Novel analogues of the scorpion venom-derived peptide, Opistoporin 1, targeting Gram-negative bacteria

By

Mandelie van der Walt

15109552

Supervisor: Prof Anabella R. M. Gaspar

Co-supervisor: Prof Megan J. Bester

Submitted in fulfilment of the requirements for the degree:

Doctor of Philosophy in Biochemistry

in the Faculty of Natural and Agricultural Sciences

University of Pretoria

November 2024

© University of Pretoria

Declaration of originality: University of Pretoria

Full names of student: ***Mandelie van der Walt***

Student number: ***15109552***

Topic of work: ***PhD Thesis- Biotherapeutics research group***

1. I understand what plagiarism is and am aware of the University's policy in this regard.

2. I declare that this thesis is my own original work. Where other people's work has been used (either from a printed source, Internet, or any other source), this has been properly acknowledged and referenced in accordance with departmental requirements.

3. I have not used work previously produced by another student or any other person to hand in as my own.

4. I have not allowed and will not allow anyone to copy my work with the intention of passing it off as his or her own work.

SIGNATURE ***MVDW***



© University of Pretoria

SUMMARY

Antimicrobial resistance among pathogens has escalated into a global crisis, significantly increasing mortality rates. Compounding this challenge is the decline in new antimicrobial drug discoveries, resulting in a scarcity of effective medicines capable of keeping pace with the rapid emergence of drug-resistant bacteria. Gram-negative bacteria, with their complex membranes and intrinsic resistance mechanisms, pose particularly daunting obstacles. Pathogens such as *Acinetobacter baumannii* and *Enterobacter cloacae*, which exhibit resistance to last resort carbapenems and cephalosporins, highlight the urgent need for novel therapeutic solutions.

Antimicrobial peptides (AMPs) are promising candidates and lead compounds for the development of next generation antimicrobials. AMPs exhibit broad-spectrum activity, selectivity towards bacteria, ability to disrupt biofilms, and possess bactericidal and/or immunomodulatory capabilities. One of the attractive features of AMPs is the potential for lower resistance development compared with conventional antimicrobial drugs. Although AMPs can be structurally modified, formulated, or used in combination with existing drugs, only a few AMPs have successfully transitioned into clinical use. Therefore, to improve the success of preclinical efficacy studies and advance hit-to-lead efforts for AMPs, this thesis utilised a combination of *in silico*, *in vitro*, and *in vivo* screenings, conducted mechanism of action studies, and employed effective sequence modification strategies. These approaches resulted in the identification of a novel array of AMPs, including the potent scorpion venom-derived peptide Opis16a. This peptide was subsequently modified to create four analogues with improved efficacy against resistant strains of Gram-negative bacteria.

At the onset of this study, 46 AMP candidates, including 27 novel or with unknown activity, were identified from African species such as scorpions, frogs, ticks, and primates. Antimicrobial screening against a diverse panel of susceptible and resistant Gram-negative and Gram-positive bacterial strains as well as fungi was undertaken. The results revealed that while many of the AMPs exhibited potent antimicrobial activity, significant cytotoxicity towards host cells, a common challenge in AMP therapeutic development, was also identified. To address this, multivariate analyses were employed to correlate 28 physicochemical peptide properties to the antimicrobial efficacy and cytotoxicity of the 46 AMPs, aiming to identify characteristics that drive selective antimicrobial effectiveness while minimising toxicity. Principal component analysis (PCA) and quantitative structure-activity relationships (QSAR) revealed that an increase in lipophilicity, hydrophobicity, or residue side chain surface area results in increased activity as well as toxicity of an AMP. Crucially, the total negative lipophilicity contributed by polar residues (Lp) was identified as the key physicochemical property determining selective antimicrobial activity.

The scorpion derived peptides proved particularly effective against Gram-negative bacteria. Among them, Opis16a emerged as a novel peptide with significant potential for therapeutic development.

© University of Pretoria

Subsequently, a more detailed assessment of the activity, stability, and mechanism of action of Opis16a, particularly against sensitive strains and drug-resistant Gram-negative clinical isolates, was undertaken. Findings were that Opis16a effectively penetrates the intricate outer membrane of Gram-negative bacteria, leading to rapid bacterial cell death. Mechanism of action studies, conducted with a standard laboratory *Escherichia coli* ATCC 700928 strain and a multidrug-resistant *A. baumannii* NICD 15283 clinical strain, revealed that Opis16a binds to lipopolysaccharides, destabilises the outer membrane, depolarises the inner membrane and finally induces lethal permeabilisation of the cytoplasmic membrane. The strong bacterial selectivity and retained activity in serum, further supported the therapeutic potential of Opis16a for topical applications. Consequently, activity was further assessed in the *in vivo Galleria mellonella* model of *A. baumannii* burn wound infection. Treatment with Opis16a results in a three-fold improvement in larval survival compared to untreated *A. baumannii*-infected larvae, with an efficacy similar to polymyxin B. Consequently, Opis16a emerges as a novel membrane-destabilising AMP showing promising *in vitro* and *in vivo* efficacy against Gram-negative bacteria, suggesting potential for advancement in topical applications.

To further increase the activity of Opis16a through rational design, four novel analogues were designed with increased cationic charge where an Asp residue in position five was replaced with a Lys (Opis16aDtoK) or where Lys residues at various positions in the sequence were replaced with Arg (Opis16aCterKtoR, Opis16aNterKtoR and Opis16aAllKtoR). Molecular dynamics (MD) simulations analyses revealed an increase in hydrogen bonding between the analogues and Gram-negative membrane lipids, along with increased membrane insertion *in silico*. Computational findings were validated through experimental *in vitro* screenings against a panel of Gram-negative bacteria, including standard laboratory and drug-resistant clinical strains. The analogues showed improvement in activity up to 16-fold compared with the parent Opis16a peptide, while maintaining strong selectivity for bacteria over HaCat cells (human keratinocyte cell-line). The analogue with the greatest improvement in activity and selectivity, Opis16aCterKtoR, also showed increased membrane permeability and *in vivo* protection of larvae infected with a multidrug-resistant *E. cloacae* NICD 16103 clinical isolate.

In summary, novel structural characteristics for the design of AMPs were developed, and subsequently Opis16a and Opis16aCterKtoR were discovered as novel AMPs with promising therapeutic potential for the treatment of Gram-negative topical infections. Further formulation can increase the potential of these AMPs for the treatment of systemic infections while additional *in vivo* animal studies are required for translation of these AMPs for clinical applications.

Keywords: Gram-negative resistant bacteria, antimicrobial peptides, rational design, molecular dynamics simulations, mechanism of action, *Galleria mellonella*, drug discovery.

© University of Pretoria

“I don’t think it’s overstating events to say that at the end of my PhD I find myself a rather different person than when I began (and not only because of the ravages of time).”

Elizabeth Krebs

Breeding biology and parental care of the crimson rosella (1999)

© University of Pretoria

Acknowledgements

I would like to express my deepest gratitude to all who shared their knowledge and encouraged me to conduct a PhD study, to persevere and ultimately complete it with a sense of accomplishment. This project has become a reality with the kind support and assistance of many individuals, sponsors and institutions whom I would like to thank.

- Firstly, my supervisor Prof. ARM Gaspar, whom I have always admired and strive to emulate. For her continual support and guidance with my research, her motivation, enthusiasm, insights and immense knowledge that she so willingly shared. This project would not have been possible without her.

- My co-supervisor, Prof. MJ Bester, for her invaluable guidance, meticulous evaluation, constructive criticism, and insightful suggestions that have been instrumental in refining my work. She taught me the importance of optimism and was always prepared with a plan B.

- The Biotherapeutics research group, for their intellectual support, great advice, motivation, and light-hearted discussions. Dalton and Roné, you're my favourite travel companions, and I'd explore the globe with you any day. Just make sure to pack comfortable walking shoes this time!

- Prof. AJ Mason from King's College London for his expertise in the antimicrobial field, his exceptional mentorship in refining my writing skills, and above all his profound knowledge and intuition in this domain. His guidance has shaped me into a more proficient researcher and scientific writer, and I greatly respect him for the profound impact he has had on my development.

- Prof. CD Lorenz from King's College London for his kindness from day one, always willing to assist with science or anything else. His profound expertise in computational biology, along with his patient teaching style and dedication to troubleshooting failed simulation runs, even beyond regular hours, are deeply valued and appreciated.

- The Biochemistry personnel, particularly Ms. S van Wyngaard who has been a cornerstone of the department. Her unwavering assistance with equipment and apparatus, administration, advice, guidance and support throughout the years has been indispensable.

- My parents- my dad who continues to support me and my mom, whose spirit continues to inspire me daily. Their unwavering love, steadfast support, and continuous belief in me have shaped every aspect of who I am today.

- My life partner, Marno Grobler, for supporting me on the days when I felt like giving up and cheering me on during my moments of triumph. You've been my anchor through both joyful and challenging times, always reminding me of what truly matters in life.

© University of Pretoria

- All my family and friends for their encouragement and taking pride in me.

- The South African Medical Research Council for funding which not only made this degree possible but also helped me grow as a scientist by supporting travel to universities in the UK. This opportunity expanded my scientific knowledge and enriched my outlook on research and science.

- The University of Pretoria for providing top-tier research facilities, an environment that enables growth and collaboration among exceptional individuals. Without this institution, my PhD project and previous degrees would not have reached successful completion, nor would I have had the opportunity to engage with academics at this level.

© University of Pretoria

TABLE OF CONTENTS

Page

Declaration of originality II
Summary III
Acknowledgements VI
Table of contents VIII
List of figures XI
List of tables XIII
List of abbreviations and acronyms XIV
Preface XVIII
Outputs related to the study XXI

CHAPTER 1: Literature review ***pg. 1.1***

1.1 The rise of antimicrobial resistance 1.1
1.2 Gram-negative resistant bacterial infections 1.2
1.3 The Gram-negative bacterial cell wall 1.5
1.4 Antimicrobial peptides as potential next generation antibiotics 1.7
1.4.1 AMP targets and mechanisms of action 1.7
1.4.1.1 Direct bacterial cell wall targeting 1.8
1.4.1.2 Direct intracellular targeting 1.12
1.4.1.3 Direct biofilm targeting 1.12
1.4.1.4 Indirect action via immune modulation 1.14
1.4.2 AMPs in clinical trials 1.16
1.5 Strategies to increase the therapeutic application of AMPs 1.19
1.6 Modern technologies that accelerate AMP discovery, design and development 1.21
1.6.1 AMP databases 1.21
1.6.2 Machine learning and AMP prediction 1.22
1.6.3 Molecular simulation modelling 1.23
1.7 Screening of modified or rationally designed AMPs 1.24
1.7.1 *In vitro,* cell-based screening models 1.24
1.7.2 *Ex vivo,* tissue-based screening models 1.25
1.7.3 *In vivo,* animal screening models 1.27
1.8 Conclusion 1.28
1.9 References 1.29

© University of Pretoria

CHAPTER 2: QSAR reveals decreased lipophilicity of polar residues determines the selectivity of antimicrobial peptide activity ***pg. 2.1***

VAN DER WALT, M., MÖLLER, D.S., VAN WYK, R.J., FERGUSON, P.M., HIND, C.K., CLIFFORD, M., DO CARMO SILVA, P., SUTTON, J.M, MASON, J.A., BESTER, M.J. & GASPAR, A.R.M. (2024). QSAR reveals cationic residues with decreased lipophilicity determine the selectivity of antimicrobial peptide activity. *ACS Omega,* doi: 10.1021/acsomega.4c01277.

CHAPTER 3:* Scorpion venom-derived Opis16a shows potent membrane-destabilising Gram-negative activity and promising *in vivo* topical efficacy** ***pg. 3.1

3.1 Abstract 3.2
3.2 Introduction 3.3
3.3 Materials and methods 3.5
3.3.1 Opis16a purification 3.5
3.3.2 Antimicrobial activity assay 3.5
3.3.3 *In vitro* cytotoxicity screening against HepG2 cells 3.5
3.3.4 Outer membrane LPS competitive inhibition 3.6
3.3.5 Outer membrane permeabilisation 3.6
3.3.6 Cytoplasmic membrane depolarisation 3.6
3.3.7 Cytoplasmic membrane permeabilisation 3.7
3.3.8 Time-kill kinetics 3.7
3.3.9 Opis16a activity in the presence of trypsin and serum 3.7
3.3.10 *In vitro* antibacterial activity of Opis16a in a *G. mellonella* burn model 3.8
3.3.11 Activity data and statistical analysis 3.8
3.4 Results 3.9
3.4.1 Opis16a displays promising antibacterial activity with high selectivity 3.9
3.4.2 LPS pretreatment inhibits Opis16a antibacterial activity suggesting binding 3.10
3.4.3 Opis16a permeabilises the outer membrane 3.11
3.4.4 Opis16a depolarises the cytoplasmic membrane at sub-MIC 3.12
3.4.5 Opis16a shows rapid killing of *E. coli* and *A. baumannii* via cytoplasmic membrane permeabilisation 3.13
3.4.6 Opis16a retains activity in serum, but not in trypsin solution 3.15
3.4.7 Opis16a shows activity against *in vivo A. baumannii* infected wounds 3.15
3.5 Discussion 3.17
3.6 Conclusion 3.19
3.7 Acknowledgements 3.19
3.8 References 3.20

© University of Pretoria

CHAPTER 4: Enhanced Gram-negative membrane disruption and in vivo antibacterial efficacy through lysine and arginine enrichment in the Opis16a sequence pg. 4.1

4.1 Abstract 4.2
4.2 Introduction 4.3
4.3 Materials and methods 4.5
4.3.1 Materials 4.5
4.3.2 Molecular dynamic simulations 4.5
4.3.3 Circular dichroism spectroscopy 4.6
4.3.4 Antibacterial activity against laboratory strains and clinical isolates 4.7
4.3.5 *In vitro* cytotoxicity screening against epidermal HaCat cells 4.7
4.3.6 Cytoplasmic membrane permeabilisation 4.8
4.3.7 Time-kill kinetics 4.8
4.3.8 Opis16aCterKtoR activity in the presence of trypsin and serum 4.8
4.3.9 *In vivo* antibacterial activity of Opis16aCterKtoR in a *G. mellonella* burn wound model 4.9
4.3.10 Activity data and statistical analysis 4.9
4.4 Results 4.10
4.4.1 Opis16a analogues have increased hydrogen bonding with lipids 4.10
4.4.2 Decreased conformational flexibility of the Opis16a analogues 4.11
4.4.3 Opis16a analogues offer improved antibacterial potency 4.15
4.4.4 An increase in bacterial selectivity highlights the potential of the analogues 4.17
4.4.5 Opis16a analogues show better membrane insertion and permeabilisation 4.18
4.4.6 Opis16aCterKtoR shows rapid killing of resistant *E. cloacae* NICD 16103 ..... 4.21
4.4.7 Opis16aCterKtoR retains activity in serum but not in trypsin solution 4.22
4.4.8 Opis16aCterKtoR shows efficacy against *in vivo E. cloacae* NICD 16103 infected burn wounds 4.22
4.5 Discussion 4.24
4.6 Conclusion 4.28
4.7 Acknowledgements 4.28
4.8 References 4.29
Supplementary 4.32

CHAPTER 5: Conclusion and future perspectives pg. 5.1

5.1 Summary of findings and future perspectives 5.1
5.2 Last word 5.4
5.3 References 5.6

SUPPLEMENTARY INFORMATION S1

© University of Pretoria

LIST OF FIGURES

CHAPTER 1: Literature review *pg. 1.1*

Figure 1.1: Mechanisms of antimicrobial resistance 1.2
Figure 1.2: WHO 2024 list of priority pathogens grouped under critical, high and medium 1.3
Figure 1.3: Gram-negative bacterial cell envelope 1.5
Figure 1.4: The structure of LPS 1.6
Figure 1.5: Five common structural classes of AMPs 1.7
Figure 1.6: Mechanisms of action of AMPs 1.8
Figure 1.7: Phospholipids found in Gram-negative vs mammalian cytoplasmic membranes 1.9
Figure 1.8: AMPs and their cytoplasmic membrane binding specificity 1.10
Figure 1.9: Models of AMP action on microbial cell membranes 1.11
Figure 1.10: Bacterial biofilm formation 1.13
Figure 1.11: The various stages of wound healing and examples of AMPs involved 1.15
Figure 1.12: SWOT analysis of AMPs 1.17
Figure 1.13: Chemical structures of clinically approved AMPs 1.18
Figure 1.14: Example of an MD simulation 1.24
Figure 1.15: Examples of *in vitro* screening techniques 1.24
Figure 1.16: Example of *ex vivo* porcine lung and cornea models evaluating AMP efficacy 1.26
Figure 1.17: *In vivo G. mellonella* model assessing the efficacy of an AMP 1.28

CHAPTER 2: QSAR reveals decreased lipophilicity of polar residues determines the selectivity of antimicrobial peptide activity *pg. 2.1*

VAN DER WALT, M., MÖLLER, D.S., VAN WYK, R.J., FERGUSON, P.M., HIND, C.K., CLIFFORD, M., DO CARMO SILVA, P., SUTTON, J.M, MASON, J.A., BESTER, M.J. & GASPAR, A.R.M. (2024). QSAR reveals cationic residues with decreased lipophilicity determine the selectivity of antimicrobial peptide activity. *ACS Omega,* doi: 10.1021/acsomega.4c01277

CHAPTER 3: Scorpion venom-derived Opis16a shows potent membrane-destabilising Gram-negative activity and promising *in vivo* topical efficacy *pg. 3.1*

Figure 3.1: Effect of LPS on Opis16a efficacy against Gram-negative bacteria 3.10
Figure 3.2: Opis16a mediated outer membrane permeabilisation over 2h 3.12
Figure 3.3: Percentage cytoplasmic membrane depolarisation after treatment with Opis16a ... 3.13
Figure 3.4: Inner membrane permeabilisation corresponds to time-kill kinetics of Opis16a 3.14
Figure 3.5: Antibacterial efficacy of Opis16a in the presence of trypsin or serum 3.15
Figure 3.6: Opis16a provided protection in a *G. mellonella – A. baumannii* NICD 15283 burn wound infection model 3.16

© University of Pretoria

Figure 4.1: Hydrogen bonding between peptide and PEPG model lipids differ among Opis16a analogues and is driven by cationic residues 4.11

Figure 4.2: Conformation analysis of Opis16a and analogues in Gram-negative membranes .. 4.12

Figure 4.3: Average conformational flexibility of Opis16a and analogues in Gram-negative membranes 4.14

Figure 4.4: Change in conformational flexibility of Opis16a and analogues over time 4.15

Figure 4.5: Membrane activity of Opis16a and analogues in Gram-negative membranes *in silico* 4.19

Figure 4.6: Membrane activity of Opis16a and analogues in Gram-negative membranes *in vitro* 4.20

Figure 4.7: Bacterial time-kill kinetics of Opis16a compared with Opis16aCterKtoR..... 4.22

Figure 4.8: Comparison of Opis16a and Opis16aCterKtoR activity against *E. cloacae* NICD 16103 in serum, and in a *G. mellonella* burn wound infection model..... 4.23

Figure S4.1: Hydrogen bonding between peptide and PEPG model lipids differ among Opis16a analogues and is driven by cationic residues..... 4.33

Figure S4.2: Steady-state secondary structure analysis of Opis16a and analogues..... 4.33

Figure S4.3: Membrane permeabilisation of Opis16a and analogues against Gram-negative bacterial membranes 4.35

Figure S4.4: Comparison of membrane permeabilisation in *E. cloacae* NICD 16103 induced by 1x MIC of Opis16a and analogues at different times..... 4.36

© University of Pretoria

LIST OF TABLES

CHAPTER 1: Literature review ***pg. 1.1***

Table 1.1: Various AMPs, their targets and mechanism of action 1.8

Table 1.2: Mechanisms of action of intracellular targeting AMPs 1.12

Table 1.3: Bacterial targets, mode of administration and structural characteristics of AMPs in different phases of clinical trials 1.17

CHAPTER 2: QSAR reveals decreased lipophilicity of polar residues determines the selectivity of antimicrobial peptide activity ***pg. 2.1***

VAN DER WALT, M., MÖLLER, D.S., VAN WYK, R.J., FERGUSON, P.M., HIND, C.K., CLIFFORD, M., DO CARMO SILVA, P., SUTTON, J.M, MASON, J.A., BESTER, M.J. & GASPAR, A.R.M. (2024). QSAR reveals cationic residues with decreased lipophilicity determine the selectivity of antimicrobial peptide activity. *ACS Omega,* doi: 10.1021/acsomega.4c01277

CHAPTER 3:* Scorpion venom-derived Opis16a shows potent membrane-destabilising Gram-negative activity and promising *in vivo* topical efficacy** ***pg. 3.1

Table 3.1: The sequence and physicochemical properties of opistoporin 1 and Opis16a 3.4

Table 3.2: Antibacterial activity and selectivity of Opis16a against Gram-negative strains 3.9

CHAPTER 4: Rational design and screening of 2nd generation AMPs from the parent scorpion venom peptide, Opis16a ***pg. 4.1***

Table 4.1: Physicochemical properties of Opis16a and its four analogues 4.5

Table 4.2: Antibacterial activity of Opis16a analogues against Gram-negative bacteria 4.16

Table 4.3: The toxicity and bacterial selectivity indexes of Opis16a and analogues 4.18

Table S4.1: Antimicrobial susceptibility profile provided by the NICD 4.32

Table S4.2: Antibacterial activity of four clinically used antibacterial agents, and melittin, against Gram-negative bacterial strains 4.32

Table S4.3: Peptide secondary structure determined with BestSel using CD spectra 4.34

CHAPTER 5: Conclusion and future perspectives ***pg. 5.1***

Table 5.1: Summary of the activities, mechanisms of action and clinical potential of Opis16a and Opis16aCterKtoR 5.5

SUPPLEMENTARY INFORMATION ***S1***

Table S1: A summary of all the peptides purified S16

© University of Pretoria

LIST OF ABBREVIATIONS AND ACRONYMS

A

A. baumannii	*Acinetobacter baumannii*
ADMET	Absorption, distribution, metabolism, excretion and toxicity
Ala	Alanine
AN	Acetonitrile
AmB	Amphotericin B
AMP	Antimicrobial peptide
AMR	Antimicrobial resistance
ANOVA	One-way analysis of variance
APD3	Antimicrobial peptide database
Arg	Arginine
Asn	Asparagine
Asp	Aspartic acid
ATCC	American Type Culture Collection
ATP	Adenosine triphosphate

B

BMRB	Biological magnetic resonance bank
BTD	Baboon theta defensin

C

$CAMP_{R3}$	Collection of antimicrobial peptides
CD	Circular dichroism
CDC	Centers for Disease Control and Prevention
CFU	Colony forming units
CPF	Caerulein precursor fragment
CPP	Cell penetrating peptide
Cys	Cysteine

D

DADP	Database of Anuran defense peptides
ddH_2O	Double distilled water
DMEM	Dulbecco's Modified Eagles medium
DNA	Deoxyribonucleic acid
DRAMP	Data repository of antimicrobial peptides

E

E. coli	*Escherichia coli*
E. cloacae	*Enterobacter cloacae*
Em	Emission wavelength
EUCAST	European Committee on Antimicrobial Susceptibility Testing

© University of Pretoria

Ex	Excitation wavelength
F	
FCS	Foetal calf serum
G	
g	Gravity
Gln	Glutamine
Glu	Glutamic acid
Gly	Glycine
GPU	Graphics processing unit
GPI	Glycosylphosphatidylinositol
H	
<H>	Hydrophobicity
HAI	Hospital acquired infection
HBD	Human β-defensin
HGT	Horizontal gene transfer
His	Histidine
I	
ICU	Intensive care unit
Ile	Isoleucine
K	
Kb	Binding affinity
L	
LAL	*Limulus amoebocyte* lysate
LB	Luria broth
Leu	Leucine
LP	Lipophilicity of polar residues
LPS	Lipopolysaccharide
Lys	Lysine
M	
MBC	Minimum bactericidal concentration
MBEC	Minimum biofilm eradication concentration
MBIC	Minimum biofilm inhibition concentration
MBPC	Minimum biofilm prevention concentration
MD	Molecular dynamics
MDR	Multidrug-resistant
Met	Methionine
MGE	Mobile gene element
MHB	Mueller Hinton broth
MIC	Minimum inhibitory concentration

© University of Pretoria

MW	Molecular weight
N	
NaP	Sodium phosphate
nm	Nanometre
NMR	Nuclear magnetic resonance
NVT	Fixed number of simulated particles (N), simulation cell volume (V) and temperature (T)
NPT	Fixed number of simulated particles (N), simulation pressure (P) and temperature (T)
O	
OD	Optical density
OmDef	*Ornithodoros moubata* defensin isoform
ORAC	Oxygen radical absorbance capacity
OsDef	*Ornithodoros savignyi* defensin isoform
Os-C	Synthetic derivative of OsDef2 from C-terminus end by omitting 3 cysteine residues
P	
PBS	Phosphate buffered saline
PC	Phosphatidylcholine
PCA	Principal component analysis
PE	Phosphatidylethanolamine
PG	Phosphatidylglycerol
PHE	Public Health England
Phe	Phenylalanine
POPG	1-Palmitoyl-2-oleoyl-sn-glycero-3- phospho-(1′-rac-glycerol)
POPE	1-Palmitoyl-2-oleoyl-sn-glycero-3- phosphoethanolamine
Pro	Proline
Q	
QSAR	Quantitative structure-activity relationship
R	
RBC	Red blood cells
RDA	Radial diffusion assay
ROS	Reactive oxygen species
RP-HPLC	Reverse phase- high performance liquid chromatography
rpm	Rotations per minute
RPMI	Roswell Park Memorial Institute medium
RTD	Rhesus θ-defensin
S	
SDS	Sodium dodecyl sulphate
SE	Standard error of the mean

© University of Pretoria

T

TCA	Trichloroacetic acid
TFA	Trifluoroacetic acid
TGF	Transforming growth factor
Thr	Threonine
TNF	Tumour necrosis factor
Trp	Tryptophan
TSA	Tryptic soy agar
TSB	Tryptic soy broth
Tyr	Tyrosine

U

UPLC-MS	Ultra performance liquid chromatography – mass spectrometer

V

Val	Valine
v/v	Volume per volume

W

w/v	Weight per volume
WHO	World Health Organization

X

XDR	Extensive drug-resistant
XPF	Xenopsin precursor fragments

Y

YPD	Yeast peptone dextrose

© University of Pretoria

Preface

The emergence of multidrug-resistant Gram-negative infections, particularly those with profound healthcare implications, highlights an urgent need for innovative therapeutic approaches. Recognising the severity of this issue, the World Health Organization (WHO) has designated antimicrobial resistance as a critical public health threat of the 21st century. At the forefront of concern are Gram-negative bacteria such as multidrug-resistant *Acinetobacter baumannii*, *Enterobacter cloacae*, *Pseudomonas aeruginosa*, and *Klebsiella pneumoniae*.

The main aim of this study was to contribute to the mitigation of the antimicrobial resistance crisis by identifying potent AMPs from diverse African species and evaluating the potential of the most promising candidates for future development and clinical applications. In this thesis, Chapter 1 provides an overview of the global impact of antimicrobial resistance, highlighting the growing challenges posed by antibiotic failures. It explores AMPs as a potential solution to combat these issues. Chapter 2 delves into the antibacterial and antifungal activity of 46 AMPs sourced from African species including frogs, scorpions, ticks, and primates. It identifies scorpion venom-derived peptides as the most promising candidates for further antibacterial development. The chapter also expands on understanding the structural features crucial for effective and selective activity.

Chapter 3 is centred on investigating the most promising peptide, Opis16a, among those identified, examining its mechanism of action, anti-Gram-negative potential, and suitability for development as a topical treatment for burn wound infections. The final experimental chapter utilises all-atom MD simulations in a rational design strategy to develop analogues of Opis16a, with the aim of enhancing antibacterial efficacy, especially against Gram-negative bacteria (Chapter 4). These rational design strategies yielded positive outcomes in *in vitro* screenings, showing improved and selective antibacterial activity. Further investigation examined the mechanism of action and suitability of the most promising analogue for topical application. Chapter 5 provides a summary of the findings from each of the preceding chapters, along with proposals for future research directions. The experimental chapters of this thesis were structured as independent entities with the intention of facilitating future publication. While unavoidable repetitions may occur in some chapters, every effort was made to minimise redundancy.

The first objective of the study was twofold: first, to identify a novel group of diverse, linear AMPs from various African species with potential antimicrobial activity; and second, to utilise this extensive group of AMPs to broaden our understanding of the structural features crucial for effective and selective AMP function. The sub-objectives were to:

- Identify short AMPs from African species with predicted antimicrobial activity that have not been extensively researched or patented before, by using sources such as the Antimicrobial Peptide Database (APD3), the Data Repository of Antimicrobial Peptides (DRAMP), the

© University of Pretoria

Collection of Anti-Microbial Peptides (CAMPR3), and other published sources.

- Screen the group of 46 identified African derived AMPs for activity *in vitro* against susceptible and resistant strains of Gram-negative and -positive bacteria and fungi.
- Determine the bacterial over mammalian cell selectivity of these peptides *in vitro* against human erythrocytes and HaCat keratinocytes.
- Solve the secondary structure of all peptides in Tris buffer, sodium dodecyl sulphate (SDS) and membrane-mimicking environments using circular dichroism (CD) spectroscopy.
- Employ principal component analysis (PCA) and quantitative structure-activity relationship (QSAR) correlations to identify and summarise the physicochemical properties crucial for antimicrobial activity and selectivity of these 46 peptides.

The second objective of the study was to further explore the selectivity, mechanism of action, stability, and lastly the potential for topical treatment of infections with the most active scorpion AMP (identified from objective one), Opis16a. The sub-objectives were to:

- Confirm the antibacterial activity of Opis16a against Gram-negative strains, including a multidrug-resistant clinical isolate (*A. baumannii* NICD 15283) and bacterial over mammalian cell selectivity using HaCat and HepG2 cells.
- Investigate the mechanism of action of Opis16a through time-kill kinetics studies, outer membrane lipopolysaccharide (LPS) binding, and the depolarisation and permeabilisation of the inner cytoplasmic membrane of *E. coli* ATCC 700928 and *A. baumannii* NICD 15283.
- Determine the antibacterial activity of Opis16a against *A. baumannii* NICD 15283 in the presence of trypsin or foetal calf serum (FCS)
- Evaluate the ability of Opis16a to provide effective therapy in a *Galleria mellonella* burn wound *A. baumannii* NICD 15283 infection model.

The final objective was to employ strategic design methods to enhance the efficacy of Opis16a specifically against Gram-negative bacteria. The sub-objectives were to:

- Design four novel analogues (Opis16aDtoK, Opis16aCterKtoR, Opis16aNterKtoR and Opis16aAllKtoR) of Opis16a via amino acid substitution to increase anti-Gram-negative efficacy.
- Use MD simulations to evaluate the potential of the four rationally designed peptides to interact *in silico* with a Gram-negative model membrane.
- Determine the secondary structures of the four rationally designed peptides in Tris buffer, SDS and membrane-mimicking environments using CD spectroscopy.
- Evaluate the activity of the four rationally designed peptides, compared with the parent peptide Opis16a, against a panel of Gram-negative bacteria, six standard laboratory strains and two clinical isolates including *A. baumannii* NICD 15283 and *E. cloacae* NICD 16103.

© University of Pretoria

- Determine the bacterial over mammalian HaCat cell selectivity of the four rationally designed peptides.
- Evaluate the time-kill kinetics and mechanism of action of the most promising AMP, Opis16aCterKtoR, compared with Opis16a, against *E. cloacae* NICD 16103.
- Determine the antibacterial activity of Opis16aCterKtoR compared with Opis16a against *E. cloacae* NICD 16103 in the presence of trypsin or FCS.
- Evaluate the potential of Opis16aCterKtoR, compared with Opis16a, for topical applications by assessing the peptide ability to treat *G. mellonella* burn wounds infected with *E. cloacae* NICD 16103.

© University of Pretoria

Research outputs related to this PhD study

Peer-reviewed articles:

- **VAN DER WALT, M**., MÖLLER, D.S., VAN WYK, R.J., FERGUSON, P.M., HIND, C.K., CLIFFORD, M., DO CARMO SILVA, P., SUTTON, J.M, MASON, A.J., BESTER, M.J. & GASPAR, A.R.M. (2024). QSAR reveals cationic residues with decreased lipophilicity determine the selectivity of antimicrobial peptide activity. ***ACS Omega,*** **doi: 10.1021/acsomega.4c01277.**
- MÖLLER, D.S., **VAN DER WALT, M**., OOSTHUIZEN, C.B., SERIAN, M., LORENZ, C.D., MASON, A.J., SEREM, J.C., BESTER, M.J. & GASPAR, A.R.M. (2024). Improving the activity and selectivity of a scorpion-derived peptide, A3a, against *Acinetobacter baumannii* through rational design. ***ACS Omega*** **(under review).**
- **VAN DER WALT, M**., OOSTHUIZEN, C.B., MASON, A.J., BESTER, M.J. & GASPAR, A.R.M. (2024/5). Opis16a, a scorpion-derived membrane destabilising peptide with potent Gram-negative activity and promising *in vivo* topical efficacy **(manuscript in preparation).**
- **VAN DER WALT, M**., OOSTHUIZEN, C.B., SERIAN, M., LORENZ, C.D., MASON, A.J., BESTER, M.J. & GASPAR, A.R.M. (2024/5). Sequence modifications of Opis16a delivers analogues with increased antibacterial potency **(manuscript in preparation).**
- **VAN DER WALT, M**., MÖLLER, D.S., VAN WYK, R.J., BESTER, M.J. & GASPAR, A.R.M. (2024/5). Exploring the mechanism of action of two tick derived antimicrobial peptides, Os and Os-C, against planktonic *C. albicans* **(manuscript in preparation).**

Oral presentations:

- **VAN DER WALT, M**., MÖLLER, D.S., VAN WYK, R.J., BESTER, M.J. & GASPAR, A.R.M. (2022). Exploring the mechanism of action of two tick derived antimicrobial peptides, Os and Os-C, against planktonic *C. albicans.* SASBMB 2022 Congress (23-26 January 2022). **Oral presentation**.
- **VAN DER WALT, M.**, MÖLLER, D. S. & VAN WYK, R. J. (2022). Tapping the biodiversity of Africa for antimicrobial peptide discovery. Monthly seminar (22 March 2022), School of Life Sciences, Microbiology, University of Warwick, Coventry, United Kingdom. **Oral presentation**.
- **VAN DER WALT, M.** (2024). Novel analogues of the scorpion venom-derived peptide, Opistoporin 1, targeting Gram-negative bacteria. Department of Biochemistry, Genetics and Microbiology (BGM) seminar (26 August 2024), University of Pretoria, Pretoria, South Africa. **Oral presentation**.

Poster presentations:

- MÖLLER, D.S, VAN WYK, R.J. & **VAN DER WALT, M**. (2022). Molecular dynamics simulation of the interaction of peptide analogues derived from the tick OsDef2 defensin with model Gram-positive and Gram-negative bacterial cell membranes. SASBMB 2022 Congress (23-26 January 2022), Virtual. **Poster presentation.**
- **VAN DER WALT, M.**, MÖLLER, D.S., VAN WYK, R.J., FERGUSON, P.M., HIND, C.K., CLIFFORD, M., DO CARMO SILVA, P., SUTTON, J.M, LORENZ, C.D., MASON, A.J., BESTER, M.J. & GASPAR, A.R.M. (2023). Peptides from scorpion venom: The solution to antimicrobial resistance? BGM symposium (1 December 2023), University of Pretoria, Pretoria, South Africa. **Poster presentation**.

© University of Pretoria

CHAPTER 1: Literature review

1.1 The rise of antimicrobial resistance

Antimicrobials, such as antibiotics and antifungals, have been pivotal in the history of medicine and have saved millions of lives, substantially contributing to the control and prevention of infectious diseases that were the main cause of human deaths (Aminov, 2010). Initially, the antibiotic era inspired hope that virtually any bacterial infection could be effectively treated. However, this optimism was tempered by the emergence of antimicrobial resistance (AMR). The consequences of AMR are profound and global. A comprehensive study conducted by Murray *et al.* (2019) highlighted the staggering toll of AMR, reporting an estimated 4.95 million deaths in 2019 attributed to bacterial infections resistant to antimicrobials. Most of these fatalities occurred in sub-Saharan Africa, highlighting the disparities in healthcare access and treatment efficacy.

Regardless of many attempts at discovering new and lasting antibiotics, only a handful remain effective. This is due to the natural ability of pathogens to withstand environmental challenges and the effects of harmful molecules, such as antimicrobial agents. Every use or misuse of these drugs selects for resistant strains. Resistance mechanisms are diverse and complex, involving mutations that lead to changes in cellular targets such as DNA, mRNA and proteins, the development of efflux pumps to counteract drug uptake, inactivation of enzymes involved in drug metabolism and the use of alternative metabolic pathways (Davies, 1997; Bush *et al.,* 1995; Nikaido, 1998; Uddin *et al.,* 2021) (Fig. 1.1). Resistant genes can also be acquired through horizontal gene transfer, a process facilitated by mobile genetic elements such as plasmids and transposons. This mechanism plays a crucial role in the spread of resistance genes among bacterial populations (Davies, 1997; Michaelis & Grohmann, 2023). This highlights the urgent need for innovation in drug discovery to prevent a potential post-antibiotic era where infections could become virtually untreatable.

© University of Pretoria

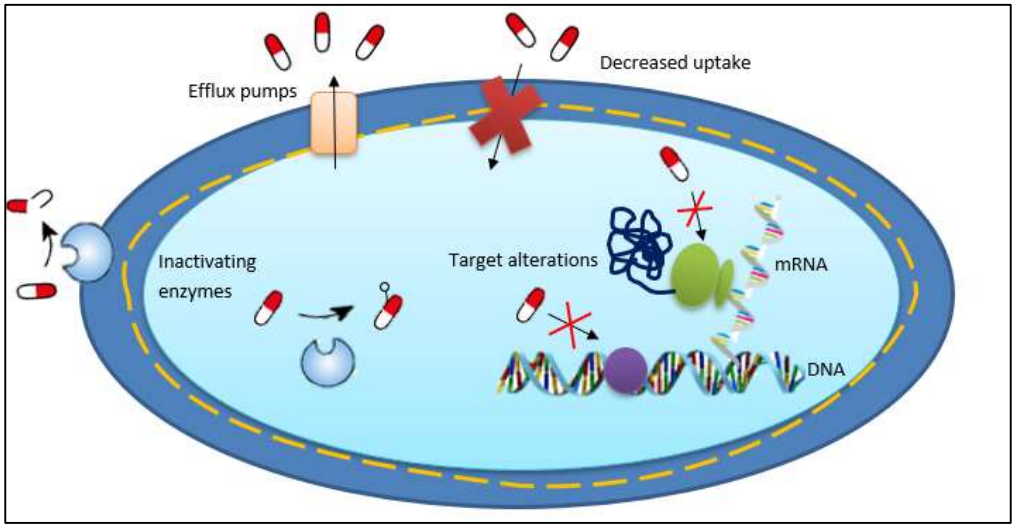


***Figure 1.1: Mechanisms of antimicrobial resistance**. Microorganisms can change intra- and extracellular targets, increase the expression of efflux pumps, decrease drug uptake, inactivate metabolic enzymes, and alternate biochemical pathways, to resist the action of antimicrobial drugs. (Modified from: Antibiotic resistance strategies in bacteria, ReAct, 2015 used under CC-BY-NC 2.0 license).*

1.2 Gram-negative resistant bacterial infections

Antibiotic-resistant bacterial infections have become a critical global issue, with Gram-negative bacteria such as *Acinetobacter baumannii*, *Pseudomonas aeruginosa*, *Enterobacter cloacae*, and *Klebsiella pneumoniae* significantly contributing to high mortality rates (Murray *et al.,* 2019). In response to this growing threat, the World Health Organization (WHO) prioritised antibiotic-resistant microorganisms in 2017, categorising them by the urgency of the need for new treatment options. This list was updated in 2024, as summarised below (Fig. 1.2). Gram-negative pathogens are predominantly represented, with drug-resistant *A. baumannii* or *Enterobacterales* and third-generation cephalosporin-resistant *Enterobacterales* classified as critical priorities for intervention.

A. baumannii has emerged as a notorious opportunistic pathogen capable of causing a wide range of infections, particularly in healthcare settings where it exhibits a remarkable ability to develop resistance against multiple antimicrobial agents. The ability of this bacterium to survive and persist on medical equipment and surfaces within hospital environments has made it a common cause of nosocomial infections (Brady *et al.,* 2023).

While *A. baumannii* predominantly affects immunocompromised patients and those with underlying health conditions, it can also infect otherwise healthy individuals, particularly in scenarios involving prolonged exposure to healthcare facilities or equipment, or in individuals where the integrity of the skin is compromised (Peleg *et al.*, 2008). Wound infections caused by *A. baumannii*, associated with traumatic injuries, surgical wounds, and burns, highlight its capacity to colonise damaged dermal tissues and form biofilms on various surfaces (Ruamsap *et al.,* 2023). These biofilms provide protection against host immune responses and antimicrobial treatments, contributing to chronic and challenging infections (Fattahian *et al.*, 2011).

© University of Pretoria

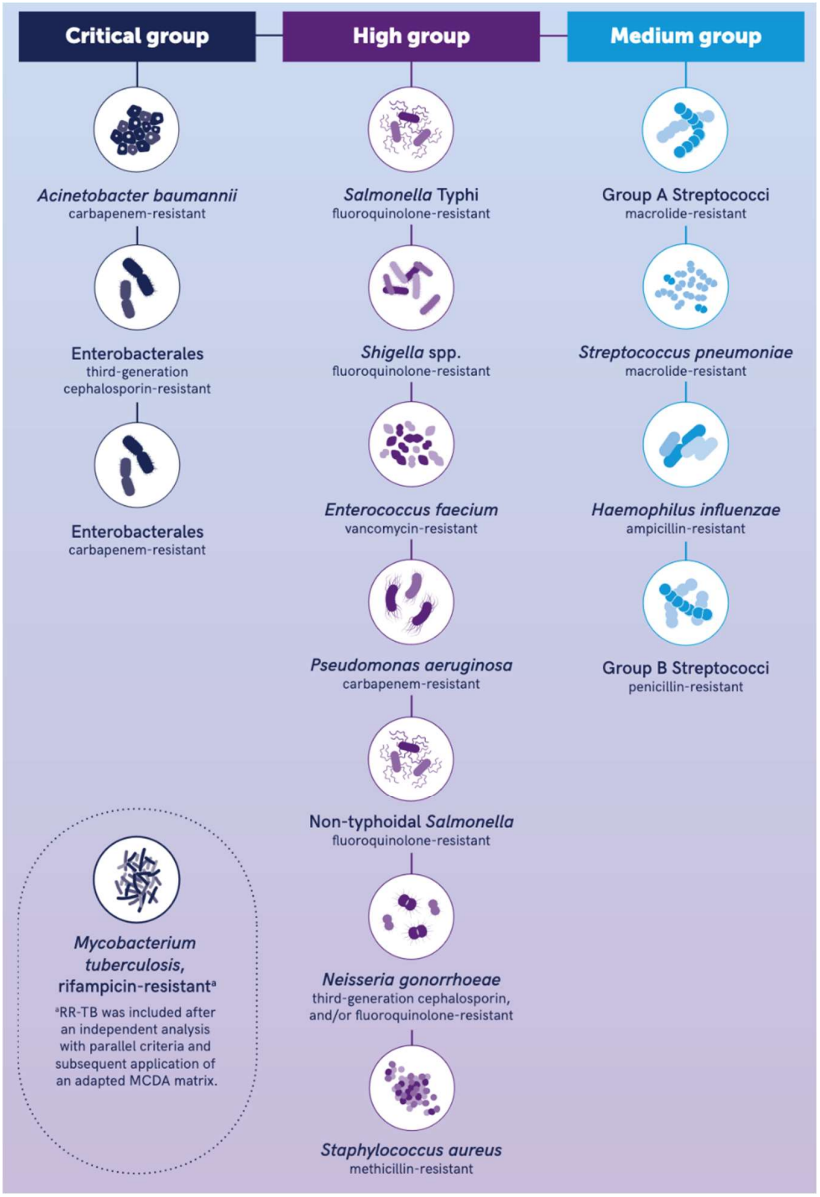


Figure 1.2: WHO updated 2024 list of priority pathogens grouped under critical, high, and medium priority based on their antibiotic resistance. *Gram-negative bacteria are more resistant than Gram-positive bacteria and thus make up most of this list. (Used under CC-BY-NC-SA 3.0 IGO license).*

In addition to biofilm formation, *A. baumannii* employs intrinsic resistance mechanisms, such as reduced outer membrane permeability and efflux pumps, which actively expel antibiotics from the bacterial cell. Moreover, *A. baumannii* readily acquires resistance genes through horizontal gene transfer, allowing it to rapidly evolve and adapt to new environmental pressures, including exposure to antibiotics (Peleg *et al.*, 2008).

These mechanisms make efforts to combat *A. baumannii* infections challenging and limit the effectiveness of available antibiotics. Multidrug-resistant strains, particularly those resistant to carbapenems, considered as last-resort antibiotics, are increasingly prevalent worldwide (Peleg *et al.*, 2008). In Europe, studies indicate rising rates of multidrug-resistant *A. baumannii* infections

© University of Pretoria

exceeding 50% across multiple antibiotic classes (European Centre for Disease Prevention and Control, 2021). The rise of carbapenem-resistant *A. baumannii* strains highlights the urgent need for novel antimicrobial therapies and improved infection control measures to mitigate the impact of this resilient pathogen in healthcare settings (Hawkey *et al.,* 2018).

In addition, *Enterbobacterales* that include *E. cloacae* has been designated by the WHO as a critical pathogen necessitating urgent attention due to its capability to cause severe infections and its high levels of antibiotic resistance (Bennett *et al.*, 2023). *E. cloacae* thrives particularly well in hospital settings, where it contributes substantially to nosocomial infections. These infections are often associated with an ability to form biofilms on medical devices and colonise tissues making it challenging to eradicate with conventional antimicrobial therapies (Misra *et al.*, 2022). In burn wound infections specifically, *E. cloacae* has been reported as a causative agent, where tissue damage is exacerbated and recovery is complicated due to the ability of this bacterium to colonise and persist in damaged tissues (Misra *et al.*, 2022).

A significant concern is the propensity of *E. cloacae* to exhibit intrinsic resistance mechanisms, including the production of extended-spectrum beta-lactamases and AmpC beta-lactamases. These enzymes confer resistance to a broad spectrum of antibiotics, including cephalosporins and penicillins, commonly used to treat bacterial infections (Annavajhala *et al.*, 2019). Moreover, the bacterium can acquire additional resistance genes through horizontal gene transfer, further complicating treatment options and leading to the emergence of multidrug-resistant strains, including those resistant to carbapenems (Annavajhala *et al.*, 2019).

The impact of *E. cloacae* is particularly severe in developing countries, where healthcare infrastructure challenges and limited access to effective antibiotics exacerbate the problem. Studies have indicated alarmingly high rates of multidrug resistance among clinical isolates of *E. cloacae* in these regions, with resistance recorded to key antibiotics like third-generation cephalosporins and carbapenems (Annavajhala *et al.*, 2019). This resistance not only compromises treatment efficacy but also necessitates more stringent infection control measures and enhanced surveillance to curb its spread and impact on public health (Annavajhala *et al.*, 2019).

Other bacterial pathogens of significant concern, which fall into the high and medium priority groups, include *Salmonella* species, *Shigella* species, and *P. aeruginosa*. *Salmonella* species are notorious for causing foodborne illnesses and typhoid fever while *Shigella* species are responsible for shigellosis, a severe form of dysentery. *P. aeruginosa* is especially troubling, having been classified in the critical priority group in 2017 due to its role in hospital-acquired infections and the capacity to develop resistance to a broad spectrum of antibiotics. This highlights the urgent need for novel antimicrobial therapies and improved infection control measures to effectively combat infections, particularly those caused by the increasingly prevalent Gram-negative bacteria, and reduce their impact.

© University of Pretoria

In an endeavour, to design drugs that effectively target Gram-negative bacteria, several structural features of these bacteria must be considered and the most challenging is related to the complexity of the cell wall compared with Gram-positive bacteria.

1.3 The Gram-negative bacterial cell wall

Gram-negative bacteria have a distinctive three-layered cell envelope (Fig1.3). The first layer of Gram-negative bacteria is the outer membrane, a distinctive and protective feature absent in Gram-positive bacteria. This membrane comprises an inner leaflet of phospholipids and an outer leaflet of lipopolysaccharides (LPS).

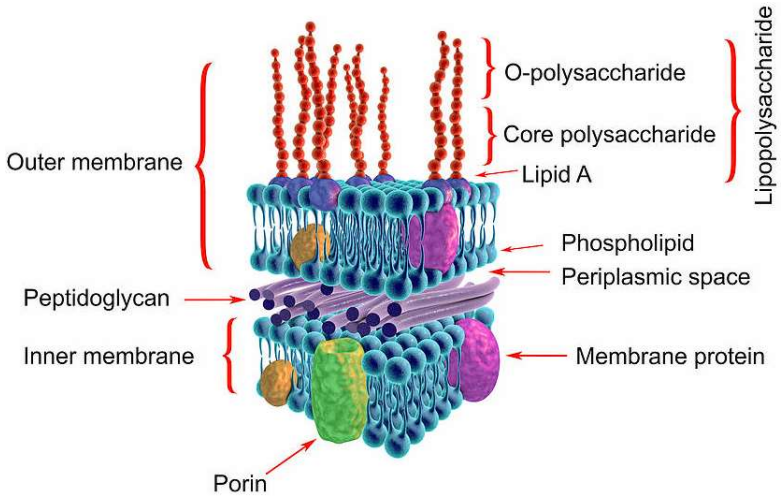


Figure 1.3: Gram-negative bacterial cell envelope. *The cell wall layers include both an outer and inner membrane, containing transmembrane proteins (green, yellow, and purple). The membranes are separated by a thin peptidoglycan layer. The outer surface is usually a LPS layer with lipids (purple) in the membrane, and long saccharide side chains (red) extending out (Available from: Avopix.com; Free photos on Avopix are released free of copyrights under Creative Commons CC0 (public domain)).*

The LPS molecule is composed of three main regions: lipid A, a core oligosaccharide, and an O-antigen polysaccharide chain (Fig. 1.4). Lipid A anchors the LPS to the outer membrane and is responsible for its endotoxic effects, which can trigger severe inflammatory responses in the host (Galgano *et al.,* 2022). It consists of highly acylated β-1′-6-linked glucosamine disaccharides that can also be phosphorylated as seen in *E. coli* (Galgano *et al.,* 2022). The core oligosaccharide links lipid A to the O-antigen and provides additional structural stability. The consists mostly of hexoses, heptoses, and/or octoses which can be modified by coupling with phosphates or other groups like phosphoethanolamine. The O-antigen polysaccharide chain, extending from the core, varies greatly among different bacterial strains and contributes to the antigenic diversity of Gram-negative bacteria (Galgano *et al.,* 2022). The O-antigen is the most variable part of LPS and is typically composed of repeating oligosaccharides of up to eight sugars in linear or branched structures. In *E. coli*, N-acetylglucosamine-phosphate mannose, rhamnose, and galactose are the sugars commonly found in the O-antigen oligosaccharide (Galgano *et al.,* 2022).

LPS acts as a formidable barrier to many antibiotics. The hydrophobic nature of lipid A and the large size and complexity of the O-antigen chain impede the diffusion of antibiotics through the outer

© University of Pretoria

membrane (Snyder *et al.,* 1999; Wang *et al.,* 2021; Saxena *et al.*, 2023). This barrier significantly reduces the effectiveness of antibiotics that target intracellular components or bacterial metabolism, such as β-lactams.

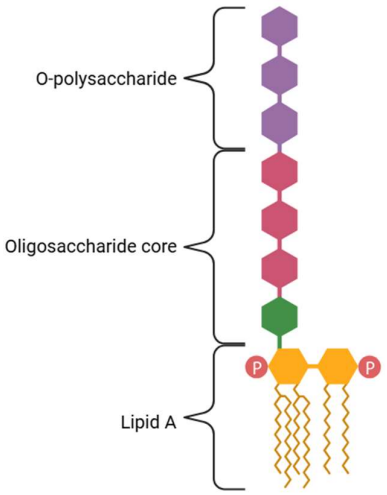


Figure 1.4: The structure of LPS. *LPS is a complex Gram-negative membrane molecule consisting of lipids and carbohydrates. The lipid A component (yellow) is situated in the outer membrane and interacts with TLR4 through phosphate groups and acyl chains. The central core consists of oligosaccharides of hexoses, heptoses, or octoses (pink and green) that connect lipid A to the O-polysaccharide. The O-polysaccharide is composed of repeating polysaccharide units such as mannose, galactose, and rhamnose (purple) and serves as a shield to prevent antibody recognition. (Image adapted under CC-BY 4.0 license from Galgano et al., 2022 using Biorender.com).*

β-lactams e.g., penicillins and cephalosporins, are often hindered by the LPS layer because their mechanism of action includes binding to penicillin-binding proteins within the periplasmic space (Bertani *et al.*, 2018). The impermeability of the outer membrane reduces the access of these antibiotics to PBPs, limiting their efficacy.

The LPS layer also exhibits selective permeability, regulating the entry of small molecules through the outer membrane (Saxena *et al.*, 2023). This selectivity is managed by outer membrane proteins, including porins, that form channels allowing certain molecules to pass while restricting others (Saxena *et al.*, 2023). Porins are crucial for facilitating the transport of nutrients and small molecules across the outer membrane, but they also influence antibiotic susceptibility by controlling the access of antibiotics to their intracellular targets.

This selective permeability can significantly impede the entry of antibiotics that rely on passive diffusion or active transport mechanisms to cross the outer membrane. For example, aminoglycosides such as gentamicin and streptomycin depend on specific transport systems to penetrate the outer membrane and reach their ribosomal targets. The selective LPS containing layer, combined with the restricted porin channels, reduces the uptake of these antibiotics, thereby diminishing their effectiveness against Gram-negative bacteria (Saxena *et al.*, 2023).

Beneath the outer membrane lies a thin peptidoglycan layer, a heteropolymer of alternating (β1 →4) linked *N*-acetyl glucosamine and *N*-acetylmuramic acid residues aiding structural rigidity (Fig. 1.3).

© University of Pretoria

This layer is relatively sparse in Gram-negative bacteria when compared with Gram-positive bacteria and consequently Gram-negative bacteria are inherently less susceptible to certain antibiotics that target cell wall synthesis (Typas *et al.*, 2016). Finally, the inner membrane composed of phospholipids and proteins harbours essential cellular machinery for various cellular functions including nutrient transport, energy production and biosynthesis (Silhavy *et al.*, 2010).

While the bacterial cell envelope provides a protective barrier against antibiotic treatment, it is a distinctive structural feature that is absent in mammalian cells, making it an attractive target for drug discovery. Many antimicrobial peptides (AMPs) exert their antimicrobial effects by targeting and disrupting bacterial membranes. This membrane-targeting mechanism positions AMPs as valuable lead compounds in the development of new treatments for Gram-negative bacterial infections. Their ability to penetrate and disrupt the bacterial cell envelope provides a promising avenue for designing effective antimicrobial agents specifically aimed at overcoming the defences of Gram-negative pathogens.

1.4 Antimicrobial peptides as potential next generation antibiotics

Also known as host defence peptides, AMPs, comprise of 5 to 100 amino acids and usually contain positively charged residues such as Lys and Arg with hydrophobic regions, making them amphipathic (Epand & Vogel, 1999). Their secondary structure varies greatly and can be α-helical, β-stranded, looped, extended, cyclic configurations or combinations of these structures, among others (Fig. 1.5) (Epand & Vogel, 1999; Lei *et al.,* 2019). In solution, AMPs are generally unstructured and only fold into their final conformation upon interacting with membranes (Ramazi *et al.,* 2022).

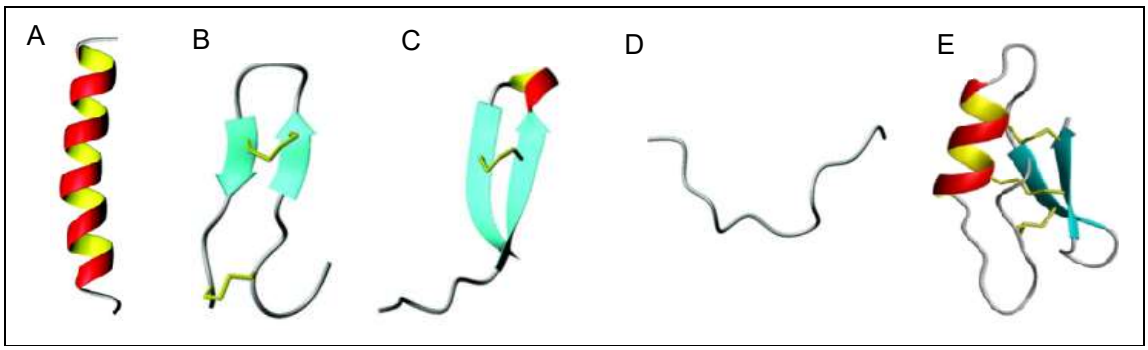


Figure 1.5: Five common structural classes of AMPs. *(A) α-helical structure, (B) β-pleated sheet, (C) looped (D) extended structure and (E) mixed structure (Modified from: Biljana & Havard, 2015, used under CC-BY-NC 2.0 license).*

1.4.1 AMP targets and mechanisms of action

Due to their membrane-targeting properties, AMPs exhibit broad-spectrum activity against various infections, including bacterial, viral, fungal, and parasitic pathogens, as well as certain cancers (Zasloff, 1987; Huan *et al.,* 2020; Table 1.1). In addition to their membrane interactions, a range of intracellular

© University of Pretoria

mechanisms of action have also been identified. Importantly, many AMPs can target different pathways or cellular components simultaneously, leading to synergistic effects that enable rapid microbial killing at low dosages, thus reducing the probability of resistance development (Flamm *et al.,* 2015).

***Table 1.1**: Various AMPs, their targets and mechanism of action.*

AMP	Target	Mechanism	Reference
Cecropins	Bacteria	Disrupts bacterial membrane integrity	Wang *et al.,* 2016
BMAP-12	Viruses	Destruction of viral RNA	Miao *et al.,* 2018
Rabbit defensin: NP-2	Fungi	Membrane permeabilisation	Yeung *et al.,* 2011
SMAP-29	Parasites	Local membrane permeabilisation	McGwire *et al.,* 2003
Temporin-1Cea	Cancer	Targets phosphatidylserine in membranes of cancer cells	Wang *et al.,* 2016

In addition to having multiple targets, AMPs are also multifunctional. They can directly kill pathogens via targeting the membrane or inhibiting intracellular functions and/or indirectly kill pathogens by modulating the immune response (Fig. 1.6).

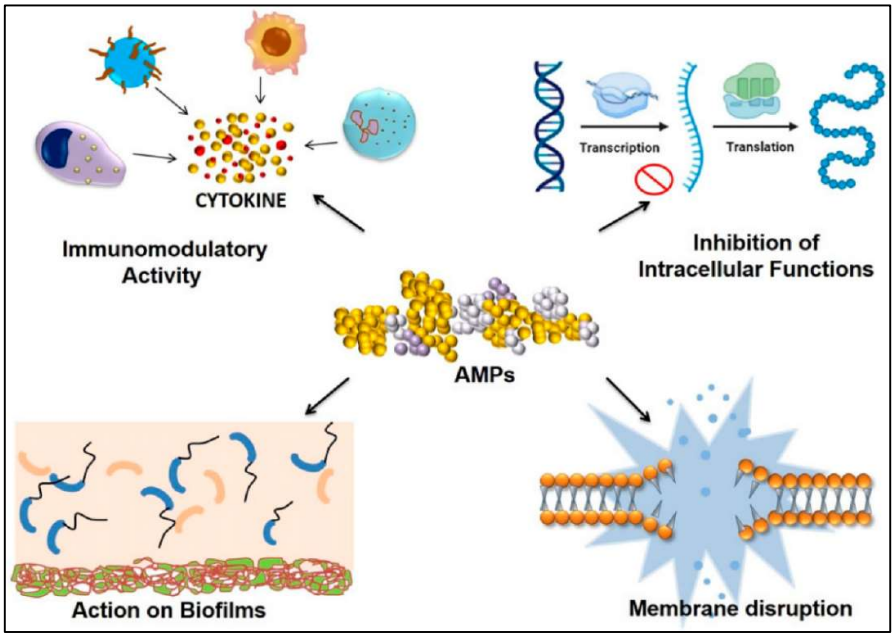


***Figure 1.6: Mechanisms of action of AMPs.** AMPs have direct mechanisms of action such as the inhibition of intracellular function of cells, direct killing of pathogens by disrupting the membrane, or targeting biofilms produced by bacteria or/and indirect mechanisms of action such as regulating the immune system (Saha et al., 2024, used under CC-BY 4.0 license).*

1.4.1.1 Direct bacterial cell membrane targeting

Although anionic AMPs exist, most research focuses on cationic AMPs because of their ability to electrostatically interact with microbial membranes (Epand & Vogel, 1999; Huan *et al.,* 2020). As described earlier, the Gram-negative cell wall consists of three distinct layers; the outer membrane,

© University of Pretoria

a thin peptidoglycan layer and an inner cytoplasmic membrane (Fig. 1.3). The first anionic target an AMP will encounter is LPS on the outer membrane of Gram-negative bacteria. Although LPS typically acts as a barrier to antibiotics due to its complex structure, it is an ideal target for certain AMPs (Pulido *et al.* 2012). AMPs, which are positively charged and often hydrophobic, can interact with LPS by binding to the negatively charged phosphate groups and lipid components. Notable examples of AMPs that target and neutralise LPS include cathelicidins and cecropins (Golec, 2007; Lin *et al.,* 2008; Van Moll *et al.,* 2023). The interaction between AMPs and LPS results in increased membrane permeability, which can cause leakage of cellular contents leading to bacterial cell death. By binding to LPS, AMPs can also neutralise the toxic effects of endotoxins, reducing harmful immune responses or systemic inflammation (Pulido *et al.* 2012).

However, not all AMPs have the ability to bind LPS. The primary mechanism of action for most AMPs involves permeabilising the cytoplasmic membrane through their affinity for negatively charged phospholipids. The cytoplasmic membrane of microorganisms such as bacteria are enriched with acidic phospholipids like phosphatidylglycerol on the outer leaflet (Fig. 1.7 A), giving the cell an overall negative charge at physiological pH (Deschamps *et al.,* 2019, Strahl & Errington, 2017). The quantity of each lipid class has been shown to differ in different growth medias (Deschamps *et al.,* 2021).

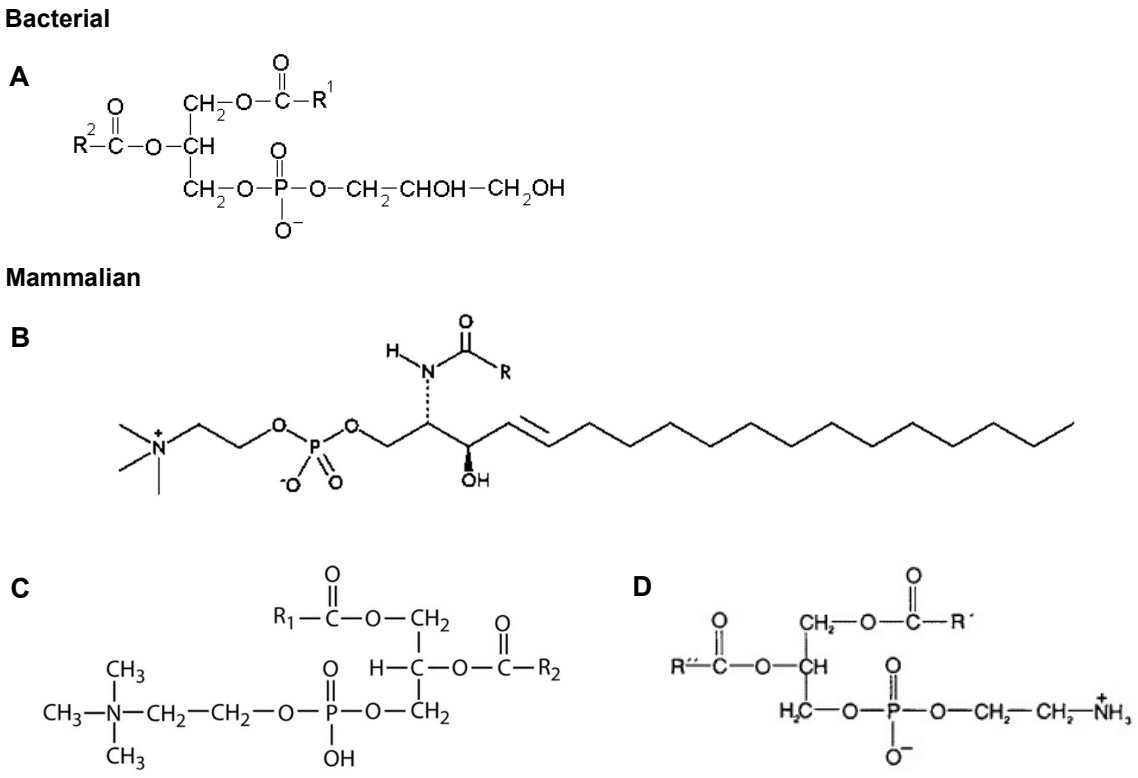


Figure 1.7: Phospholipids found in Gram-negative and mammalian cytoplasmic membranes. *The negatively charged (A) phosphatidylglycerol is more commonly found in bacterial cell membranes whereas the zwitterionic (B) sphingomyelin, (C) phosphatidylcholine and (D) phosphatidylethanolamine are more abundantly found in mammalian cell membranes (Modified from Lodish et al., 2008 under CC-BY 4.0 license).*

© University of Pretoria

In contrast, mammalian plasma membranes typically feature anionic phospholipids in their inner leaflets and zwitterionic lipids such as sphingomyelin, phosphatidylcholine, and phosphatidylethanolamine on their outer leaflets, rendering their surface more neutral (Fig. 1.7 B-D) (Strahl & Errington, 2017). Thus, cationic peptides will selectively bind the more anionic cytoplasmic membranes of microorganisms like bacteria at physiological pH, rather than neutral mammalian membranes and this selectivity is an important feature that is considered in the development of AMPs for therapeutic purposes (Fig. 1.8).

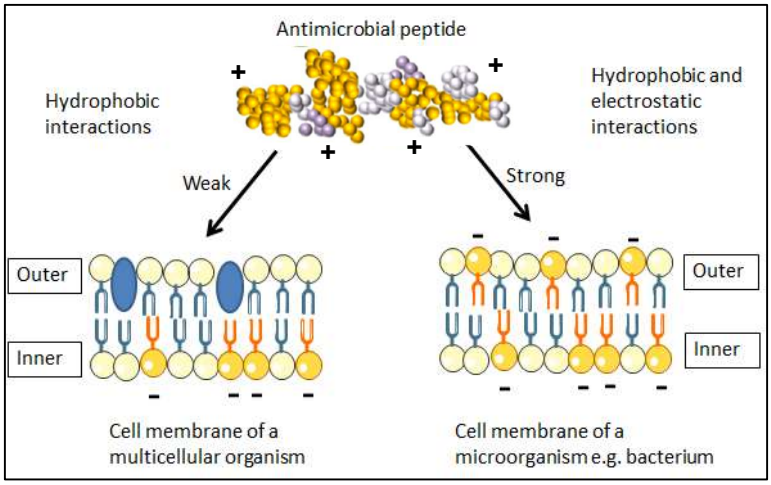


Figure 1.8: AMPs and their cytoplasmic membrane binding specificity*. The cell membrane of a multicellular organism versus that of simpler organisms and the AMP specificity toward these membranes. The outer leaflet of the plasma membrane of the bacterium is much more anionic than that of the multicellular organism, making it a target for AMP binding (Modified from: Molecular basis for membrane discrimination by antimicrobial peptides (Parchebafi et al., 2022, used under CC-BY 4.0 license).*

The interaction of AMPs with pathogen cell membranes is traditionally described by the carpet, barrel-stave, toroidal pore, and aggregated models (Fig. 1.9). In the carpet model, AMPs aggregate on the cell surface until a critical concentration is reached that leads to detergent-like micelle formation resulting in an irreversible loss of membrane integrity and leakage of cellular contents (Gazit *et al.,* 1996; Gera *et al.,* 2022). For the barrel-stave model, AMPs first bind to the surface of the bacterial membrane and following aggregation their hydrophobic regions are inserted into the lipid bilayer, forming a transmembrane channel (He *et al.,* 1996). The hydrophilic regions of the peptides line the inner pore of the channel, allowing the passage of ions and other small molecules. This structure resembles a barrel with the peptides forming the staves and the lipid bilayer forming the barrel wall. In the toroidal-pore model, AMPs interact with the bacterial membrane and induce local curvature (Sengupta *et al.,* 2008). This curvature involves both the lipid bilayer and the peptides themselves. AMPs disrupt the lipid packing by binding to the membrane surface and inserting perpendicularly to form a continuous pore structure where both the peptide and lipid components contribute to the pore lining. Insertion of peptides into the membrane occurs via a specific arrangement to form pores with a uniform size. This model often involves peptides that prefer binding to negatively charged lipids, common in bacterial membranes. Lastly, in the disordered toroidal-pore

© University of Pretoria

model, also known as the aggregate model, AMPs insert perpendicularly into the membrane bilayer in a non-specific arrangement, resulting pores that differ in size and lifetime (Hancock *et al.,* 2002). Peptides aggregate in a way that sequesters membrane lipids, leading to disruption of lipid bilayer integrity (Fig. 1.9). When these aggregates collapse, the peptides can translocate into the cell cytoplasm. This process can destabilise the membrane and lead to leakage of cellular components.

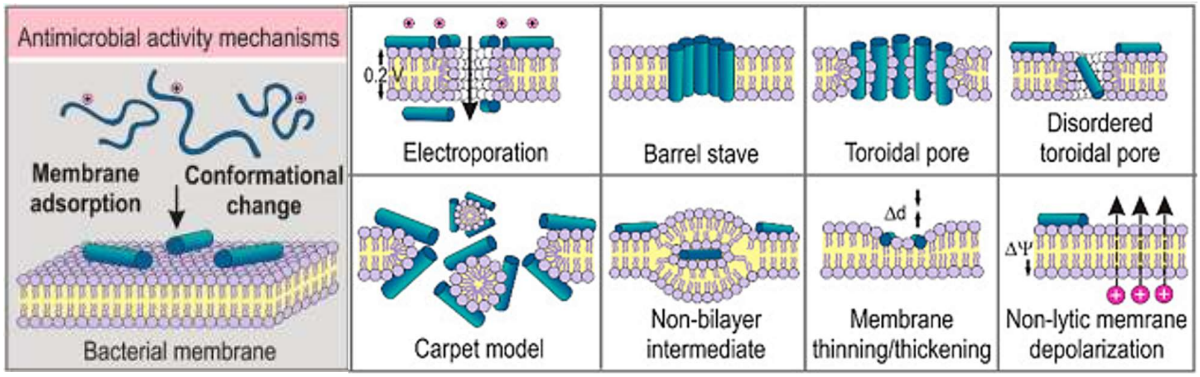


Figure 1.9: Models of AMP action on microbial cell membranes. *Microbial cell membranes are shown as yellow fatty acid bilayers with purple phosphate head groups and active peptides in blue. (Modified from: Gera et al., 2022, used under CC-BY 4.0 license).*

More recently, additional models and variations on existing models have been proposed which include the molecular electroporation, non-lytic depolarisation, membrane thinning via the sinking raft and dynamic peptide-lipid interaction models (Fig. 1.9). The molecular electroporation model describes a mechanism by which cationic AMPs interact with the negatively charged components of bacterial membranes, such as LPS or phospholipid headgroups, and alter the electrical potential of the membrane. When the local electric potential difference reaches a critical threshold, it triggers a series of events leading to the formation of transient pores in the membrane (Nayab *et al.,* 2022). The process of electroporation involves the disruption of lipid packing and bilayer integrity due to the electrostatic interactions and local electric field induced by AMPs.

In the membrane thinning sinking raft model, AMPs form clusters or rafts on the bacterial membrane surface (Fig. 1.9). These clusters then sink into the membrane, disrupting lipid packing and inducing membrane curvature. This process can lead to the formation of transient pores or structural changes that compromise membrane integrity (Nayab *et al.,* 2022), allowing the passage of ions, small molecules, and water across the membrane, disrupting cellular homeostasis and eventually leading to bacterial cell death.

Lastly, the dynamic peptide-lipid interaction model emphasises the dynamic nature of peptide-membrane interactions. It suggests that AMPs can switch between different modes of membrane interaction depending on the peptide concentration, lipid composition, and environmental conditions (Pirtskhalava *et al.,* 2021). For example, peptides may initially interact with the membrane in a carpet-like manner but then transition to forming pores or inducing membrane curvature.

© University of Pretoria

It is proposed that the development of resistance against membrane-active AMPs is less likely than against conventional antibiotics, as AMPs do not target a specific molecule such as an enzyme but rather interact with a broader range of cellular components, including the cell membrane. As a result, overcoming the antibacterial effects of AMPs would require a significant and widespread rearrangement of the entire cell membrane, which is a more complex and challenging adaptation compared to the targeted resistance mechanisms developed against traditional antibiotics.

However, resistance has been observed against some AMPs, such as polymyxin B, by modifications in the lipid A component of LPS in Gram-negative bacteria, leading to reduced binding affinity of the peptide to the bacterial membrane (Schaenzer & Wright, 2020). Additionally, certain bacterial strains have shown upregulation of efflux pumps that can actively expel AMPs (Moravej *et al.,* 2018). This demonstrates that while the emergence of resistance may be less common, it is not entirely absent.

1.4.1.2 Direct intracellular targeting

Although most AMPs are membrane acting, many studies have demonstrated that some AMPs are able to exploit intracellular targets as a primary or supportive mechanism of killing. Examples of intracellular mechanisms of action are presented in Table 1.2 and include the inhibition of nucleic acid synthesis, protein synthesis, enzyme activity and cell wall synthesis. Additional activities include the production of reactive oxygen species (ROS), initiation of apoptosis, mitochondrial dysfunction and degradation of vacuoles (Lei *et al.,* 2019).

Table 1.2: *Mechanisms of action of intracellular targeting AMPs*

AMP	Intracellular mechanism	Reference
Lactoferrin	Degrades DNA, increases ROS production	Andres *et al.,* 2008
Indolicidin	Inhibits DNA topoisomerase	Le *et al.,* 2017
Sordarin	Inhibitor of elongation factor – 2 during fungal protein synthesis	Dominguez *et al.,* 1998
Histatin 5	Induces oxidative stress and mitochondria malfunction	Puri & Edgerton, 2014
Microcin J25	Inhibits RNA polymerase	Le *et al.,* 2017
hGAPDH	Initiates apoptosis and inhibits proteases	Wagener *et al.,* 2013
Buforin II	Interrupts DNA and RNA synthesis	Park *et al.,* 1998

1.4.1.3 Direct biofilm targeting

In addition to their planktonic antimicrobial functions, some AMPs have direct antibiofilm activities (Luo & Song, 2021). Biofilms are complex, structured communities of microorganisms that adhere to surfaces and are encased in a self-produced extracellular matrix (Ramanathan *et al.,* 2021) (Fig. 1.10). The matrix is composed of polysaccharides, proteins, and nucleic acids, which provide structural stability and protection to the embedded cells. It acts as a physical barrier that can limit the penetration of antimicrobial agents. This makes it difficult for antimicrobials to reach bacteria protected within the biofilm, at effective concentrations (Ramanathan *et al.,* 2021).

© University of Pretoria

Bacteria within biofilms also often exhibit altered metabolic activity compared with their planktonic counterparts (Ramanathan *et al.,* 2021). This can include a slower growth rate, which makes them less susceptible to antimicrobials that target actively dividing cells and less visible to immune responses.

Biofilms can form on a wide range of surfaces, both biotic such as tissues in the human body and abiotic such as medical devices and industrial equipment (Ramanathan *et al.,* 2021). The ability of AMPs to interact with and disrupt these biofilms presents a promising avenue for both preventing and treating biofilm-associated infections. Studies have demonstrated that certain AMPs possess the ability to inhibit biofilm formation or to eradicate established biofilms (Luo & Song, 2021). AMPs with biofilm inhibitory properties can interfere with the initial adhesion or attachment of bacteria to surfaces (Fig. 1.10). This inhibitory activity is crucial for applications in various settings where biofilm formation can lead to persistent infections or contamination (Luo & Song, 2021).

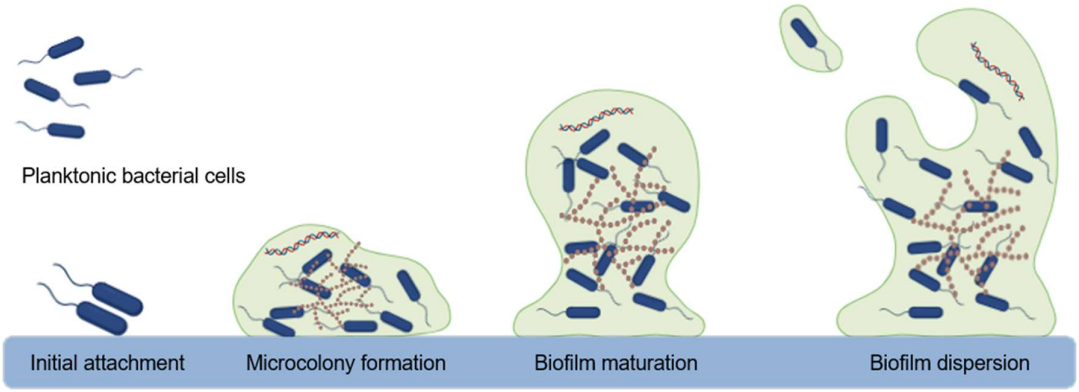


Figure 1.10: Bacterial biofilm formation. *Biofilm formation involves four stages, and these are the initial attachment of the planktonic cells, then microcolony formation followed by biofilm maturation and dispersion. (Image adapted under CC-BY 4.0 license from: Ramanathan et al. (2021) using Biorender.com.*

This characteristic makes AMPs valuable for coating medical devices, such as catheters, implants, and prosthetics, as well as for use on hospital equipment and other surfaces where biofilm formation poses a risk. By preventing the initial stages of biofilm development, AMPs help in reducing the likelihood of chronic infections and device-related complications. AMPs like LL-37 and HNP-1 have shown promise in biofilm prevention by interfering with bacterial adhesion and biofilm matrix production (Luo & Song, 2021; Moazzezy *et al.*, 2020).

Other AMPs exhibit the capability to disrupt and dismantle mature biofilms (Fig. 1.10, biofilm maturation). These AMPs can penetrate the biofilm matrix and target the bacteria within, leading to the breakdown of the biofilm structure and the elimination of bacterial cells (Luo & Song, 2021). This property is particularly useful for treating established biofilm-associated infections, such as those in chronic wounds or in cases where biofilms have formed on medical devices. Peptides such as bovine lactoferricin and temporal defensins have demonstrated the ability to disrupt mature biofilms and kill associated bacteria (Ulvatne *et al.*, 2004; Luo & Song, 2021). These AMPs are being explored for their potential use in treating chronic infections.

© University of Pretoria

1.4.1.4 Indirect action via immune modulation

An indirect mechanism of action exhibited by some AMPs is their ability to modulate the immune system. This immunomodulatory effect can serve as a primary mechanism of action or complement the direct mechanisms employed by peptides that target cell membranes or intracellular components. By enhancing the immune response, AMPs can activate and recruit crucial immune cells, such as macrophages, platelets, monocytes, lymphocytes, and polymorphonuclear leukocytes, to the site of infection leading to improved pathogen clearance (Jenssen & Hancock, 2010).

AMPs can also play a significant role in regulating inflammation by balancing pro-inflammatory and anti-inflammatory signals. For example, AMPs like TCP25 or CAMP have been shown to bind to LPS, reduce the availability thereof and mitigate excessive inflammatory responses that can disrupt healing (Bartlett *et al.,* 2004, Puthia *et al.*, 2020). Additionally, certain AMPs, such as LL-37 and human defensins, modulate ROS levels (Oyinloye *et al.,* 2015). While ROS are important for pathogen destruction, the overproduction thereof can lead to oxidative stress, hindering healing (Oyinloye *et al.,* 2015). By maintaining a favourable oxidative environment, AMPs support cellular health and the proper functioning of immune cells.

Moreover, some AMPs such as human defensins contribute to immune regulation by enhancing the expression of antigens on antigen-presenting cells (APCs) (Fruitwala *et al.,* 2019). This facilitates a more robust adaptive immune response critical for long-term immunity. Other AMPs, such as CaTx- II or β-defensins can directly interact with signalling pathways involved in immune responses, such as activating NF-κB, which is essential for the transcription of various pro-inflammatory genes (Samy *et al.*, 2014).

This multifunctional nature of AMPs makes them particularly well-suited for the treatment of chronic wound infections, where persistent inflammation hinders healing. The diverse roles of AMPs allow enhanced antimicrobial therapy through broad-spectrum activity, which is crucial in wounds that often harbour multiple pathogens and at the same time facilitate wound healing and recovery through their immune-modulating effects.

Wound healing is an intricate process that involves various structural and immune cells. The coordinated secretion of chemokines, cytokines, and growth factors orchestrates the four distinct phases of wound healing: haemostasis, inflammation, proliferation, and maturation or tissue remodelling (Raziyeva *et al.*, 2021) (Fig. 1.11). Each of these phases must function effectively to ensure proper healing. However, when this organised process is disrupted, such as in cases of antimicrobial-resistant infections, tissue healing is delayed, ultimately resulting in chronic wounds (Raziyeva *et al.*, 2021). Common characteristics of non-healing wounds include excessive exudation, recurring infections, tissue necrosis, impaired re-epithelialisation, reduced angiogenesis, and an overabundance of ROS (Raziyeva *et al.*, 2021).

© University of Pretoria

Given their multifunctional properties, AMPs are increasingly explored as novel therapies for promoting wound healing. Some AMPs, such as LL-37 and defensins, initiate the first phase of wound healing by stimulating the secretion of chemokines and cytokines that recruit and activate immune cells (Gera *et al.,* 2022). Other AMPs can influence the differentiation of immune cells. For instance, peptides like cathelicidins may promote the polarisation of macrophages toward a pro-inflammatory phenotype (M1) initially to combat pathogens (Raziyeva *et al.*, 2021). This M1 phenotype is characterised by the production of inflammatory cytokines and the activation of various immune mechanisms aimed at eradicating invading pathogens. Following this initial response, a transition to an anti-inflammatory phenotype (M2) occurs, which supports tissue repair and regeneration (Raziyeva *et al.*, 2021).

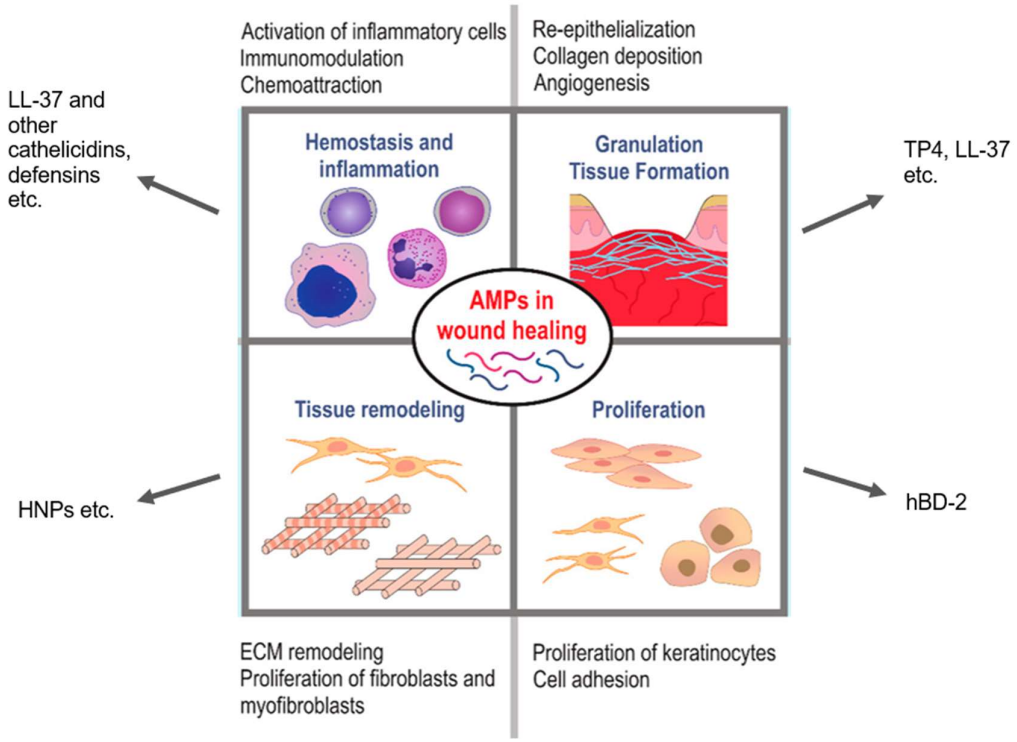


Figure 1.11: The various stages of wound healing and examples of AMPs involved. *(1) The first stage is haemostasis and inflammation, supported by AMPs such as cathelicidins and defensins. (2) The second stage, angiogenesis and re-epithelialisation, is facilitated by AMPs like TP4 and LL-37. (3) The third stage involves tissue remodelling, aided by AMPs such as human neutrophil peptides (HNPs). (4) The final stage is the proliferation of keratinocytes, which is promoted by AMPs like human beta-defensin 2 (hBD-2). (Image adapted from: Gera et al., 2022, used under CC-BY 4.0 license).*

In the second phase of wound healing, several AMPs have demonstrated the ability to stimulate angiogenesis, the formation of new blood vessels, that is critical for the supply of nutrients and oxygen to healing tissues (Schuerholz *et al.*, 2012; Biragyn, A., 2005; Mader & Hoskins, 2006; Malan *et al.,* 2016). For example, AMPs like Tilapia Piscidin 4 (TP4) have been shown to enhance endothelial cell proliferation and migration, key processes in angiogenesis (Huang *et al.,* 2015).

© University of Pretoria

During the third phase, certain AMPs can modulate the expression of key enzymes involved in tissue remodelling. For instance, the activity of matrix metalloproteinases (MMPs) may be influenced, which play a critical role in breaking down extracellular matrix components during tissue restoration (Raziyeva *et al.*, 2021). The regulation of MMP expression by AMPs is vital because while MMPs are necessary for normal tissue remodelling, their excessive activity can lead to degradation of the newly formed tissue, hindering the healing process (Raziyeva *et al.*, 2021). By striking a balance in MMP activity, AMPs help facilitate proper wound healing and maintain tissue integrity. Examples of AMPs that have shown such regulatory functions include human neutrophil peptides (HNPs) and certain defensins (Musrati *et al.,* 2016).

Finally, in the fourth phase of wound healing, AMPs such as human beta-defensin 2 (hBD-2) has been shown to enhance the migration and proliferation of keratinocytes, the primary cells involved in re-epithelialisation (Gera *et al.,* 2022). This activity is crucial for closing the wound and restoring the protective barrier of the skin. The interplay of these AMPs throughout the various phases of wound healing highlights their multifaceted roles in not only combating infection but also fostering an environment conducive to effective tissue repair.

1.4.2 AMPs in clinical trials

Although AMPs present promising advantages in treating infections and enhancing wound healing, they also have a few limitations for clinical use. Under certain physiological conditions, AMPs may exhibit reduced antimicrobial activity. High salt concentrations, for example, can interfere with the binding of some AMPs to bacterial membranes (Kerenga *et al.*, 2019). Additionally, AMPs often bind preferentially to anionic proteins present in serum, saliva, or sputum, which can prevent them from effectively targeting bacterial membranes (Shao *et al.,* 2019). These peptides are also vulnerable to endogenous proteinases (Shao *et al.,* 2019) which further limits their effectiveness and often confines their use to topical applications. Moreover, issues related to tissue toxicity and allergenicity must be carefully considered. Fosgerau & Hoffmann (2015) conducted a SWOT (strengths, weaknesses, opportunities and threats) analysis to show the various advantages and limitations of using peptides as therapeutics. This was adapted in Fig. 1.12 to show the characteristics of AMPs specifically.

Despite the potential weaknesses and threats, results from preclinical studies showed that AMPs that target Gram-negative bacteria could be applied in the prevention and treatment of numerous conditions. For example, the coating of catheters with a novel peptide E6 prevented catheter associated infections in murine models (Yu *et al.*, 2017). PXL150 showed potency against *P. aeruginosa* infected burn wounds in murine models (Björn *et al.*, 2015). Peptides LL-37 and IDR-1 strengthened respiratory function in mice suffering with pneumonia (Hou *et al.*, 2013).

© University of Pretoria

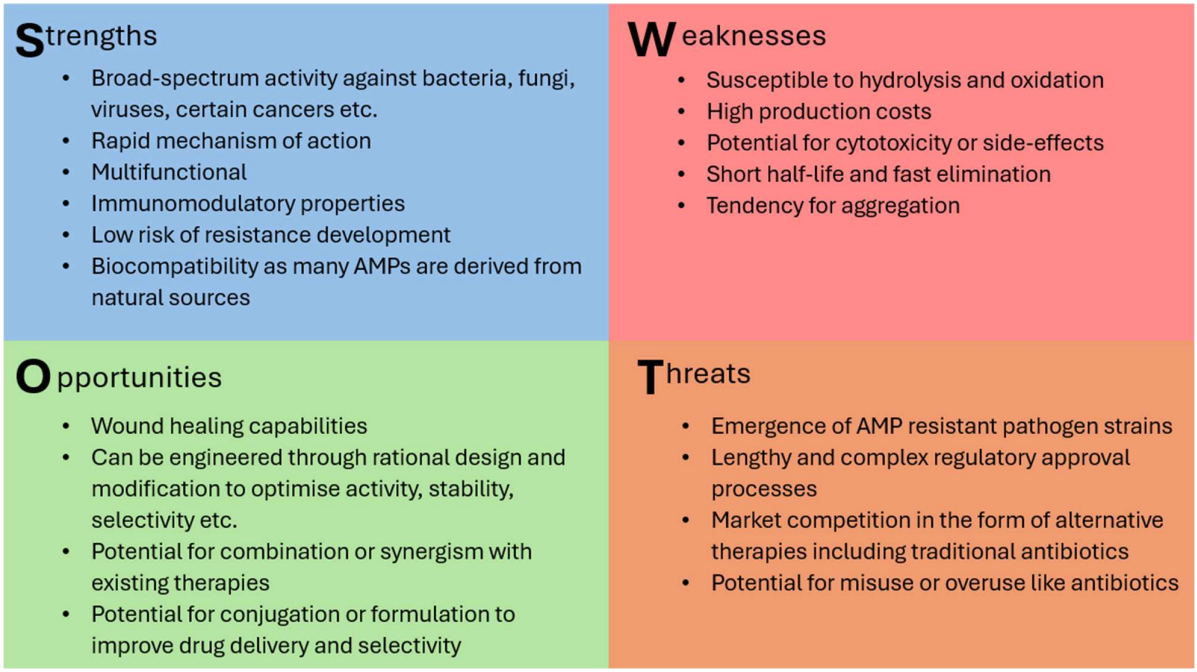


Figure 1.12: SWOT analysis of the strengths, weaknesses, opportunities and threats of AMPs as potential therapeutics. *Adapted from Fosgerau & Hoffmann (2015).*

Furthermore, several AMPs including LL-37 displayed *in vivo* antibiofilm activity (Segev-Zarko *et al.*, 2015, Batoni *et al.,* 2016). Based on successful preclinical studies, numerous AMPs are being investigated in human clinical trials to demonstrate efficacy and safety (Table 1.3).

Table 1.3: Bacterial targets, mode of administration, and structural characteristics of AMPs in different phases of clinical trials

AMP	Target	Administration	Phase	Clinical Trial ID	Length	Net charge	Reference
Friulimicin	MRSA/ pneumonia	Intravenous	I	NCT00492271	12	-2	Schneider *et al.*, 2009
LL-37	Leg ulcers	Topical	II	EUCTR2012-002100-41	37	+6	Gronberg *et al.*, 2021
Murepavadin	*P. aeruginosa K. pneomaniae*	Intravenous	II	EUCTR2017-003933-27-EE	14	+4	Srinivas *et al.*, 2010
Gramicidin S	Infected wounds	Topical	III	NCT00534391	16	+2	David & Rajasekaran, 2015
Polymyxin B	Gram-negative bacteria	Topical	III	NCTOO490477	10	+5	Rigatto *et al.*, 2019
Colistin (Polymyxin E)	*A. baumanniil* pneumonia	Intravenous	III	NCT01292031	10	+5	Yu *et al.*, 2015
Nisin	*Gram-positive bacteria*	Oral	III	NCT02928042	34	+4	Prince *et al.*, 2016
Daptomycin	Skin infections/ bacteraemia	Intravenous	III	NCT01922011	13	0	Taylor & Palmer, 2016

© University of Pretoria

Approved AMPs, include gramicidin S from *Bacillus brevis* (Swierstra *et al.*, 2016), nisin an AMP derived from *Lactococcus lactis* (Prince *et al.,* 2016), daptomycin from *Streptomyces roseosporus* (Taylor & Palmer, 2016) and colistin derived from *Paenibacillus* bacteria (Falagas *et al.,* 2005). All of these are naturally occurring and bacterially produced peptides characterised by cyclic portions in their structures and are either gene encoded or non-ribosomally produced (Fig. 1.13).

Nonetheless, the number of AMPs, particularly those effective against Gram-negative bacteria, remains limited, with many still in early phase I and II clinical trials. As a result, there is a pressing need to design new AMPs that demonstrate superior efficacy compared with conventional antibiotics. These peptides should be fast-acting, exhibit minimal side effects, and maintain their activity in physiological environments relevant to oral, intravenous, and topical applications.

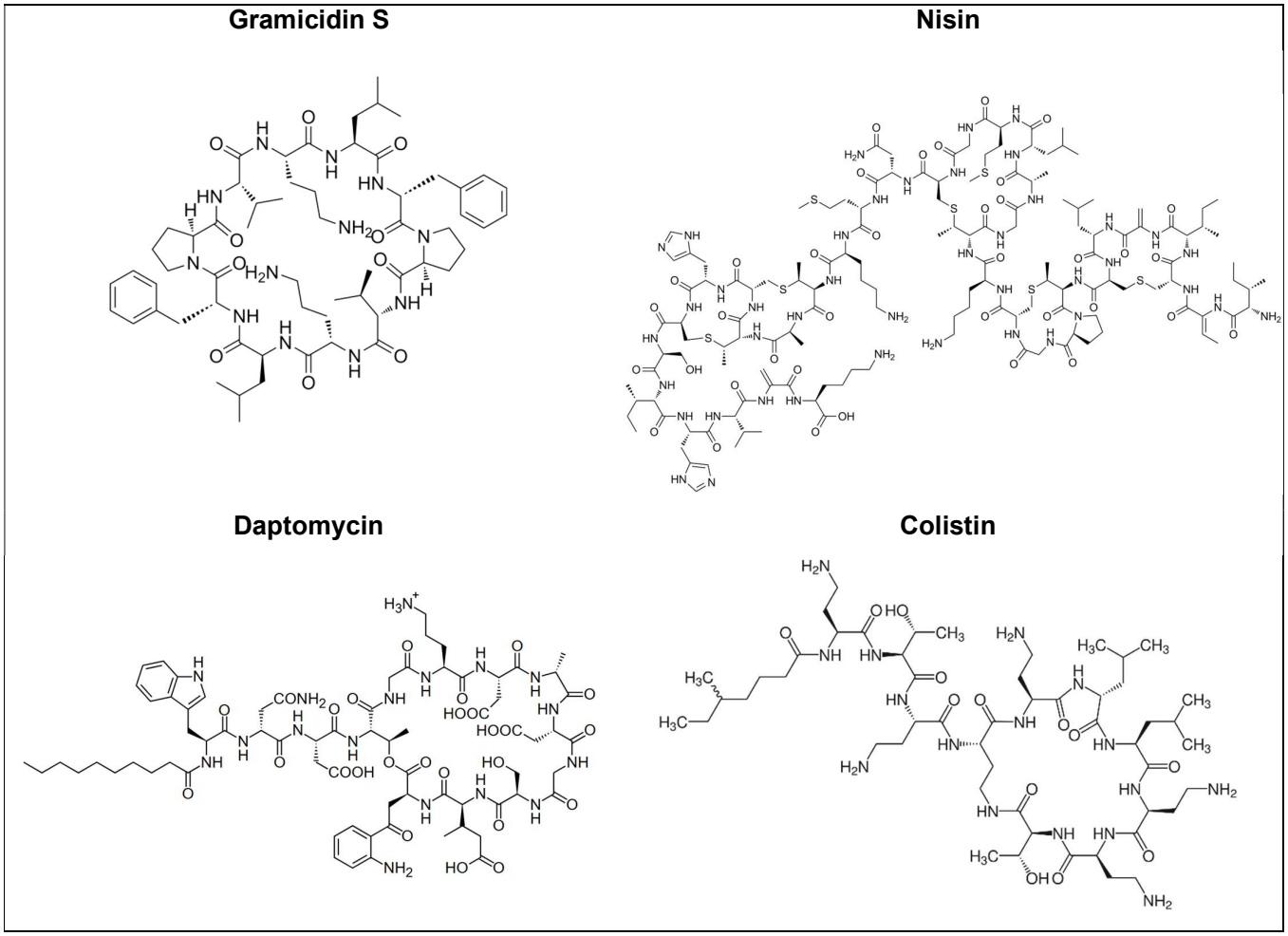


Figure 1.13: Chemical structures of clinically approved AMPs: gramicidin S, nisin, daptomycin, and colistin. *(Obtained free of copyrights).*

© University of Pretoria

1.5 Strategies to increase the therapeutic application of AMPs

To optimise AMPs for therapeutic application, it is crucial to understand how various physiological characteristics influence their performance. Recent advancements in structure-activity relationship research have led to the development of modification strategies aimed at overcoming some of the typical limitations of AMPs and enhancing their therapeutic potential. Antimicrobial activity and toxicity of AMPs are influenced by several physicochemical properties, including overall charge, hydrophobicity, amphipathicity, length, and other structural features.

A crucial determinant is the overall positive charge, which facilitates initial electrostatic binding of the AMP to the negatively charged microbial membrane, contrasting with the neutral membranes of eukaryotic cells (Fig. 1.8).

Therefore, a common modification strategy to enhance bacterial targeting and selectivity involves incorporating more positively charged amino acids such as Arg or Lys into the AMP sequence (Li *et al.*, 2013). This approach aims to increase electrostatic interactions with the negatively charged microbial membranes, thereby improving binding and disruption of bacterial cells, while minimising interactions with mammalian cells.

AMP hydrophobicity also significantly influences activity and toxicity. Greater hydrophobicity facilitates insertion into and disruption of cellular membranes, crucial for antimicrobial efficacy (Dathe & Wieprecht, 1999). However, heightened hydrophobicity is also correlated with increased haemolytic activity, highlighting the need to balance hydrophobicity (or lipophilicity) with charge to achieve optimal selectivity.

AMP activity also depends on chain length, however longer chains are usually accompanied by greater toxicity to mammalian cells (Van der Walt *et al.,* 2024). Consequently, shorter AMPs are preferred, as they can be synthesised more quickly and easily. Additionally, shorter peptides are easier to modify and optimise at a lower cost, and they are less likely to provoke unwanted immune responses (Carotenuto *et al.,* 2008; Bagheri *et al.,* 2016; Mikut *et al.,* 2016). This balance between efficacy and safety makes shorter AMPs a more practical choice in therapeutic applications.

Charge, hydrophobicity and length alone, do not account for the antimicrobial activity of AMPs, and increasingly there is a need to identify other contributing structural features to increase hit-to-lead discovery.

While modifying the properties of AMPs can enhance their activity and selectivity, it does not address the critical issue of peptide stability in physiological environments. AMPs face significant challenges *in vivo* when exposed to proteases present in serum, the digestive tract, or secreted by bacteria. In addition, AMPs are also sensitive to varying salt concentrations, pH levels and serum proteins (Shao *et al.,* 2019). Infected tissues, such as those in cystic fibrosis lungs, as well as topical areas like

© University of Pretoria

infected eyes or chronic wounds, often exhibit elevated proteolytic activity (Norstrom & Malmsten, 2017).

To address these stability issues and enhance the therapeutic potential of AMPs, various modification strategies can be implemented. These include cyclisation to resemble naturally occurring AMPs like gramicidin S and daptomycin (Fig. 1.13), the addition of hydrophobic side chains akin to those in daptomycin and colistin (Fig. 1.13), and the incorporation of unnatural or D-enantiomer amino acids, similar to gramicidin S (Fig. 1.13). Other effective strategies involve N- and C-terminal amidation and acetylation, the introduction of disulfide bonds, nitrogen alkylation, and specific amino acid substitutions (Akkam, Y. 2016; Pasupuleti *et al.,* 2012).

Proteolytic enzymes responsible for AMP degradation are broadly classified into two categories: exopeptidases, which cleave amide bonds at the N- or C-termini, and endopeptidases, which cleave bonds within the peptide molecule (Ceuleers *et al.* 2016). One particularly effective but modest strategy, which was incorporated in this study, involves C-terminal amidation. This modification offers several advantages, such as potential increased resistance to enzymatic exopeptidases and an increase in overall charge which is usually associated with enhanced antimicrobial activity and membrane interaction.

Peptide cyclisation also increases resistance to exopeptidases and entails creating a cyclic backbone that effectively constrains the termini of the peptide. This strategy limits the flexibility of AMPs while maintaining their charge, amphipathicity, and molecular volume (Andreev *et al.,* 2016). A prime example of this approach is daptomycin, a cyclic AMP that is clinically utilised for its potent antimicrobial activity (Table 1.3, Fig. 1.13). The cyclic structure of daptomycin not only facilitates its incorporation into microbial membranes but also enhances its resistance to terminal proteolysis, significantly boosting its antimicrobial activity.

The substitution of amino acids with unnatural amino acids, such as D-amino acids (Ong *et al.*, 2014), hexafluoroleucine (Meng & Kumar, 2007), α-amino-3-guanidino-propionic acid (Knappe *et al.*, 2010), α-aminoisobutyric acid (De Zotti *et al.*, 2011), (*S*)-2-amino-4-guanidinobutyric acid (Agb) or homo-Arg (hArg) (Arias *et al.,* 2018), and other chemically modified residues with varying cationicity and side chains, is also often undertaken. These unnatural amino acids are less likely to be recognised by proteases, thereby minimising proteolytic degradation when incorporated into AMP sequences. For instance, D-pleurocidin has demonstrated significant antimicrobial activity when administered intravenously, largely due to its enhanced resistance to proteolytic breakdown (Manzo *et al.,* 2020). Additionally, gramicidin S, which contains D-amino acids, has been clinically approved, showcasing the effectiveness of this modification in developing therapeutically viable AMPs.

© University of Pretoria

1.6 Modern technologies that accelerate AMP discovery, design and development

While significant progress has been made in overcoming AMP limitations, the transition from discovery to clinical application remains both time-consuming and often uncertain. To develop a novel AMP candidate, it is crucial to thoroughly understand its physicochemical properties, structural characteristics, biological activities and particularly its specific molecular targets. The peptide must also exhibit bioavailability, stability in human plasma, and demonstrate both high affinity and selectivity towards its intended pathogen target (Wang *et al.*, 2010). These properties can be experimentally validated for AMP prediction however, the *in vitro* experiments required to collect this data are usually laborious, time-consuming and expensive.

This is where modern technology becomes indispensable for enabling accurate AMP discovery and strategic rational design (Xu *et al.,* 2021). Advanced techniques like genome sequencing, nuclear magnetic resonance (NMR), machine learning, molecular modelling and other bioinformatic tools allow for swift and accurate identification, along with *in silico* screening of novel compounds, well before any resources are committed to production or *in vitro* screening (Terekhov *et al.,* 2018). These technologies streamline the initial phases of drug development, potentially accelerating the path of promising AMP candidates from research to clinical implementation.

1.6.1 AMP databases

Thousands of AMPs are now available in public databases including APD3 (Antimicrobial Peptide Database, http://aps.unmc.edu/AP/), CAMPR3 (Collection of Anti-Microbial Peptides, https://camp.bicnirrh.res.in/), DRAMP (Data Repository of Antimicrobial Peptides, http://dramp.cpu-bioinfor.org/) and Defensins Knowledgebase (http://defensins.bii.a-star.edu.sg/). The APD3, CAMPR3 and DRAMP databases are similar comprehensive repositories that catalogue a vast array of AMPs from various sources including natural organisms and synthetic designs. The databases provide detailed information on peptide sequences, structures, antimicrobial activities, and experimental data. This facilitates the exploration of AMP properties through interactive search tools and allows users to filter peptides based on specific criteria such as antimicrobial spectrum, target organism, and peptide length. Over the years, these databases evolved to incorporate advanced features like peptide modelling, structure prediction, and comparative analysis, making it invaluable resources for both experimentalists and computational biologists involved in AMP research.

The Defensins Knowledgebase focuses on a specific class of AMPs known as defensins that are widely distributed in plants, animals, and microorganisms. This database compiles information on defensin sequences, structures, genetic variations, and functional activities derived from experimental studies and genomic analyses. It supports comparative genomics and evolutionary

© University of Pretoria

studies to elucidate the diversity and evolutionary conservation of defensin peptides across species. The Defensins Knowledgebase also serves as a resource for exploring defensin interactions with microbial membranes, mechanisms of antimicrobial action, and potential applications in biotechnology and medicine.

Databases play a crucial role in computational prediction and discovery of active AMPs as researchers can query these databases to identify patterns, common motifs, and structural features associated with effective antimicrobial action. By leveraging these resources, researchers can efficiently identify promising candidates without the need to screen potentially inactive natural peptides. Moreover, these databases not only provide access to annotated sequences but also aid in the development of new algorithms and predictive models for AMP design.

1.6.2 Machine learning and AMP prediction

Machine learning techniques have revolutionised the prediction of active AMPs by leveraging computational algorithms to analyse large datasets. These algorithms can identify hidden patterns and relationships between sequence, structure, physicochemical properties, and antimicrobial activity of peptides (Fernandes *et al.,* 2023).

Supervised learning methods, such as Support Vector Machines (SVM), Random Forests, and Neural Networks, are commonly used to classify peptides based on training data from experimental assays (Fernandes *et al.,* 2023). These algorithms distinguish between active and inactive peptides, facilitating the identification of promising candidates for further study. Unsupervised learning techniques, like clustering and dimensionality reduction methods such as Principal Component Analysis (PCA) or Quantitative Structure Activity Relationship analysis (QSAR), help in exploring peptide properties and identifying novel AMP candidates.

PCA is a statistical technique that simplifies complex data sets by reducing the dimensionality while preserving essential information (Abdi & Williams, 2010). In AMP research, PCA can be applied to analyse large datasets of peptide sequences and multiple physicochemical properties, identifying dominant patterns and correlations that contribute to antimicrobial activity. By extracting principal components, researchers can uncover key features that differentiate active AMPs from inactive ones, facilitating the design and optimisation of new peptide candidates.

QSAR modelling is another powerful tool used in computational chemistry and pharmacology to predict the biological activity of molecules based on their structural and physicochemical properties (Roy *et al.,* 2015). In the context of AMPs, QSAR models help elucidate the relationships between peptide structure, physicochemical properties (such as hydrophobicity, charge, and secondary structure), and antimicrobial activity against specific pathogens. By quantifying these relationships, QSAR models provide insights into the design principles underlying effective AMPs, guiding rational design efforts and accelerating the discovery of novel antimicrobial therapies.

© University of Pretoria

Machine learning approaches to predict peptide structure also exist. AlphaFold, developed by DeepMind, has revolutionised protein structure prediction by employing deep learning to predict the 3D structures of proteins from their amino acid sequences with unprecedented accuracy (Jumper *et al.*, 2021). This advancement is particularly relevant for AMP research as it enables the prediction of how peptides fold into functional structures that interact with microbial membranes, thereby influencing their antimicrobial efficacy.

Integrating bioinformatics and computational biology with AMP research enhances accuracy and efficiency in predicting bioactive peptides. It can accelerate the discovery of novel AMPs and the optimisation of existing antimicrobial therapies.

1.6.3 Molecular simulation modelling

Molecular simulation modelling is a recent advancement in computational biology that allows an understanding of the interaction between AMPs and microbial membranes at the atomic level, all without the need for extensive experimental work (Irvine *et al.,* 2023). Techniques such as molecular dynamics (MD) simulations simulate the behaviour of peptides in a biological environment, providing insights into their structural dynamics, membrane insertion mechanisms, and stability. MD simulations can predict binding affinities, energetics of interaction, and potential modifications to enhance peptide efficacy and selectivity (La Rocca *et al.,* 1999; Mondal, J., 2019). One primary advantage of MD simulations is the ability to reduce costs associated with AMP discovery by minimising the need for laborious and resource-intensive experimental assays (Mondal, J., 2019).

These simulations have been successfully used to investigate the interactions of various AMPs with microbial membranes on a molecular level. One notable example is LL-37. Despite extensive experimental studies, the precise mechanism of action of LL-37 has remained elusive. MD simulations involving LL-37 in the presence of 1-palmitoyl-2-oleoyl-sn-glycero-3-phosphoglycerol (POPG), a bacterial membrane model, and 1-palmitoyl-2-oleoyl-sn-glycero-3-phosphocholine (POPC), a mammalian membrane model, provided valuable insights (Zhao *et al.,* 2018). The simulations demonstrated that LL-37 rapidly associates with the bacterial bilayer while maintaining its helical conformation in the core region, aligning parallel to the bilayer. Notably, this interaction resulted in a noticeable deformation of the bacterial membrane. In contrast, LL-37 exhibited slower kinetics when interacting with the POPC mammalian bilayer, leading to a significant loss of its helical structure. Furthermore, LL-37 only partially penetrated the POPC bilayer, with minimal deformation observed. The differing behaviours of LL-37 on the two bilayers can be largely attributed to the overall positive charge of the peptide, the negative charge of the POPG bilayer, and the neutral nature of the POPC bilayer (Zhao *et al.,* 2018).

© University of Pretoria

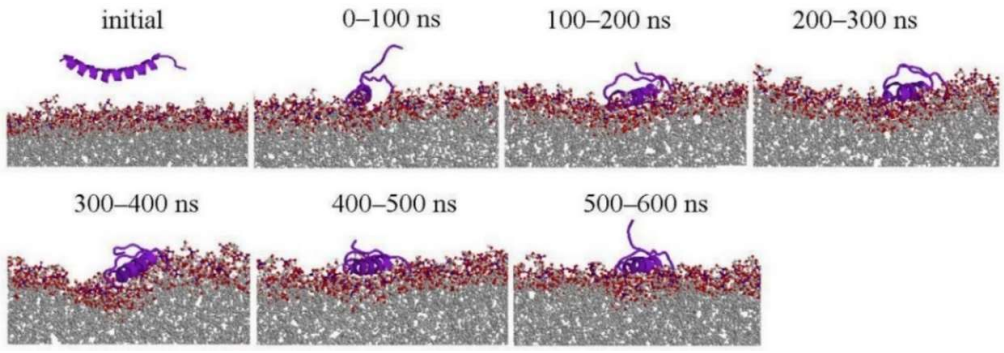


Figure 1.14: Example of an MD simulation showing the interaction of LL-37 with a model bacterial membrane over 600 ns. *This simulation demonstrates how the peptide interacts with and inserts into the membrane, how this affects the membrane structure and also how the conformation of LL-37 changes as it comes into close proximity with the membrane. (Obtained from: Zhao et al., 2018, under CC-BY 4.0 license).*

1.7 Screening of modified or rationally designed AMPs

Following *in silico* and computational design, AMPs with the highest potential can subsequently undergo screening through *in vitro*, *ex vivo*, and *in vivo* experiments. These experiments are designed to assess the potential efficacy of an AMP in various environments, progressively resembling topical or systemic applications with each screen.

1.7.1 In vitro, cell-based screening models

In vitro screening methods play a crucial role in evaluating the antimicrobial activity, stability, and safety profile of AMPs before advancing promising candidates to more complex biological systems (Fig. 1.15). One of the most popular methods to screen for antimicrobial activity is the microdilution assay, due to its precision and quantitative nature (Hosain, T.J., 2024). This method determines the minimum inhibitory concentration (MIC) of AMPs, the lowest concentration required to inhibit microbial growth in a liquid culture (Hosain, T.J., 2024). By using a series of diluted peptide concentrations, the AMP potency can accurately be assessed across various microbial strains. The microbroth dilution method allows for a high-throughput analysis of multiple samples and conditions simultaneously, offering detailed and reproducible data on AMP activity (CLSI, 2012).

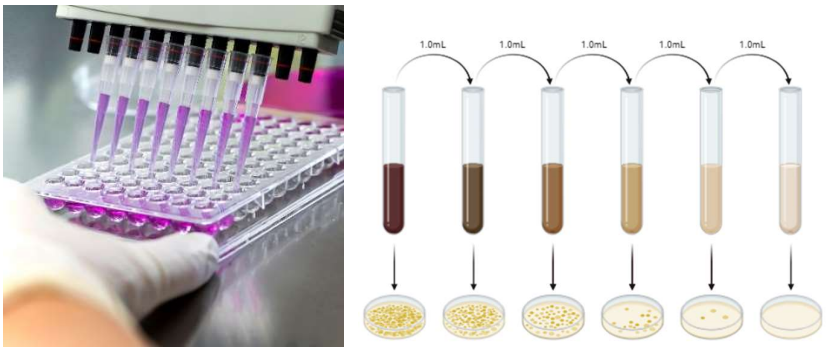


Figure 1.15: Examples of in vitro screening techniques. *The left image illustrates the method for plate dilutions where in this case in a multichannel pipette and 96-well plate is used. The right image depicts test tubes with different cell dilutions, highlighting the tube dilution approach. (Images obtained free of copyrights).*

© University of Pretoria

To screen for selectivity, haemolysis and cytotoxicity assays are also critical *in vitro* tests that assess the potential toxicity of AMPs by evaluating their ability to lyse red blood cells or damage mammalian cells. These assays, which can be seen as extensions of the microdilution assay, provide valuable insights into the safety profile and therapeutic index of a peptide in environments that mimic either topical or systemic applications (Khalef *et al.,* 2024).

A limitation of traditional *in vitro* screening is its potential inability to accurately replicate complex physiological conditions of real-life settings, which can lead to either an overestimation or underestimation of peptide activity. To address this challenge, synthetic and more complex *in vitro* models have been developed that closely simulate actual conditions (Hofmann *et al.,* 2023). These models provide a controlled environment to study how AMPs perform in for example a wound-like setting, allowing researchers to evaluate their efficacy, safety, and mechanisms of action before progressing to *in vivo* studies.

One example is the use of cultured epidermal cells to create a monolayer that mimics the epidermal layer of skin. A "wound" is induced by physically or chemically disrupting the cell monolayer (Hofmann *et al.*, 2023). This model is useful for studying cellular responses to AMPs, such as cell migration, proliferation, and wound healing processes. Another predictive *in vitro* model of high complexity that has potential for the evaluation of AMPs, is the co-culture model of the human cystic fibrosis bronchial epithelial cell line CFBE41o-and THP-1 monocyte-derived macrophages, mimicking an infection of the human bronchial mucosa by *P. aeruginosa* at air-liquid interface (ALI) conditions (Montefusco-Pereira *et al.,* 2020). This model assesses epithelial barrier integrity, macrophage transmigration, bacterial survival, and inflammation simultaneously.

1.7.2 Ex vivo, tissue-based screening models

In vivo testing in drug discovery and development faces ethical considerations and limitations. Ethical concerns about animal welfare have led to increased regulatory scrutiny and public pressure to find alternatives. The ethical debate focuses the 3Rs that aims to replace animals with new alternative models, to reduce the number of animals used, and to refine experiments to minimise suffering (Strech & Dirnagl, 2019). As such, *ex vivo* models offer significant advantages in the evaluation of AMPs and other therapeutic agents by bridging the gap between *in vitro* and *in vivo* testing.

Ex vivo models provide a more accurate representation of physiological conditions compared with traditional *in vitro* assays. These models involve the use of tissue or organ samples from living organisms, such as discarded tissue from surgical procedures, which are then maintained in a controlled environment outside the body (Xu *et al.,* 2021). This allows for a more precise assessment of peptide efficacy, tissue compatibility, and potential side effects (Xu *et al.,* 2021). *Ex vivo* models also enable the evaluation of localised effects of AMPs on specific tissues or organs. For instance, *ex vivo* skin models can assess how AMPs interact with dermal tissues (Okurowska *et al.,* 2020),

© University of Pretoria

while *ex vivo* lung tissue models can evaluate the impact on respiratory infections (Harrison and Diggle, 2016). This localised approach helps in understanding peptide behaviour in targeted settings.

In these models, tissue samples from animals or humans that are obtained from existing procedures or would otherwise be discarded are used. This significantly reduces the number of live animals required, aligning with ethical principles that emphasise the humane treatment of animals. Additionally, *ex vivo* models allow for extensive preliminary testing of peptides, helping to identify promising candidates and refine their profiles before progressing to *in vivo* studies. This preselection process enhances the likelihood of success in subsequent *in vivo* experiments.

An example of an *ex vivo* model that also indicates the suitability of an AMP for systemic application is the porcine lung model developed by Harrison and Diggle (2016), which simulates cystic fibrosis (Fig. 1.16). The efficacy of antimicrobials such as colistin and tobramycin has been evaluated with this model (Sweeney *et al.,* 2020). Another *ex vivo* model is the porcine corneal model of bacterial keratitis developed by Okurowska *et al.* (2020), which closely replicates keratitis infections (Fig. 1.16). This model provides insights into the suitability of antimicrobials for topical eye applications. It has been used to evaluate the efficacy of antimicrobials like moxifloxacin and ciprofloxacin, demonstrating the potential of AMPs to effectively treat bacterial infections in ocular contexts (Okurowska *et al.* 2024).

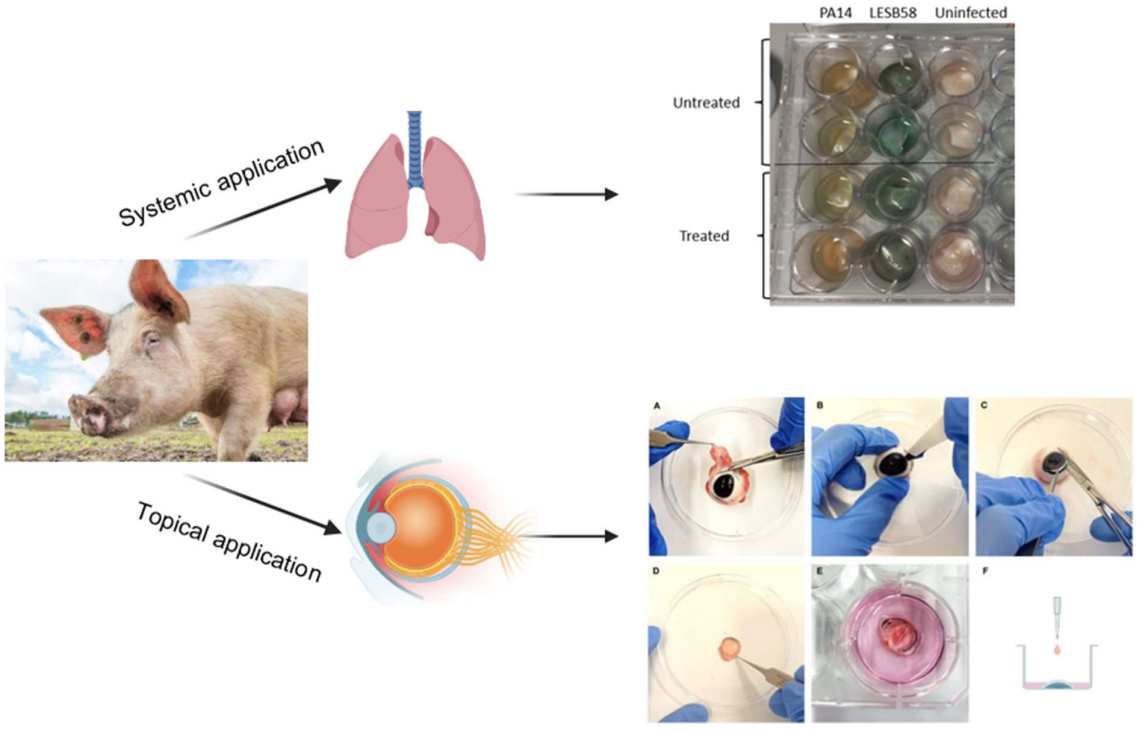


Figure 1.16: Example of ex vivo porcine lung and cornea models evaluating AMP efficacy. *Lung tissue and corneas can be sourced from a local butchery. Bronchioles are dissected, sterilised, and maintained in artificial sputum medium, then inoculated with bacterial isolates, such as P. aeruginosa 14 or LESB58, for biofilm development. The biofilm is subsequently treated with an antimicrobial agent. Corneas are sterilised, incised, and infected with bacteria, allowing for biofilm formation before topical antimicrobial treatment. In both models, infected tissues are homogenised and spot-plated after 24 h of treatment to assess bacterial eradication. (Figure created using Biorender.com)*

© University of Pretoria

1.7.3 In vivo, animal screening models

Unlike *in vitro* models, which analyse biological processes in isolated systems, *in vivo* testing evaluates the effects of treatments within a living organism and provides a comprehensive understanding of how a drug interacts with the complex environment of a whole body, including its various tissues, organs, and biological systems.

The primary advantage of *in vivo* testing is the ability to capture intricate physiological and biochemical interactions that cannot be fully replicated *in vitro* or *ex vivo*. This includes metabolism, pharmacokinetics such as drug absorption, distribution, metabolism, excretion and toxicity (ADMET), and the immune response (Xu *et al.,* 2021). Observing how a drug performs in a living organism allows researchers to better predict its efficacy, safety, and potential side effects in humans (Xu *et al.,* 2021).

Several *in vivo* models are employed to assess the therapeutic potential and safety of AMPs. Animal models, particularly small mammals like mice, rats, and other rodents, are extensively used during the preclinical drug discovery and development phase (Lewis *et al.,* 2016). Their genetic similarities to humans, rapid turnover rates, and availability make them ideal for initial testing (Lewis *et al.,* 2016; Girkin *et al.,* 2019). This stage helps determine optimal dosing and routes of administration before advancing to human trials.

A challenge in AMP research is the cost implications associated with testing in mice, rats, and pigs. Therefore, a smaller but still relevant model such as the *Galleria mellonella* model (Fig. 1.17), commonly known as the greater wax moth larvae, has emerged as a promising alternative to traditional animal models, particularly for testing the efficacy of AMPs for systemic or topical infections (McCloskey *et al.,* 2019). This model is increasingly used due to its simplicity, cost-effectiveness, and ease of maintenance (Wojda *et al.,* 2020). The larvae are naturally susceptible to a range of pathogens, including bacteria and fungi, making them ideal for studying infectious diseases and evaluating antimicrobial treatments. In addition, these insects are not considered sentient in the same way as mammals, which reduces the moral and ethical issues associated with their use (Wojda *et al.,* 2020). Maintaining *G. mellonella* larvae is also relatively inexpensive compared with vertebrate models. These larvae require minimal space and resources, and their short life cycle allows for rapid experimentation and turnover. Additionally, the larvae are easy to handle and manipulate, and experiments can be conducted with a relatively small number of specimens.

Despite their simplicity, *G. mellonella* larvae possess an innate immunity that responds to infections in similar ways to human responses (Wojda *et al.,* 2020). This simplicity allows for straightforward administration of treatments and observation of outcomes, facilitating experimental reproducibility. This model has successfully been used to evaluate the activity of AMPs like gentamicin, vancomycin, D-pleurocidin and more (Di Blasio *et al.,* 2022; Manzo *et al.,* 2020).

© University of Pretoria

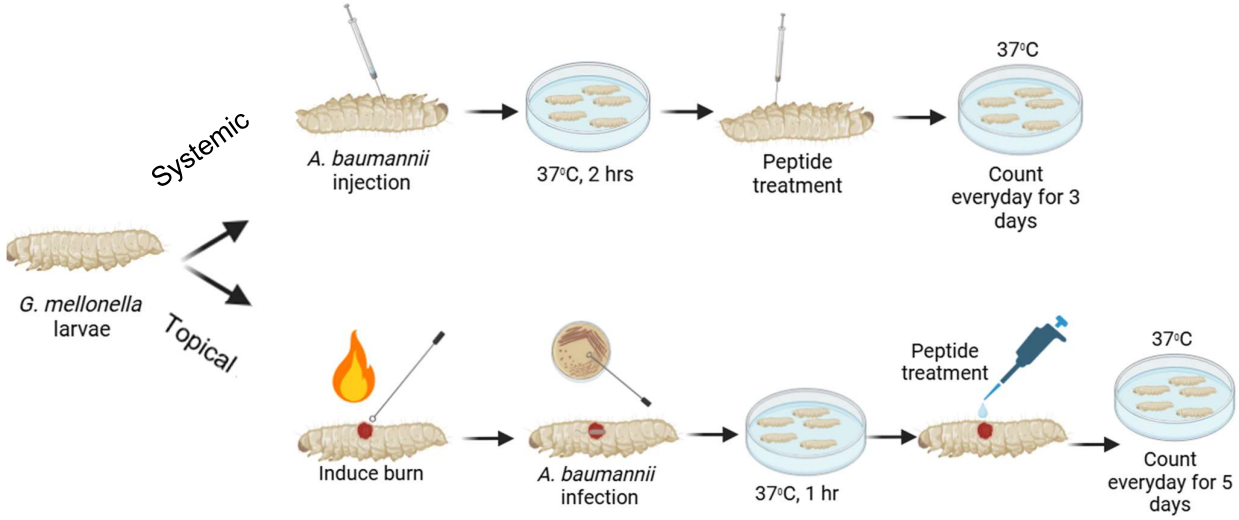


Figure 1.17: In vivo G. mellonella model assessing the efficacy of an AMP against systemic and topical infections. *To evaluate the effectiveness of systemic AMP administration, bacterial pathogens, such as A. baumannii, are injected into a proleg of the larvae. After allowing the infection to progress for approximately 2 h, systemic peptide treatment is administered. For the topical infection model, a burn wound is created on the larvae's back, followed by infection with a bacterial pathogen for about 1 h, after which topical peptide treatment is applied. In both scenarios, larval survival is monitored over several days. (Figure created using Biorender.com).*

More complex animal models, such as murine infection models, remain crucial for the thorough preclinical evaluation of promising AMPs, as demonstrated with SMAP-29, TP4, and D-pleurocidin-KR (Jung *et al.,* 2021; Manzo *et al.,* 2020). However, *in vitro*, *ex vivo* and simpler *in vivo* animal models are valuable in the evaluation of AMPs before progressing to human clinical trials. This thorough preclinical assessment ensures that promising AMP candidates are not only effective but also safe and suitable for further development in clinical settings.

1.8 Conclusion

In conclusion, AMPs represent promising candidates in the lead-to-hit discovery of new drugs to combat drug-resistant infections, particularly those caused by Gram-negative bacteria. However, the complexity and impermeability of the Gram-negative cell wall pose significant challenges to their effectiveness. Therefore, investigating the interactions between AMPs and the Gram-negative cell wall is crucial.

Our current understanding of structure-activity relationships and the structural requirements for selectivity is still limited. Additionally, the stability of AMPs in physiological environments presents further complications for their development. To address these challenges, ongoing research focused on optimising AMP stability, selectivity, and delivery mechanisms is vital.

This thesis delves into these issues, presenting novel AMPs with potent activity and elucidated mechanisms of action. It also proposes rational design methods and formulations aimed at overcoming stability, toxicity, and delivery obstacles.

© University of Pretoria

1.8 References

ABDI, H. & WILLIAMS, L. J. (2010). Principal component analysis. *Wiley Interdisciplinary Reviews: Computational Statistics,* 2 (4), pg. 433–459. https://doi.org/10.1002/wics.101

AMINOV, R. I. (2010). A brief history of the antibiotic era: Lessons learned and challenges for the future. *Frontiers in Microbiology,* 1 (1), pg. 1-134.

ANNAVAJHALA, M. K., GOMEZ-SIMMONDS, A., & UHLEMANN, A. C. (2019). Multidrug-resistant *Enterobacter cloacae* complex emerging as a global, diversifying threat. *Frontiers in Microbiology, 10* (44). https://doi.org/10.3389/fmicb.2019.00044

ARIAS, M., PIGA, K. B., HYNDMAN, M. E. & VOGEL, H. J. (2018). Improving the activity of Trp-rich antimicrobial peptides by Arg/Lys substitutions and changing the length of cationic residues. *Biomolecules,*8 (2), article 19, pg. 19-32. doi: 10.3390/biom8020019.

BARTLETT, K.H., MCCRAY, P.B., & THORNE, P.S. (2004). Reduction in the bactericidal activity of selected cathelicidin peptides by bovine calf serum or exogenous endotoxin. *International Journal of Antimicrobial Agents*, 23 (6), pg. 606-612. https://doi.org/10.1016/j.ijantimicag.2004.02.018.

BENNETT, W., MENDE, K., CAMPBELL, W.R., BECKIUS, M., STEWART, L., SHAIKH, F., RAHMAN, A., TRIBBLE, D.R. & YABES, J.M. (2023). *Enterobacter cloacae* infection characteristics and outcomes in battlefield trauma patients. *PLoS One*, 18 (8), e0290735. doi: 10.1371/journal.pone.0290735.

BERTANI, B., & RUIZ, N. (2018). Function and biogenesis of lipopolysaccharides. *EcoSal Plus,* 8 (1), 10.1128/ecosalplus. ESP-0001-2018. https://doi.org/10.1128/ecosalplus.

BRADY, M. F., JAMAL, Z. & PERVIN, N. (2024). Acinetobacter. *Treasure Island (FL): StatPearls.* Available at: https://www.ncbi.nlm.nih.gov/books/NBK430784/. Accessed August 2024.

BUSH, K., JACOBY, G. A., & MEDEIROS, A. A. (1995). A functional classification scheme for beta-lactamases and its correlation with molecular structure. *Antimicrobial Agents and Chemotherapy,* 39 (6), pg. 1211–1233. https://doi.org/10.1128/aac.39.6.1211

CENTERS FOR DISEASE CONTROL AND PREVENTION. (2013). *Antimicrobial Resistance Threat Report*. Available at: http://www.cdc.gov/drugresistance/threat-report-2013/. Accessed March 2019.

CEULEERS, H. VAN SPAENDONK, H., HANNING, N., HEIRBAUT, J., LAMBEIR, A. M., JOOSSENS, J., AUGUSTYNS, K., DE MAN, J., MEESTER, I. & DE WINTER, B. (2016). Visceral hypersensitivity in inflammatory bowel diseases and irritable bowel syndrome: The role of proteases. *World Journal of Gastroenterology*, 22 (47), article 10275.

CHIRAMBA, C. K., MÖLLER, D. S., LORENZ, C. D., CHIROMBO, R. R., MASON, A. J., BESTER, M. J., & GASPAR, A. R. M. (2024). Tryptophan end-tagging confers antifungal activity on a tick-derived peptide by triggering reactive oxygen species production. *ACS Omega,* 9 (13), pg. 15556-15572. https://doi.org/10.1021/acsomega.4c00478

CHU, H. L., CHIH, Y. H., PENG, K. L., WU, C. L., YU, H. Y., CHENG, D., CHOU, Y. T., & CHENG, J. W. (2020). Antimicrobial peptides with enhanced salt resistance and antiendotoxin properties. *International Journal of Molecular Sciences,* 21 (18), Article 6810. https://doi.org/10.3390/ijms21186810

CLINICAL AND LABORATORY STANDARDS INSTITUTE (CLSI). (2012). Methods for dilution antimicrobial susceptibility tests for bacteria that grow aerobically. *Approved Standard—Ninth Edition*. CLSI document M07-A9. Clinical and Laboratory Standards Institute.

CYTRYŃSKA, M., & ZDYBICKA-BARABAS, A. (2015). Defense peptides: recent developments, *Biomolecular Concepts*, 6 (4), pg. 237-251.

© University of Pretoria

DAVIES, J. E. (1997). Origins, acquisition, and dissemination of antibiotic resistance determinants. *Ciba Foundation Symposium,* 207, pg. 15–27. https://doi.org/10.1002/9780470516005.ch2

DESCHAMPS, E., SCHMITZ-AFONSO, I., SCHAUMANN, A., DE, E., LOUTELIER-BOURHIS, C., ALEXANDRE, S. & AFONSO, C. (2019). Determination of the collision cross sections of cardiolipins and phospholipids from *Pseudomonas aeruginosa* by traveling wave ion mobilityspectrometry-mass spectrometry using a novel correction strategy. *Analytical and Bioanalytical Chemistry*, 411 (34), pg. 8123-8131.

DESCHAMPS, E., SCHAUMANN, A., SCHMITZ-AFONSO, I., AFONSO, C., DÉ, E., LOUTELIER-BOURHIS, C. & ALEXANDRE, S. (2021). Membrane phospholipid composition of *Pseudomonas aeruginosa* grown in a cystic fibrosis mucus-mimicking medium. *Biochimica et Biophysica Acta (BBA) - Biomembranes*, 1863 (1), pg. 183482-183501. https://doi.org/10.1016/j.bbamem.2020.183482.

DI BLASIO, S., CLARKE, M., HIND, C.K., ASAI, M., LAURENCE, L., BENVENUTI, A., HASSAN, M., SEMENYA, D., MAN, D.K., HORROCKS, V., MANZO, G., VAN DER LITH, S., LAM, C., GENTILE, E., ANNETTE, C., BOSSE, J., LI, Y., PANARETOU, B., LANGFORD, P.R., ROBERTSON, B.D., LAM, J.K.W, SUTTON, J.M., MCARTHUR, M. & MASON, A. J. (2022). Bolaamphiphile analogues of 12-bis-THA Cl2 are potent antimicrobial therapeutics with distinct mechanisms of action against bacterial, mycobacterial, and fungal pathogens. *mSphere*, 8 (1), article e0050822. https://doi.org/10.1128/msphere.00508-22.

EPAND, R. M., & VOGEL, H. J. (1999). Diversity of antimicrobial peptides and their mechanisms of action. *Biochimica et Biophysica Acta (BBA) - Biomembranes,* 1462 (1–2), pg. 11–28. https://doi.org/10.1016/S0005-2736(99)00253-5

EUROPEAN CENTRE FOR DISEASE PREVENTION AND CONTROL. (2021). Antimicrobial resistance in the EU/EEA (EARS-Net)—Annual epidemiological report for 2020. *ECDC*. Available at: https://www.ecdc.europa.eu/en/publications-data/surveillance-antimicrobial-resistance-europe-2020. Accessed July 2024.

FATTAHIAN, Y., RASOOLI, I., GARGARI, S. L. M., RAHBAR, M. R., ASTANEH, S. D. & AMANI, J. (2011). Protection against *Acinetobacter baumannii* infection via its functional deprivation of biofilm associated protein (Bap). *Microbial Pathogenesis*, 51 (1), pg. 402–406. doi: 10.1016/j.micpath.2011.09.004.

FERNANDES, F. C., CARDOSO, M. H., GIL-LEY, A., LUCHI, L. V., DA SILVA, M. G. L., MACEDO, M. L. R., DE LA FUENTE-NUNEZ, C., & FRANCO, O. L. (2023). Geometric deep learning as a potential tool for antimicrobial peptide prediction. *Frontiers in Bioinformatics*, 3, article 1216362. https://doi.org/10.3389/fbinf.2023.1216362

FOSGERAU, K. & HOFFMANN, T. (2015). Peptide therapeutics: Current status and future directions. *Drug Discovery Today*, 20 (1), pg.122-128. doi: 10.1016/j.drudis.2014.10.003.

FRUITWALA, S., EL-NACCACHE, D.W., & CHANG, T.L. (2019). Multifaceted immune functions of human defensins and underlying mechanisms. *Seminars in Cell & Developmental Biology*, 88 (1), pg. 163-172. doi: 10.1016/j.semcdb.2018.02.023.

GALGANO, L., GUIDETTI, G. F., TORTI, M. & CANOBBIO, I. (2022). The controversial role of LPS in platelet activation *in vitro*. *International Journal of Molecular Sciences*, 23 (1), article 10900. https://doi.org/10.3390/ijms231810900

GERA, S., KANKURI, E. & KOGERMANN, K. (2022). Antimicrobial peptides – Unleashing their therapeutic potential using nanotechnology. *Pharmacology & Therapeutics*, 232, article 107990. https://doi.org/10.1016/j.pharmthera.2021.107990

GIRKIN, J., MALTBY, S., SINGANAYAGAM, A., BARTLETT, N. & MALLIA, P. (2019). *In vivo* experimental models of infection and disease. *Rhinovirus Infections*, pg. 195–238. doi: 10.1016/B978-0-12-816417-4.00008-1.

© University of Pretoria

GOLEC, M. (2007). Cathelicidin LL-37: LPS-neutralizing, pleiotropic peptide. *Annals of Agricultural and Environmental Medicine,* 14 (1), pg. 1–4.

HANCOCK, R. E. W., & PATRZYKAT, A. (2002). Clinical development of cationic antimicrobial peptides: From natural to novel antibiotics. *Current Drug Targets - Infectious Disorders,* 2 (1), pg. 79–83.

HARRISON, F. & DIGGLE, S. P. (2016). An *ex vivo* lung model to study bronchioles infected with *Pseudomonas aeruginosa* biofilms. *Microbiology*, 162 (1), pg. 1755–1760.

HE, K., LUDTKE, S. J., HELLER, W. T., & HUANG, H. W. (1996). Mechanism of alamethicin insertion into lipid bilayers. *Biophysical Journal,* 71 (5), pg. 2669–2679. https://doi.org/10.1016/S0006-3495(96)79458-4.

HOFMANN, E., FINK, J., PIGNET, A. L., SCHWARZ, A., SCHELLNEGGER, M., NISCHWITZ, S. P., HOLZER-GEISSLER, J. C. J., KAMOLZ, L. P. & KOTZBECK, P. (2023). Human *in vitro* skin models for wound healing and wound healing disorders. *Biomedicines*, 11 (4), pg. 1056-1078. https://doi.org/10.3390/biomedicines11041056.

HOSSAIN, T.J. (2024). Methods for screening and evaluation of antimicrobial activity: A review of protocols, advantages, and limitations. *European Journal of Microbiology and Immunology (Bp)*, 14 (2), pg. 97-115. doi: 10.1556/1886.2024.00035.

HUAN, Y., KONG, Q. & MOU, H. (2020). Antimicrobial peptides: Classification, design, application and research progress in multiple fields. *Frontiers in Microbiology*, 11 (1), article 582779. doi: 10.3389/fmicb.2020.582779.

HUANG, H.N., CHAN, Y.L., WU, C.J. & CHEN, J.Y. (2015). Tilapia Piscidin 4 (TP4) stimulates cell proliferation and wound closure in MRSA-Infected wounds in mice. *Marine Drugs*, 13 (5), pg. 2813-2833. https://doi.org/10.3390/md13052813

IRVINE, A., MCKENZIE, D., MCCOY, C.J., GRAHAM, R.L.J., GRAHAM, C., HUWS, S.A., ATKINSON, L.E. & MOUSLEY, A. (2023). Novel integrated computational AMP discovery approaches highlight diversity in the helminth AMP repertoire'. *PLoS Pathogens*, 19 (7), article e1011508. doi: 10.1371/journal.ppat.1011508.

JUMPER, J., EVANS, R., PRITZEL, A. & HASSABIS, D. (2021). Highly accurate protein structure prediction with AlphaFold. *Nature,* 596 (1), pg. 583–589. https://doi.org/10.1038/s41586-021-03819-2

KHALEF, L., LYDIA, R., FILICIA, K. & MOUSSA, B. (2024). Cell viability and cytotoxicity assays: Biochemical elements and cellular compartments. *Cell Biochemistry and Function*. 42 (1), pg. e4007- e4022. doi:10.1002/cbf.4007

LA ROCCA, P., BIGGIN, P.C., TIELEMAN, D.P. & SANSOM, M.S.P. (1999). Simulation studies of the interaction of antimicrobial peptides and lipid bilayers. *Biochimica et Biophysica Acta*, 1462 (1), pg. 185-200. doi: 10.1016/S0005-2736(99)00206-0.

LEWIS, A. J., SEYMOUR, C. W. & ROSENGART, M. R. (2016). Current murine models of sepsis. *Surgical Infections (Larchmt),* 17 (4), pg. 385-93. doi: 10.1089/sur.2016.021.

LI, L., VOROBYOV, I. & ALLEN, T.W. (2013). The different interactions of lysine and arginine side chains with lipid membranes. *Journal of Physical Chemistry B*, 117 (40), pg.11906–11920.

LIN, Q.P., ZHOU, L.F., LI, N.N., CHEN, Y.Q., LI, B.C., CAI, Y.F., & ZHANG, S.Q. (2008). Lipopolysaccharide neutralization by the antibacterial peptide CM4. *European Journal of Pharmacology,* 596 (1–3), pg. 160–165. https://doi.org/10.1016/j.ejphar.2008.08.017.

© University of Pretoria

LUO, Y. & SONG, Y. (2021). Mechanism of antimicrobial peptides: antimicrobial, anti-inflammatory and antibiofilm activities. *International Journal of Molecular Sciences*, 22 (21), article 11401. doi: 10.3390/ijms222111401.

MCCLOSKEY, A. P., LEE, M., MEGAW, J., MCEVOY, J., COULTER, S. M., PENTLAVALLI, S., & LAVERTY, G. (2019). Investigating the *in vivo* antimicrobial activity of a self-assembling peptide hydrogel using a *Galleria mellonella* infection model. *ACS Omega,* 4 (2), pg. 2584-2589. https://doi.org/10.1021/acsomega.8b03578.

MICHAELIS, C. & GROHMANN, E. (2023). Horizontal gene transfer of antibiotic resistance genes in biofilms. *Antibiotics*, 12 (2), pg. 328-341. doi: 10.3390/antibiotics12020328.

MISRA, T., TARE, M. & JHA, P.N. (2022). Insights into the dynamics and composition of biofilm formed by environmental isolate of *Enterobacter cloacae*. *Frontiers in Microbiology,* 13 (1), pg. 877060 - 877071.doi: 10.3389/fmicb.2022.877060.

MOAZZEZY, N., ASADI KARAM, M.R., RAFATI, S., BOUZARI, S. & OLOOMI, M. (2020). Inhibition and eradication activity of truncated α-defensin analogs against multidrug resistant uropathogenic *Escherichia coli* biofilm. *PLoS One*, 15 (7), article e0235892. doi: 10.1371/journal.pone.0235892.

MONDAL, J. (2019). A brief appraisal of computational modeling of antimicrobial peptides' activity'. *Drug Development Research*, 80 (1), pg. 28-32. doi: 10.1002/ddr.21472.

MONTEFUSCO-PEREIRA, C.V., HORSTMANN, J.C., EBENSEN, T., BEISSWENGER, C., BALS, R., GUZMÁN, C.A., SCHNEIDER-DAUM, N., CARVALHO-WODARZ, C.D.S. & LEHR, C.M. (2020). *P. aeruginosa* infected 3D co-culture of bronchial epithelial cells and macrophages at air-liquid interface for preclinical evaluation of anti-infectives. *Journal of Visualized Experiments*, (160), article e61069. doi:10.3791/61069.

MORAVEJ, H., MORAVEJ, Z., YAZDANPARAST, M., HEIAT, M., MIRHOSSEINI, A., MOOSAZADEH MOGHADDAM, M. & MIRNEJAD, R. (2018). Antimicrobial peptides: features, action, and their resistance mechanisms in bacteria. *Microbial Drug Resistance*, 24 (6), pg. 747-767. doi: 10.1089/mdr.2017.0392.

MURRAY, C.J.L., IKUTA, K.S., RAO, P., WOOL, E., AGARWAL, R., BEKKER, A., DAY, N.P.J., DUNACHIE, S.J., HAY, S.I., NANAVATI, R., NOVOTNEY, A., STEENKESTE, N., SARTORIUS, B., LOPEZ, A.D., MOORE, C.E. & NAGHAI, M. (2019). Global burden of bacterial antimicrobial resistance in 2019: a systematic analysis. *The Lancet*, 399 (10325), pg. 629 – 655.

MUSRATI, A.A., TERVAHARTIALA, T., GÜRSOY, M., KÖNÖNEN, E., FTEITA, D., SORSA, T., UITTO, V.J. & GÜRSOY, U.K. (2016). Human neutrophil peptide-1 affects matrix metalloproteinase-2, -8 and -9 secretions of oral squamous cell carcinoma cell lines *in vitro*. *Archives of Oral Biology*, 66 (1), pg. 1-7. doi: 10.1016/j.archoralbio.2016.02.003.

NIKAIDO, H. (1998). Multiple antibiotic resistance and efflux. *Current Opinion in Microbiology,* 1 (5), pg. 516–523. https://doi.org/10.1016/s1369-5274(98)80083-0.

OKUROWSKA, K., ROY, S., THOKALA, P., PARTRIDGE, L., GARG, P., MACNEIL, S., MONK, P. N. & KARUNAKARAN, E. (2020). Establishing a porcine *ex vivo* cornea model for studying drug treatments against bacterial keratitis. *Journal of Visualized Experiments: JoVE*, 12 (159), article 61156. doi: 10.3791/61156.

OKUROWSKA, K., MONK, P.N. & KARUNAKARAN, E. (2024). Increased tolerance to commonly used antibiotics in a *Pseudomonas aeruginosa ex vivo* porcine keratitis model. *Microbiology*, 170 (5), article 001459.

© University of Pretoria

OYINLOYE, B.E., ADENOWO, A.F., & KAPPO, A.P. (2015). Reactive oxygen species, apoptosis, antimicrobial peptides, and human inflammatory diseases. *Pharmaceuticals (Basel)*, 8 (2), pg. 151-175. doi: 10.3390/ph8020151.

PARCHEBAFI, A., TAMANAEE, F., EHTERAM, H., AHMAD, E., NIKZAD, H. & HADDAD KASHANI, H. (2022). The dual interaction of antimicrobial peptides on bacteria and cancer cells; mechanism of action and therapeutic strategies of nanostructures. *Microbial Cell Factories*, 21 (118), pg. 1-18. doi: 10.1186/s12934-022-01848-8.

PELEG, A. Y., SEIFERT, H., & PATERSON, D. L. (2008). *Acinetobacter baumannii*: Emergence of a successful pathogen. *Clinical Microbiology Reviews*, 21(3), pg. 538-582.

PULIDO, D., NOGUÉS, M. V., BOIX, E., & TORRENT, M. (2012). Lipopolysaccharide neutralization by antimicrobial peptides: A gambit in the innate host defense strategy. *Journal of Innate Immunity,* 4 (4), pg. 327-336. https://doi.org/10.1159/000336713.

PUTHIA, M., BUTRYM, M., PETRLOVA, J., STRÖMDAHL, A.C., ANDERSSON, M.Å., KJELLSTRÖM, S., & SCHMIDTCHEN, A. (2020). A dual-action peptide-containing hydrogel targets wound infection and inflammation. *Science Translational Medicine*, 12 (524), article eaax6601.

RAMANATHAN, S., SIVASUBRAMANIAN, S., PANDURANGAN, P., MANI, G., MADHU, D., & LIN, X. (2021). Bacterial biofilm inhibition: A focused review on recent therapeutic strategies for combating biofilm-mediated infections. *Frontiers in Microbiology,* 12 (1), article 676458. https://doi.org/10.3389/fmicb.2021.676458

RAMAZI, S., MOHAMMADI, N., ALLAHVERDI, A., KHALILI, E. & ABDOLMALEKI, P. (2022). A review on antimicrobial peptides databases and the computational tools. *Database: The Journal of Biological Databases and Curation*, pg. 1-17. doi: 10.1093/database/baac011.

RAZIYEVA, K., KIM, Y., ZHARKINBEKOV, Z., KASSYMBEK, K., JIMI, S., & SAPAROV, A. (2021). Immunology of acute and chronic wound healing. *Biomolecules*, 11 (5), pg. 700-721. doi: 10.3390/biom11050700.

REACT. (2015) Bacteria, antibiotics and antibiotic resistance. *Lecture,* Available from: http://www.reactgroup.org/wp-content/uploads/2016/09/TBx_basic_lecture_ABR.pdf. Accessed February 2019.

ROY, K., KAR, S. & DAS, R. N. (2015). Chapter 9 – Newer QSAR techniques. *Understanding the Basics of QSAR for Applications in Pharmaceutical Sciences and Risk Assessment,* pg. 319-356.

RUAMSAP, N., THOMAS, M.C.S., IMERBSIN, R., REED, M.C., GONWONG, S., LURCHA-CHAIWONG, W., ISLAM, D., WOJNARSKI, M., VESELY, B.A., LUGO-ROMAN, L.A., WATERS, N.C. & ZURAWSKI, D.V. (2023). Chronic wound infection model of *Acinetobacter baumannii* in outbred mice. *Military Medicine*, 188 (7), pg. e1708-e1716.

SAHA, S., BARIK, D. & BISWAS, D. (2024). AMPs as host-directed immunomodulatory agents against skin infections caused by opportunistic bacterial pathogens. *Antibiotics*, 13 (5), pg. 439-454. doi: 10.3390/antibiotics13050439.

SAMY, R.P., KANDASAMY, M., GOPALAKRISHNAKONE, P., STILES, B.G., ROWAN, E.G., BECKER, D., & CHOW, V.T. (2014). Wound healing activity and mechanisms of action of an antibacterial protein from the venom of the eastern diamondback rattlesnake (*Crotalus adamanteus*). *PLoS One*, 9 (1), Article e80199.

SAXENA, D., MAITRA, R., BORMON, R., CZEKANSKA, M., MEIERS, J., TITZ, A., VERMA, S. & CHOPRA, S. (2023). Tackling the outer membrane: facilitating compound entry into Gram-negative bacterial pathogens. *Nature Portfolio Journal: Antimicrobials and Resistance*, 1 (1), pg. 17-29. doi: 10.1038/s44259-023-00016-1.

© University of Pretoria

SILHAVY, T. J., KAHNE, D. & WALKER, S. (2010).The bacterial cell envelope. *Cold Spring Harbor Perspectives in Biology,* 2 (5), article a000414. doi:10.1101/cshperspect.a000414.

SNYDER, S., KIM, D., & MCINTOSH, T. J. (1999). Lipopolysaccharide bilayer structure: Effect of chemotype, core mutations, divalent cations, and temperature. *Biochemistry,* 38 (33), pg. 10758–10767. https://doi.org/10.1021/bi990867d

STRECH, D. & DIRNAGL, U. (2019). 3Rs missing: animal research without scientific value is unethical. *BMJ Open Science*, 3 (1), article 2018-000048. doi: 10.1136/bmjos-2018-000048.

SWEENEY, E., SABNIS, A., EDWARDS, A.M. AND HARRISON, F. (2020). Effect of host-mimicking medium and biofilm growth on the ability of colistin to kill *Pseudomonas aeruginosa*. *Microbiology (Reading)*, 166 (12), pg. 1171-1180. doi:10.1099/mic.0.000962.

TYPAS, A., BANZHAF, M., GROSS, C. A., & VOLLMER, W. (2016). From the regulation of peptidoglycan synthesis to bacterial growth and morphology. *Nature Reviews Microbiology*, 14 (3), pg. 224-236. doi:10.1038/nrmicro.2016.7

UDDIN, T. M., CHAKRABORTY, A. J., KHUSRO, A., MATIN, B. M. R. M. Z., MITRA, S., EMRAN, T. B., DHAMA, K., RIPON, M. K. H., GAJDÁCS, M., SAHIBZADA, M. U. K., HOSSAIN, M. J. & KOIRALA, N. (2021). Antibiotic resistance in microbes: History, mechanisms, therapeutic strategies and future prospects. *Journal of Infection and Public Health*, 14 (12), pg. 1750-1766. doi: 10.1016/j.jiph.2021.10.020.

ULVATNE, H., SAMUELSEN, Ø., HAUKLAND, H.H., KRÄMER, M. & VORLAND, L.H. (2004). Lactoferricin B inhibits bacterial macromolecular synthesis in *Escherichia coli* and *Bacillus subtilis*. *FEMS Microbiology Letters*, 237 (1), pg. 377-384. doi: 10.1111/j.1574-6968.2004.tb09720.x

VAN DER WALT, M., MÖLLER, D. S., VAN WYK, R. J., FERGUSON, P. M., HIND, C. K., CLIFFORD, M., DO CARMO SILVA, P., SUTTON, J. M, MASON, J. A., BESTER, M. J. & GASPAR, A. R. M. (2024). QSAR reveals cationic residues with decreased lipophilicity determine the selectivity of antimicrobial peptide activity. *ACS Omega,* 1 (1). doi: 10.1021/acsomega.4c01277.

VAN MOLL, L., WOUTERS, M., DE SMET, J., DE VOOGHT, L., DELPUTTE, P., VAN DER BORGHT, M. & COS, P. (2023). In-depth biological characterization of two black soldier fly anti-Pseudomonas peptides reveals LPS-binding and immunomodulating effects. *mSphere*, 8 (1), article e00454-23. doi: 10.1128/msphere.00454-23.

WANG, J., MA, W., FANG, Y., LIANG, H., YANG, H., WANG, Y., DONG, X., ZHAN, Y. & WANG, X. (2021) Core oligosaccharide portion of lipopolysaccharide plays important roles in multiple antibiotic resistance in *Escherichia coli. Antimicrobial Agents and Chemotherapy*, 65 (1), article 10.1128/aac.00341-21. doi: 10.1128/aac.00341-21.

WOJDA, I., STANIEC, B., SUŁEK, M. & KORDACZUK, J. (2020). The greater wax moth *Galleria mellonella*: biology and use in immune studies. *Pathogens and Disease*, 78 (9), article ftaa057. doi: 10.1093/femspd/ftaa057.

WORLD HEALTH ORGANIZATION. (2017). Antibacterial agents in clinical development: an analysis of the antibacterial clinical development pipeline, including tuberculosis. [Internet] Available from: http://www.who.int/medicines/areas/rational_use/antibacterial_agents_clinical_development/en/, Accessed July 2021.

WORLD HEALTH ORGANIZATION. (2024). WHO bacterial priority pathogens list, 2024: Bacterial pathogens of public health importance to guide research, development and strategies to prevent and control antimicrobial resistance. [Internet] Available from: WHO bacterial priority pathogens list, 2024: Bacterial pathogens of public health importance to guide research,

© University of Pretoria

development and strategies to prevent and control antimicrobial resistance, Accessed August 2024.

XU, Y., SHRESTHA, N., PRÉAT, V., & BELOQUI, A. (2021). An overview of *in vitro*, *ex vivo* and *in vivo* models for studying the transport of drugs across intestinal barriers. *Advanced Drug Delivery Reviews,* 175 (1), article 113795. https://doi.org/10.1016/j.addr.2021.05.005.

Zasloff, M. (1987). Magainins, a class of antimicrobial peptides from Xenopus skin: Isolation and structure. *Proceedings of the National Academy of Sciences,* 84 (15), pg. 5449–5453. https://doi.org/10.1073/pnas.84.15.5449.

© University of Pretoria

CHAPTER 2:

QSAR reveals decreased lipophilicity of polar residues determines the selectivity of antimicrobial peptide activity

This chapter has been published in ACS Omega, volume 9, June 2024, pages 26030-26049; **Van der Walt, M. (writing of article as first author, responsible for principal component analysis and QSAR analysis data, equally contributed to experimental work performed during training at King's College London (UK), including processing of physiochemical data used for PCA and QSAR analysis),** Möller, D.S. (contributed to writing of article as co-author, equally contributed to experimental work including processing of physiochemical data used for PCA and QSAR analysis), Van Wyk, R.J. (contributed to writing of article as co-author, equally contributed to experimental work including processing of physiochemical data used for PCA and QSAR analysis), Ferguson, P.M. (contributed to purification of 46 AMPs using RP-HPLC), Hind, C.K., Clifford, M., Do Carmo Silva, P. (screening of 46 peptides for antimicrobial and haemolytic activity), Sutton, J.M. (co-writer and editing, critical evaluation of the study and data interpretation), Mason, A.J. (communicating author, co-writer and editing, critical evaluation of the study and data interpretation), Bester, M.J. (co-supervisor of study, co-writer and editing, critical evaluation of the study and data analysis) and Gaspar, A.R.M. (study supervisor and communicating author, co-writer and editing, critical evaluation of the study and data analysis). This article appears as published, together with supplementary data, as Chapter 2 to form part of this thesis.

© University of Pretoria

ACS OMEGA

UNIVERSITEIT VAN PRETORIA
UNIVERSITY OF PRETORIA
YUNIBESITHI YA PRETORIA

Open Access

This article is licensed under CC-BY 4.0

http://pubs.acs.org/journal/acsodf

Article

QSAR Reveals Decreased Lipophilicity of Polar Residues Determines the Selectivity of Antimicrobial Peptide Activity

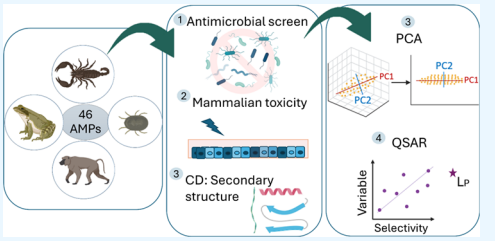
Mandelie van der Walt, Dalton S. Möller, Rosalind J. van Wyk, Philip M. Ferguson, Charlotte K. Hind, Melanie Clifford, Phoebe Do Carmo Silva, J. Mark Sutton, A. James Mason,* Megan J. Bester, and Anabella R. M. Gaspar*

Cite This: https://doi.org/10.1021/acsomega.4c01277

Read Online

ACCESS | Metrics & More | Article Recommendations | Supporting Information

ABSTRACT: Antimicrobial resistance has increased rapidly, causing daunting morbidity and mortality rates worldwide. Antimicrobial peptides (AMPs) have emerged as promising alternatives to traditional antibiotics due to their broad range of targets and low tendency to elicit resistance. However, potent antimicrobial activity is often accompanied by excessive cytotoxicity toward host cells, leading to a halt in AMP therapeutic development. Here, we present multivariate analyses that correlate 28 peptide properties to the activity and toxicity of 46 diverse African-derived AMPs and identify the negative lipophilicity of polar residues as an essential physiochemical property for selective antimicrobial activity. Twenty-seven active AMPs are identified, of which the majority are of scorpion or frog origin. Of these, thirteen are novel with no previously reported activities. Principal component analysis and quantitative structure−activity relationships (QSAR) reveal that overall hydrophobicity, lipophilicity, and residue side chain surface area affect the antimicrobial and cytotoxic activity of an AMP. This has been well documented previously, but the present QSAR analysis additionally reveals that a decrease in the lipophilicity, contributed by those amino acids classified as polar, confers selectivity for a peptide to pathogen over mammalian cells. Furthermore, an increase in overall peptide charge aids selectivity toward Gram-negative bacteria and fungi, while selectivity toward Gram-positive bacteria is obtained through an increased number of small lipophilic residues. Finally, a conservative increase in peptide size in terms of sequence length and molecular weight also contributes to improved activity without affecting toxicity. Our findings suggest a novel approach for the rational design or modification of existing AMPs to increase pathogen selectivity and enhance therapeutic potential.



1. INTRODUCTION

Antimicrobial resistance is a global health crisis with a severe impact on developing countries,[1] where infections due to drug resistance are difficult to treat, especially in patients with compromised immune systems.[2,3] Additional costs of prolonged hospitalization and medical expenses have placed a strain on healthcare systems.[4] This heightens the urgency in the search and development of new antimicrobial drugs, and antimicrobial peptides (AMPs) have emerged as promising drug candidates.

Cationic AMPs are found in the innate immune systems of a variety of living organisms. These peptides have bactericidal, fungicidal, antibiofilm, immunomodulatory, and anticancer properties[5−7] identifying AMPs as multifunctional peptides. The broad-spectrum activity,[5,6,8] superior pharmacodynamic properties,[7,9−12] and multifaceted bactericidal mechanisms[12,13] of AMPs are thought to lower the potential for drug resistance.

Despite these advantages, there are several drawbacks that hinder the breakthrough of AMPs into therapeutic use. Compared with antibiotics, AMPs tend to act against less specific targets, and this may cause a lack of selectivity.[14] A side effect of this is the potential lysis of mammalian cell membranes causing hemolysis or cytotoxicity in humans.[15,16] AMPs such as colistin, polymyxin B, and gramicidins have been approved for medical use but, due to toxic side effects, applications are limited.[14] Thus, engineering AMPs capable of selectively targeting microbial over mammalian cells is an important consideration in AMP therapeutic development.

Rational design is a current approach used in recent studies aimed at developing new or optimizing natural AMPs to improve antimicrobial efficacy.[7,18] Strategies include increasing the net positive charge to increase electrostatic interactions with microbial membranes, increasing peptide hydrophobicity to promote membrane insertion, or combining both strategies to increase peptide amphipathicity.[17] While these strategies may enhance antimicrobial activity, microbial over mammalian selectivity is generally harder to address, leaving mammalian cell toxicity unresolved and hindering therapeutic application. Thus, for the successful rational design of effective and

Received: February 8, 2024
Revised: May 15, 2024
Accepted: May 20, 2024

Downloaded via 92.18.251.191 on June 3, 2024 at 16:31:18 (UTC).
See https://pubs.acs.org/sharingguidelines for options on how to legitimately share published articles.

© XXXX The Authors. Published by American Chemical Society

© University of Pretoria

UNIVERSITEIT VAN PRETORIA
UNIVERSITY OF PRETORIA
YUNIBESITHI YA PRETORIA

selective AMPs, it is essential to understand the sequence-driven features that confer not only target efficacy but also selectivity.

Molecular and experimentally determined properties aid in describing the relationship between the peptide structure and antimicrobial potency. In addition to charge and hydrophobicity, Krauson et al., Mai et al., and Li et al. consider peptide secondary structure and helicity as essential parameters for antimicrobial success,[18−20,62,63] while others report AMP size and sequence length as important determinants.[17,21] Due to the many parameters involved in the structure−activity relationships of AMPs, rational design, and optimization strategies often contain exceptions and contradictions, making it difficult to establish standard criteria.

The increase in information on AMP structure and function has contributed to the development of in silico chemo-informatic tools to analyze the structure−function relationships of peptides. This is useful in summarizing multidimensional data sets to find consistencies among variables.[22] This approach can then be used to analyze the activity and selectivity of AMPs by focusing on AMP structure which in turn is defined by numerical physiochemical properties.[23] Here, multivariate methods such as principal component analysis (PCA) and quantitative structure−activity relationship (QSAR) correlations are used to identify and then summarize the structural parameters of 46 AMPs with the aim of potentially simplifying future drug design and development.

Briefly, PCA reduces the dimensionality of a data set by transforming the input variables into reduced, linear groups called principal components (PCs).[24] The PCs that show the largest variations indicate the relationships that exist in the multivariate data set, which were not initially observed in the input data. The first few PCs summarize the properties responsible for most of the variation.[24] QSAR is a mathematical model that quantitatively relates a numerical measure of chemical structure e.g., a physiochemical property to a biological effect e.g., antimicrobial activity or toxicity.[25] This type of analysis is gaining increased acceptance by medicinal researchers and related fields due to its ability to prioritize ideas in lead optimization and increase the rate of drug discovery.[26]

Although PCA analysis has not yet been featured regularly, QSAR multivariate methods have been used in previous studies involving AMPs. Ostberg and Kaznessis[27] performed an extensive QSAR study on the antimicrobial, hemolytic, and cytotoxic effects of 62 AMPs derived from protegrins. The study included molecular descriptors that were correlated with activity against four Gram-negative, one Gram-positive bacteria, and one fungus. The complexity and vast amount of data made the results difficult to interpret without clear guidelines for future peptide design. Frecer[28] quantitatively analyzed the antimicrobial and hemolytic activities of 97 cyclic AMPs, derived from Protegrin-1, by making use of simple additive molecular properties. QSAR modeling correlated antimicrobial potencies of cyclic peptides to charge and amphipathicity, while the lipophilicity of residues forming the nonpolar face correlated with increased hemolysis.[28]

The current study focuses on a new group of more diverse, linear AMPs that were identified in various African species. A total of 46 AMPs, of which 27 are novel or have unknown activity, were subjected to antimicrobial screening against a large panel of eight Gram-negative, four Gram-positive bacteria, and six fungi, including susceptible and resistant strains. Cytotoxicity was evaluated against human erythrocytes and immortalized keratinocytes. The secondary structures of each AMP in Tris buffer, as well as three different membrane-mimicking environments, were determined with circular dichroism (CD) spectroscopy. CD conformation together with molecular parameters such as charge, length, mass, lipophilicity, hydrophobicity, etc. of the diverse group of peptides allowed for conclusive, wide-spectrum PCA and QSAR analyses.

2. MATERIALS AND METHODS

2.1. Peptide Selection and Modification. At first, 116 AMP candidates were identified in indigenous African species including scorpions, frogs, ticks, and primates using the Antimicrobial Peptide Database (APD3), the Data Repository of Antimicrobial Peptides (DRAMP), the Collection of Antimicrobial Peptides ($CAMP_{R3}$) and other published sources. The list was reduced by selecting only short peptides of 25 amino acids or less in length to ensure cost-effective synthesis and screening. From large sequences, shorter sequences were identified using $CAMP_{R3}$ prediction of antimicrobial regions within peptides. Amino acid sequences from 8 to 22 amino acids with increments of 2 amino acids were screened for predicted activity. Sequences with AMP prediction >0.95 (SVM, Random Forest, Discriminant Analysis) were selected and from these the shortest sequences with the highest charge (although not necessarily a predictor of activity), and not previously identified using DRAMP and APD3 were selected. This resulted in a total of 55 peptides. Furthermore, only the analogues derived from parent peptides with validated activity against *Escherichia coli* were included. Peptides that are under clinical investigation such as magainin[29] or already extensively researched and/or patented (identified with DRAMP) were removed from the list. To increase positive charge, several of these peptides were amidated, resulting in the final 46 peptides (Table 1).

Frog peptides such as Xenoxin-1, DRAMP02272a, or the large Caerulein peptides of *Xenopus petersii* and *X. muelleri* previously showed promising antibacterial and antifungal activity.[30−32] From these parent peptides, shorter sequences like DRAMP02273a, the xenopsin-precursor fragments (XPFs), or Caerulein-precursor fragments (CPFs) were derived and included in the study. For comparative purposes, some larger peptides were also included such as CPF-P2, CPF-P3, and CPF-MW1.

Scorpion peptides such as Opistoporin 1 or 2 (Opis1 or 2) and Parabutoporin (PBP) from the venom of the South-African *Opistophthalmus carinatus* or *Parabuthus schlechteri* species previously showed potent antibacterial activity, especially against Gram-negative bacteria.[33] For this study, shorter derivatives with predicted activity such as Opis16a and Opis8a based on the sequence of Opis1 or PS-PB-8a, PS-PB-14a, PS-PB-16a and PS-PB-20a based on PBP, were included. Three synthetic derivatives of the broad-spectrum *Androctonus amoreuxi* scorpion peptide, AamAP1, namely, AamAP-S1, A3, and AamAP1-Lys[34−37] as well as their novel amidated forms were included in the study. Lastly, derivatives such as K3-IsCTa, K7P8K11-IsCTa, and A1F5K11-IsCTa[38,39] from the potent *Opisthacanthus madagascariensis* scorpion peptide, IsCT, were added to the list of 16 scorpion peptides.

Eleven AMPs screened for antimicrobial activity originate from African tick species such as *Ornithodoros savignyi* and *O. moubata*. Research by Ismail et al.[40] showed anti-Gram-positive

© University of Pretoria
https://doi.org/10.1021/acsomega.4c01277
ACS Omega XXXX, XXX, XXX−XXX

Table 1. Physiochemical Properties of 46 AMPs Derived from Sequences Identified in African Frog, Scorpion, Tick, and Primate Species[a]

	species	peptide	sequence	MW (g/mol)	length; charge	ElutionTime (min)[b]	L[c]	SCSA (Å)[d]	HBtot[e]
frogs	*Xenopus laevis* (Southern Africa)	XPF	GWASKIGQTLGKIAKVGLKELIQPK	2664	25; +4	45,8	7.85	1245,9	30
		XPF10a^{N}	LGKIAKVGLK-NH_2	1025	10; +4	22	3.76	511,8	9
		DRAMP02272a	GMASKAGAIAGKIAKVALKAL-NH_2	1968	21; +5	44	7.62	658,2	15
		DRAMP02273a	KIAKVALKAL-NH_2	1053	10; +4	28	4.38	472,6	9
		X1−20a*,^{N}	KCLTLRSLKKTLKFCASGRT-NH_2	2254	20; +7	31,7	6.70	1057,4	36
	Xenopus petersii (Southern Africa)	CPF-P2	GLASFLGKALKAGLKIGSHLLGGAPQ	2505	27; +3	50,5	12.39	1085,9	26
		CPF-P2a^{N}	FLGKALKAGLKIGSHL-NH_2	1652	16; +4	33	8.13	1085,9	26
		CPF-P3	GFGSFLGKALKAALKIGANVLGGAPQQ	2614	27; +3	54,3	11.62	1081,9	25
		CPF-P3−10a^{N}	KALKAALKIG-NH_2	1011	10; +4	22,7	3.16	421,5	9
		CPF-P3−12a^{N}	KALKAALKIGAN-NH_2	1196	12; +4	26	2.87	516,4	12
		CPF-P3−20a^{N}	GKALKAALKIGANVLGGAPQ-NH_2	1876	20; +4	35,5	6.60	729,2	20
	Xenopus muelleri (Central/Southern Africa)	CPF-MW1	GLGSLLGKAFKFGLKTVGKMMGGAPREQ	2879	28; +4	46,6	8.14	1279,3	33
		CPF-MW-10a^{N}	KAFKFGLKTV-NH_2	1137	10; +4	24,9	4.10	602,7	11
		CPF-MW-12a^{N}	KAFKFGLKTVGK-NH_2	1323	12; +5	25	3.11	693,4	14
		CPF-MW-20a^{N}	GKAFKFGLKTVGKMMGGAPR-NH_2	2081	20; +6	32,5	5.48	909,6	26
scorpions	*Parabuthus schlectheri* (Southern Africa)	PS−PB-8a^{N}	WKSKLAKK-NH_2	987	8; +5	14	0.26	560,9	15
		PS−PB-14a^{N}	KKAWKSKLAKKLRAKGK-NH_2	1968	17; +10	22	−2.39	994,1	32
		PS−PB-16a^{N}	GSFLKKAWKSKLAKKL-NH_2	1832	16; +7	28,8	3.74	981,4	23
		PS−PB-20a^{N}	GSFLKKAWKSKLAKKLRAKG-NH_2	2245	20; +9	29	2.05	1092,2	31
	Opistophthalmus carinatus (Southern Africa)	Opis16a^{N}	GKVWDWIKSTAKKLWN-NH_2	1959	16; +4	41,2	4.87	1134,9	14
		Opis8a^{N}	WIKSTAKK-NH_2	960	8; +4	15	1.61	513,5	24
	Androctonus amoreuxi (North Africa)	AamAP1	FLFSLIPHAIGGLISAFK	1931	18; +1	50	16.27	911,8	14
		AamAP-S1	FLFSLIPKAIGGLISAFK	1922	18; +2	52,3	15.15	926,8	15
		AamAP-S1a^{N}	FLFSLIPKAIGGLISAFK-NH_2	1921	18; +3	55	15.15	926,8	15
		AamAP1-Lys	FLFKLIPKAIKKLISKFK	2162	18; +6	45,5	10.92	1282,5	25
		AamAP1-Lys-a^{N}	FLFKLIPKAIKKLISKFK-NH_2	2162	18; +7	43	10.92	1282,5	25
		A3	FLFSLIRKAIGGLISAFK	1981	18; +3	53	13.42	926,8	15
		A3a^{N}	FLFSLIRKAIGGLISAFK-NH_2	1980	18; +4	58	13.42	926,8	15
	Opisthacanthus madagascariensis (Madagascar)	K3-IsCTa	ILKKIWEGIKSLF-NH_2	1575	13; +3	46,8	7.54	918,7	14
		K7P8K11-IsCTa	ILGKIWKPIKKLF-NH_2	1584	13; +5	38	9.60	960,8	18
		A1F5K8-IsCTa	ALGKFWEKIKSLF-NH_2	1567	13; +3	46,1	6.04	854,5	14
ticks	*Ornithodoros savignyi* (Southern Africa)	Os*	KGIRGYKGGYCKGAFKQTCKCY	2460	22; +6	24,7	5.48	1169,5	37
		Osa*,^{N}	KGIRGYKGGYCKGAFKQTCKCY-NH_2	2459	22; +7	24,5	5.48	1169,5	37
		Os-C	KGIRGYKGGYKGAFKQTKY	2150	19; +6	21,8	0.86	1056,7	31
		Os(3−12)a	IRGYKGGYCK-NH_2	1143	10; +4	17	2.27	531,1	17
		Os(11−22)a*	CKGAFKQTCKCY-NH_2	1379	12; +4	21,3	4.75	676	22
		W3(Os-C)a	WWWKGIRGYKGGYKGAFKQTKY-NH_2	2709	22; +6	31	7.61	1420	34
		W(Os-C)a^{N}	WKGIRGYKGGYKGAFKQTKY-NH_2	2336	20; +7	25	3.11	1177,8	32
	Ornithodoros moubata (Southern Africa)	OmDefB*,^{N}	RGIRGYKGGYCTGRFKQTCKCY	2546	22; +6	25	5.39	1131,9	43
		OmDefB19^{N}	RGIRGYKGGYTGRFKQTKY	2237	19; +6	20	0.77	1019,1	37
		W-OmC-Ca	WSGIRGYKGGYKGLFKQTNY-NH_2	2323	20; +5	29,5	5.84	1227,1	31
		W-OmB-Ca^{N}	WRGIRGYKGGYTGRFKQTKY-NH_2	2422	20; +7	25	3.02	1140,2	38

© University of Pretoria

https://doi.org/10.1021/acsomega.4c01277
ACS Omega XXXX, XXX, XXX−XXX

UNIVERSITEIT VAN PRETORIA
UNIVERSITY OF PRETORIA
YUNIBESITHI YA PRETORIA

UNIVERSITEIT VAN PRETORIA
UNIVERSITY OF PRETORIA
YUNIBESITHI YA PRETORIA

Table 1. continued

	species	peptide	sequence	MW (g/mol)	length; charge	ElutionTime (min) [b]	L [c]	SCSA (Å)^2 [d]	HBtot [e]
primates	*Papio anubis/Papio ursinus* (Africa)	ThetaDefA*,U	RCVCTRGFC	1044	9; +2	22	5.87	380,3	18
		ThetaDefB*,U	RCVCRRGVC	1051	9; +3	20	4.60	334.1	21
		BTD11a*,N	RRGVCRCVCRR-NH_2	1363	11; +6	16	2.01	413.5	31
		BTD15a*,N	RCVCRRGVCRCVCRR- NH_2	1824	15; +7	20	5.30	579.5	40

[a]* – AMPs containing more than one cysteine residue were evaluated in their reduced forms throughout the study. N – Novel derivative. U – Unknown antimicrobial activity. [b]This is the retention time for the major fraction collected during semipreparative HPLC of each peptide supplied at c 80% purity. [c]The sum of the lipophilicity of the constituent amino acids of the peptides was determined from Frecer[28] calculated using $\pi_{FP} = \log P_{o/w}(a.a.) - \log P_{o/w}(Gly)$ (Suppl. Table S1). [d]The sum of the side chain surface areas (SCSA) of the constituent amino acids of the peptides were determined from Frecer[28] as calculated from the Connolly surfaces method[46] (Suppl. Table S1). [e]The sum of the hydrogen bond acceptors and donors calculated using in house scripts (Suppl. Table S1).

and -negative activity for the defensin-derived Os, Os(3−12), and Os(11−22) peptides with negligible erythrocyte hemolysis. Amidated forms of these derivatives were included in the current study. From *O. moubata* three defensins have been identified namely OmDefA, OmDefB, and OmDefC, with similar activities against Gram-positive bacteria.[41,42] To increase antimicrobial activity, analogues with higher charges or those that are carboxy-amidated were included in this study.[43] Trp residues, especially at the N-termini, are known to drive the interaction of an AMP with the lipid core of bilayers through hydrophobic forces and are likely also responsible for increased activity.[44] Tryptophan residues were added to the N-termini of several tick-derived analogues, and amidated versions were included.

In their study on primate AMPs, Garcia et al.[45] predicted 10 theoretical cyclic θ-defensins, BTD-1 to BTD-10. BTD-2 had the most promising antimicrobial activity in vitro. Shorter linear sequences BTD15a and BTD11a contained within the cyclic peptide sequence have been identified and amidated for this study. Two other derivatives, ThetaDefA and ThetaDefB, the nine residues on the N-terminus or the C-terminus of BTD-1, are included in this study with an aim to identify the active region of the parent peptide.

2.2. Peptide Synthesis and Purification. A total of 46 peptides were supplied by Cambridge Research Biochemicals (Cleveland, UK) at ∼80% purity. They were further purified using water/acetonitrile gradients in reverse-phase high-performance liquid chromatography (RP-HPLC) on a Waters SymmetryPrep C8, 7 mm, 19 × 300 mm column.

Crude peptides, made up to 10 mg/mL in 0.1% TFA (v/v) in ddH_2O, were subjected to preparative RP-HPLC purification on an Agilent 1100 system, with elution in gradient. A gradient program at a flow rate of 8 mL/min and column temperature of 25 °C was used to achieve elution with solvent A (0.1% trifluoroacetic acid (TFA) in water (v/v)) and solvent B (0.1% TFA in 100% acetonitrile (ACN) (v/v)). The elution program was as follows: (1) At 0−73 min, 100% solvent A to 0% solvent B; (2) at 73−77 min, 40% solvent A to 60% solvent B; (3) at 77−93 min, 10% solvent A to 90% solvent B; (4) at 93−105 min, 100% solvent A to 0% solvent B. Data collected were the retention time of the major fraction for each peptide in minutes as RP-HPLC ElutionTime (ElutionTime). Absorbance was detected at 254 nm, and fractions were collected manually. The fractions collected were spun in a speed-vac to remove ACN and the contents lyophilized. After freeze-drying for 24 h the peptides were dissolved in 10% (v/v) acetic acid before being lyophilized for a second time and then stored at −20 °C.

2.3. Antimicrobial Activity against a Panel of Sensitive and Resistant Pathogens. Antimicrobial activity was evaluated against a panel of 18 pathogens consisting of eight Gram-negative strains (*E. coli* NCTC 12923, *E. coli* LEC001, *Pseudomonas aeruginosa* PAO1, *P. aeruginosa* NCTC 13437, *Acinetobacter baumannii* ATCC 17978, *A. baumannii* AYE, *Klebsiella pneumoniae* M6, *K. pneumoniae* NCTC 13368), four Gram-positive strains (*Staphylococcus aureus* ATCC 9144, *S. aureus* NCTC 13616, *S. aureus* USA300, *S. aureus* 1199B) and six fungi (*Candida auris* TDG 1912, *C. albicans* NCPF 8018, *C. krusei* NCPF 3876, *C. tropicalis* NCPF 8760, and *C. parapsilosis* NCPF 3209). Pathogens were grown in noncation adjusted Mueller Hinton broth (MHB, for bacteria) or Roswell Park Memorial Institute (RPMI 1640) + 2% glucose (for fungi) at 37 °C with 180 rpm shaking and maintained on solid

© University of Pretoria
https://doi.org/10.1021/acsomega.4c01277
ACS Omega XXXX, XXX, XXX−XXX

UNIVERSITEIT VAN PRETORIA
UNIVERSITY OF PRETORIA
YUNIBESITHI YA PRETORIA

media (tryptic soy agar for bacteria and Sabouraud dextrose agar for fungi). For an antibiogram, see Suppl. Table S2.

The 46 peptides were serially diluted (128 to 2 μg/mL) in media down polypropylene 96-well plates. Bacteria or fungi, diluted from an overnight culture to an OD_{600} of 0.01, were added to the serially diluted peptides at a 1:1 ratio resulting in a starting cell density of $\sim 5 \times 10^5$ CFU/mL. Plates were incubated at 37 °C for 20 h, and the optical density was determined spectrophotometrically at 600 nm. Minimum inhibition concentrations (MICs) were determined from a minimum of three biological repeats and are reported in μg/mL as well as μM. The MIC is defined as the lowest concentration that resulted in pathogen growth of <0.1 above the background absorbance. The MIC_{50} or MIC_{90} is defined as the lowest peptide concentration that results in 50% or 90% growth inhibition over a 20 h treatment period, respectively.

2.4. In Vitro Hemolytic Activity. Potential erythrocyte hemolysis was tested by incubating serial dilutions of the AMPs in PBS with freshly collected erythrocytes at a ratio of 1:1 in 96-well polypropylene V-shape plates for 1 h at 37 °C. Control wells were treated with 0.1% Triton-X-100 to ensure complete lysis or PBS-only to represent no lysis. The erythrocytes were collected by centrifugation and the OD_{550} of the supernatant was measured using a plate reader. The percentage hemolysis was calculated as

$$\text{Hemolysis}\ (\%) = 100 - 100\left(\frac{A_{\text{peptide}} - A_{\text{blank}}}{A_{\text{growth control}} - A_{\text{blank}}}\right) \quad (1)$$

where A_{peptide} is the absorbance value of erythrocytes exposed to a known peptide concentration, $A_{\text{growth control}}$ is the absorbance of erythrocytes exposed to 0.1% Triton-X-100 and A_{blank} is the absorbance of erythrocytes exposed to the PBS. The concentrations at which a peptide caused 10% (HC_{10}) and 50% (HC_{50}) hemolysis was determined from the dose response curves.

2.5. In Vitro HaCat Cytotoxicity. The HaCat cell line (Cellonex, South Africa) was cultured in Dulbecco's Modified Eagle Medium (DMEM) supplemented with 10% heat-inactivated fetal calf serum (FCS) and 1% antibiotic-antimycotic (Abs) and maintained at 5−10% CO_2, 37 °C, 95% humidity. For cytotoxicity screening, 5.56×10^4 cells/mL were plated in a 96-well plate. After 24 h incubation, the cells are initially exposed to each peptide at a concentration of 256 μg/mL or 0.1% Triton-X-100 as the control for 21 h. If cytotoxicity was observed, at a level of significance of $p < 0.0001$ compared with the untreated control after 21 h, a dose-response assay was undertaken. Cell viability was determined by adding 10% 3-(4,5-dimethyl-2-thiazolyl)-2,5-diphenyl-2H-tetrazolium bromide (MTT) (1 mg/mL), to each well and after a further 3 h incubation the media was discarded, and the formazan crystals dissolved by adding 25% DMSO in ethanol. The absorbance was measured at OD_{570} by using the FLUOstar Omega multidetection microplate reader (BMG Labtech). Percentage cell viability was calculated relative to the untreated control. The LC_{50} was defined as the concentration of AMP treatment that results in 50% lethality of HaCat cells and was determined from the dose-response curves.

2.6. Circular Dichroism Spectroscopy. Far-UV CD spectra of the peptides (50 μM) were obtained in Tris buffer (5 mM, pH 7.4), sodium dodecyl sulfate (SDS) micelles (50 mM prepared in 5 mM Tris, pH 7.4), and in the presence of small unilamellar vesicles (SUVs) using a Chirascan and a ChriscanPlus spectrometer (Applied Photophysics, Leatherhead, UK). For the preparation of SUVs, 1-palmitoyl-2-oleoyl-*sn*-glycero-3-phospho-(1′-rac-glycerol) (POPG) and 1-palmitoyl-2-oleoyl-*sn*-glycero-3-phosphoethanolamine (POPE) purchased from Avanti Polar Lipids, Inc. (Alabaster, AL) were used without any purification. The lipid powders were solubilized in chloroform and dried under rotor evaporation. To completely remove the organic solvent, the lipid films were left overnight under a vacuum and hydrated in 5 mM Tris buffer (pH 7.4). The lipid suspension was subjected to five rapid freeze−thaw cycles for further sample homogenization. POPE/POPG (75:25, mol:mol) and POPG SUVs were obtained by sonicating the lipid suspensions on Soniprep 150 (Measuring and Scientific Equipment, London, UK) for 2 × 5 min with an amplitude of six micrometers in the presence of ice to avoid lipid degradation. The SUVs were stored at 4 °C and used within 5 days of preparation.

CD spectra were recorded from 260 to 180 nm at a constant temperature of 296.15 K, a bandwidth of 2 nm, a step size of 1 nm, and a path length of 0.5 mm. The POPE/POPG or POPG SUV suspensions at a final concentration of 5 mM were used to dissolve the peptides to give a final peptide concentration of 50 μM. The same experimental conditions were used to investigate the peptide secondary structure in 5 mM Tris and 50 mM SDS micelles. For data processing, a spectrum of the peptide-free Tris solution, SDS solution, or lipid suspension was subtracted and Savitsky−Golay smoothing with a convolution width of 4 points was applied.

Peptide structures were quantitatively and qualitatively identified by examining the CD spectra and mean residue molar ellipticities (MRME, $[\theta]$, deg cm^2 dmol^{-1}). Peptides with a higher tendency to form a typical α-helical structure were identified by a positive band at ~190 nm and two negative ellipticity minima around 208 and 222 nm[47,48] (Table 2). Peptides with a tendency to form β-sheeted structures were identified by a positive ellipticity maximum at 195 nm and one negative ellipticity minimum at 215 nm. Similarly, a peptide with a positive ellipticity maximum at ~205 nm and a minimum between 222−230 nm was identified to have a higher tendency to form a β-turn type I structure.[47] Increased MRME intensity at the negative bands indicates a higher tendency of the peptide to form ordered structures. Lastly, CD spectra with no positive bands were identified as disordered structures.[49−51]

2.7. PCA. Principal component analysis (PCA) is a method that reduces higher dimensional data to lower dimensional data while preserving the most important information. This is achieved by replacing the variables in a data set with a smaller number of derived variables.[52] The goal of PCA was to extract a number of principal components (PCs) that can be used as clustering variables.

PCA was performed for all 46 peptides using JMP 17.0.0 software. The data matrix consisted of 46 samples (i.e., peptides) and 28 peptide molecular variables per pathogen group. Each column is centered and standardized individually, and PCs are calculated based on the Pearson correlation matrix. The overall antimicrobial potency of each peptide against each pathogen group (Gram-negative and -positive bacteria as well as fungi) was obtained by averaging the MIC values over the panel of strains tested.

To assess the correctness of PCA for the interpretation of the data sets, Bartlett's test of sphericity was performed, where the null hypothesis (H_0) states that there are no significant

© University of Pretoria
https://doi.org/10.1021/acsomega.4c01277
ACS Omega XXXX, XXX, XXX−XXX

Table 2. CD Spectroscopy MRME Intensities of 46 African-Derived AMPs Elucidate the Predominant Secondary Structures Present in SDS, POPG, or POPG/POPE Liposomes[a]

		SDS				POPG				POPG/POPE			
species	peptide	λ of + $[\theta]$ (nm)[b]	$[\theta]_{207-215}$	$[\theta]_{218-230}$	predominant structure	λ of + $[\theta]$ (nm)[b]	$[\theta]_{207-215}$	$[\theta]_{218-230}$	predominant structure	λ of + $[\theta]$ (nm)[b]	$[\theta]_{207-215}$	$[\theta]_{218-230}$	predominant structure
frogs	XPF	191	−16087,3	−12730	α-helix	188	−15537,8	−15368,4	α-helix	191	−20857,8	−17786,7	α-helix
	XPF10a				disordered				disordered				disordered
	DRAMP02272a	191	−22372,2	−18563	α-helix	187	−16645,4	−18315,5	α-helix	190	−22234,8	−20072,1	α-helix
	DRAMP02273a	189	−10960,2	−5227,58	α-helix	188	−10823,6	−6096,34	α-helix	190	−12172,1	−5727,87	α-helix
	X1−20a	191	−11762,2	−10837,6	α-helix	197	−17718.7		β-sheet	193	−12131,2	−9901,79	α-helix
	CPF-P2	191	−11370,6	−9750,67	α-helix	189	−15114,6	−13831,7	α-helix	191	−27693,3	−24540,2	α-helix
	CPF-P2a	191	−10661,7	−7410,17	α-helix	186	−17674,1	−15410,2	α-helix	189	−14419,8	−11214,2	α-helix
	CPF-P3	192	−17908	−15106,1	α-helix	192	−15273,5	−13510,8	α-helix	192	−16291	−14066,2	α-helix
	CPF-P3-10a				disordered	197	−11718.3		β-sheet				disordered
	CPF-P3-12a				disordered	193	−4755.56		β-sheet				disordered
	CPF-P3-20a	191	−16959,1	−13504,2	α-helix	190	−17202	−14925,6	α-helix	191	−13974,2	−10927,9	α-helix
	CPF-MW1	191	−16090,9	−14897,4	α-helix	191	−17516,5	−17929	α-helix	190	−21024	−19769,6	α-helix
	CPF-MW-10a				disordered				disordered				disordered
	CPF-MW-12a				disordered	198	−3847.47		β-sheet				disordered
	CPF-MW-20a	191	−11091,2	−9544,57	α-helix	191	−3973.63		β-sheet	187	−11802,6	−8513,79	α-helix
scorpions	PS-PB-8a				disordered				disordered				disordered
	PS-PB-14a	191	−11466,1	−10672,9	α-helix	189	−14020	−11913,8	α-helix	189	−11898,7	−8431,4	α-helix
	PS-PB-16a	191	−12721,5	−7759,48	α-helix	189	−11801,8	−8608,36	α-helix	188	−12830,9	−7113,86	α-helix
	PS-PB-20a	191	−12815,3	−8142,95	α-helix	195	−12897,6	−9317	α-helix	191	−42170,4		P-II/α-helix
	Opis16a	192	−25651	−20167,6	α-helix	190	−20930,3	−15307,2	α-helix	188	−25929,2	−19734	α-helix
	Opis8a				disordered				disordered				disordered
	AamAP1	194	−9593,38	−9199,36	α-helix	192	−5013,64	−4705,86	α-helix	195	−4428,61	−4221,84	α-helix
	AamAP-S1	194	−12965,5	−12586,2	α-helix	192	−13047,3	−12862,1	α-helix	191	−13175,9	−13149,1	α-helix
	AamAP-S1a	193	−14571,1	−14745,9	α-helix	194	−14457,8	−14909,5	α-helix	194	−18872	−18677,2	α-helix
	AamP1-Lys	194	−14778,4	−14640,6	α-helix	190	−9234,91	−10738,3	α-helix	190	−12204,7	−11286,9	α-helix
	AamP1-Lysa	194	−14569,5	−14209,1	α-helix	195	−14491,8	−14824,9	α-helix	195	−13900,6	−13409,3	α-helix
	A3	193	−20899,3	−16918,5	α-helix	194	−18896,2	−20397	α-helix	191	−16406,4	−16536,2	α-helix
	A3a	192	−17674,8	−15326,7	α-helix	190	−6069,55	−6266,98	α-helix	194	−17351,6	−16210	α-helix
	K3-IsCTa	193	−14176,5	−9122,25	α-helix	190	−21973,5	−15284,4	α-helix	188	−20182	−14588,9	α-helix
	K7P8K11-IsCTa	194	−6578,13	−5694,38	α-helix	188	−6955,99	−7397,42	α-helix	189	−7209,07	−7240,37	α-helix
	A1F5K8-IsCTa	194	−12642,8	−7083,27	α-helix	188	−13386,5	−8670,74	α-helix	189	−14724,9	−10264,6	α-helix
ticks	Os	196	−2335,81	−1725,27	α-helix	189	−4350,35	−3789,7	α-helix	204		−2458,25	β-turn type I
	Osa	194	−4487,05	−4216,23	α-helix	193	−2114,6	−1968,74	α-helix	195	−2417,51	−2338,34	α-helix
	Os-C				disordered	197	−905.33		β-sheet				disordered
	Os(3−12)a				disordered				disordered				disordered
	Os(11−22)a	191	−6391,03		β-sheet	195	−7768,55		β-sheet	195	−6159,43		β-sheet
	W3(Os-C)a				disordered				disordered				disordered
	W(Os-C)a				disordered				disordered				disordered
	OmDefB				disordered				disordered				disordered
	OmDefB19				disordered				disordered				disordered

© University of Pretoria

https://doi.org/10.1021/acsomega.4c01277
ACS Omega XXXX, XXX, XXX−XXX

UNIVERSITEIT VAN PRETORIA
UNIVERSITY OF PRETORIA
YUNIBESITHI YA PRETORIA

UNIVERSITEIT VAN PRETORIA
UNIVERSITY OF PRETORIA
YUNIBESITHI YA PRETORIA

Table 2. continued

		SDS				POPG				POPG/POPE			
species	peptide	λ of + $[\theta]$ (nm)[b]	$[\theta]_{207-215}$	$[\theta]_{218-230}$	predominant structure	λ of + $[\theta]$ (nm)[b]	$[\theta]_{207-215}$	$[\theta]_{218-230}$	predominant structure	λ of + $[\theta]$ (nm)[b]	$[\theta]_{207-215}$	$[\theta]_{218-230}$	predominant structure
primate	W-OmC-Ca				disordered	192	−6508,76	−9435,85	α-helix				disordered
	W-OmB-Ca				disordered				disordered				disordered
	ThetaDefA				disordered				disordered				disordered
	ThetaDefB				disordered				disordered				disordered
	BTD11a				disordered				disordered				disordered
	BTD15a	185	−7204,69	−6479,47	α-helix	195	−1616.22		β-sheet	193	−6404.7		β-sheet

[a]All CD spectra are shown in Suppl. Figures S3−S6. MRME intensities are not calculated for CD spectra obtained in Tris buffer (5 mM) as all peptides adopted disordered conformations in this environment. [b]Indicates the wavelength in nanometres where a positive MRME maximum is recorded.

correlations between the variables in a data matrix, i.e., all correlation coefficients are <0.1 (Suppl. Table S13). This indicates that if the value for one variable is known, it cannot be used to predict the value of another variable. An alternative hypothesis (H_A) is in contradiction to H_0 stating that there is a correlation between variables. Thus, rejection of H_0 would confirm the correctness of PCA application in this study.[55]

2.8. Quantitative Structure−Activity Relationship Analysis. Molecular descriptors used in the QSAR analysis included: charge, sequence length, overall lipophilicity (L), lipophilicity contributed by the polar or nonpolar residues (L_P and L_N), summation of the side chain surface areas of the total peptide, polar or nonpolar residues (SCSA, $SCSA_P$, and $SCSA_N$), the molecular weight of the entire peptide, polar or nonpolar residues (Mw, MwP, and MwN), count of small lipophilic residues (CSL) or aromatic residues (CAR), the total number of hydrogen bond donor and acceptor centers (HBtot, HBdon, and HBacc), the total number of rotatable bonds (#RotBonds) and various amphipathicity descriptors (L_P/L, L_P/L_N, L/L_N, Q/L, Q/L_N, $SCSA_P/SCSA_N$, MwP/MwN, Q/CSL, and Q/CAR) (Suppl. Table S1). Experimentally determined characteristics included ElutionTime as an indicator of overall peptide hydrophobicity and the CD structure of each peptide determined in POPG/POPE lipids representing Gram-negative membranes, POPG lipids for Gram-positive membranes, and SDS micelles for fungal membranes. AMPs with an α-helical structure were labeled 4, β-sheets were labeled 3, β-turns and mixed conformations were labeled 2, and disordered structures were labeled 1.

The molecular charge was calculated as the sum of qi, where qi is the formal charge of a residue at pH 7, which depends on the side chain pK_a constant.[53] Lipophilicity parameters, L, L_P, and L_N, were defined by the residue side chain lipophilicity parameter, πFP, described by Frecer[28] and Fauchere and Pliska,[54] as a total of all the residues of the peptide (L) or only the contribution of the polar (P) or nonpolar (N) residues. The πFP parameter represents the difference between the experimental partitioning coefficients in the n-octanol/water system, log $P_{o/w}$, of a given amino acid and glycine:

$$\pi\mathrm{FP} = \log P_{o/w}\ (\text{a. a. }) - \log P_{o/w}\ (\mathrm{Gly}) \quad (2)$$

Lipophilicity parameters, L, L_P, and L_N, calculated with the more recent Wimley−White bilayer/water scale[76] were also assessed to determine the robustness of the QSAR to different lipophilicity scales (Suppl. Table S15).

The surface areas of the peptide describe the bulkiness due to the residue side chains and were obtained from Frecer[28] that used the Connolly surface calculation method.[46] Molecular weights of the analogues (Mw, MwP, and MwN) were calculated as the sum of the relevant residue contributions. The count of CSL within the nonpolar face was also considered. Amphipathicity descriptors were defined as the ratio of certain molecular properties. Peptide flexibility was expressed as the total number of rotatable bonds in the residue side chains obtained with Shrodinger-Maestro version 13.1 released 2022-1. #RotBonds = sum of all the R.B.i, where R.B.i is the number of rotatable bonds in an amino acid side chain: R.B.i = R.B.(a.a.) - R.B.(Gly).

A Pearson correlation between the molecular descriptors and the average MIC per peptide was determined for Gram-negative, Gram-positive, and antifungal activity as well as cytotoxic activity against HaCat cells by using multivariate correlations in JMP 17.0.0 software and row-wise estimation.

© University of Pretoria
https://doi.org/10.1021/acsomega.4c01277
ACS Omega XXXX, XXX, XXX−XXX

UNIVERSITEIT VAN PRETORIA
UNIVERSITY OF PRETORIA
YUNIBESITHI YA PRETORIA

The Pearson product-moment correlation coefficient measures the strength of the linear relationship between the two variables. For response variables X and Y, it is denoted as r and computed as follows:

$$r = \frac{\sum (x - \overline{x})(y - \overline{y})}{\sqrt{\sum (x - \overline{x})^2} \sqrt{\sum (y - \overline{y})^2}} \quad (3)$$

If there is an exact linear relationship between two variables, the correlation is 1 or −1, depending on whether the variables are positively or negatively related. If there is no linear relationship, then the correlation tends toward zero. In this study, the data matrix consisted of 46 samples (i.e., peptides) and the 28 molecular/experimental descriptors described earlier.

2.9. Activity Data and Statistical Analysis. Triplicate dose-response assays with three technical repeats each were performed per peptide against the target pathogens. All data analyses were performed using GraphPad Prism V 7.0 software (San Diego, CA, USA). The selectivity indices (SI) were determined by ratios of LC_{50}/MIC. Statistical analyses were performed by determining Row totals/means with standard deviation (SD) or standard error of the mean (SEM) followed by One-way analysis of variance (ANOVA) with Dunnett's multiple/selected comparison post-test.

3. RESULTS

3.1. Novel African-Derived AMPs Show Promising Antimicrobial Activity In Vitro. AMP potency was evaluated against a panel of resistant and susceptible Gram-negative and Gram-positive bacteria by determining modal MICs (Suppl. Tables S3−S6), comparable to previous work where the potency of AMPs such as the WF peptides, Temporin B, Temporin L and Pleurocidin were determined against similar bacterial panels.[77−81] Antifungal potency was evaluated against a panel of six fungi by measuring the modal MIC_{50} and MIC_{90} values (Suppl. Tables S7−S10). The EUCAST and CLSI definitions of an antifungal MIC value vary depending on the antifungal class, with amphotericin B having a 90% growth inhibition (MIC_{90}) readout, while all other clinically used antifungals have a 50% growth inhibitory readout (MIC_{50}). Overall, the peptides are more active against susceptible and resistant strains of *E. coli*, *A. baumannii*, *S. aureus*, and *C. tropicalis* NCPF 8760, requiring lower concentrations to inhibit these strains compared to others. *P. aeruginosa* PAO1 is the least sensitive bacterial strain as only seven AMPs have MICs ≤ 128 μg/mL. *C. auris* TDG 1912 is the least sensitive fungal strain as none of the peptides show MIC_{90} activity and only BTD11a shows MIC_{50} activity. Out of the 46 AMPs, 27 show strong antibacterial activity, and 22 show some antifungal activity, indicating a preference for prokaryotic cells. Noticeably, shorter peptides such as XPF10a, DRAMP02273a, CPF-P3-10a, CPF-P3-12a, CPF-MW-10a, CPF-MW-12a, PS-PB-8a, Opis8a, ThetaDefA, and ThetaDefB, with sequence lengths of 12 or less, have no activity.

For the frog-derived AMP group, nine out of 15 peptides have broad-spectrum antibacterial activity with MICs ≤ 128 μg/mL while only six have antifungal activity (Suppl. Tables S3 and S7). For this group, the antibacterial potential is greater than the antifungal potential. Three peptides, CPF-P2, CPF-P3, and CPF-MW1, show activity against all Gram-negative and Gram-positive bacteria except *P. aeruginosa* PAO1. XPF is the only frog AMP that shows antibacterial activity against the entire bacterial panel, including the *P. aeruginosa* strains (Suppl. Tables S3 and S3B). The bacterially active peptides inhibit only one or two fungal strains and require moderately high MICs to achieve fungal inhibition. Noticeably, peptides CPF-P2a and CPF-MW-20a show antibacterial activity against at least four bacterial strains but no antifungal activity.

The scorpion-derived group of peptides shows the highest activity. Thirteen of 16 peptides have MICs ≤ 128 μg/mL against bacteria or fungi (Suppl. Tables S4 and S8). Opis16a, AamAP-S1a, AamAP1-Lys, AamAP1-Lysa, A3, A3a, K3-IsCTa, K7P8K11-IsCTa, and A1F5K8-IsCTa all demonstrate potent activity against multiple different bacterial and fungal strains, with generally low MIC values. Opis16a, AamP1-Lys, AamP1-Lysa, and A3a are the most promising antibacterial peptides of the 46 AMPs with activity against all 12 bacterial strains with low MICs. The C-terminal amidation of parent peptides AamAP1-S1, AamAP1-Lys, and A3 results in peptides with increased overall activity.

The tick-derived AMP group has the lowest activity in the tested environments. Of the 11 AMPs, only four show significant antibacterial activity with MICs between 16 and 128 μg/mL and all peptides lack antifungal activity (Suppl. Tables S5 and S9). These results differ from previous studies that found activity for the Os peptides but could be explained by the previously described salt susceptibility of these peptides in different media.[40,61] N-terminal tryptophan tagging and C-terminal amidation of parent peptides Os-C and OmDefB result in W3(Os-C)a, W(Os-C)a, W-OmB-Ca and W-OmC-Ca with increased potency against at least two bacterial strains but did not improve antifungal activity.

One of the four primate AMPs, BTD15a, shows promising antibacterial activity against all bacteria except the *P. aeruginosa* strains (Suppl. Tables S6 and S6B). BTD15a is also active against five of the six fungal species, with slightly higher concentrations (Suppl. Tables S10 and S10B). Under the conditions used BTD11a proved ineffective against bacteria but showed efficacy against all the tested fungal pathogens, making it the most promising antifungal AMP and the only peptide with activity against the resistant *C. auris* TDG 1912 strain (Suppl. Tables S10 and S10B).

3.2. Mammalian Toxicity Is Mostly Caused by the Microbially Active Scorpion-Derived AMPs. An ideal candidate for antimicrobial therapeutic applications must demonstrate selective activity against pathogens at low concentrations while exhibiting limited mammalian cell toxicity. To further characterize the potential of the 46 peptides, cytotoxicity was determined using human erythrocytes and the HaCat cell line. Erythrocyte hemolysis represents membrane lytic effects, while with the HaCat cell line, the effect on viability is determined and in addition to membrane effects includes the effect on cellular processes such as cellular metabolism, growth, and replication.

At the initial screening concentration of 256 μg/mL, 12 of the 46 AMPs caused hemolysis of more than 10% while eight caused 50% hemolysis at ≤256 μg/mL (Suppl. Table S11). Significant HaCat toxicity is observed for 20 AMPs and generally corresponds to those that showed hemolytic activity (Suppl. Figures S1 and S2). For the 12 most cytotoxic peptides ($p < 0.0001$), dose-response curves (1024−4 μg/mL) were generated from which the LC_{50} values were determined (Suppl. Table S12).

Overall, the frog peptides show low to moderate hemolytic activity and cytotoxicity indicating pathogen over mammalian

© University of Pretoria
https://doi.org/10.1021/acsomega.4c01277
ACS Omega XXXX, XXX, XXX−XXX

UNIVERSITEIT VAN PRETORIA
UNIVERSITY OF PRETORIA
YUNIBESITHI YA PRETORIA



Figure 1. Peptide potency and selectivity shown by the relationship between the average Gram-negative MIC and (A) hemolysis or (B) HaCat toxicity both at 256 μg/mL. Boxed peptides show HaCat toxicity but not hemolysis or vice versa. Purple circle labeled peptides show increased selectivity for Gram-positive bacteria. Red square labeled peptides show increased selectivity for Gram-negative bacteria.

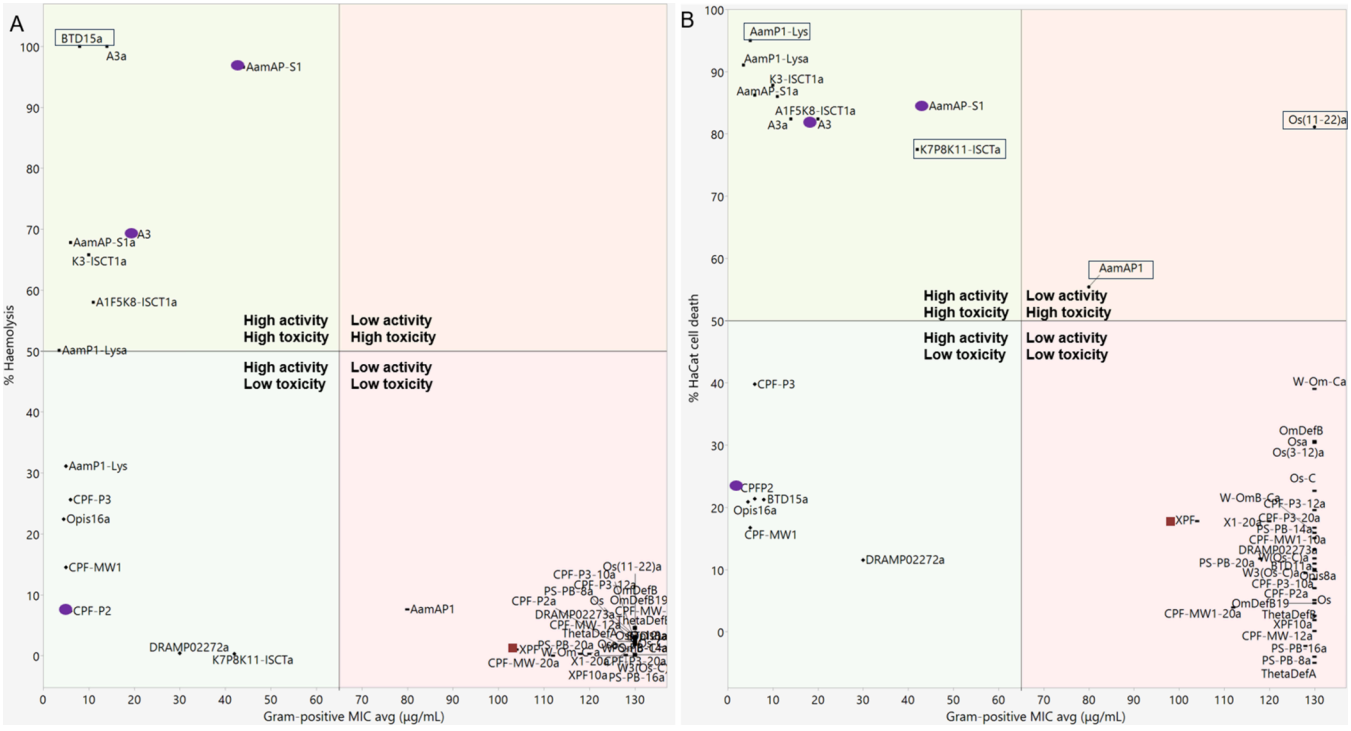


Figure 2. Peptide potency and selectivity shown by the relationship between the average Gram-positive MIC and (A) hemolysis or (B) HaCat toxicity both at 256 μg/mL. Boxed peptides show HaCat toxicity but not hemolysis or vice versa. Purple circle labeled peptides show increased selectivity for Gram-positive bacteria. Red square labeled peptides show increased selectivity for Gram-negative bacteria.

cell selectivity (Suppl. Table S11, Figures S1 and S2). Most of these peptides show an average hemolysis of less than 10% with HC_{10} values larger than 256 μg/mL. Only CPF-P3 and CPF-MW1 show slightly higher hemolytic activities of more than 10% at 256 μg/mL, but their HC_{50} values remain above 256 μg/mL which is higher than their MICs. Similarly, HaCat viability remains at 80% or more after treatment with most of the frog peptides. CPF-P3 is the only cytotoxic frog peptide

© University of Pretoria

https://doi.org/10.1021/acsomega.4c01277
ACS Omega XXXX, XXX, XXX−XXX

UNIVERSITEIT VAN PRETORIA
UNIVERSITY OF PRETORIA
YUNIBESITHI YA PRETORIA



Figure 3. Peptide potency and selectivity shown by the relationship between the average antifungal MIC and (A) hemolysis or (B) HaCat toxicity both at 256 μg/mL. Boxed peptides show HaCat toxicity but not hemolysis or vice versa. Blue triangle labeled peptides show selectivity toward fungi only.

that causes a 39.9% reduction in HaCat cell viability with an average LC_{50} of 283.5 μg/mL (Suppl. Figure S2 and Table S12). This LC_{50} is still higher than the bacterial MICs of this peptide. Therefore, due to their bacterial potency and overall low cytotoxicity, the three most active frog AMPs, XPF, CPF-MW1, and CPF-P3 show noteworthy Gram-negative and -positive selectivity over mammalian cells (Figures 1 and 2).

The most active scorpion-derived AMP group shows the highest proportion of toxic peptides. Nine out of the 13 active peptides display an average hemolysis of more than 10% at 256 μg/mL while 10 peptides reduce HaCat cell viability by 44% or more (Suppl. Table S11, Figures S1 and S2). Peptides AamAP1-S1, AamAP1-S1a, A3, A3a, K3-IsCTa, and A1F5K8-IsCTa show the highest hemolysis with HC_{50} values lower than 256 μg/mL. The active scorpion AMPs also show HaCat toxicity with LC_{50} values ranging between 59.3 and 279.7 μg/mL (Suppl. Table S12). Peptides AamAP1-S1a and K3-IsCTa are the most toxic with the lowest LC_{50} values of 59.3 and 69.4 μg/mL, respectively (Suppl. Table S12). The four most active peptides, AamAP1-Lys, AamAP1-Lysa, A3a, and Opis16a have LC_{50} values of 124.4, 101.4, 279.7, and 311.2 μg/mL, respectively. AamAP1-Lysa and AamAP1-Lys are considered cytotoxic with LC_{50} < 256 μg/mL, while A3a shows less toxicity. Opis16a is regarded as the least toxic of the four most active scorpion peptides, making it the best candidate for potent bacterial activity and selectivity (Figures 1 and 2).

Peptides identified in African tick species cause significantly more HaCat toxicity than hemolytic activity (Suppl. Table S12, Figures S1 and S2). Six out of the 11 peptides, Osa, Os(3−12)a, Os(11−22)a, Os-C, W-OmC-Ca, and OmDefB, show significant decreases in HaCat cell viability compared to the growth control (Suppl. Figure S2). This is notable as the tick group shows little to no bactericidal, fungicidal, or hemolytic activity. Once again this can be attributed to the salt susceptibility of these peptides in different broth environments.[40,61] Os(11−22)a is the most cytotoxic peptide in this group, reducing HaCat cell viability by 59.5% with an average LC_{50} of 163.2 μg/mL (Suppl. Table S12).

Lastly, only one out of the four primate-derived AMPs shows significant hemolysis (Suppl. Table S10 and Figure S1). BTD15a, the only peptide in this group with antibacterial activity, causes 100% hemolysis at 256 μg/mL. The HC_{10} and HC_{50} of this peptide is also the lowest of all 46 AMPs tested at 9 and 33 μg/mL, respectively. Although obtained under different conditions, these concentrations overlap with the MIC range of this peptide, suggesting little selectivity for pathogen cells over mammalian red blood cells (Figure 1 A). In terms of HaCat toxicity, at 256 μg/mL BTD15a only causes a 20% reduction in cell viability (Suppl. Figure S2). This shows that BTD15a is active toward pathogens and mammalian erythrocytes but not toward mammalian HaCat cells, suggesting some selectivity (Figure 1 B). The other three peptides in this group are considered noncytotoxic, causing on average less than 10% hemolysis or HaCat toxicity. Noticeably, the most active antifungal peptide, BTD11a, shows no hemolytic or cytotoxic activity and is the only peptide with pronounced selectivity for fungal rather than bacterial or mammalian cells (Figure 3).

3.3. CD Spectroscopy MRME Intensities Indicate Structured Secondary Conformations for Active AMPs.

One molecular descriptor that is considered to play an important role in determining antimicrobial potency is the secondary structure of an AMP. AMPs tend to fold and form higher secondary structures when in close proximity to membranous environments.[50,51] Mai et al.[62] and Li et al.[63] previously reported that peptides with more ordered secondary structures exhibit improved antibacterial potency. Here, far-UV

© University of Pretoria
https://doi.org/10.1021/acsomega.4c01277
ACS Omega XXXX, XXX, XXX−XXX

UNIVERSITEIT VAN PRETORIA
UNIVERSITY OF PRETORIA
YUNIBESITHI YA PRETORIA

CD analysis indicates that, in general, the peptides adopt a disordered conformation in Tris buffer (Suppl. Figures S3−S6). However, in three membrane-mimicking environments, the AMPs that have promising activity adopt predominantly α-helical or β-sheet conformations upon interaction with the SDS, Gram-positive, and -negative model membranes (Table 2 and Suppl. Figures S3−S6). This is consistent with previous studies that have shown that ordered secondary structures play a vital role in the membranolytic action of AMPs.[62,63] A decrease in activity was also observed for shorter peptides that are unable to adopt stable secondary structures, possibly preventing the membranolytic action.

For 27 out of the 46 peptides, CD spectra are observed consistent with substantial α-helix conformation in the SDS environment: a positive band around 195 nm and two negative bands around 208 and 222 nm (Table 2). These peptides predominantly have longer sequences and correspond mostly to the 27 AMPs that showed activity against the bacterial panel. Only four peptides, DRAMP02273a, PS−PB14a, Os, and Osa, that have substantial α-helical content in SDS show no activity against bacteria. The activity of these peptides might have been affected by experimental conditions such as the salt concentration of the media used. These results are similar to what is reported by Pan et al.[64] where an analogue of aurein 2.3 also adopts an α-helix similar to the active natural form, but in contrast, has no antimicrobial action.

On the other hand, peptides like W3(Os-C)a, W(Os-C)a, W-OmC-Ca, and W-OmB-Ca showed some activity against bacteria without adopting an ordered structure in SDS. This suggests that a structured secondary conformation such as an α-helix or β-sheet increases the probability of potent antimicrobial action but does not always guarantee activity. More likely, other physiological factors such as hydrophobicity, length, charge, or amphipathicity, in conjunction with secondary structure confer activity rather than secondary structure alone. The CD spectrum obtained for the most toxic tick AMP, Os(11−22)a, is consistent with β-sheet folding in the SDS environment, which is also observed in other membranous environments (Suppl. Figure S5E). Opis16a, one of the most potent and selective AMPs, showed the deepest MRME minima, indicating the strongest predominance for α-helicity of all 46 peptides in this environment.

In the POPG (Gram-positive) environment, peptides generally adopt more ordered structures with only 13 disordered peptides compared to 18 in SDS (Table 2). This can be explained by the greater size of POPG SUVs in contrast to SDS micelles therefore resulting in a stronger anionic attraction to the cationic peptides.[65] As a result, peptides exhibit reduced flexibility when anchored in this membrane interaction. CD spectra of CPF-P3-10a, CPF-P3-12a, CPF-MW-12a, and Os-C are now consistent with β-sheet (Suppl. Figures S3I,J,N and S5C), with an increase in the intensity of a single negative band at 220 nm (Table 2). In POPG, W-OmC-Ca adopts a more α-helical instead of disordered conformation, with an increase in the intensity of two MRME minima recorded (Suppl. Figure S5J). Of the 27 α-helical AMPs in SDS, 25 remain α-helical in POPG, with X1-20a and CPF-MW-20a now showing stronger β-sheet tendencies (Suppl. Figure S3E,O and Table 2).

In the POPG/POPE (Gram-negative) environment, the structural tendencies of the peptides closely resemble those observed in SDS, rather than in POPG, with the same 18 peptides having disordered structures. This could be explained by the difference in charge between the SUVs. POPG is greatly anionic, whereas mixed POPG/POPE contains less anionic lipids and is more zwitterionic overall. As explained by Urushibara and Hicks,[66] even slight differences in local charge density or hydrophobicity between membranes will result in different physiochemical surface properties that can dramatically affect the binding and consequently the conformational flexibility of AMPs. The 27 α-helical AMPs in SDS remain α-helical in POPG/POPE, except for PS-PB-20a which has a mixed P-II/α-helical conformation (Suppl. Figure S4D), BTD15a with stronger β-sheet tendencies and a loss in the 218−230 nm negative band (Suppl. Figure S6D) and Os with β-turn Type I tendencies with a loss in the 207−215 nm negative band (Figure S5A).

Generally, the less active tick and primate groups are mostly disordered, while the most active scorpion group showed the highest number of α-helical AMPs. Only two of the scorpion peptides, PS-PB-8a and Opis8a with short sequences of eight residues, remain disordered throughout all membrane environments, which explains the lack of activity. The same trends were observed for the frog- and primate-derived peptides. Active AMPs such as XPF, CPF-P2, CPF-P3, CPF-MW1, and BTD15a adopt predominantly α-helical conformations, whereas inactive shorter AMPs like XPF10a, CPF-MW10a, ThetaDefA and ThetaDefB are disordered.

Overall, the truncation of parent peptides to 15 amino acids or less resulted in decreased activity and a loss of secondary structure. This suggests that the optimal length for these AMPs to be able to adopt stable secondary structures and to exert their antimicrobial action is 16 amino acids or more. These findings are similar to those by Gagnon et al.[67] and Liu et al.[68] who also reported a decrease in antimicrobial action as the sequence length of the involved AMPs decreased.

Noticeably, six peptides from the tick or primate groups, Os, Osa, OmDefB, ThetaDefA, ThetaDefB, and BTD15a, contain two or more Cys residues (Suppl. Figures S5A,B,H and S6A,B,D). These residues can form disulfide bonds in oxidizing environments, which could result in different secondary structures than reported here.

3.4. Principal Component Analysis Highlights the Importance of Balance between Nonpolar and Polar Peptide Properties in Antimicrobial Activity. In this study, PCA is used to identify distinctive structural features in peptides that confer antimicrobial activity. Knowledge of these structural attributes can facilitate the design of novel antimicrobial agents and accelerate drug discovery. For PCA, 28 molecular peptide parameters were evaluated to identify specific structural features associated with Gram-negative, Gram-positive, or antifungal activities. The data matrices were composed of 46 peptides and 28 variables. Peptides were grouped according to their average MIC.

The Bartlett's test of sphericity revealed χ^2 is 2016.25 (PC-1) and 1643.94 (PC-2) for Gram-negative activity, 2004.10 (PC-1) and 1639.63 (PC-2) for Gram-positive activity, and 2037.89 (PC-1) and 1671.67 (PC-2) for antifungal activity (Suppl. Table S13). The p values calculated for the three populations are <0.0001 which is lower than the chosen significance level of 0.05 indicating that the data sets are suitable for factor analysis. Thus, there are no grounds for accepting H_0 and it can be assumed that the correlation matrix is not an identity matrix. The adequate results for Bartlett's test as well as the high number of peptides included in this study

© University of Pretoria
https://doi.org/10.1021/acsomega.4c01277
ACS Omega XXXX, XXX, XXX−XXX

UNIVERSITEIT VAN PRETORIA
UNIVERSITY OF PRETORIA
YUNIBESITHI YA PRETORIA

Table 3. Variable Composition of Each PC Obtained for Peptide Activity against Gram-Negative and Gram-Positive Bacteria and Fungi

	Gram-negative		Gram-positive		fungi	
principal component	variable	correlation coefficient	variable	correlation coefficient	variable	correlation coefficient
PC-1	L	−0.816	L	−0.808	L	−0.744
	L_N	−0.768	L_N	−0.758	HBdon	0.705
	ElutionTime	−0.752	ElutionTime	−0.750	HBtot	0.708
	$SCSA_N$	−0.741	$SCSA_N$	−0.734	MW_P/MW_N	0.718
	CSL	−0.700	MW_P	0.715	charge	0.765
	MW_P	0.716	charge	0.726	$SCSA_P$	0.775
	charge	0.723	MW_P/MW_N	0.730	MW_P	0.777
	MW_P/MW_N	0.734	Q/CSL	0.785	Q/CSL	0.786
	Q/CSL	0.780	$SCSA_P/SCSA_N$	0.850	$SCSA_P/SCSA_N$	0.861
	$SCSA_P/SCSA_N$	0.856	Q/L_N	0.921	Q/L_N	0.892
	Q/L_N	0.925				
PC-2	#RotBonds	0.879	#RotBonds	0.878	MW_N	0.754
	SCSA	0.932	SCSA	0.935	#RotBonds	0.808
	length	0.937	length	0.939	SCSA	0.916
	MW	0.972	MW	0.972	length	0.937
					MW	0.942
PC-3	L_P	0.859	L_P	0.865	L_P	0.873
PC-4	L_P/L	−0.828	L_P/L	−0.828	L_P/L	−0.836
	Q/L	0.797	Q/L	0.798	Q/L	0.809

confirm the appropriate application of PCA for studying the main molecular parameters that affected antimicrobial activity.

Eigenvalues, percentages of variance, and cumulative variance were calculated for the parameters involved in peptide activity against Gram-negative and -positive bacteria as well as fungi (Suppl. Table S14). The number of principal components (PCs) specified for each group was determined based on the percentage cumulative variance.[56] This agrees with other examples in the literature where the number of PCs is defined by a threshold cumulative variance.[52,56,57] This specific threshold value depends on the specificity of the data and is usually at least 70%.[56] For this study, the number of PC selections was determined at a threshold cumulative variance value of at least 80% (Suppl. Table S14).

For each group, four PCs are enough to describe over 80% of the cumulative variance. The four PCs result in 84.42% cumulative variance for activity against the Gram-negative bacteria, 83.95% for activity against the Gram-positive bacteria, and 84.82% for activity against fungi. The number of PCs selected for each group is also confirmed with a screen plot suggested by Kaiser's criterion (Suppl. Figures S7−S9).[57] The PCs with eigenvalues greater than 1.5 qualify to be used for the interpretation of results (Suppl. Table S14).

For anti-Gram-negative activity, PC-1 accounts for 37.9% and PC-2 for 29.36% of the variation (Suppl. Table S14) with the composition of individual PCs listed in Table 3. PC-1 is responsible for the highest amount of variability in the data indicating that the variables that make up PC-1 have the greatest impact on how the data are separated into active and nonactive peptides. PC-1 consists of 11 variables with absolute loading matrices of ≥0.7 (Table 3). Five of the variables show a negative correlation to PC-1 and relate mostly to the lipophilicity and nonpolar properties of peptides, including L, L_N, ElutionTime, $SCSA_N$, and CSL. Six of the variables show a positive correlation to PC-1 and include mostly the polar properties such as MW_P, charge, MW_P/MW_N, Q/CSL, $SCSA_P/SCSA_N$, and Q/L_N (Table 3). PC-2 consists of four variables with positive loading matrices of ≥0.7. The size of the peptide (MW and length), or peptide side chains factors (SCSA and #RotBonds) have the largest impact on PC-2. L_P is the biggest contributor to PC-3 with a positive correlation of >0.7. PC-4 contains two amphipathic variables with L_P/L having the biggest impact followed by Q/L (Table 3).

On a PCA biplot for anti-Gram-negative activity, the 46 peptides are split into two distinct groups (Figure 4). Potent peptides that have lower MIC_{avg} are shown in blue and accumulate mostly to the upper left quadrant and are associated with molecular properties such as increased L_N residues, increased SCSA of nonpolar residues, and increased ElutionTime, indicating greater hydrophobicity, increased MW of nonpolar residues, increased CSL residues, and CD

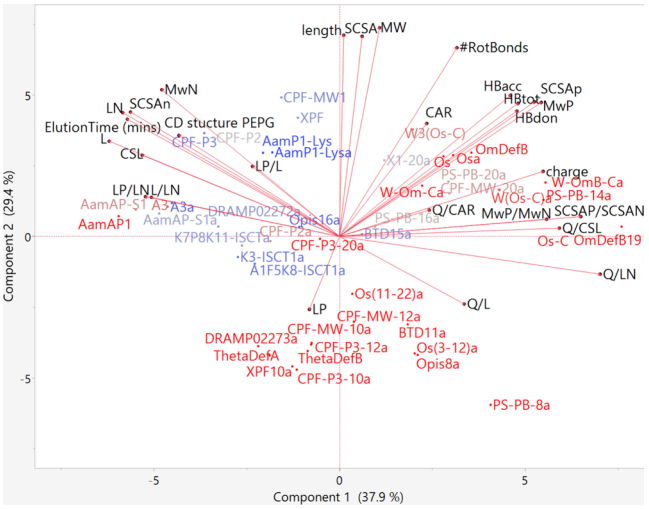


Figure 4. PCA biplot showing the molecular properties of AMPs that impact their MIC_{avg} against Gram-negative bacteria. A clustering of active (blue) AMPs are shown in the region of $SCSA_N$, L_N, ElutionTime etc. while less active (red) AMPs cluster in regions of L_P, $SCSA_P$, HB, charge, $SCSA_P/SCSA_N$, Q/CSL etc.

© University of Pretoria
https://doi.org/10.1021/acsomega.4c01277
ACS Omega XXXX, XXX, XXX−XXX

structure. Less active peptides with a higher MIC_{avg} accumulate mostly on the right. These peptides are generally less lipophilic, hydrophobic, and have fewer nonpolar residues. Inactive peptides are associated with molecular properties related to polarity such as increased L_P, change in the peptide charge or the number of hydrogen bonds, increased SCSA of polar residues, and an increase in various amphipathic molecular descriptors.

The PC composition for anti-Gram-positive activity is very similar to that of anti-Gram-negative activity. PC-1 accounts for 37.4% and PC-2 for 29.5% of the variation within the data (Suppl. Table S14). PC-1 consists of ten peptide descriptors with absolute loading matrices of ≥0.7, similar to the PC-1 of the Gram-negative group (Table 3). Contributions to PC-1 include four negative correlations by L, L_N, ElutionTime, and $SCSA_N$ and 6 positive correlations by MW_P, charge, MW_P/MW_N, Q/CSL, $SCSA_P/SCSA_N$, and Q/L_N (Table 3). The compositions of PC-2, -3, and -4 are also practically identical to the anti-Gram-negative PCs with peptide size and side chain (MW, length, SCSA, and #RotBonds), L_P and amphipathic variables making the greatest contributions, respectively (Table 3).

On the PCA biplot for anti-Gram-positive activity, the peptides are also split into two distinct groups (Figure 5).

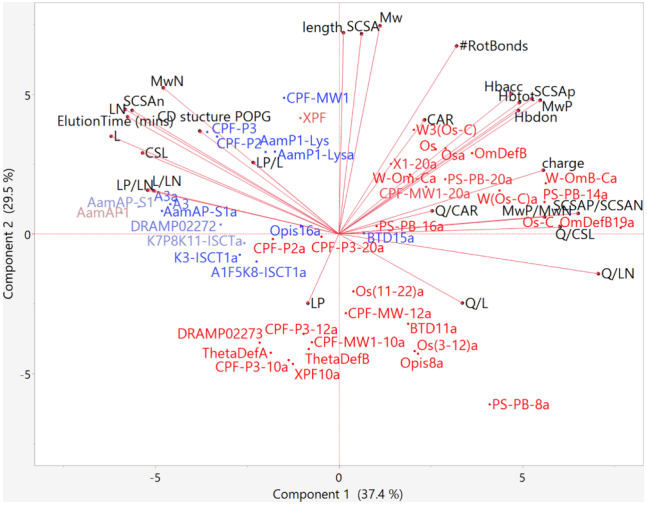


Figure 5. PCA biplot showing the molecular properties of AMPs that impact their MIC_{avg} against Gram-positive bacteria. A clustering of active (blue) AMPs are shown in the region of ElutionTime, $SCSA_N$, L_N etc. while less active (red) AMPs cluster in regions of L_P, Q/L, HB, charge, $SCSA_P/SCSA_N$ etc.

Potent peptides (blue) that have lower MIC_{avg} cluster mostly to the upper left quadrant associated with similar molecular properties as anti-Gram-negative activity such as increased lipophilicity, increased nonpolar residue SCSA, increased ElutionTime indicating greater hydrophobicity, increased CSL residues, and increased MW of nonpolar residues. The less active peptides (red) that have higher MIC_{avg} are scattered on the opposite side of the plot indicating decreased lipophilicity and hydrophobicity (Figure 5). The less active peptides are associated with molecular properties such as increased L_P, change in peptide charge or number of HB, increased SCSA of polar residues, as well as an increase in amphipathic molecular descriptors like Q/L_N.

For the PCA on both bacterial groups, peptides are categorized into active or inactive peptides first on their lipophilicity and nonpolar properties versus their polarity, then their size and side chain properties and last the lipophilicity of their polar residues and their amphipathic properties.

In contrast to the antibacterial activity, most of the AMPs are inactive against fungi or had high MIC_{90} values in the screenings, apart from BTD11a. Therefore, the composition and correlation coefficients for PC-1 of antifungal activity are different from those of antibacterial activity. PC-1 consists of ten peptide descriptors with absolute loading matrices of ≥0.7, with L being the only negative correlation (Table 3). Properties such as L_N, ElutionTime, and $SCSA_N$ that appear in the PC-1 of bacterial activity have lower than 0.7 negative correlation coefficients in the PC-1 of antifungal activity. Nine variables show a positive correlation to antifungal PC-1 and include mostly polar properties such as HBdon and HBtot, not associated with antibacterial PC-1, MW_P/MW_N, charge, $SCSA_P$, MW_P, Q/CSL, $SCSA_P/SCSA_N$, and Q/L_N. The compositions of PC-2, -3, and -4 are more similar to those of antibacterial activity with the peptide size and side chain (MW, length, SCSA and #RotBonds), L_P and amphipathic variables making the greatest contributions, respectively (Table 3).

On a PCA biplot, the most active antifungal AMPs, shown in blue, with MIC_{90} below 80 μg/mL do not group together or associate with any molecular property in particular (Figure 6).

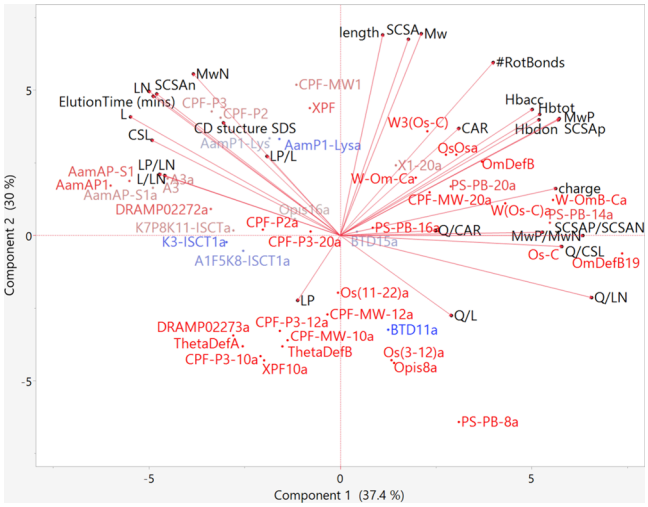


Figure 6. PCA biplot showing the molecular properties of AMPs that impact their MIC_{avg} against fungi. A clustering of active (light red/blue) AMPs is shown in different regions including L, CSL, L_P/L_N, L/L_N etc. while less active (red) AMPs cluster in regions of L_P, HB, charge, $SCSA_P/SCSA_N$ etc.

AMPs with some activity and MIC_{90} between 90 and 110 μg/mL group around the upper left quadrant in the vicinity of hydrophobic nonpolar molecular properties such as MW_N, L, and CSL and amphipathic properties such as L_P/L_N and L/L_N. Those that are completely inactive, shown in bright red, are scattered in the other three quadrants associated with polarity such as L_P and charge (Figure 6).

3.5. QSAR Analysis Show That Certain Peptide Descriptors Including Lipophilicity and Size Can Be Manipulated To Achieve Broad-Spectrum Pathogen over Mammalian Selectivity.

QSAR analysis was performed

© University of Pretoria
https://doi.org/10.1021/acsomega.4c01277
ACS Omega XXXX, XXX, XXX−XXX

UNIVERSITEIT VAN PRETORIA
UNIVERSITY OF PRETORIA
YUNIBESITHI YA PRETORIA

Table 4. Correlation of Single Molecular Descriptors of the 46 AMPs with Antimicrobial and Cytotoxic Activities

		R^2				
	property	Gram-negative bacteria MIC_{avg}	Gram-positive bacteria MIC_{avg}	fungi MIC_{avg}	%hemolysis	%HaCat cell death
1	ElutionTime (min)	−0.7203	−0.8032	−0.4590	0.5567	0.6485
2	L	−0.5246	−0.6713	−0.3576	0.5413	0.6376
3	L_N	−0.7464	−0.8027	−0.5531	0.5855	0.6343
4	$SCSA_N$	−0.7492	−0.7920	−0.4968	0.5230	0.6082
5	MwN	−0.6832	−0.7462	−0.4162	0.4500	0.4865
6	CD structure	−0.7250	−0.5670	−0.3425	0.4597	0.4548
7	L_P/L_N	−0.2103	−0.3396	−0.0510	0.3103	0.4426
8	L/L_N	−0.1928	−0.3099	−0.0362	0.2763	0.4097
9	CSL	−0.5204	−0.5914	−0.3447	0.3155	0.2755
10	L_P/L	−0.1358	−0.1675	−0.0890	0.1297	0.2489
11	SCSA	−0.4589	−0.3225	−0.1024	0.0341	0.2350
12	CAR	−0.0190	−0.0051	0.1287	0.0498	0.2250
13	Mw	−0.3691	−0.2877	−0.1111	0.0576	0.1195
14	sequence length	−0.3623	−0.3182	−0.0633	0.0297	0.0748
15	L_P	0.5258	0.2956	0.4575	−0.0711	0.0330
16	#RotBonds	−0.3049	−0.1062	−0.0739	−0.0619	0.0321
17	Q/CAR	−0.0162	0.1919	0.1001	−0.2490	−0.1772
18	HBacc	0.0344	0.1853	0.0936	−0.2188	−0.2010
19	$SCSA_P$	0.0653	0.2597	0.2801	−0.3813	−0.2144
20	HBtot	0.0447	0.1872	0.0260	−0.1794	−0.2305
21	HBdon	0.0486	0.1828	−0.0091	−0.1543	−0.2389
22	MwP	0.1253	0.2805	0.2178	−0.3133	−0.2675
23	Charge	0.0364	0.2892	0.0388	−0.2451	−0.2776
24	Q/L	0.2370	0.2561	0.1781	−0.1804	−0.2803
25	Q/CSL	0.3733	0.4251	0.3222	−0.3037	−0.3021
26	$SCSA_P/SCSA_N$	0.4631	0.5194	0.4496	−0.4156	−0.3158
27	MwP/MwN	0.4330	0.5075	0.3644	−0.3871	−0.3630
28	Q/L_N	0.5264	0.6058	0.3810	−0.4363	−0.4634

to relate the selectivity of the 46 AMPs to specific molecular properties that contribute to their potency and mechanism of action. Quantifying the structure−activity relationship of active peptides is essential for the future rational design of potent and selective antimicrobial peptides.

The MIC values were averaged over the panel of strains tested per group to facilitate the assessment of the overall antimicrobial potency of the peptides against Gram-negative bacteria, Gram-positive bacteria, or fungi. QSAR analysis that involves the averaged MIC (MIC_{avg}) reflects the antimicrobial potency of a peptide better than analyses based on MICs against the individual strains, where the actual effect may be strongly dependent on the specific membrane composition, cell growth rate, and life cycle of the particular strain.[28] The MIC_{avg} gives an overall indication of these factors and accentuates the role of the peptide sequence and structure in the achieved antimicrobial effect. Additionally, the development of a QSAR model for peptides that are active against a wide spectrum of Gram-negative and Gram-positive bacteria or fungi is preferable to structure−activity relationships described only for a specific individual strain. The relationships between sequences and observed bioactivities were analyzed in terms of physio-chemical molecular properties as well as experimentally determined characteristics of the peptides.

Table 4 shows the pairwise correlations between the averaged antimicrobial (MIC_{avg}), hemolytic (% hemolysis), or cytotoxic (% HaCat cell death) activities and the respective molecular properties of the peptides. Consistent with the PCA analysis, descriptors such as L_N, $SCSA_N$, and ElutionTime show strong negative correlations with Gram-negative, Gram-positive, and antifungal activity (Table 4 and S15). This suggests that an increase in nonpolar lipophilic amino acids, nonpolar residues with bulkier side chains, or increased overall hydrophobicity leads to an increase in broad-spectrum antimicrobial activity. These three descriptors are also strongly correlated with hemolysis and HaCat cell death (Table 4) regardless of the lipophilicity scale used (Suppl. Table S15). This is consistent with several other studies[58−60] which report that AMP lipophilicity and hydrophobicity closely correlate with mammalian toxicity. Thus, an increase in lipophilic nonpolar residues as well as overall hydrophobicity may lead to improved broad-spectrum activity but also decreased pathogen selectivity.

Similar to the findings of the PCA analyses, the AMP secondary structure correlates strongly with Gram-negative activity with an R^2 of −0.7250 surpassing the R^2 of −0.5670 and −0.3425 for Gram-positive or antifungal activity, respectively. The more ordered the overall secondary structure of the peptide e.g., α-helical or β-sheeted, the lower the average MIC against Gram-negative bacteria. This indicates a narrow-spectrum association. Although the correlation is stronger toward Gram-negative activity, an association between CD structure and toxicity also exists with an R^2 of 0.4597 for hemolysis and 0.4548 for HaCat toxicity. Therefore, an increase in the ordered secondary structure of an AMP can potentiate anti-Gram-negative activity but might also lead to an increase in toxicity.

Gram-positive antibacterial activity, in turn, is much more dependent on peptide lipophilicity and hydrophobicity, especially of the nonpolar residues, rather than the secondary

© University of Pretoria
https://doi.org/10.1021/acsomega.4c01277
ACS Omega XXXX, XXX, XXX−XXX

UNIVERSITEIT VAN PRETORIA
UNIVERSITY OF PRETORIA
YUNIBESITHI YA PRETORIA

structure. The R^2 values for ElutionTime and L_N of >0.8 show the strongest correlations of all 28 molecular descriptors across the three pathogen groups. This highlights the importance of these descriptors for anti-Gram-positive activity. Another property that showed a relatively strong correlation with Gram-positive activity is the count of small lipophilic residues (CSL). This implies that increasing the count of small lipophilic residues in a peptide sequence or the overall hydrophobicity or lipophilicity of the nonpolar face will increase anti-Gram-positive activity but might contribute to toxicity.

Similarly, the antifungal activity is also more dependent on the lipophilicity and hydrophobicity of a peptide. Although, out of the 28 properties L_N, $SCSA_N$, and ElutionTime show the highest correlation with antifungal activity, the R^2 values are much lower than the R^2 values for antibacterial or HaCat activity and similar to the R^2 values of hemolysis. This suggests that these properties might slightly increase the antifungal activity of a peptide but are not ideal in conferring fungal selectivity over bacterial or mammalian selectivity.

Thus, there are several properties that correlate well with antimicrobial activity showing an absolute R^2 of >0.5, which can be manipulated to increase the potency of an AMP but will most likely also cause an undesired cytotoxic side-effect. Therefore, to increase pathogen over mammalian selectivity and reduce the risk of toxicity, descriptors that show little to no correlation with hemolytic or HaCat toxicity but some association with antimicrobial activity, and vice versa, should be considered. L_P (Table S1) describes the lipophilicity of those amino acids classified as polar (Arg, Asn, Asp, Gln, Glu, His, Lys, Ser, Thr, Tyr). As such it is possible to vary this parameter alongside, or independently of, a change in charge and potentially independently of overall hydrophobicity as nonpolar residues Cys, Ile, Leu, Met, Phe, Pro, Trp, and Val do not contribute. Most notably, L_P shows strong positive correlations with the MIC for all three pathogens and no association with toxicity. Therefore, including more polar cationic residues to reduce the lipophilicity of the polar groups will decrease the L_P resulting in an improved broad-spectrum MIC with no concomitant increase in cytotoxic effects. This result is also obtained when using the Wimley-White scale (Suppl. Table S15). For antibacterial activity, it is however important to retain a balance between L_P and L_N. A drastic decrease in L_P to increase activity and selectivity can lead to an imbalance in the L_P/L_N ratio, which could result in decreased activity. Thus, having a few L_N residues is important to balance activity and toxicity.

For antifungal activity, L_P is the only parameter that can be manipulated to increase activity and have no effect on toxicity. All other parameters that increase the antifungal activity also cause an increase in toxicity. Here, the L_P/L_N ratio is not as important. Thus, reducing the lipophilicity contributed by the polar residues will decrease the overall L_P value and increase antifungal activity, with no effect on hemolytic or HaCat toxicity. Increasing the charge or the number of hydrogen bond-forming residues is also an effective strategy for decreasing HaCat toxicity and thus increasing antifungal selectivity.

The peptide size in terms of the sequence length and molecular weight also shows notable correlations with antibacterial activity and a negligible association with toxicity. This suggests that an increased sequence length and, consequently, Mw can lead to increased antibacterial activity and no change in toxicity. The same was observed in the MIC screens, where peptides shorter than 12 residues showed no antibacterial activity. Peptide size does not seem to be essential for the antifungal activity.

Lastly, the #RotBonds in an AMP sequence correlate with anti-Gram-negative activity and have no effect on toxicity. Thus, an increase in residues that contain higher amounts of side chain rotational bonds, such as Lys or Arg, will increase anti-Gram-negative activity without affecting cytotoxicity.

Other properties that show a correlation with toxicity but no association with antimicrobial activity can also be manipulated to reduce toxicity and achieve selectivity. One example is the count of aromatic residues (CAR) in a peptide sequence. This property correlates with HaCat cell death and somewhat with antifungal activity but shows no association with antibacterial activity. Hence, a decrease in the CAR could potentially reduce the HaCat toxicity of an AMP without affecting its antibacterial activity. Similarly, properties like charge and the number of hydrogen bonds (HB) a peptide can form correlate with both hemolysis and HaCat cell death but have no effect on Gram-negative or antifungal activity. Thus, increasing the overall charge and consequently the number of HB of an AMP would mean a decrease in the toxicity and an increase in Gram-negative or fungal selectivity. This, however, is not the case for Gram-positive antibacterial activity, as an increase in charge might lead to a loss in activity.

For a Gram-negative targeting AMP, an increase in polar residues with bulkier side chains would increase the $SCSA_P$ value, which would decrease toxicity without affecting activity. For a fungal targeting AMP, a decrease in L_P would result in a decrease in the L_P/L_N or L/L_N ratios, which can reduce the toxicity of the compound without affecting its antifungal potency.

4. DISCUSSION

AMPs show great potential for development into therapeutic drugs to address the global antimicrobial resistance crisis. However, despite their many advantages, AMPs have some drawbacks that limit their translation into therapeutic drugs. Potent AMPs often exhibit low target selectivity and are accompanied by unacceptable toxicity toward host cells.[14−16] More than 70 of the peptides deposited in DRAMP have entered the antimicrobial drug development stage with 27 in clinical trials and 34 in the preclinical stage.[69] Thus far, only eight have made it to market including colistin, polymyxin B, vancomycin, gramicidin, bacitracin, daptomycin, enfuvirtide, and telaprevir, with many other trials being halted due to unwanted toxicity.[69,70] Several clinically approved peptides including the well characterized Gramicidins and Polymyxins were initially denied due to their toxicity but have since been approved as last-resort therapeutics with limited applications.[14,69,70] As a result, AMP toxicity is regarded as one of the main challenges to overcome in the design and development of peptides as therapeutic drugs.

The biological effects of AMPs are directly associated with their structural features, and it is therefore essential to understand the sequence-driven features that confer activity and, more importantly, target selectivity. Various physiochemical properties such as the peptide charge, hydrophobicity, amphipathicity, or secondary structure have been associated with structure−activity relationships (SAR) of AMPs.[17−20] Due to the huge diversity in structural or physiochemical properties characteristic of AMPs, it is often difficult to

© University of Pretoria
https://doi.org/10.1021/acsomega.4c01277
ACS Omega XXXX, XXX, XXX−XXX

UNIVERSITEIT VAN PRETORIA
UNIVERSITY OF PRETORIA
YUNIBESITHI YA PRETORIA

pinpoint the exact molecular property or combination of properties required to obtain a potent and selective AMP for therapeutic use. Quantitative analyses of the SAR of AMPs could simplify large data sets to summarize the key physiochemical properties that determine selectivity; however, QSAR studies on AMP selectivity are scarce. Most available QSAR studies on AMPs utilize machine-learning techniques to define mathematical models that can predict AMP activity.[27,28,71,72] Very few QSAR models explicitly address target selectivity and rarely define which physiochemical properties and amino acid residues contribute to selectivity.

In this study, a QSAR based on 28 molecular properties of 46 diverse African-derived AMPs, identifies L_P as an essential molecular parameter to consider for broad-spectrum antimicrobial selectivity. L_P showed a strong correlation with peptide activity against Gram-negative, Gram-positive, and fungal pathogen classes and a much lower correlation with mammalian cytotoxicity. This suggests that an increase in the number of polar residues to reduce the overall L_P of the peptide can lead to an increase in activity without affecting toxicity, thus increasing the selectivity of an AMP. Similar results were obtained using the Wimley-White scale, demonstrating the robustness of L_P as a parameter for selectivity regardless of the lipophilicity scale used.

The interaction with, and diffusion across, a pathogenic phospholipid-bilayer requires a peptide to be lipophilic and hydrophobic enough to interact with the lipid chains but also be polar enough to selectively target a pathogen over mammalian cell membranes. Several SAR studies show the importance of amphipathicity with a balance between hydrophobic and cationic regions in an active AMP sequence.[18−20,58,73] A peptide with increased hydrophobicity or lipophilic nonpolar residues will show enhanced cytolytic activities, whereas a peptide with an imbalance in net charge will show decreased selectivity and antimicrobial potency.[58−60,73] The QSAR model established by Frecer[28] also correlated peptide lipophilicity and amphipathicity to potent antimicrobial action. This agrees with the current QSAR results that show a strong correlation between hydrophobicity or lipophilicity and peptide activity, but there is also a strong correlation with toxicity as well. Thus, increasing the overall hydrophobicity or lipophilicity of a peptide alone will improve activity but not selectivity. L_P represents a polar property that can be manipulated to balance lipophilicity and charge to achieve target selectivity.

In this study, three scorpion-derived peptides, namely, A3a, AamAP-Lysa, and Opis16a, and two frog-derived peptides, XPF and CPF-MW1 were identified as the best antibacterial peptides of the 46 AMPs with activity against all or all but one of the tested bacterial strains. Their activities correlate with their high overall hydrophobicity (ElutionTime) and lipophilicities (Table 1). Only Opis16a, XPF, and CPF-MW1 showed selective microbial killing and low cytotoxicity. This selectivity is correlated to low L_P values of −6.91 for Opis16a, −7.46 for XPF, and −7.26 for CPF-MW1. A3a and AamAP-Lysa with higher L_P values of −3.07 and −0.94, respectively, showed more toxicity and less pathogen selectivity.

Although a balance between hydrophobicity and polarity has been identified as a strategy to improve selectivity in previous SAR studies,[18−20,58,73] manipulating the L_P of an AMP as a way of achieving this balance has, to our knowledge, not been suggested as of yet. At pH 7, there are four polar residues with negative L_P values including anionic Asp (L_P of −2.57) and Glu (L_P of −2.29), and cationic Arg (L_P of −1.01) and Lys (L_P of −0.99) (Suppl. Table S1). The cationic side chains of Arg or Lys have been shown to increase the selectivity for anionic pathogens rather than neutral mammalian membranes.[74] Therefore, Arg and Lys fulfill both the cationic charge and negative L_P requirements making these residues the preferable choice to achieve pathogen over mammalian selectivity.

In the past, polar cationic residues were incorporated into peptide sequences to improve antimicrobial activity by increasing the overall charge; however, the QSAR shows that an increase in charge alone has no effect on Gram-negative or fungal activity of the peptide. Rather the increased charge caused by these residues reduces mammalian toxicity and decreases the L_P to improve microbial selectivity.

As an example, the usefulness of the present QSAR findings can be determined through the understanding of the results of an SAR study of a small group of AMPs by Fields et al.[75] In their study, four linear peptides were derived from a parent SynSaf-P1 peptide using stepwise amino acid substitutions to improve antimicrobial activity. To obtain the first derivative, SynSaf-P8, a Thr residue was changed for a Lys resulting in an increased overall charge but also a very substantial drop in L_P. Activity studies revealed that this increase in overall charge did not significantly alter the antimicrobial activity, consistent with the prediction of the current QSAR. However, further substitutions of Gly residues to more hydrophobic Trp residues, increasing L_N, in derivatives SynSaf-P24, SynSaf-P56, and SynSaf-P96 significantly improved the antimicrobial activity. The current QSAR shows that AMPs with increased numbers of lipophilic and bulky nonpolar residues such as Trp or Phe result in increased hydrophobicity and generally display promising MIC results. As mentioned previously, a strong correlation between these molecular properties and peptide cytotoxicity also exists. An increase in overall hydrophobicity or lipophilicity would not only result in lower MICs but also lead to increased erythrocyte and HaCat toxicity. As predicted by the current QSAR, the improved SynSaf-P24, SynSaf-P56, and SynSaf-P96 derivatives with increased lipophilicity and hydrophobicity did not show increased toxicity.[73] This is because of the initial incorporation of Lys which, on its own, did not improve the activity of SynSaf-P8, but did manage to cause a sufficient reduction in L_P to mitigate the toxicity, caused by the increased hydrophobicity and lipophilicity of the Trp residues in SynSaf-P24, SynSaf-P56, and SynSaf-P96, and achieve microbial over mammalian selectivity.

Although the most effective, L_P and charge are not the only descriptors involved in the antimicrobial selectivity. Other properties such as CAR, HB, #RotBonds and SCSA can be manipulated to achieve selectivity to specific pathogen groups over others as well as over mammalian cells. For example, decreasing the CAR in a peptide sequence could potentially reduce the HaCat toxicity without affecting its antibacterial activity. To further improve Gram-negative activity and selectivity the #RotBonds in the residues of a peptide sequence can be increased. Once again, Lys and Arg residues can be considered due to their long and flexible hydrocarbon side chains. For Gram-positive selectivity, a more balanced overall charge is preferred and may be achieved by including smaller, neutral lipophilic residues such as Ala, Gly, Leu, or Ile.[28]

Finally, peptide size in terms of sequence length and molecular weight can also be considered to improve peptide activity and selectivity, as shorter sequences show little activity. This could be due to the potential impact of peptide size on

© University of Pretoria
https://doi.org/10.1021/acsomega.4c01277
ACS Omega XXXX, XXX, XXX−XXX

UNIVERSITEIT VAN PRETORIA
UNIVERSITY OF PRETORIA
YUNIBESITHI YA PRETORIA

various other molecular properties, including the conformational state and flexibility of an AMP. A conservative increase in the sequence length and molecular weight would allow an increase in activity without affecting the toxicity.

Overall, the results show that the antimicrobial and cytotoxic effects of AMPs are proportional to their hydrophobicity and lipophilicity. Although this is well documented in the literature, the identification of properties such as L_P, charge, hydrogen bonding, #RotBonds and CAR that confer selectivity to certain pathogen classes over mammalian or other pathogens represents a relatively novel finding. This may help overcome the major challenge of cytotoxic side effects of potent AMPs that restrict them from entering the drug development stage.

5. CONCLUSIONS

Analysis of 46 diverse peptides, with a focus on antimicrobial, hemolytic, and cytotoxic activity supplied the data required to obtain a better overall picture of what physiochemical properties are required for an effective and selective AMP. PCA and QSAR revealed that, at least for this sample of peptides, characteristics such as overall hydrophobicity, nonpolar lipophilic residues, and residue side chain surface area affect the antimicrobial and cytotoxic activity of an AMP. Some of these characteristics outweigh others, depending on the specific target pathogen. QSAR further identified the lipophilicity of polar residues to be the main molecular property that can be manipulated to improve pathogen over mammalian selectivity. Furthermore, an increase in the overall peptide charge specifically confers Gram-negative and fungal selectivity, while Gram-positive selectivity is obtained through small lipophilic residues. The PCA and QSAR results herein obtained grant valuable information for future rational AMP design strategies that could lead to antimicrobial and cytotoxic activity improvement.

■ ASSOCIATED CONTENT

Supporting Information

The Supporting Information is available free of charge at https://pubs.acs.org/doi/10.1021/acsomega.4c01277.

Peptide properties per residue; antimicrobial activity; antibiogram; antibacterial activity; antifungal activity; hemolytic activity; cytotoxicity against HaCat cells; circular dichroism spectra; PCA; and QSAR -Wimley-White (PDF)

■ AUTHOR INFORMATION

Corresponding Authors

A. James Mason − *Institute of Pharmaceutical Science, School of Cancer & Pharmaceutical Science, King's College London, London SE1 9NH, United Kingdom;* orcid.org/0000-0003-0411-602X; Email: james.mason@kcl.ac.uk

Anabella R. M. Gaspar − *Department of Biochemistry, Genetics and Microbiology, Faculty of Natural and Agricultural Sciences, University of Pretoria, Pretoria 0002, South Africa;* orcid.org/0000-0003-2035-3084; Email: anabella.gaspar@up.ac.za

Authors

Mandelie van der Walt − *Department of Biochemistry, Genetics and Microbiology, Faculty of Natural and Agricultural Sciences, University of Pretoria, Pretoria 0002, South Africa*

Dalton S. Möller − *Department of Biochemistry, Genetics and Microbiology, Faculty of Natural and Agricultural Sciences, University of Pretoria, Pretoria 0002, South Africa*

Rosalind J. van Wyk − *Department of Biochemistry, Genetics and Microbiology, Faculty of Natural and Agricultural Sciences, University of Pretoria, Pretoria 0002, South Africa*

Philip M. Ferguson − *Institute of Pharmaceutical Science, School of Cancer & Pharmaceutical Science, King's College London, London SE1 9NH, United Kingdom*

Charlotte K. Hind − *Antimicrobial Discovery Development and Diagnostics, Vaccine Evaluation and Development Centre, UK Health Security Agency, Salisbury SP4 0JG, United Kingdom*

Melanie Clifford − *Antimicrobial Discovery Development and Diagnostics, Vaccine Evaluation and Development Centre, UK Health Security Agency, Salisbury SP4 0JG, United Kingdom;* Present Address: Defense Science and Technology Laboratory, Porton Down, Salisbury SP4 0JQ, United Kingdom

Phoebe Do Carmo Silva − *Antimicrobial Discovery Development and Diagnostics, Vaccine Evaluation and Development Centre, UK Health Security Agency, Salisbury SP4 0JG, United Kingdom;* Present Address: School of Life Sciences, University of Warwick, Coventry CV4 7AL, United Kingdom.

J. Mark Sutton − *Antimicrobial Discovery Development and Diagnostics, Vaccine Evaluation and Development Centre, UK Health Security Agency, Salisbury SP4 0JG, United Kingdom;* orcid.org/0000-0002-2288-0446

Megan J. Bester − *Department of Anatomy, Faculty of Health Sciences, University of Pretoria, Pretoria 0002, South Africa*

Complete contact information is available at: https://pubs.acs.org/10.1021/acsomega.4c01277

Notes

The authors declare no competing financial interest.

■ ACKNOWLEDGMENTS

Research reported in this publication was supported by the South African Medical Research Council with funds received from the South African National Department of Health and a SA-UK Newton Fund Antibiotic Accelerator (MC_PC_MR/T029552/1), awarded to AJM and ARMG, and administered by the Medical Research Council (UK). Antimicrobial and hemolytic testing was performed at UKHSA as part of their Open Innovation model under Grant-in-aid funding 113361. We thank Dr. T. Bui for technical assistance with CD spectroscopy, Dr. J. Serem for assistance and expertise regarding HaCat cytotoxicity studies, and Prof. Z. Apostolides for recommendations regarding PCA analysis.

■ ABBREVIATIONS

AMP, antimicrobial peptide; MIC, minimum inhibition concentration; PCA, principal component analysis; QSAR, quantitative structure−activity relationship

■ REFERENCES

(1) Ayukekbong, J. A.; Ntemgwa, M.; Atabe, A. N. The threat of antimicrobial resistance in developing countries: causes and control strategies. *Antimicrobial Resistance & Infection Control* **2017**, *6* (1), 1−8.

(2) Jemal, M.; Deress, T.; Belachew, T.; Adem, Y. Antimicrobial resistance patterns of bacterial isolates from blood culture among

© University of Pretoria

UNIVERSITEIT VAN PRETORIA
UNIVERSITY OF PRETORIA
YUNIBESITHI YA PRETORIA

HIV/AIDS patients at Felege Hiwot Referral Hospital, Northwest Ethiopia. *International Journal of Microbiology* **2020**, *2020*, 1−8.
(3) Ioana, D. O.; Evelina, T.; Shunmay, Y.; Rashida, A. F.; Richard, A. S.; Heidi, H.; Alexander, M. A.; Kranzer, K. The association between antimicrobial resistance and HIV infection: a systematic review and meta-analysis. *Clin. Microbiol. Infect.* **2021**, *27* (6), 846−853.
(4) Nelson, R. E.; Hyun, D.; Jezek, A.; Samore, M. H. Mortality, length of stay, and healthcare costs associated with multidrug-resistant bacterial infections among elderly hospitalized patients in the United States. *Clinical Infectious Diseases* **2022**, *74* (6), 1070−1080.
(5) Amso, Z.; Hayouka, Z. Antimicrobial random peptide cocktails: a new approach to fight pathogenic bacteria. *Chemical Communications (Camb)* **2019**, *55*, 2007−2014.
(6) Lei, J.; Sun, L.; Huang, S.; Zhu, C.; Li, P.; He, J.; Mackey, V.; Coy, D. H.; He, Q. The antimicrobial peptides and their potential clinical applications. *Am. J. Transl. Res.* **2019**, *11* (7), 3919−3931.
(7) Huan, Y.; Kong, Q.; Mou, H.; Yi, H. Antimicrobial peptides: Classification, design, application and research progress in multiple fields. *Frontiers in Microbiology* **2020**, *11*, 2559−2578.
(8) Mahlapuu, M.; Hakansson, J.; Ringstad, L.; Bjorn, C. Antimicrobial peptides: An emerging category of therapeutic agents. *Frontiers in Cellular and Infection Microbiology* **2016**, *6* (194), 1−12.
(9) Hancock, R. E. W. Host defence (cationic) peptides: what is their future clinical potential? *Drugs* **1999**, *57*, 469−473.
(10) Mosca, D. A.; Hurst, M. A.; So, W.; Viajar, B. S. C.; Fujii, C. A.; Falla, T. J. IB-367, a protegrin peptide with in vitro and in vivo activities against the microflora associated with oral mucositis. *Antimicrob. Agents Chemother.* **2000**, *44*, 1803−1808.
(11) El Shazely, B.; Yu, G.; Johnston, P. R.; Rolff, J. Resistance evolution against antimicrobial peptides in *Staphylococcus aureus* alters pharmacodynamics beyond the MIC. *Frontiers in Microbiology* **2020**, *11* (103), 1−11.
(12) Yu, G.; Baeder, D. Y.; Regoes, R. R.; Rolff, J. Predicting drug resistance evolution: insights from antimicrobial peptides and antibiotics. *Proc. Biol. Sci.* **2018**, *285* (1874), 20172687.
(13) Nguyen, T. N.; Teimouri, H.; Medvedeva, A.; Kolomeisky, A. B. Cooperativity in bacterial membrane association controls the synergistic activities of antimicrobial peptides. *J. Phys. Chem. B* **2022**, *126* (38), 7365−7372.
(14) Boto, A.; Pérez De La Lastra, J. M.; González, C. C. The road from host-defense peptides to a generation of antimicrobial drugs. *Molecules* **2018**, *23* (2), 311−320.
(15) Greco, I.; Molchanova, N.; Holmedal, E.; Jenssen, H.; Hummel, B. D.; Watts, J. L.; Hakkanson, J.; Hansen, P. R.; Svenson, J. Correlation between hemolytic activity, cytotoxicity and systemic in vivo toxicity of synthetic antimicrobial peptides. *Sci. Rep.* **2020**, *10* (1), 13206.
(16) Sarkar, T.; Chetia, M.; Chatterjee, S. Antimicrobial peptides and proteins: From nature's reservoir to the laboratory and beyond. *Frontiers in Chemistry* **2021**, *9*, 1−40.
(17) Han, Y.; Zhang, M.; Lai, R.; Zhang, Z. Chemical modifications to increase the therapeutic potential of antimicrobial peptides. *Peptides* **2021**, *146*, No. 170666.
(18) Krauson, A. J.; Hall, O. M.; Fuselier, T.; Starr, C. G.; Kauffman, W. B.; Wimley, W. C. Conformational fine-tuning of pore-forming peptide potency and selectivity. *J. Am. Chem. Soc.* **2015**, *137*, 16144−16152.
(19) Liu, Y.; Du, Q.; Ma, C.; Xi, X.; Wang, L.; Zhou, M.; Burrows, J. F.; Chen, T.; Wang, H. Structure-activity relationship of an antimicrobial peptide, Phylloseptin-PHa: balance of hydrophobicity and charge determines the selectivity of bioactivities. *Drug Design, Development and Therapy* **2019**, *13*, 447−458.
(20) Duque, H. M.; Rodrigues, G.; Santos, L. S.; Franco, O. L. The biological role of charge distribution in linear antimicrobial peptides. *Expert Opinion on Drug Discovery* **2023**, *18* (3), 287−302.
(21) Park, Y.; Park, S. C.; Park, H. K.; Shin, S. Y.; Kim, Y.; Hahm, K. S. Structure-activity relationship of hp (2−20) analog peptide: Enhanced antimicrobial activity by n-terminal random coil region deletion. *Biopolymers* **2007**, *88*, 199−207.
(22) Iwaniak, A.; Minkiewicz, P.; Darewicz, M.; Protasiewicz, M.; Mogut, D. Chemometrics and cheminformatics in the analysis of biologically active peptides from food sources. *Journal of Functional Foods* **2015**, *16*, 334−351.
(23) Scotti, L.; Júnior, F. J. B. M.; Ishiki, H. M.; Ribeiro, F. F.; Duarte, M. C.; Santana, G. S.; Oliveira, T. B.; Formiga Melo Diniz, M. F.; Quintans-Júnior, L. J.; Scotti, M. T. In *Computer-aided drug design studies in food chemistry. Natural and artificial flavoring agents and food dyes*; Grumezescu, A. M.; Holban, A. M., Eds.; Elsevier BV: Amsterdam, 2018; pp 261−297.
(24) Abdi, H.; Williams, L. J. Principal component analysis. *Wiley Interdisciplinary Reviews: Computational Statistics* **2010**, *2* (4), 433−459.
(25) Pittinger, C.; Mohapatra, A. Chapter 69 - Software tools for toxicology and risk assessment. In *Information Resources in Toxicology (Fourth Edition)*; 2009; pp 631−638.
(26) Roy, K.; Kar, S.; Das, R. N. Chapter 9 − Newer QSAR techniques. In *Understanding the Basics of QSAR for Applications in Pharmaceutical Sciences and Risk Assessment*; 2015; pp 319−356.
(27) Ostberg, N.; Kaznessis, Y. Protegrin structure-activity relationships: using homology models of synthetic sequences to determine structural characteristics important for activity. *Peptides* **2005**, *26*, 197−206.
(28) Frecer, V. QSAR analysis of antimicrobial and haemolytic effects of cyclic cationic antimicrobial peptides derived from protegrin-1. *Bioorg. Med. Chem.* **2006**, *14*, 6065−6074.
(29) Jacob, L.; Zasloff, M. Potential therapeutic applications of magainins and other antimicrobial agents of animal origin. [Review]. *Ciba Found. Symp.* **1994**, *186*, 197−216.
(30) Lohner, K.; Prossnigg, F. Biological activity and structural aspects of PGLa interaction with membrane mimetic systems. *Biochim. Biophys. Acta, Biomembr.* **2009**, *1778* (8), 1656−1666.
(31) Conlon, J. M.; Mechkarska, M. Host-defense peptides with therapeutic potential from skin secretions of frogs from the family Pipidae. *Pharmaceuticals* **2014**, *7*, 58−77.
(32) King, J. D.; Mechkarska, M.; Coquet, L.; Leprince, J.; Jouenne, T.; Vaudry, H.; Takada, K.; Conlon, J. M. Host-defense peptides from skin secretions of the tetraploid frogs Xenopus petersii and *Xenopus pygmaeus*, and the octoploid frog *Xenopus lenduensis* (Pipidae). *Peptides* **2012**, *33* (1), 35−43.
(33) Cesa-Luna, C.; Munoz-Rojas, J.; Saab-Rincon, G.; Baez, A.; Morales-Garcia, Y. E.; Juarez-Gonzalez, V. R.; Quintero-Hernandez, V. Structural characterization of scorpion peptides and their bactericidal activity against clinical isolates of multidrug-resistant bacteria. *PLoS One* **2019**, *14* (11), No. e0222438.
(34) Almaaytah, A.; Zhou, M.; Wang, L.; Chen, T.; Walker, B.; Shaw, C. Antimicrobial/cytolytic peptides from the venom of the North African scorpion, *Androctonus amoreuxi*: Biochemical and functional characterization of natural peptides and a single site-substituted analog. *Peptides* **2012**, *35*, 291−299.
(35) Almaaytah, A.; Farajallah, A.; Abualhaijaa, A.; Al-Balas, Q. A3, a scorpion venom derived peptide analogue with potent antimicrobial and potential antibiofilm activity against clinical isolates of Multi-Drug Resistant Gram-positive bacteria. *Molecules* **2018**, *23*, 1603−1615.
(36) Almaaytah, A.; Abualhaijaa, A.; Alqudah, O. The evaluation of the synergistic antimicrobial and antibiofilm activity of AamAP1-Lysine with conventional antibiotics against representative resistant strains of both Gram-positive and Gram-negative bacteria. *Infection and Drug Resistance* **2019**, *12*, 1371−1380.
(37) Song, C.; Wen, R.; Zhou, J.; Zeng, X.; Kou, Z.; Zhang, J.; Wang, T.; Chang, P.; Lv, Y.; Wu, R. Antibacterial and antifungal properties of a novel antimicrobial peptide GK-19 and its application in skin and soft tissue infections induced by *MRSA* or *Candida albicans*. *Pharmaceutics* **2022**, *14* (9), 1937−1949.
(38) Lee, K.; Shin, S. Y.; Kim, K.; Lim, S. S.; Hahm, K. S.; Kim, Y. Antibiotic activity and structural analysis of the scorpion-derived

© University of Pretoria
https://doi.org/10.1021/acsomega.4c01277
ACS Omega XXXX, XXX, XXX−XXX

UNIVERSITEIT VAN PRETORIA
UNIVERSITY OF PRETORIA
YUNIBESITHI YA PRETORIA

antimicrobial peptide, IsCT, and its analogs. *Biochem. Biophys. Res. Commun.* **2004**, *323* (2), 712−719.
(39) Acevedo, I. C. C.; Silva, P. I.; Silva, F. D.; Araújo, I.; Alves, F. L.; Oliveira, C. S.; Oliveira, V. X. IsCT-based analogs intending better biological activity. *Journal of Peptide Science: an Official Publication of the European Peptide Society* **2019**, *25* (12), No. e3219.
(40) Ismail, N. O.; Odendaal, C.; Serem, J. C.; Stromstedt, A. A.; Bester, M. J.; Sayed, Y.; Neitz, A. W. H.; Gaspar, A. R. M. Antimicrobial function of short amidated peptide fragments from the tick-derived OsDef2 defensin. *Journal of Peptide Science* **2019**, *25*, 1−9.
(41) Nakajima, Y.; Van Der Goes Van Naters-Yasui, A.; Taylor, D.; Yamakawa, M. Two isoforms of a member of the arthropod defensin family from the soft tick *Ornithodoros moubata* (Acari: Argasidae). *Insect Biochem. Mol. Biol.* **2001**, *31*, 747−751.
(42) Nakajima, Y.; Van Der Goes Van Naters-Yasui, A.; Taylor, D.; Yamakawa, M. Antibacterial peptide defensin is involved in midgut immunity of the soft tick, *Ornithodoros moubata*. *Insect Mol. Biol.* **2002**, *11*, 611−618.
(43) Dennison, S. R.; Harris, F.; Bhatt, T.; Singh, J.; Phoenix, D. A. The effect of C-terminal amidation on the efficacy and selectivity of antimicrobial and anticancer peptides. *Molecular and cellular biochemistry* **2009**, *332* (1−2), 43−50.
(44) Pasupuleti, M.; Chalupka, A.; Morgelin, M.; Schmidtchen, A.; Malmsten, M. Tryptophan end-tagging of antimicrobial peptides for increased potency against *Pseudomonas aeruginosa*. *Biochim. Biophys. Acta* **2009**, *1790*, 800−808.
(45) Garcia, A. E.; Osapay, G.; Tran, P. A.; Yuan, J.; Selsted, M. E. Isolation, synthesis, and antimicrobial activities of naturally occurring theta-defensin isoforms from baboon leukocytes. *Infect. Immun.* **2008**, *76* (12), 5883−5891.
(46) Connolly, M. L. Analytical molecular surface calculation. *J. Appl. Crystallogr.* **1983**, *16*, 548−558.
(47) Kelly, S. M.; Jess, T. J.; Price, N. C. How to study proteins by circular dichroism. *Biochimica et Biophysica Acta - Proteins Proteomics* **2005**, *1751* (2), 119−139.
(48) Rogers, D. M.; Jasim, S. B.; Dyer, N. T.; Auvray, F.; Réfrégiers, M.; Hirst, J. D. Electronic circular dichroism spectroscopy of proteins. *Chemistry* **2019**, *5* (11), 2751−2774.
(49) Baldwin, R. L.; Rohl, C. A. Deciphering rules of helix stability in peptides. *Methods Enzymol.* **1998**, *295*, 1−26.
(50) Fairlie, D. P.; Shepherd, N. E.; Hoang, H. N.; Abbenante, G. Single turn peptide alpha helices with exceptional stability in water. *J. Am. Chem. Soc.* **2005**, *127* (9), 2974−2983.
(51) Wang, D.; Cheng, K.; Kulp, J. L.; Arora, P. S. Evaluation of biologically relevant short alpha-helices stabilized by a main-chain hydrogen-bond surrogate. *J. Am. Chem. Soc.* **2006**, *128* (28), 9248−9256.
(52) Iwaniak, A.; Hrynkiewicz, M.; Bucholska, J.; Darewicz, M.; Minkiewicz, P. Structural characteristics of food protein-originating di- and tripeptides using principal component analysis. *European Food, Research and Technology* **2018**, *244*, 1751−1758.
(53) Dawson, R. M. C.; Elliott, D. C.; Elliott, W. H.; Jones, K. M. *Data for Biochemical Research*, 3rd ed.; Oxford Science Publications: 1986; pp 1−31.
(54) Fauchere, J. L.; Pliska, V. Hydrophobicity scale (pi-r). *Eur. J. Med. Chem.* **1983**, *18*, 369−375.
(55) Bartlett, M. S. A note on multiplying factors for various chi-squared approximations. *Journal of the Royal Statistical Society: Series B* **1954**, *16*, 296−298.
(56) O'rourke, N.; Hatcher, L.; Stepanski, E. J. Principal component analysis. In *A step-by-step approach to using SAS for univariate and multivariate statistics*, 2nd ed.; O'Rourke, N.; Hatcher, L.; Stepanski, E. J. *Eds.;* SAS Institute: Cary, 2005; pp 453−455.
(57) Stanisz, A. Statistical course with an application of STATISTICA PL on medicine examples. In *Principal component analysis*; Stanisz, A. Ed.; StatSoft Cracow: Poland, 2007; pp 165−181.
(58) Gong, H.; Zhang, J.; Hu, X.; Li, Z.; Fa, K.; Liu, H.; Waigh, T. A.; Mcbain, A.; Lu, J. R. Hydrophobic control of the bioactivity and cytotoxicity of de novo designed antimicrobial peptides. *ACS Appl. Mater. Interfaces* **2019**, *11* (38), 34609−34620.
(59) Frecer, V.; Ho, B.; Ding, J. L. De novo design of potent antimicrobial peptides. *Antimicrob. Agents Chemother.* **2004**, *48* (9), 3349−3357.
(60) Yeaman, M. R.; Yount, N. Y. Mechanisms of antimicrobial peptide action and resistance. *Pharmacol. Rev.* **2003**, *55*, 27−55.
(61) Mbuayama, K. R.; Taute, H.; Strömstedt, A. A.; Bester, M. J.; Gaspar, A. R. M. Antifungal activity and mode of action of synthetic peptides derived from the tick OsDef2 defensin. *J. Pept. Sci.* **2022**, *28* (5), No. e3383.
(62) Mai, X. T.; Huang, J.; Tan, J.; Huang, Y.; Chen, Y. Effects and mechanisms of the secondary structure on the antimicrobial activity and specificity of antimicrobial peptides. *Journal of Peptide Science: an official publication of the European Peptide Society* **2015**, *21* (7), 561−568.
(63) Li, S.; Wang, Y.; Xue, Z.; Jia, Y.; Li, R.; He, C.; Chen, H. The structure-mechanism relationship and mode of actions of antimicrobial peptides: A review. *Trends in Food ScienceTechnology* **2021**, *109*, 103−115.
(64) Pan, Y. L.; Cheng, J. T.; Hale, J.; Pan, J.; Hancock, R. E.; Straus, S. K. Characterization of the structure and membrane interaction of the antimicrobial peptides aurein 2.2 and 2.3 from Australian southern bell frogs. *Biophys. J.* **2007**, *92* (8), 2854−2864.
(65) Wojciechowska, M.; Miszkiewicz, J.; Trylska, J. Conformational changes of Anoplin, W-MreB1−9, and (KFF)3K peptides near the membranes. *International Journal of Molecular Sciences* **2020**, *21* (24), 9672.
(66) Urushibara, T.; Hicks, R. Effect of liposome surface charge and peptide side chain charge density on antimicrobial peptide-membrane binding as determined by circular dichroism. *J. Membr. Sci. Technol.* **2013**, *3* (3), 124.
(67) Gagnon, M.; Strandberg, E.; Grau-Campistany, A.; Wadhwani, P.; Reichert, J.; Bürck, J.; Rabanal, F.; Auger, M.; Paquin, J. F.; Ulrich, A. S. Influence of the length and charge on the activity of alpha-helical amphipathic antimicrobial peptides. *Biochemistry* **2017**, *56* (11), 1680−1695.
(68) Liu, Z.; Brady, A.; Young, A.; Rasimick, B.; Chen, K.; Zhou, C.; Kallenbach, N. R. Length effects in antimicrobial peptides of the (RW)n series. *Antimicrob. Agents Chemother.* **2007**, *51* (2), 597−603.
(69) Wang, C.; Hong, T.; Cui, P.; Wang, J.; Xia, J. Antimicrobial peptides towards clinical application: Delivery and formulation. *Adv. Drug Delivery Rev.* **2021**, *175*, No. 113818.
(70) Mahlapuu, M.; Björn, C.; Ekblom, J. Antimicrobial peptides as therapeutic agents: opportunities and challenges. *Critical Reviews in Biotechnology* **2020**, *40* (7), 978−992.
(71) Cardoso, M. H.; Orozco, R. Q.; Rezende, S. B.; Rodrigues, G.; Oshiro, K. G. N.; Cândido, E. S.; Franco, O. L. Computer-aided design of antimicrobial peptides: Are we generating effective drug candidates? *Frontiers in Microbiology* **2020**, *10*, 3097.
(72) Toropova, M. A.; Aleksandar, M. V.; Veselinović, J. B.; Stojanović, D. B.; Toropov, A. A. QSAR modeling of the antimicrobial activity of peptides as a mathematical function of a sequence of amino acids. *Comput. Biol. Chem.* **2015**, *59* (Pt A), 126−130.
(73) Hwang, P. M.; Vogel, H. J. Structure-function relationships of antimicrobial peptides. *Biochemistry and Cell Biology* **1998**, *76* (2), 235−246.
(74) De Planque, M. R. R.; Kruijtzer, J. A. W.; Liskamp, R. M. J.; Marsh, D.; Greathouse, D. V.; Koeppe, R. E.; De Kruijff, B.; Killian, J. A. Different membrane anchoring positions of tryptophan and lysine in synthetic transmembrane α-helical peptides. *J. Biol. Chem.* **1999**, *274*, 20839−20846.
(75) Fields, F. R.; Manzo, G.; Hind, C. K.; Janardhanan, J.; Foik, I. P.; Do Carmo Silva, P.; Balsara, R. D.; Clifford, M.; Vu, H. M.; Ross, J. N.; Kalwajtys, V. R.; Gonzalez, A. J.; Bui, T. T.; Ploplis, V. A.; Castellino, F. J.; Siryaporn, A.; Chang, M.; Sutton, J. M.; Mason, A. J.; Lee, S. Synthetic antimicrobial peptide tuning permits membrane disruption and interpeptide synergy. *ACS Pharmacol. Transl. Sci.* **2020**, *3* (3), 418−424.

© University of Pretoria
https://doi.org/10.1021/acsomega.4c01277
ACS Omega XXXX, XXX, XXX−XXX

UNIVERSITEIT VAN PRETORIA
UNIVERSITY OF PRETORIA
YUNIBESITHI YA PRETORIA

(76) Wimley, W.; White, S. Experimentally determined hydrophobicity scale for proteins at membrane interfaces. *Nature Structural & Molecular Biology* **1996**, *3*, 842−848.
(77) Clarke, M.; Hind, C. K.; Ferguson, P. M.; Manzo, G.; Mistry, B.; Yue, B.; Romanopulos, J.; Clifford, M.; Bui, T. T.; Drake, A. F.; Lorenz, C. D.; Sutton, J. M.; Mason, A. J. Synergy between Winter Flounder Antimicrobial peptides. *npj Antimicrobials & Resistance* **2023**, *1* (8), 1−16.
(78) Ferguson, P. M.; Clarke, M.; Manzo, G.; Hind, C. K.; Clifford, M.; Sutton, J. M.; Lorenz, C. D.; Phoenix, D. A.; Mason, A. J. Temporin B forms heterooligomers with Temporin L, modifies its membrane activity and increases the cooperativity of its antibacterial pharmacodynamic profile. *Biochemistry* **2022**, *61*, 1029−1040.
(79) Manzo, G.; Hind, C. K.; Ferguson, P. M.; Amison, R. T.; Hodgson-Casson, A. C.; Ciazynska, K. A.; Weller, B. J.; Clarke, M.; Lam, C.; Man, R. C. H.; O'shaughnessy, B. G.; Clifford, M.; Bui, T. T.; Drake, A. F.; Atkinson, R. A.; Lam, J. K. W.; Pitchford, S. C.; Page, C. P.; Phoenix, D. A.; Lorenz, C. D.; Sutton, J. M.; Mason, A. J. A Pleurocidin analogue with greater conformational flexibility, enhanced antimicrobial potency and in vivo therapeutic efficacy. *Commun. Biol.* **2020**, *3* (1), 697.
(80) Manzo, G.; Ferguson, P. M.; Hind, C.; Clifford, M.; Gustilo, V. B.; Ali, H.; Bansal, S. S.; Bui, T. T.; Drake, A. F.; Atkinson, R. A.; Sutton, J. M.; Lorenz, C. D.; Phoenix, D. A.; Mason, A. J. Temporin L and aurein 2.5 have identical conformations but subtly distinct membrane and antibacterial activities. *Sci. Rep.* **2019**, *9* (1), 10934.
(81) Manzo, G.; Ferguson, P. M.; Gustilo, V. B.; Hind, C.; Clifford, M.; Bui, T. T.; Drake, A. F.; Atkinson, R. A.; Sutton, M. J.; Batoni, G.; Lorenz, C. D.; Phoenix, D. A.; Mason, A. J. Minor sequence modifications in temporin B cause drastic changes in antibacterial potency and selectivity by fundamentally altering membrane activity. *Sci. Rep.* **2019**, *9* (1385), 1−16.

© University of Pretoria
https://doi.org/10.1021/acsomega.4c01277
ACS Omega XXXX, XXX, XXX−XXX

QSAR reveals decreased lipophilicity of polar residues determines the selectivity of antimicrobial peptide activity

Mandelie van der Walt[a], Dalton S. Moller[a], Rosalind J. van Wyk[a], Philip M. Ferguson[b], Charlotte K. Hind[c], Melanie Clifford[c], Phoebe Do Carmo Silva[c], J. Mark Sutton[c], A. James Mason[b]*, Megan J. Bester[d], Anabella R. M. Gaspar[a]*

[a] Department of Biochemistry, Genetics and Microbiology, Faculty of Natural and Agricultural Sciences, University of Pretoria, 0002, South Africa
[b] Institute of Pharmaceutical Science, School of Cancer & Pharmaceutical Science, King's College London, Franklin-Wilkins Building, 150 Stamford Street, London, SE1 9NH, United Kingdom
[c] Antimicrobial Discovery Development and Diagnostics, Vaccine Evaluation and Development Centre, UK Health Security Agency, SP4 0JG, United Kingdom
[d] Department of Anatomy, Faculty of Health Sciences, University of Pretoria, 0002, South Africa

***Corresponding authors:**

Prof. A.J. Mason, Institute of Pharmaceutical Science, King's College London, james.mason@kcl.ac.uk

Prof. A.R.M. Gaspar, Department of Biochemistry, Genetics and Microbiology, Faculty of Natural and Agricultural Sciences, University of Pretoria, anabella.gaspar@up.ac.za

SUPPLEMENTARY MATERIALS

© University of Pretoria

1. Peptide properties per residue

Table S1: *Sidechain descriptors of amino acids used in PCA and QSAR analyses*

Amino acid	charge	L_P[a]	L_N[a]	L_P[b]	L_N[b]	$SCSA_P$ (Å)[c]	$SCSA_N$ (Å)[c]	MwP	MwN	CSL[d]	CAR[d]	HBacc	HBdon	R.B.i[e]
Ala	*0*	*0*	*0.31*	*0*	*-0.17*	*0*	*19.6*	*0*	*71.1*	*1*	*0*	*0*	*0*	*0*
Arg	*+1*	*-1.01*	*0*	*-0.81*	*0*	*39.7*	*0*	*156.2*	*0*	*0*	*0*	*1*	*4*	*4*
Asn	*0*	*-0.6*	*0*	*-0.42*	*0*	*114.5*	*0*	*114.1*	*0*	*0*	*0*	*1*	*2*	*2*
Asp	*-1*	*-2.57*	*0*	*-1.23*	*0*	*53.0*	*0*	*115.1*	*0*	*0*	*0*	*2*	*0*	*2*
Cys	*0*	*0*	*1.54*	*0*	*0.24*	*0*	*37.6*	*0*	*103.1*	*1*	*0*	*1*	*1*	*2*
Gln	*0*	*-0.22*	*0*	*-0.58*	*0*	*71.7*	*0*	*146.1*	*0*	*0*	*0*	*1*	*2*	*3*
Glu	*-1*	*-2.29*	*0*	*-2.02*	*0*	*61.6*	*0*	*129.1*	*0*	*0*	*0*	*2*	*0*	*3*
Gly	*0*	*0*	*0*	*0*	*-0.01*	*0*	*0*	*0*	*57.1*	*0*	*0*	*0*	*0*	*0*
His	*0*	*0.13*	*0*	*-0.17*	*0*	*75.7*	*0*	*137.1*	*0*	*0*	*0*	*1*	*1*	*2*
Ile	*0*	*0*	*1.8*	*0*	*0.31*	*0*	*68.4*	*0*	*113.2*	*1*	*0*	*0*	*0*	*2*
Leu	*0*	*0*	*1.7*	*0*	*0.56*	*0*	*69.9*	*0*	*113.2*	*1*	*0*	*0*	*0*	*2*
Lys	*+1*	*-0.99*	*0*	*-0.99*	*0*	*90.7*	*0*	*128.2*	*0*	*0*	*0*	*1*	*2*	*5*
Met	*0*	*0*	*1.23*	*0*	*0.23*	*0*	*78.2*	*0*	*131.2*	*1*	*0*	*1*	*0*	*3*
Phe	*0*	*0*	*1.79*	*0*	*1.13*	*0*	*92.2*	*0*	*147.2*	*0*	*1*	*0*	*0*	*2*
Pro	*0*	*0*	*0.72*	*0*	*-0.45*	*0*	*39.7*	*0*	*97.1*	*1*	*0*	*0*	*-1*	*0*
Ser	*0*	*-0.04*	*0*	*-0.13*	*0*	*26.7*	*0*	*87.1*	*0*	*0*	*0*	*1*	*1*	*2*
Thr	*0*	*0.26*	*0*	*-0.14*	*0*	*44.8*	*0*	*101.1*	*0*	*0*	*0*	*1*	*1*	*2*
Trp	*0*	*0*	*2.25*	*0*	*1.85*	*0*	*121.1*	*0*	*186.2*	*0*	*1*	*0*	*1*	*2*
Tyr	*0*	*0.96*	*0*	*0.94*	*0*	*102.0*	*0*	*163.2*	*0*	*0*	*1*	*1*	*1*	*3*
Val	*0*	*0*	*1.22*	*0*	*-0.07*	*0*	*51.1*	*0*	*99.1*	*1*	*0*	*0*	*0*	*1*

[a]The lipophilicity of polar or nonpolar amino acids at pH 7.0 taken from Frecer (28) and Fauchere & Pliska (54) calculated using $\pi_{FP} = \log P_{o/w}(\text{a.a.}) - \log P_{o/w}(\text{Gly})$
[b]The lipophilicity of polar or nonpolar amino acids at pH 7.0 according to the Wimley-white bilayer/water scale (74)
[c]The side chain surface areas (SCSA) of amino acids taken from Frecer (28) as calculated by Connolly surfaces method (46)
[d]Count of small lipophilic (CSL) or aromatic (CAR) residues taken from Frecer (28)
[e]The number of rotatable bonds in an amino acid side chain: R.B.i = Rotatable Bonds (a.a.) - Rotatable Bonds (Gly)

© University of Pretoria

2. Antimicrobial activity

Table S2: *Antibiogram employed in the AMP susceptibility testing for susceptible and resistant (A) Gram-negative and -positive bacteria and (B) fungi.*

A

Isolate	Modal MICs (µg/mL)				
	Colistin	Tobra-mycin	Cipro-floxacin	Gentamycin	Ceftazidime
Gram-negative					
E. coli NCTC 12923 (S)	0.0625	16	≤0.125	1	≤0.125
E. coli LEC001 (R)	2	8	32	4	128
P. aeruginosa PAO1 (S)	2	2	0.5	4	1
P. aeruginosa NCTC 13437 (R)	4	64	64	256	>128
A. baumannii ATCC 17978 (S)	1	4	0.5	0.5	<0.5
A. baumannii AYE (R)	1	64	128	>512	>128
K. pneumoniae M6 (S)	2	8	<0.5	0.25	<0.5
K. pneumoniae NCTC 13368 (R)	1	64	0.5	4	512
Gram-positive					
S. aureus (MSSA) ATCC 9144 (S)	ND	0.25-0.5	1	0.25	16
S. aureus (MRSA) NCTC 13616 (R)	>128	0.5	64	0.25	128
S. aureus (MRSA) USA300 (R)	ND	ND	64	4	32
S. aureus (MRSA) 1199B (R)	ND	0.25	8	0.25	8

B

Isolate	Modal MICs (µg/mL)				
	Fluconazole	Caspofungin	Voriconazole	Ampho-tericin B	Abafungin
Fungi					
C. auris TDG 1912	>128	0.03	1	0.03	>128
C. albicans NCPF 3281	0.06-0.125	≤0.007	≤0.007	0.015	>128
C. glabrata NCPF 8018	4	≤0.007	0.125	0.03	>128
C. krusei NCPF 3876	8	≤0.007	0.06	0.06	0.25
C. tropicalis NCPF 8760	16	≤0.007	0.5	0.03	>128
C. parapsilosis NCPF 3209	0.25	0.125	≤0.007	≤0.007	0.25-0.5

© University of Pretoria

Table S3: *Inhibitory activity of 15 frog derived AMPs against a panel of susceptible and resistant bacteria*

Isolate	Modal MICs (µg/mL)														
	X. laevis					***X. petersii***						***X. muelleri***			
	XPF	**XPF10a**	**DRAMP 02272**	**DRAMP 02273**	**X1-20a**	**CPF-P2**	**CPF-P2a**	**CPF-P3**	**CPF-P3-10a**	**CPF-P3-12a**	**CPF-P3-20a**	**CPF-MW1**	**CPF-MW-10a**	**CPF-MW-12a**	**CPF-MW-20a**
Gram-negative															
E. coli NCTC 12923 (S)	**4**	>128	**4**	>128	**8**	**8**	**32**	**8**	>128	>128	**128**	**8**	>128	>128	**16**
E. coli LEC001 (R)	**4**	>128	**8**	>128	>128	**16**	**64**	**8**	>128	>128	>128	**8**	>128	>128	**64**
P. aeruginosa PAO1 (S)	**128**	>128	>128	>128	>128	>128	>128	>128	>128	>128	>128	>128	>128	>128	>128
P. aeruginosa NCTC 13437 (R)	**128**	>128	>128	>128	>128	**128**	>128	**64**	>128	>128	>128	**128**	>128	>128	>128
A. baumannii ATCC 17978 (S)	**4**	>128	**4**	>128	**16**	**4**	**32**	**4**	>128	>128	**128**	**4**	>128	>128	**32**
A. baumannii AYE (R)	**4**	>128	**2**	>128	**16**	**8**	**64**	**8**	>128	>128	**128**	**4**	>128	>128	**32**
K. pneumoniae M6 (S)	**64**	>128	**32**	>128	**32**	**128**	>128	**32**	>128	>128	>128	**16**	>128	>128	>128
K. pneumoniae NCTC 13368 (R)	**32**	>128	**64**	>128	**64**	**128**	>128	**32**	>128	>128	>128	**32**	>128	>128	>128
Gram-positive															
S. aureus (MSSA) ATCC 9144 (S)	**32**	>128	**8**	>128	**16**	**4**	>128	**4**	>128	>128	>128	**4**	>128	>128	**64**
S. aureus (MRSA) NCTC 13616 (R)	**128**	>128	**16**	>128	>128	**4**	>128	**4**	>128	>128	>128	**4**	>128	>128	**128**
S. aureus (MRSA) USA300 (R)	**128**	>128	**32**	>128	>128	**8**	>128	**8**	>128	>128	>128	**8**	>128	>128	**128**
S. aureus (MRSA) 1199B (R)	**128**	>128	**64**	>128	>128	**8**	>128	**8**	>128	>128	>128	**4**	>128	>128	**128**

© University of Pretoria

Table S3 B: *Inhibitory activity of 15 frog derived AMPs against a panel of susceptible and resistant bacteria* ***shown in µM***

Isolate	Modal MICs (µM)													
	X. laevis					*X. petersii*						*X. muelleri*		
	XPF	XPF10a	DRAMP 02272	DRAMP 02273	X1-20a	CPF-P2	CPF-P2a	CPF-P3	CPF-P3-10a	CPF-P3-12a	CPF-P3-20a	CPF-MW1	CPF-MW-10a	CPF-MW-12a	CPF-MW-20a
Gram-negative															
E. coli NCTC 12923 (S)	**1.5**	>120.6	**2**	>117.5	**3.4**	**2.9**	**18.6**	**2.9**	>122	>103.8	**65.7**	**2.7**	>110.8	>95.5	**6.5**
E. coli LEC001 (R)	**1.5**	>120.6	**4**	>117.5	>55	**5.8**	**37.1**	**2.9**	>122	>103.8	>65.7	**2.7**	>110.8	>95.5	**25.8**
P. aeruginosa PAO1 (S)	**46.5**	>120.6	>64	>117.5	>55	>46	>74	>47	>122	>103.8	>65.7	>43.1	>110.8	>95.5	>51.7
P. aeruginosa NCTC 13437 (R)	**46.5**	>120.6	>64	>117.5	>55	**46**	>74	**23.5**	>122	>103.8	>65.7	**43.1**	>110.8	>95.5	>51.7
A. baumannii ATCC 17978 (S)	**1.5**	>120.6	**2**	>117.5	**6.9**	**1.4**	**18.6**	**1.5**	>122	>103.8	**65.7**	**1.4**	>110.8	>95.5	**12.9**
A. baumannii AYE (R)	**1.5**	>120.6	**1**	>117.5	**6.9**	**2.9**	**37.1**	**2.9**	>122	>103.8	**65.7**	**1.4**	>110.8	>95.5	**12.9**
K. pneumoniae M6 (S)	**23.2**	>120.6	**16**	>117.5	**13.8**	**46**	>74	**11.8**	>122	>103.8	>65.7	**5.4**	>110.8	>95.5	>51.7
K. pneumoniae NCTC 13368 (R)	**11.6**	>120.6	**32**	>117.5	**27.5**	**46**	>74	**11.8**	>122	>103.8	>65.7	**10.8**	>110.8	>95.5	>51.7
Gram-positive															
S. aureus (MSSA) ATCC 9144 (S)	**11.6**	>120.6	**4**	>117.5	**6.9**	**1.4**	>74	**1.5**	>122	>103.8	>65.7	**1.4**	>110.8	>95.5	**25.8**
S. aureus (MRSA) NCTC 13616 (R)	**46.5**	>120.6	**8**	>117.5	>55	**1.4**	>74	**1.5**	>122	>103.8	>65.7	**1.4**	>110.8	>95.5	**51.7**
S. aureus (MRSA) USA300 (R)	**46.5**	>120.6	**16**	>117.5	>55	**2.9**	>74	**2.9**	>122	>103.8	>65.7	**2.7**	>110.8	>95.5	**51.7**
S. aureus (MRSA) 1199B (R)	**46.5**	>120.6	**32**	>117.5	>55	**2.9**	>74	**2.9**	>122	>103.8	>65.7	**1.4**	>110.8	>95.5	**51.7**

© University of Pretoria

Table S4: *Inhibitory activity of 16 scorpion derived AMPs against a panel of susceptible and resistant bacteria*

Isolate	Modal MICs (µg/mL)															
	P. schlectheri				*O. carinatus*		*A. amoeruxi*							*O. madagascariensis*		
	PS-PB-8a	PS-PB-14a	PS-PB-16a	PS-PB-20a	Opis16a	Opis8a	AamAP1	AamAP-S1	AamAP-S1a	AamAP1-Lys	AamAP1-Lysa	A3	A3a	K3-IsCTa	K7P8K11-IsCTa	A1F5K8-IsCTa
Gram-negative																
E. coli NCTC 12923 (S)	>128	>128	**16**	**32**	**4**	>128	>128	**64**	**16**	**4**	**4**	>128	**16**	**8**	**16**	**8**
E. coli LEC001 (R)	>128	>128	**64**	**64**	**4**	>128	>128	**32**	**16**	**8**	**8**	>128	**32**	**8**	**64**	**8**
P. aeruginosa PAO1 (S)	>128	>128	**64**	**128**	**128**	>128	>128	>128	>128	**32**	**16**	>128	**32**	>128	>128	>128
P. aeruginosa NCTC 13437 (R)	>128	>128	**128**	>128	**32**	>128	>128	>128	**128**	**16**	**16**	>128	**16**	**64**	**64**	**64**
A. baumannii ATCC 17978 (S)	>128	>128	**16**	**8**	**2**	>128	**128**	**64**	**8**	**4**	**2**	**8**	**8**	**4**	**8**	**4**
A. baumannii AYE (R)	>128	>128	**32**	**32**	**2**	>128	**128**	**32**	**8**	**2**	**4**	**16**	**16**	**8**	**8**	**8**
K. pneumoniae M6 (S)	>128	>128	>128	>128	**8**	>128	>128	>128	**64**	**16**	**8**	>128	**32**	**16**	**32**	**16**
K. pneumoniae NCTC 13368 (R)	>128	>128	>128	>128	**16**	>128	>128	>128	**64**	**16**	**8**	>128	**32**	**16**	**64**	**16**
Gram-positive																
S. aureus (MSSA) ATCC 9144 (S)	>128	>128	**32**	**8**	**2**	>128	**64**	**16**	**4**	**4**	**4**	**16**	**16**	**8**	**8**	**4**
S. aureus (MRSA) NCTC 13616 (R)	>128	>128	>128	>128	**4**	>128	**64**	**64**	**8**	**4**	**2**	**16**	**16**	**8**	**64**	**16**
S. aureus (MRSA) USA300 (R)	>128	>128	>128	>128	**8**	>128	**128**	**64**	**8**	**8**	**4**	**32**	**16**	**16**	**64**	**16**
S. aureus (MRSA) 1199B (R)	>128	>128	>128	>128	**4**	>128	**64**	**32**	**4**	**4**	**4**	**16**	**8**	**8**	**32**	**8**

© University of Pretoria

Table S4 B: *Inhibitory activity of 16 scorpion derived AMPs against a panel of susceptible and resistant bacteria* ***shown in µM***

Isolate	Modal MICs (µM)															
	P. schlectheri				*O. carinatus*		*A. amoeruxi*							*O. madagascariensis*		
	PS-PB-8a	PS-PB-14a	PS-PB-16a	PS-PB-20a	Opis16a	Opis8a	AamAP1	AamAP-S1	AamAP-S1a	AamAP1-Lys	AamAP1-Lysa	A3	A3a	K3-lsCTa	K7P8 K11-lsCTa	A1F5K8-lsCTa
Gram-negative																
E. coli NCTC 12923 (S)	>127.2	>63.8	**8.5**	**13.9**	**2**	>133.2	>64.8	**32.2**	**8.1**	**1.8**	**1.8**	>62.9	**7.9**	**5**	**9.9**	**5**
E. coli LEC001 (R)	>127.2	>63.8	**33.9**	**27.8**	**2**	>133.2	>64.8	**16.1**	**8.1**	**3.6**	**3.6**	>62.9	**15.7**	**5**	**39.5**	**5**
P. aeruginosa PAO1 (S)	>127.2	>63.8	**33.9**	**55.7**	**64.7**	>133.2	>64.8	>64.5	>64.8	**14.4**	**7.2**	>62.9	**15.7**	>79.5	>79	>79.9
P. aeruginosa NCTC 13437 (R)	>127.2	>63.8	**67.8**	>55.7	**16.2**	>133.2	>64.8	>64.5	**64.8**	**7.2**	**7.2**	>62.9	**7.9**	**39.8**	**39.5**	**39.9**
A. baumannii ATCC 17978 (S)	>127.2	>63.8	**8.5**	**3.5**	**1**	>133.2	**64.8**	**32.2**	**4.1**	**1.8**	**0.9**	**3.9**	**3.9**	**2.5**	**4.9**	**2.5**
A. baumannii AYE (R)	>127.2	>63.8	**17**	**13.9**	**1**	>133.2	**64.8**	**16.1**	**4.1**	**0.9**	**1.8**	**7.9**	**7.9**	**5**	**4.9**	**5**
K. pneumoniae M6 (S)	>127.2	>63.8	>67.8	>55.7	**4**	>133.2	>64.8	>64.5	**32.4**	**7.2**	**3.6**	>62.9	**15.7**	**9.9**	**19.8**	**10**
K. pneumoniae NCTC 13368 (R)	>127.2	>63.8	>67.8	>55.7	**8.1**	>133.2	>64.8	>64.5	**32.4**	**7.2**	**3.6**	>62.9	**15.7**	**9.9**	**39.5**	**10**
Gram-positive																
S. aureus (MSSA) ATCC 9144 (S)	>127.2	>63.8	**17**	**3.5**	**1**	>133.2	**32.4**	**8.1**	**2**	**1.8**	**1.8**	**7.9**	**7.9**	**5**	**4.9**	**2.5**
S. aureus (MRSA) NCTC 13616 (R)	>127.2	>63.8	>67.8	>55.7	**2**	>133.2	**32.4**	**32.2**	**4.1**	**1.8**	**0.9**	**7.9**	**7.9**	**5**	**39.5**	**10**
S. aureus (MRSA) USA300 (R)	>127.2	>63.8	>67.8	>55.7	**4**	>133.2	**64.8**	**32.2**	**4.1**	**3.6**	**1.8**	**15.7**	**7.9**	**9.9**	**39.5**	**10**
S. aureus (MRSA) 1199B (R)	>127.2	>63.8	>67.8	>55.7	**2**	>133.2	**32.4**	**16.1**	**2**	**1.8**	**1.8**	**7.9**	**3.9**	**5**	**19.8**	**5**

© University of Pretoria

Table S5: *Inhibitory activity of 11 tick derived AMPs against a panel of susceptible and resistant bacteria*

Isolate	Modal MICs (µg/mL)										
	O. savignyi							*O. moubata*			
	Os	Osa	Os-C	Os(3-12)a	Os(11-22)a	W3(Os-C)a	W(Os-C)a	OmDefB	OmDef19	W-OmC-Ca	W-OmB-Ca
Gram-negative											
E. coli NCTC 12923 (S)	>128	>128	>128	>128	>128	**64**	>128	>128	>128	**128**	**128**
E. coli LEC001 (R)	>128	>128	>128	>128	>128	>128	>128	>128	>128	>128	>128
P. aeruginosa PAO1 (S)	>128	>128	>128	>128	>128	>128	>128	>128	>128	>128	>128
P. aeruginosa NCTC 13437 (R)	>128	>128	>128	>128	>128	>128	>128	>128	>128	>128	>128
A. baumannii ATCC 17978 (S)	>128	>128	>128	>128	>128	**32**	**64**	>128	>128	**128**	**64**
A. baumannii AYE (R)	>128	>128	>128	>128	>128	**16**	**32**	>128	>128	**128**	**32**
K. pneumoniae M6 (S)	>128	>128	>128	>128	>128	>128	>128	>128	>128	>128	>128
K. pneumoniae NCTC 13368 (R)	>128	>128	>128	>128	>128	>128	>128	>128	>128	>128	>128
Gram-positive											
S. aureus (MSSA) ATCC 9144 (S)	>128	>128	>128	>128	>128	**32**	**128**	>128	>128	**128**	**128**
S. aureus (MRSA) NCTC 13616 (R)	>128	>128	>128	>128	>128	>128	>128	>128	>128	>128	>128
S. aureus (MRSA) USA300 (R)	>128	>128	>128	>128	>128	>128	>128	>128	>128	>128	>128
S. aureus (MRSA) 1199B (R)	>128	>128	>128	>128	>128	>128	>128	>128	>128	>128	>128

© University of Pretoria

Table S5 B: *Inhibitory activity of 11 tick derived AMPs against a panel of susceptible and resistant bacteria* ***shown in µM***

Isolate	Modal MICs (µM)										
	O. savignyi							*O. moubata*			
	Os	**Osa**	**Os-C**	**Os(3-12)a**	**Os(11-22)a**	**W3(Os-C)a**	**W(Os-C)a**	**OmDefB**	**OmDef19**	**W-OmC-Ca**	**W-OmB-Ca**
Gram-negative											
E. coli NCTC 12923 (S)	>51.7	>51.7	>59	>112	>91.7	**23.5**	>54.4	>49.9	>56.8	**54.3**	**52.5**
E. coli LEC001 (R)	>51.7	>51.7	>59	>112	>91.7	>46.9	>54.4	>49.9	>56.8	>54.3	>52.5
P. aeruginosa PAO1 (S)	>51.7	>51.7	>59	>112	>91.7	>46.9	>54.4	>49.9	>56.8	>54.3	>52.5
P. aeruginosa NCTC 13437 (R)	>51.7	>51.7	>59	>112	>91.7	>46.9	>54.4	>49.9	>56.8	>54.3	>52.5
A. baumannii ATCC 17978 (S)	>51.7	>51.7	>59	>112	>91.7	**11.7**	**27.2**	>49.9	>56.8	**54.3**	**26.2**
A. baumannii AYE (R)	>51.7	>51.7	>59	>112	>91.7	**5.9**	**13.6**	>49.9	>56.8	**54.3**	**13.1**
K. pneumoniae M6 (S)	>51.7	>51.7	>59	>112	>91.7	>46.9	>54.4	>49.9	>56.8	>54.3	>52.5
K. pneumoniae NCTC 13368 (R)	>51.7	>51.7	>59	>112	>91.7	>46.9	>54.4	>49.9	>56.8	>54.3	>52.5
Gram-positive											
S. aureus (MSSA) ATCC 9144 (S)	>51.7	>51.7	>59	>112	>91.7	**11.7**	**54.4**	>49.9	>56.8	**54.3**	**52.5**
S. aureus (MRSA) NCTC 13616 (R)	>51.7	>51.7	>59	>112	>91.7	>46.9	>54.4	>49.9	>56.8	>54.3	>52.5
S. aureus (MRSA) USA300 (R)	>51.7	>51.7	>59	>112	>91.7	>46.9	>54.4	>49.9	>56.8	>54.3	>52.5
S. aureus (MRSA) 1199B (R)	>51.7	>51.7	>59	>112	>91.7	>46.9	>54.4	>49.9	>56.8	>54.3	>52.5

© University of Pretoria

Table S6: *Inhibitory activity of 4 primate derived AMPs against a panel of susceptible and resistant bacteria*

Isolate	Modal MICs (µg/mL)			
	Papio anubis			
	ThetaDefA	ThetaDefB	BTD15a	BTD11a
Gram-negative				
E. coli NCTC 12923 (S)	>128	>128	**8**	>128
E. coli LEC001 (R)	>128	>128	**16**	>128
P. aeruginosa PAO1 (S)	>128	>128	>128	>128
P. aeruginosa NCTC 13437 (R)	>128	>128	>128	>128
A. baumannii ATCC 17978 (S)	>128	>128	**4**	>128
A. baumannii AYE (R)	>128	>128	**8**	>128
K. pneumoniae M6 (S)	>128	>128	**32**	>128
K. pneumoniae NCTC 13368 (R)	>128	>128	**32**	>128
Gram-positive				
S. aureus (MSSA) ATCC 9144 (S)	>128	>128	**8**	>128
S. aureus (MRSA) NCTC 13616 (R)	>128	>128	**8**	>128
S. aureus (MRSA) USA300 (R)	>128	>128	**8**	>128
S. aureus (MRSA) 1199B (R)	>128	>128	**8**	>128

© University of Pretoria

Table S6 B: *Inhibitory activity of 4 primate derived AMPs against a panel of susceptible and resistant bacteria* ***shown in µM***

Isolate	Modal MICs (µM)			
	Papio anubis			
	ThetaDefA	ThetaDefB	BTD15a	BTD11a
Gram-negative				
E. coli NCTC 12923 (S)	>122.6	>116.4	**4.4**	>94
E. coli LEC001 (R)	>122.6	>116.4	**8.8**	>94
P. aeruginosa PAO1 (S)	>122.6	>116.4	>70.2	>94
P. aeruginosa NCTC 13437 (R)	>122.6	>116.4	>70.2	>94
A. baumannii ATCC 17978 (S)	>122.6	>116.4	**2.2**	>94
A. baumannii AYE (R)	>122.6	>116.4	**4.4**	>94
K. pneumoniae M6 (S)	>122.6	>116.4	**17.5**	>94
K. pneumoniae NCTC 13368 (R)	>122.6	>116.4	**17.5**	>94
Gram-positive				
S. aureus (MSSA) ATCC 9144 (S)	>122.6	>116.4	**4.4**	>94
S. aureus (MRSA) NCTC 13616 (R)	>122.6	>116.4	**4.4**	>94
S. aureus (MRSA) USA300 (R)	>122.6	>116.4	**4.4**	>94
S. aureus (MRSA) 1199B (R)	>122.6	>116.4	**4.4**	>94

© University of Pretoria

Table S7: *Inhibitory activity of 15 frog derived AMPs against a panel of fungal species*

Isolate		Modal MICs (µg/mL)														
		X. laevis					***X. petersii***						***X. muelleri***			
		XPF	**XPF10a**	**DRAMP 02272**	**DRAMP 02273**	**X1-20a**	**CPF-P2**	**CPF-P2a**	**CPF-P3**	**CPF-P3-10a**	**CPF-P3-12a**	**CPF-P3-20a**	**CPF-MW1**	**CPF-MW-10a**	**CPF-MW-12a**	**CPF-MW-20a**
C. auris TDG 1912	**MIC50**	>128	>128	>128	>128	>128	>128	>128	>128	>128	>128	>128	>128	>128	>128	>128
	MIC90	>128	>128	>128	>128	>128	>128	>128	>128	>128	>128	>128	>128	>128	>128	>128
C. albicans NCPF 3281	**MIC50**	>128	>128	>128	>128	>128	>128	>128	>128	>128	>128	>128	>128	>128	>128	>128
	MIC90	>128	>128	>128	>128	>128	>128	>128	>128	>128	>128	>128	>128	>128	>128	>128
C. glabrata NCPF 8018	**MIC50**	>128	>128	>128	>128	>128	>128	>128	>128	>128	>128	>128	>128	>128	>128	>128
	MIC90	>128	>128	>128	>128	>128	>128	>128	>128	>128	>128	>128	>128	>128	>128	>128
C. krusei NCPF 3876	**MIC50**	>128	>128	**128**	>128	**64**	**64**	>128	**64**	>128	>128	>128	**64**	>128	>128	>128
	MIC90	>128	>128	**128**	>128	**64**	**64**	>128	**64**	>128	>128	>128	**64**	>128	>128	>128
C. tropicalis NCPF 8760	**MIC50**	**32**	>128	**32**	>128	**16**	**16**	>128	**8**	>128	>128	>128	**32**	>128	>128	>128
	MIC90	**32**	>128	**32**	>128	**32**	**16**	>128	**16**	>128	>128	>128	**32**	>128	>128	>128
C. parapsilosis NCPF 3209	**MIC50**	>128	>128	>128	>128	>128	>128	>128	>128	>128	>128	>128	>128	>128	>128	>128
	MIC90	>128	>128	>128	>128	>128	>128	>128	>128	>128	>128	>128	>128	>128	>128	>128

© University of Pretoria

Table S7 B: *Inhibitory activity of 15 frog derived AMPs against a panel of fungal species* ***shown in µM***

Isolate		Modal MICs (µM)														
		X. laevis					*X. petersii*						*X. muelleri*			
		XPF	XPF10a	DRAMP 02272	DRAMP 02273	X1-20a	CPF-P2	CPF-P2a	CPF-P3	CPF-P3-10a	CPF-P3-12a	CPF-P3-20a	CPF-MW1	CPF-MW-10a	CPF-MW-12a	CPF-MW-20a
C. auris TDG 1912	**MIC50**	>46.5	>120.6	>64	>117.5	>55	>46	>74	>47	>122	>103.8	>65.7	>43.1	>110.8	>95.5	>51.7
	MIC90	>46.5	>120.6	>64	>117.5	>55	>46	>74	>47	>122	>103.8	>65.7	>43.1	>110.8	>95.5	>51.7
C. albicans NCPF 3281	**MIC50**	>46.5	>120.6	>64	>117.5	>55	>46	>74	>47	>122	>103.8	>65.7	>43.1	>110.8	>95.5	>51.7
	MIC90	>46.5	>120.6	>64	>117.5	>55	>46	>74	>47	>122	>103.8	>65.7	>43.1	>110.8	>95.5	>51.7
C. glabrata NCPF 8018	**MIC50**	>46.5	>120.6	>64	>117.5	>55	>46	>74	>47	>122	>103.8	>65.7	>43.1	>110.8	>95.5	>51.7
	MIC90	>46.5	>120.6	>64	>117.5	>55	>46	>74	>47	>122	>103.8	>65.7	>43.1	>110.8	>95.5	>51.7
C. krusei NCPF 3876	**MIC50**	>46.5	>120.6	**64**	>117.5	**27.5**	**23**	>74	**23.5**	>122	>103.8	>65.7	**10.8**	>110.8	>95.5	>51.7
	MIC90	>46.5	>120.6	**64**	>117.5	**27.5**	**23**	>74	**23.5**	>122	>103.8	>65.7	**10.8**	>110.8	>95.5	>51.7
C. tropicalis NCPF 8760	**MIC50**	**11.6**	>120.6	**16**	>117.5	**6.9**	**5.8**	>74	**2.9**	>122	>103.8	>65.7	**21.6**	>110.8	>95.5	>51.7
	MIC90	**11.6**	>120.6	**16**	>117.5	**13.8**	**5.8**	>74	**5.8**	>122	>103.8	>65.7	**21.6**	>110.8	>95.5	>51.7
C. parapsilosis NCPF 3209	**MIC50**	>46.5	>120.6	>64	>117.5	>55	>46	>74	>47	>122	>103.8	>65.7	>43.1	>110.8	>95.5	>51.7
	MIC90	>46.5	>120.6	>64	>117.5	>55	>46	>74	>47	>122	>103.8	>65.7	>43.1	>110.8	>95.5	>51.7

© University of Pretoria

Table S8: *Inhibitory activity of 16 scorpion derived AMPs against a panel of fungal species*

Isolate		Modal MICs (µg/mL)															
		P. schlectheri				*O. carinatus*		*A. amoeruxi*							*O. madagascariensis*		
		PS-PB-8a	PS-PB-14a	PS-PB-16a	PS-PB-20a	Opis-16a	Opis8a	AamAP1	AamAP-S1	AamAP-S1a	AamAP1-Lys	AamAP1-Lysa	A3	A3a	K3-IsCTa	K7P8K11-IsCTa	A1F5K8-IsCTa
C. auris TDG 1912	MIC50	>128	>128	>128	>128	>128	>128	>128	>128	>128	>128	>128	>128	>128	>128	>128	>128
	MIC90	>128	>128	>128	>128	>128	>128	>128	>128	>128	>128	>128	>128	>128	>128	>128	>128
C. albicans NCPF 3281	MIC50	>128	>128	>128	>128	**64**	>128	>128	>128	**128**	**128**	**32**	>128	>128	**32**	>128	**64**
	MIC90	>128	>128	>128	>128	**128**	>128	>128	>128	**128**	>128	**64**	>128	>128	**64**	>128	**64**
C. glabrata NCPF 8018	MIC50	>128	>128	>128	>128	**128**	>128	>128	>128	>128	**128**	**128**	>128	**128**	**64**	>128	**64**
	MIC90	>128	>128	>128	>128	**128**	>128	>128	>128	>128	>128	**128**	>128	**128**	**64**	>128	**128**
C. krusei NCPF 3876	MIC50	>128	>128	>128	**128**	**32**	>128	**128**	**64**	**64**	**16**	**16**	**32**	**32**	**16**	**32**	**32**
	MIC90	>128	>128	>128	>128	**32**	>128	**128**	**128**	**64**	**32**	**16**	**64**	**32**	**32**	**64**	**32**
C. tropicalis NCPF 8760	MIC50	>128	**64**	>128	**64**	**8**	>128	**64**	**32**	**16**	**4**	**2**	**8**	**64**	**4**	**8**	**8**
	MIC90	>128	**64**	>128	**64**	**8**	>128	**64**	**32**	**16**	**8**	**2**	**16**	**64**	**8**	**16**	**8**
C. parapsilosis NCPF 3209	MIC50	>128	>128	>128	>128	**64**	>128	>128	>128	**128**	**64**	**32**	>128	>128	**64**	**64**	**64**
	MIC90	>128	>128	>128	>128	**128**	>128	>128	>128	**128**	**64**	**32**	>128	>128	**64**	**128**	**64**

© University of Pretoria

Table S8 B: *Inhibitory activity of 16 scorpion derived AMPs against a panel of fungal species* ***shown in µM***

Isolate		Modal MICs (µM)															
		P. schlectheri				*O. carinatus*		*A. amoeruxi*							*O. madagascariensis*		
		PS-PB-8a	PS-PB-14a	PS-PB-16a	PS-PB-20a	Opis-16a	Opis8a	AamAP1	AamAP-S1	AamAP-S1a	AamAP1-Lys	AamAP1-Lysa	A3	A3a	K3-IsCTa	K7P8K1 1-IsCTa	A1F5K8-IsCTa
C. auris TDG 1912	MIC50	>127.2	>63.8	>67.8	>55.7	>64.7	>133.2	>64.8	>64.5	>64.8	>57.8	>57.8	>62.9	>62.9	>79.5	>79	>79.9
	MIC90	>127.2	>63.8	>67.8	>55.7	>64.7	>133.2	>64.8	>64.5	>64.8	>57.8	>57.8	>62.9	>62.9	>79.5	>79	>79.9
C. albicans NCPF 3281	MIC50	>127.2	>63.8	>67.8	>55.7	**32.4**	>133.2	>64.8	>64.5	**64.8**	**57.8**	**14.4**	>62.9	>62.9	**19.9**	>79	**39.9**
	MIC90	>127.2	>63.8	>67.8	>55.7	**64.7**	>133.2	>64.8	>64.5	**64.8**	>57.8	**28.8**	>62.9	>62.9	**39.8**	>79	**39.9**
C. glabrata NCPF 8018	MIC50	>127.2	>63.8	>67.8	>55.7	**64.7**	>133.2	>64.8	>64.5	>64.8	**57.8**	**57.8**	>62.9	**62.9**	**39.8**	>79	**39.9**
	MIC90	>127.2	>63.8	>67.8	>55.7	**64.7**	>133.2	>64.8	>64.5	>64.8	>57.8	**57.8**	>62.9	**62.9**	**39.8**	>79	**79.9**
C. krusei NCPF 3876	MIC50	>127.2	>63.8	>67.8	**55.7**	**16.2**	>133.2	**64.8**	**32.2**	**32.4**	**7.2**	**7.2**	**15.7**	**15.7**	**9.9**	**19.8**	**19.9**
	MIC90	>127.2	>63.8	>67.8	>55.7	**16.2**	>133.2	**64.8**	**64.5**	**32.4**	**14.4**	**7.2**	**31.4**	**15.7**	**19.9**	**39.5**	**19.9**
C. tropicalis NCPF 8760	MIC50	>127.2	**31.9**	>67.8	**27.8**	**4**	>133.2	**32.4**	**16.1**	**8.1**	**1.8**	**0.9**	**3.9**	**31.4**	**2.5**	**4.9**	**5**
	MIC90	>127.2	**31.9**	>67.8	**27.8**	**4**	>133.2	**32.4**	**16.1**	**8.1**	**3.6**	**0.9**	**7.9**	**31.4**	**5**	**9.9**	**5**
C. parapsilosis NCPF 3209	MIC50	>127.2	>63.8	>67.8	>55.7	**32.4**	>133.2	>64.8	>64.5	**64.8**	**28.8**	**14.4**	>62.9	>62.9	**39.8**	**39.5**	**39.8**
	MIC90	>127.2	>63.8	>67.8	>55.7	**64.7**	>133.2	>64.8	>64.5	**64.8**	**28.8**	**14.4**	>62.9	>62.9	**39.8**	**79**	**39.8**

© University of Pretoria

Table S9: *Inhibitory activity of 11 tick derived AMPs against a panel of fungal species*

Isolate		Modal MICs (µg/mL)										
		O. savignyi							*O. moubata*			
		Os	Osa	Os-C	Os(3-12)a	Os(11-22)a	W3(Os-C)a	W(Os-C)a	OmDefB	OmDef19	W-OmC-Ca	W-OmB-Ca
C. auris TDG 1912	MIC50	>128	>128	>128	>128	>128	>128	>128	>128	>128	>128	>128
	MIC90	>128	>128	>128	>128	>128	>128	>128	>128	>128	>128	>128
C. albicans NCPF 3281	MIC50	>128	>128	>128	>128	>128	>128	>128	>128	>128	>128	>128
	MIC90	>128	>128	>128	>128	>128	>128	>128	>128	>128	>128	>128
C. glabrata NCPF 8018	MIC50	>128	>128	>128	>128	>128	>128	>128	>128	>128	>128	>128
	MIC90	>128	>128	>128	>128	>128	>128	>128	>128	>128	>128	>128
C. krusei NCPF 3876	MIC50	>128	>128	>128	>128	>128	>128	>128	>128	>128	>128	>128
	MIC90	>128	>128	>128	>128	>128	>128	>128	>128	>128	>128	>128
C. tropicalis NCPF 8760	MIC50	>128	>128	>128	>128	>128	>128	>128	>128	>128	>128	>128
	MIC90	>128	>128	>128	>128	>128	>128	>128	>128	>128	>128	>128
C. parapsilosis NCPF 3209	MIC50	>128	>128	>128	>128	>128	>128	>128	>128	>128	>128	>128
	MIC90	>128	>128	>128	>128	>128	>128	>128	>128	>128	>128	>128

© University of Pretoria

Table S9 B: *Inhibitory activity of 11 tick derived AMPs against a panel of fungal species* ***shown in µM***

Isolate		Modal MICs (µM)										
		O. savignyi							*O. moubata*			
		Os	Osa	Os-C	Os(3-12)a	Os(11-22)a	W3(Os-C)a	W(Os-C)a	OmDefB	OmDef19	W-OmC-Ca	W-OmB-Ca
C. auris TDG 1912	**MIC50**	>51.7	>51.7	>59	>112	>91.7	>46.9	>54.4	>49.9	>56.8	>54.3	>52.5
	MIC90	>51.7	>51.7	>59	>112	>91.7	>46.9	>54.4	>49.9	>56.8	>54.3	>52.5
C. albicans NCPF 3281	**MIC50**	>51.7	>51.7	>59	>112	>91.7	>46.9	>54.4	>49.9	>56.8	>54.3	>52.5
	MIC90	>51.7	>51.7	>59	>112	>91.7	>46.9	>54.4	>49.9	>56.8	>54.3	>52.5
C. glabrata NCPF 8018	**MIC50**	>51.7	>51.7	>59	>112	>91.7	>46.9	>54.4	>49.9	>56.8	>54.3	>52.5
	MIC90	>51.7	>51.7	>59	>112	>91.7	>46.9	>54.4	>49.9	>56.8	>54.3	>52.5
C. krusei NCPF 3876	**MIC50**	>51.7	>51.7	>59	>112	>91.7	>46.9	>54.4	>49.9	>56.8	>54.3	>52.5
	MIC90	>51.7	>51.7	>59	>112	>91.7	>46.9	>54.4	>49.9	>56.8	>54.3	>52.5
C. tropicalis NCPF 8760	**MIC50**	>51.7	>51.7	>59	>112	>91.7	>46.9	>54.4	>49.9	>56.8	>54.3	>52.5
	MIC90	>51.7	>51.7	>59	>112	>91.7	>46.9	>54.4	>49.9	>56.8	>54.3	>52.5
C. parapsilosis NCPF 3209	**MIC50**	>51.7	>51.7	>59	>112	>91.7	>46.9	>54.4	>49.9	>56.8	>54.3	>52.5
	MIC90	>51.7	>51.7	>59	>112	>91.7	>46.9	>54.4	>49.9	>56.8	>54.3	>52.5

© University of Pretoria

Table S10: *Inhibitory activity of 4 primate derived AMPs against a panel of fungal species*

Isolate		Modal MICs (µg/mL)			
		Papio anubis			
		ThetaDefA	ThetaDefB	BTD15a	BTD11a
C. auris TDG 1912	**MIC50**	>128	>128	>128	**64**
	MIC90	>128	>128	>128	>128
C. albicans NCPF 3281	**MIC50**	>128	>128	**32**	**32**
	MIC90	>128	>128	**64**	**64**
C. glabrata NCPF 8018	**MIC50**	>128	>128	**128**	**16**
	MIC90	>128	>128	**128**	**32**
C. krusei NCPF 3876	**MIC50**	>128	>128	**16**	**32**
	MIC90	>128	>128	**16**	**32**
C. tropicalis NCPF 8760	**MIC50**	>128	>128	**8**	**1**
	MIC90	>128	>128	**8**	**2**
C. parapsilosis NCPF 3209	**MIC50**	>128	>128	**128**	**4**
	MIC90	>128	>128	**128**	**16**

© University of Pretoria

Table S10 B: *Inhibitory activity of 4 primate derived AMPs against a panel of fungal species* ***shown in µM***

Isolate		Modal MICs (µM)			
		Papio anubis			
		ThetaDefA	ThetaDefB	BTD15a	BTD11a
C. auris TDG 1912	**MIC50**	>122.6	>116.4	>70.2	**47**
	MIC90	>122.6	>116.4	>70.2	>94
C. albicans NCPF 3281	**MIC50**	>122.6	>116.4	**17.5**	**23.5**
	MIC90	>122.6	>116.4	**35**	**47**
C. glabrata NCPF 8018	**MIC50**	>122.6	>116.4	**70.2**	**11.8**
	MIC90	>122.6	>116.4	**70.2**	**23.5**
C. krusei NCPF 3876	**MIC50**	>122.6	>116.4	**8.8**	**23.5**
	MIC90	>122.6	>116.4	**8.8**	**23.5**
C. tropicalis NCPF 8760	**MIC50**	>122.6	>116.4	**4.4**	**0.7**
	MIC90	>122.6	>116.4	**4.4**	**1.5**
C. parapsilosis NCPF 3209	**MIC50**	>122.6	>116.4	**70.2**	**2.9**
	MIC90	>122.6	>116.4	**70.2**	**11.8**

© University of Pretoria

3. Haemolytic activity

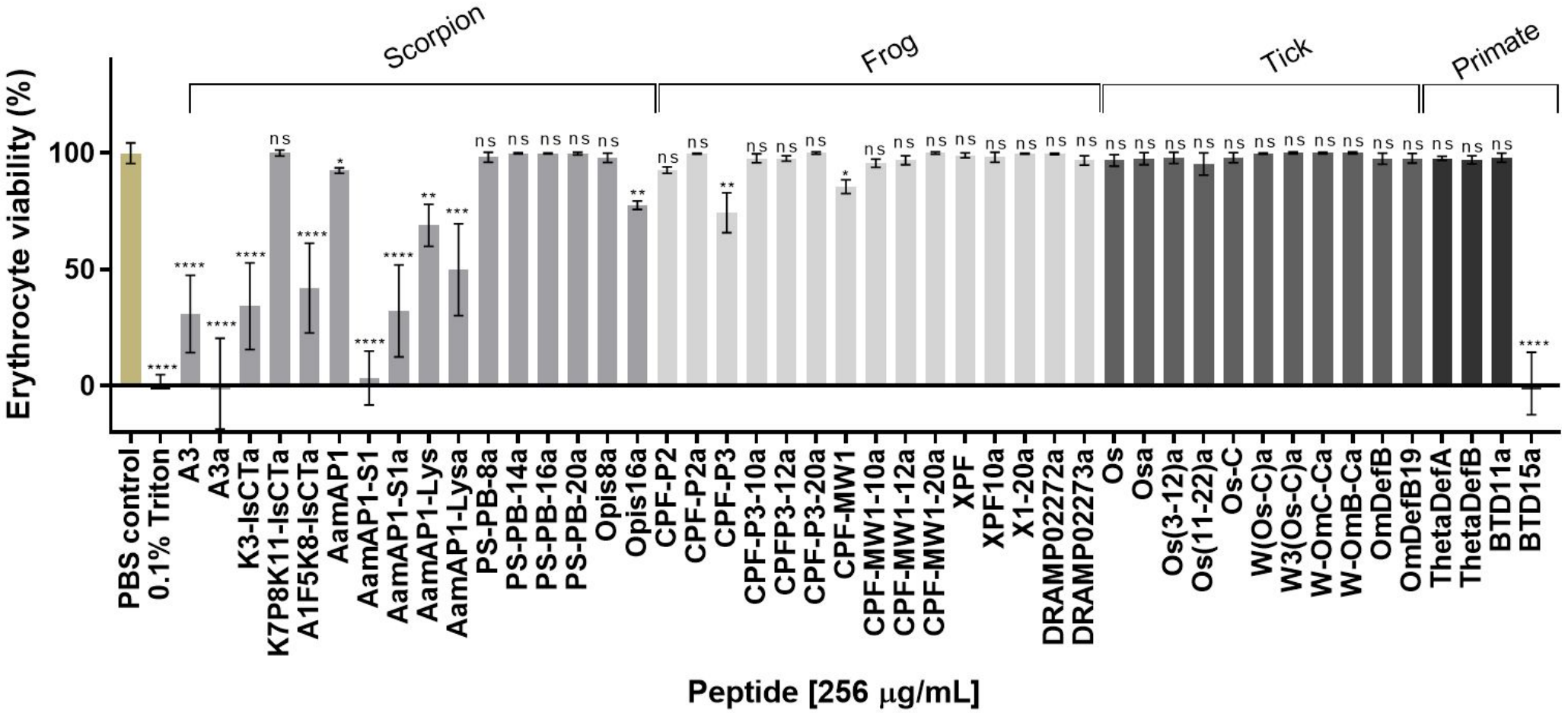


Figure S1: The percentage human erythrocyte viability after respective treatment with 46 novel AMPs. *Erythrocytes were treated with 16 scorpion, 15 frog, 11 tick and 4 primate derived AMPs at a screening concentration of 256 μg/mL each at 37 °C for 24h. Percentage viability is relative to the growth control; PBS treated cells. Error bars show the mean ± SE. Significant difference indicated by *, **, *** and **** represents p < 0.05, p < 0.01, p <0.001 and p < 0.0001 values. Results are of three independent biological repeats each performed in triplicate*

© University of Pretoria

Table S11: *Haemolytic AMPs with an HC10 or HC50 below 256 µg/mL*

Peptide	Haemolysis	
	HC10 µg/mL (µM)	HC50 µg/mL (µM)
Frog derived AMPs		
CPF-P3*	**102 (37.5)**	>256 (>94)
CPF-MW1*	**214 (72)**	>256 (>86)
Scorpion derived AMPs		
Opis16a*	**155 (78.4)**	>256 (>129)
AamAP-S1*	**128 (64.5)**	**195 (98.2)**
AamAP-S1a*	**45 (22.8)**	**112 (56.7)**
AamAP1-Lys*	**94 (42.4)**	>256 (>115.5)
AamAP1-Lysa*	**53 (23.9)**	**256 (115.5)**
A3*	**9 (4.4)**	**54 (26.5)**
A3a*	**24 (11.8)**	**78 (38.3)**
K3-IsCTa*	**84 (52.2)**	**211 (131)**
A1F5K8-IsCTa*	**102 (63.6)**	**234 (146)**
Tick derived AMPs		
Primate derived AMPs		
BTD15a*	**9 (4.9)**	**33 (18.1)**

**Most active antimicrobial peptides identified in the screens*
***AMPs with an HC10 or HC50 above 256 µg/mL are regarded as non-haemolytic and the data not shown*

© University of Pretoria

4. Cytotoxicity:

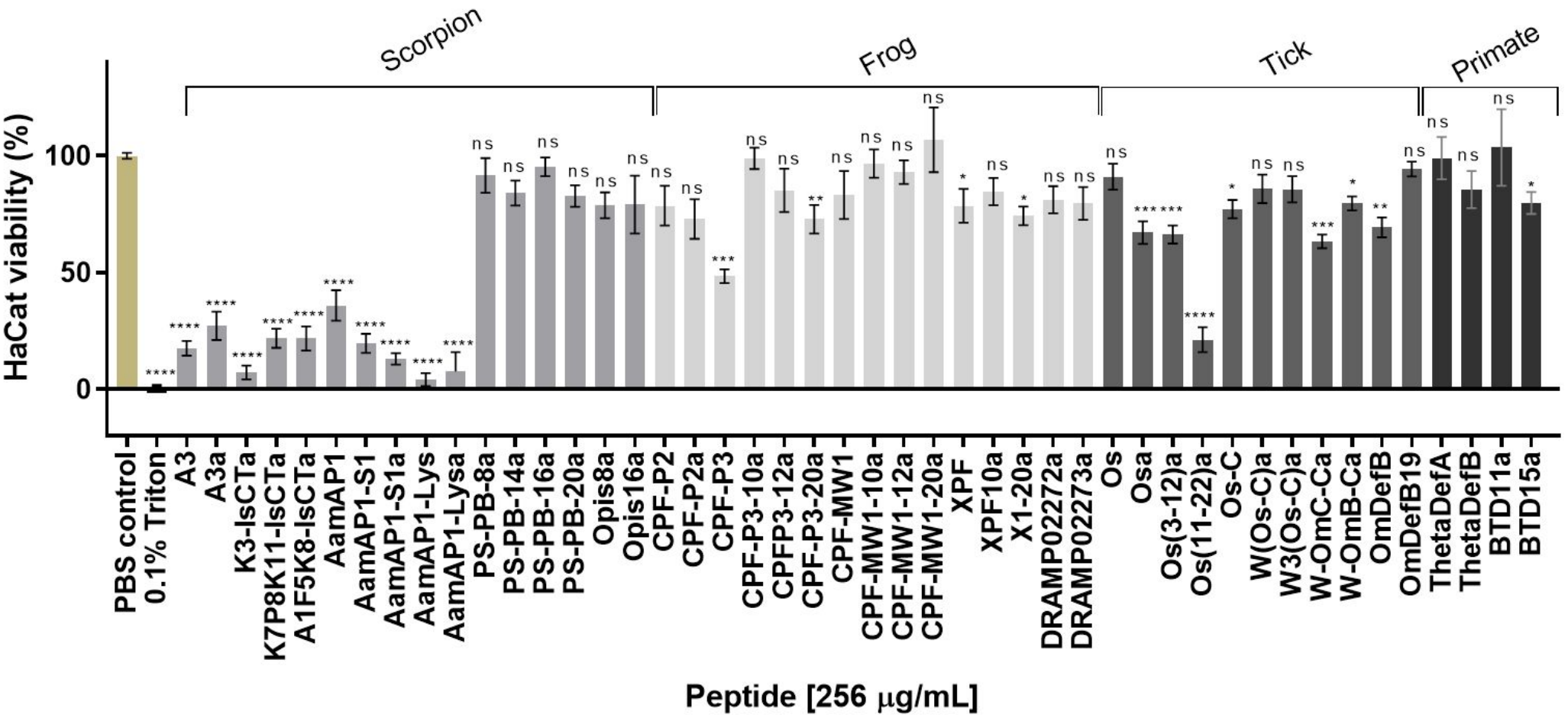


Figure S2: The percentage HaCat cell viability after respective treatment with 46 novel AMPs. *Hacat cells were treated with 16 scorpion, 15 frog, 11 tick and 4 primate derived AMPs at a screening concentration of 256 μg/mL each at 37 °C for 24h. Percentage viability is relative to the growth control; PBS treated HaCat cells. Error bars show the mean ± SE. Significant difference indicated by *, **, *** and **** represents $p < 0.05$, $p < 0.01$, $p < 0.001$ and $p < 0.0001$ values. Results are of three independent biological repeats each performed in triplicate*

© University of Pretoria

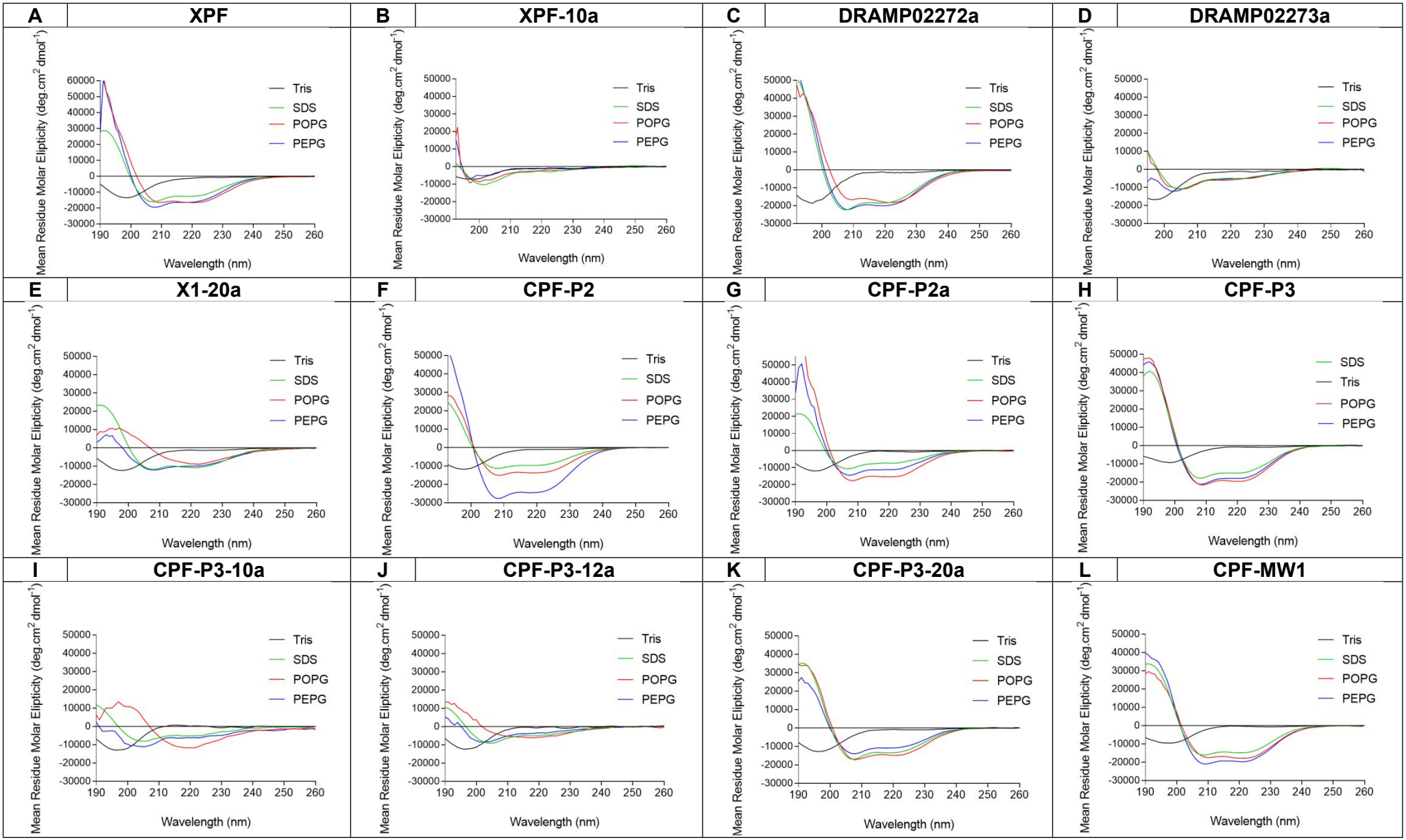
Table S12: *LC_{50} determined in the HaCat cell line of the 12 most toxic AMPs.*

	Peptide	% HaCat cell death at initial screening (256µg/mL) ± SD	HaCat LC_{50} (µg/mL) (µM)
Scorpion AMPs			
1	A3 *	*100 ± 9.7*	*113.8* (55.9)
2	A3a *	*100 ± 10.5*	*279.7* (137.5)
3	K3-IsCTa *	*104.1 ± 11.9*	*69.4* (43.1)
4	K7P8K11-IsCTa	*89.2 ± 9.1*	*142.5* (88)
5	A1F5K8-IsCTa	*83.6 ±9.2*	*168.5* (105.1)
6	AamAP1	*44.3 ±20.2*	*270.2* (136.8)
7	AamAP1-S1	*85 ±17.9*	*121* (60.9)
8	AamAP1-S1a *	*97.6 ±12.6*	*59.3* (30)
9	AamAP1-Lys *	*99.1 ± 8.7*	*124.4* (56.1)
10	AamAP1-Lysa *	*94.8 ± 8.2*	*101.4* (45.8)
Frog AMPs			
11	CPF-P3	*39.9 ±12.3*	*283.5* (104.1)
Tick AMPs			
12	Os(11-22)a	*59.5 ±13.9*	*163.2* (116.8)

* indicates peptides with the highest toxicity

© University of Pretoria

5. Circular dichroism spectra



© University of Pretoria

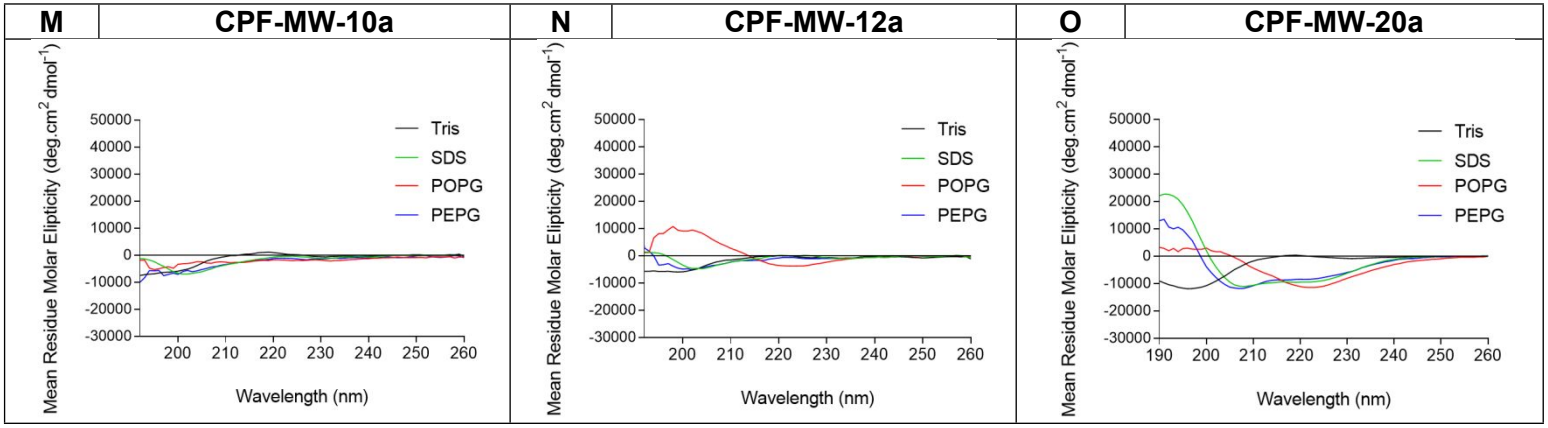
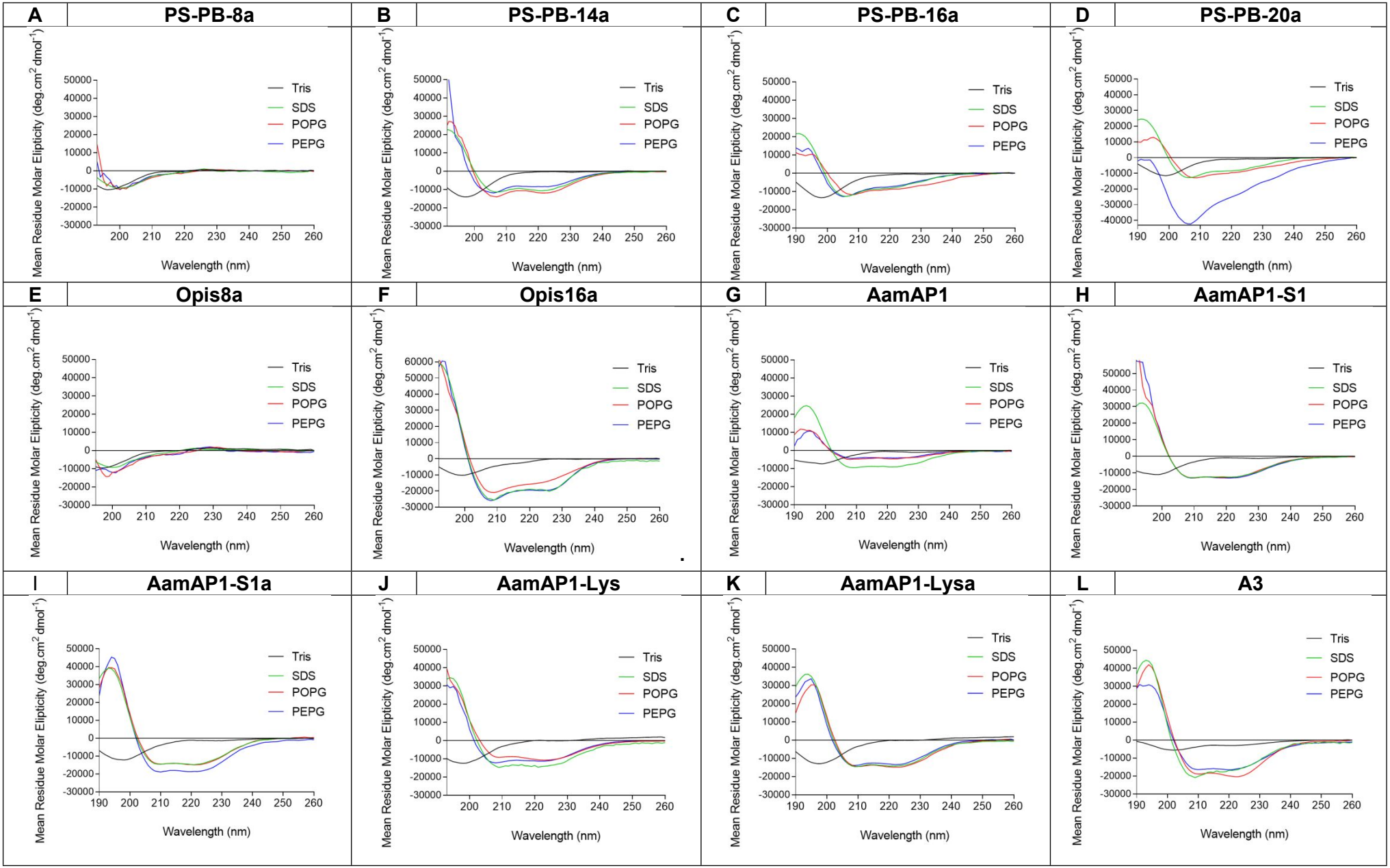


Figure S3: *CD spectra of the 15 frog derived AMPs in Tris (5mM), SDS (50mM), POPG (5mM) and PEPG (5mM) liposomes at pH of 7.4 and 23°C.*

© University of Pretoria



© University of Pretoria

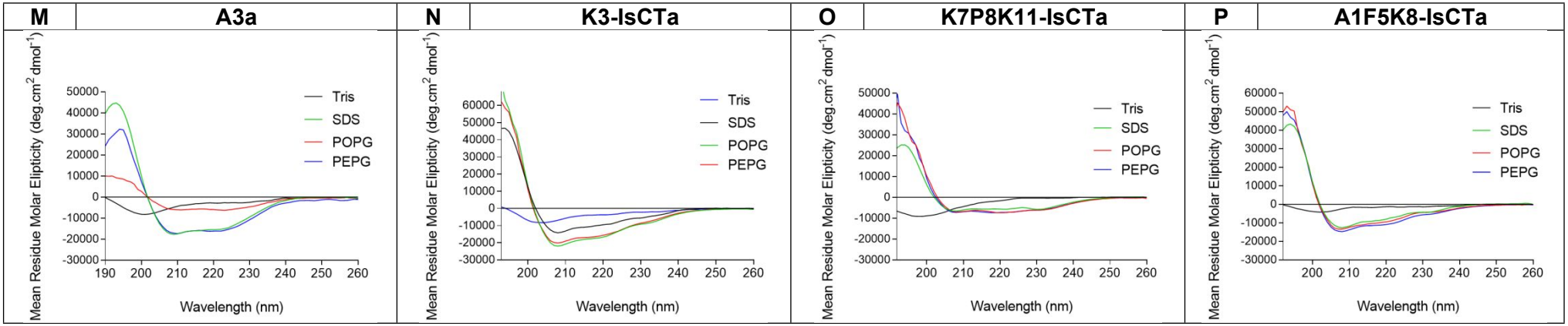


Figure S4: *CD spectra of the 16 scorpion derived AMPs in Tris (5mM), SDS (50mM), POPG (5mM) and PEPG (5mM) liposomes at pH of 7.4 and 23°C.*

© University of Pretoria

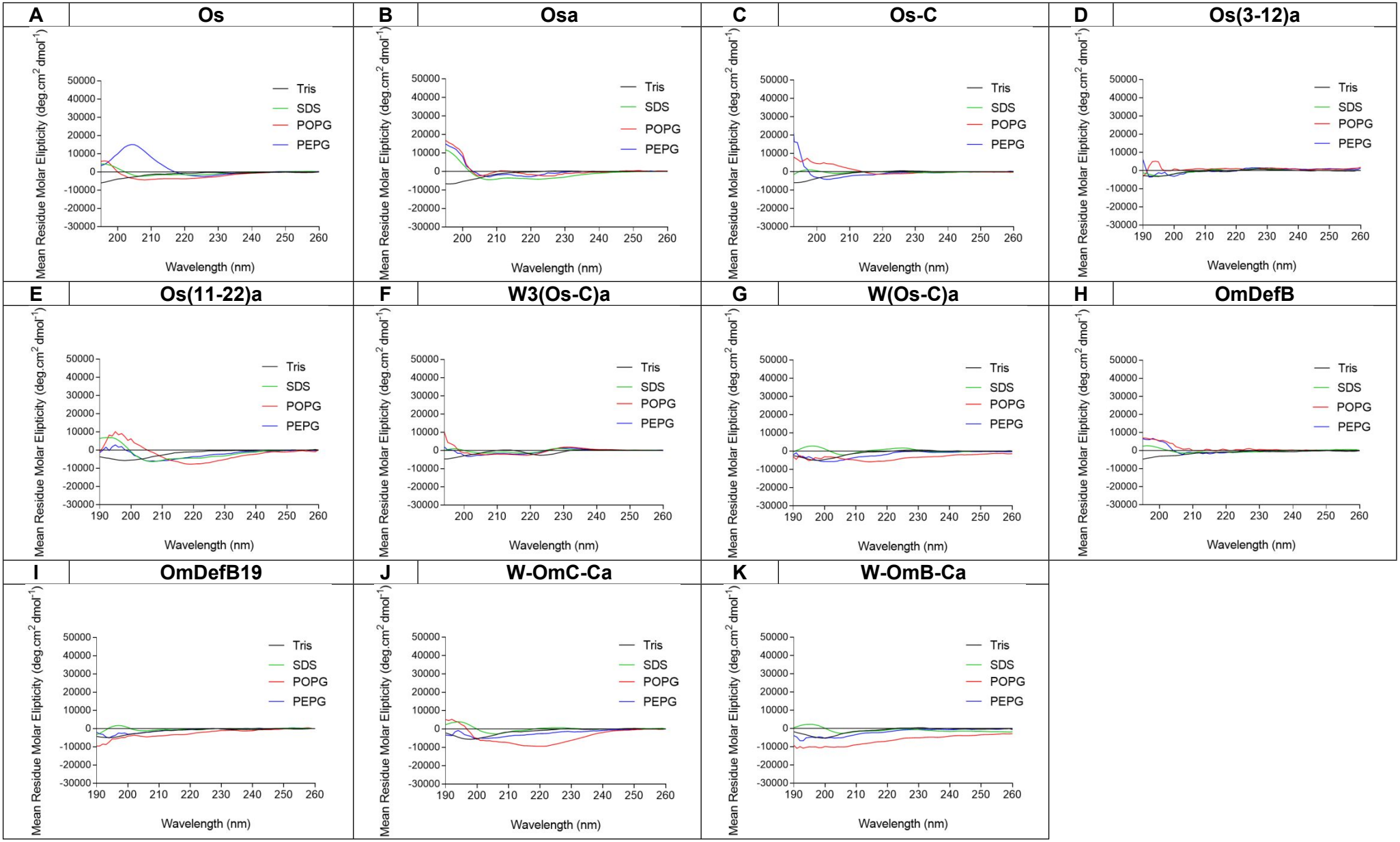


Figure S5: *CD spectra of the 11 tick derived AMPs in Tris (5mM), SDS (50mM), POPG (5mM) and PEPG (5mM) liposomes at pH of 7.4 and 23°C*

© University of Pretoria

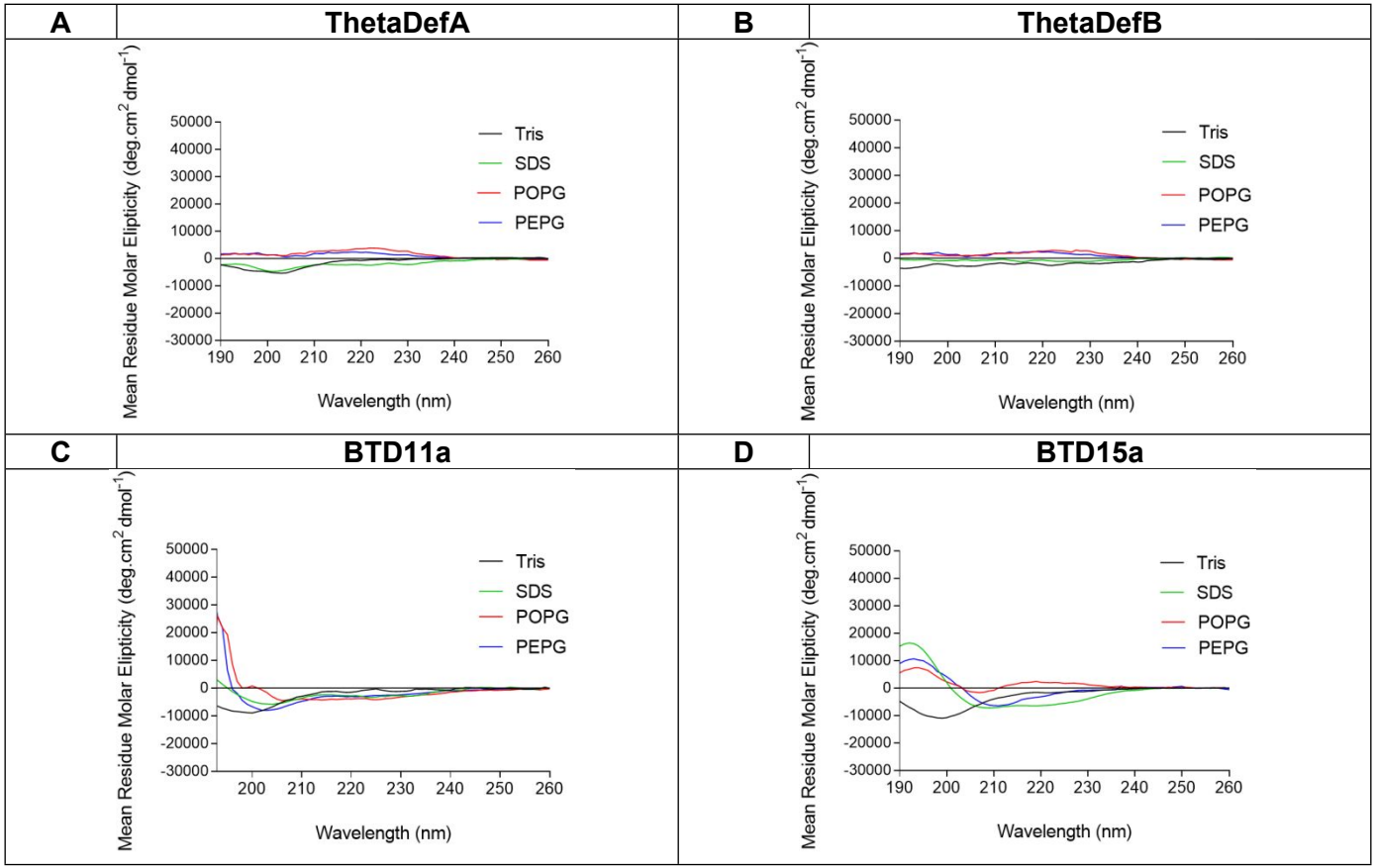


Figure S6: *CD spectra of the 4 primate derived AMPs in Tris (5mM), SDS (50mM), POPG (5mM) and PEPG (5mM) liposomes at pH of 7.4 and 23°C*

© University of Pretoria

6. PCA

Bartlett's test of PCA appropriateness

Table S13: *Results of Bartlett's test calculated for all 46 peptides against Gram-positive and -negative bacteria*

	Gram-negative bacteria	Gram-positive bacteria	Fungi
Approximate χ^2			
PC-1	2016.25	2004.10	2037.89
PC-2	1643.94	1639.63	1671.67
Degrees of freedom			
PC-1	373.77	373.72	373.59
PC-2	365.94	365.61	365.56
Significance	<0.0001	<0.0001	<0.0001

Number of PCs selected per group for data interpretation based on a cumulative variance above 80%

Table S14: *Parameters determining the no. of PCs selected for Gram-negative, -positive and fungal data interpretation*

Principal component	Eigenvalue	Variance (%)	Cumulative variance (%)
Gram-negative bacteria			
PC-1	10.61	37.90	37.902
PC-2	8.22	29.36	67.26
PC-3	3.09	11.03	78.29
PC-4	1.72	6.13	84.42
Gram-positive bacteria			
PC-1	10.46	37.37	37.37
PC-2	8.25	29.48	66.85
PC-3	3.07	10.96	77.81
PC-4	1.72	6.15	83.95
Fungi			
PC-1	10.48	37.45	37.45
PC-2	8.39	29.95	67.40
PC-3	3.16	11.28	78.68
PC-4	1.72	6.142	84.82

© University of Pretoria

Scree plots:

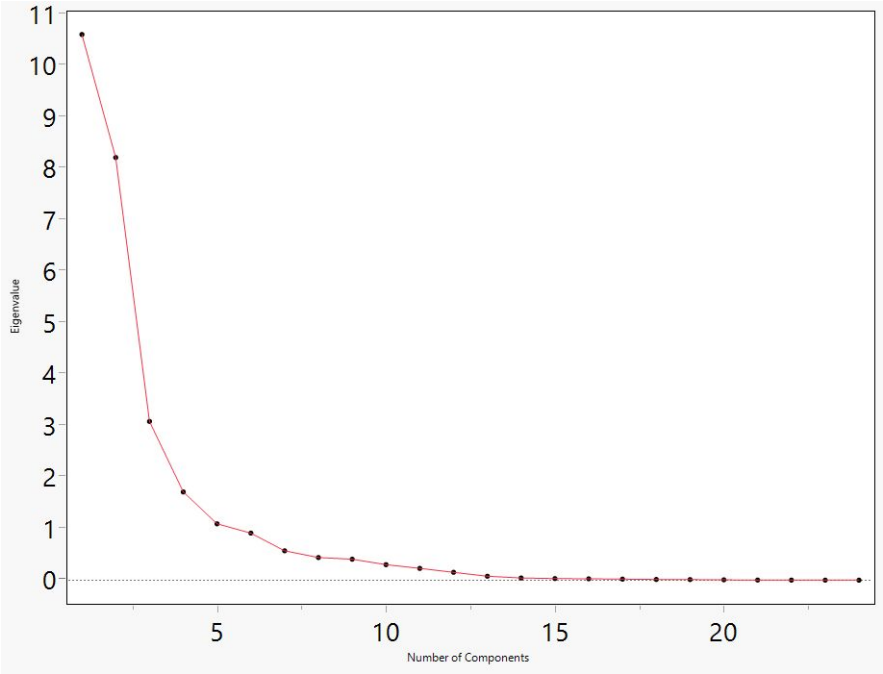


Figure S7: Scree plot for Gram-negative PCA showing the number of PCs with eigenvalues greater than 1.5. *PC-1, PC-2, PC-3, and PC-4 show eigenvalues greater than 1.5 and thus qualify to be used for the interpretation of results.*

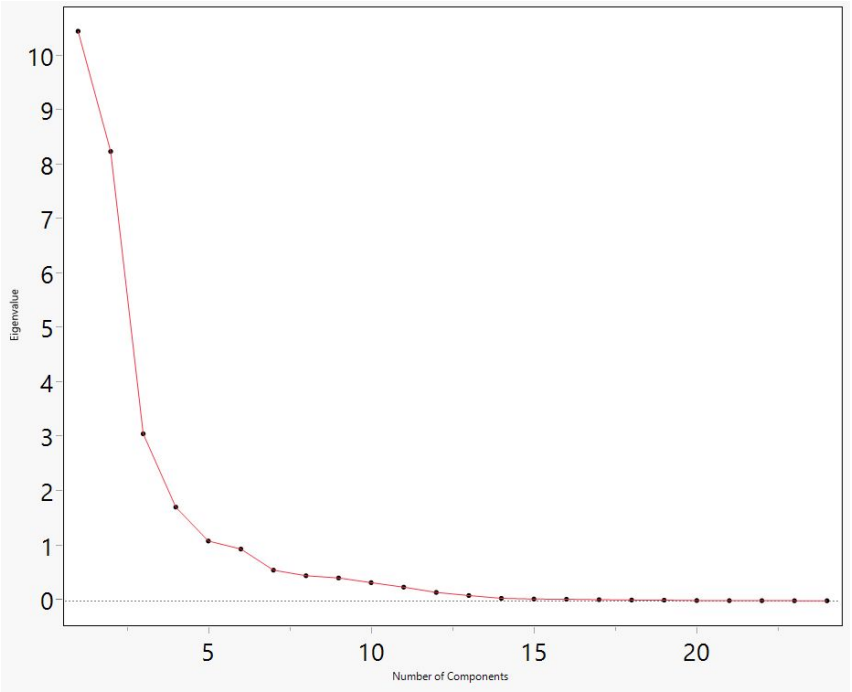


Figure S8: Scree plot for Gram-positive PCA showing the number of PCs with eigenvalues greater than 1.5. *PC-1, PC-2, PC-3, and PC-4 show eigenvalues greater than 1.5 and thus qualify to be used for the interpretation of results.*

© University of Pretoria

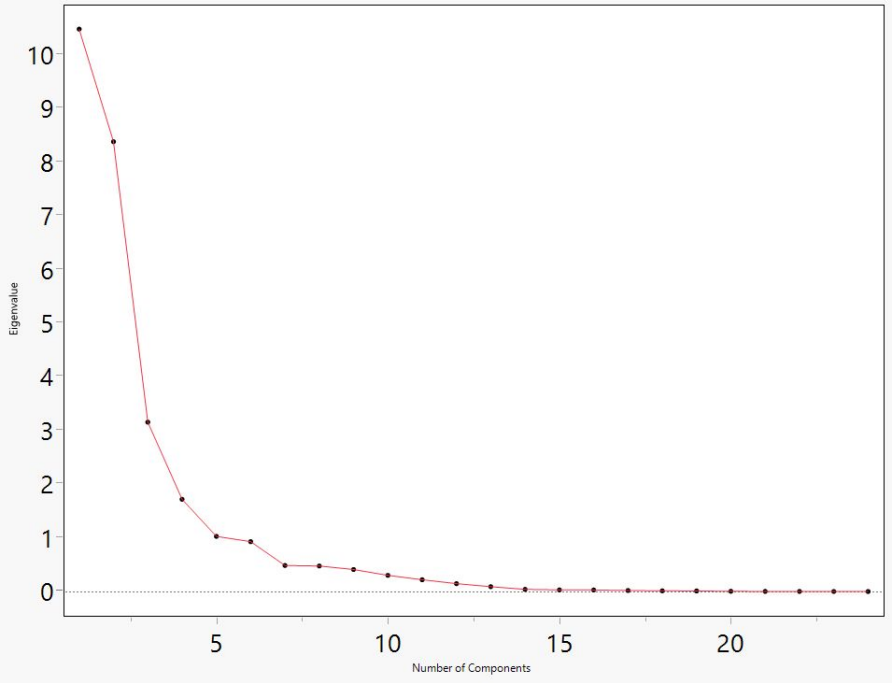


Figure S9: Scree plot for fungal PCA showing the number of PCs with eigenvalues greater than 1.5. *PC-1, PC-2, PC-3, and PC-4 show eigenvalues greater than 1.5 and thus qualify to be used for the interpretation of results.*

© University of Pretoria

7. QSAR

***Table S15**: Correlation of single molecular descriptors of the 46 AMPs with antimicrobial and cytotoxic activities – Lipophilicity parameters determined with the Wimley-White bilayer/water scale at pH 7.0*

	Property	R^2				
		Gram-negative bacteria MIC_{avg}	Gram-positive bacteria MIC_{avg}	Fungi MIC_{avg}	%Haemolysis	%HaCat cell death
1	ElutionTime (mins)	-0.7203	-0.8032	-0.4590	0.5567	0.6485
2	$SCSA_N$	-0.7492	-0.7920	-0.4968	0.5230	0.6082
3	**L_N**	**-0.6213**	**-0.4232**	**-0.2635**	**0.4503**	**0.5828**
4	**L**	**-0.1027**	**-0.1691**	**0.0327**	**0.3917**	**0.5214**
5	MwN	-0.6832	-0.7462	-0.4162	0.4500	0.4865
6	CD Structure	-0.7250	-0.5670	-0.3425	0.4597	0.4548
7	**L_P/L_N**	**-0.2107**	**-0.1939**	**0.0976**	**0.2000**	**0.3794**
8	**L/L_N**	**-0.2107**	**-0.1939**	**0.0976**	**0.2000**	**0.3794**
9	CSL	-0.5204	-0.5914	-0.3447	0.3155	0.2755
10	SCSA	-0.4589	-0.3225	-0.1024	0.0341	0.2350
11	CAR	-0.0190	-0.0051	0.1287	0.0498	0.2250
12	**L_P/L**	**-0.1072**	**-0.0870**	**-0.1665**	**0.1140**	**0.2182**
13	Mw	-0.3691	-0.2877	-0.1111	0.0576	0.1195
14	Sequence length	-0.3623	-0.3182	-0.0633	0.0297	0.0748
15	**L_P**	**0.5005**	**0.2365**	**0.3458**	**0.0272**	**0.0531**
16	#RotBonds	-0.3049	-0.1062	-0.0739	-0.0619	0.0321
17	Q/CAR	-0.0162	0.1919	0.1001	-0.2490	-0.1772
18	**Q/L**	**0.0765**	**0.0361**	**0.0935**	**-0.0877**	**-0.1908**
19	HBacc	0.0344	0.1853	0.0936	-0.2188	-0.2010
20	$SCSA_P$	0.0653	0.2597	0.2801	-0.3813	-0.2144
21	HBtot	0.0447	0.1872	0.0260	-0.1794	-0.2305
22	HBdon	0.0486	0.1828	-0.0091	-0.1543	-0.2389
23	MwP	0.1253	0.2805	0.2178	-0.3133	-0.2675
24	Charge	0.0364	0.2892	0.0388	-0.2451	-0.2776
25	Q/CSL	0.3733	0.4251	0.3222	-0.3037	-0.3021
26	$SCSA_P/SCSA_N$	0.4631	0.5194	0.4496	-0.4156	-0.3158
27	MwP/MwN	0.4330	0.5075	0.3644	-0.3871	-0.3630
28	**Q/L_N**	**0.3642**	**0.3229**	**-0.0081**	**-0.2258**	**-0.3787**

© University of Pretoria

CHAPTER 3:

Scorpion venom-derived Opis16a shows potent membrane-destabilising Gram-negative activity and promising *in vivo* topical efficacy

Van der Walt, M., Oosthuizen, C.B., Mason, A.J., Bester, M.J. & Gaspar, A.R M. (2024).

This chapter is in preparation for publication. **Van der Walt, M. (writing of article as first author, responsible for most of the experimental work and all data analysis),** Oosthuizen, C.B. (screening of Opis16a peptide for antimicrobial activity and HepG2 toxicity, co-writer and editor), Mason, A.J. (co-writer and editor, critical evaluation of the study and data interpretation), Bester, M.J. (co-supervisor of study, co-writer and editor, critical evaluation of the study and data analysis) and Gaspar, A.R.M. (study supervisor and communicating author, co-writer and editor, critical evaluation of the study and data analysis).

© University of Pretoria

3.1 Abstract

Antimicrobial peptides (AMPs) are lead candidates for antibacterial drug development, crucial amid rising antimicrobial resistance. A fundamental challenge is the development of antimicrobials effective against multidrug-resistant Gram-negative bacteria, largely due to the complexity of the outer membrane. In a previous study we showed the broad-spectrum and potent activity of Opis16a, a novel scorpion venom-derived AMP, against a large panel of Gram-negative bacteria, including drug-resistant strains, all while maintaining minimal toxicity to mammalian cells. However, the exact mechanism by which Opis16a acts even against antibiotic-resistant pathogens has not yet been elucidated. Here we show Opis16a effectively penetrates the intricate outer membrane of Gram-negative bacteria, leading to rapid bacterial cell death via cytoplasmic membrane disruption. *In vitro* screening confirms the efficacy of this peptide with activity against Gram-negative bacteria and potent selectivity toward bacteria over human HaCat and HepG2 cell lines. Mechanistic studies in *Escherichia coli* ATCC 700928 and *Acinetobacter baumannii* NICD 15283 reveal that Opis16a binds to lipopolysaccharides in a comparable way to polymyxin B and destabilises the outer membrane. The peptide also depolarises and permeabilises the cytoplasmic membrane similar to melittin. This indicates that Opis16a exhibits high efficacy akin to both polymyxin B and melittin, while offering the added benefit of minimal toxicity. The strong bacterial selectivity and effective membrane penetration of *A. baumannii*, combined with retained activity in serum, enable successful therapy in an *in vivo Galleria mellonella* model of gentamicin-resistant *A. baumannii* burn wound infections. Treatment with Opis16a nearly rescues all larvae from infection, demonstrating efficacy comparable to that of polymyxin B. This study identifies Opis16a as a novel membrane destabilising AMP with promising *in vitro* and *in vivo* activity against Gram-negative bacteria, with potential to be further developed for topical applications.

Keywords: Antimicrobial resistance, antimicrobial peptides, Gram-negative bacteria, Opis16a, lipopolysaccharides, permeabilisation, *E. coli*, *A. baumannii*

Abbreviations: AMP, antimicrobial peptide; MIC, minimum inhibition concentration; LC, lethal concentration; SI, selectivity index; LPS, lipopolysaccharides

© University of Pretoria

3.2 Introduction

Drug resistant infections, particularly those caused by Gram-negative bacteria, contribute substantially to escalating healthcare expenditures and are the leading cause of morbidity and mortality in intensive care units world-wide[1]. Compounding this challenge is the decline in antimicrobial drug discovery over recent years, resulting in an insufficient supply of novel antimicrobials capable of keeping pace with the rapid proliferation of drug-resistant pathogens. Consequently, the World Health Organization (WHO) recognised antimicrobial resistance as a major public health threat of the 21st century[2]. At the top of the WHO list of critical bacteria requiring targeted intervention are Gram-negative bacteria including carbapenem-resistant *Acinetobacter baumannii*, as well as other pathogens such as *Escherichia coli* and *Enterobacter cloacae*, which belong to the order *Enterobacterales*[2]. These bacteria are associated with a wide spectrum of infections, once considered manageable with conventional antibiotics, but have now become life-threatening due to the emergence of resistance[3]. Frequently implicated in hospital-acquired infections, *A. baumannii* is the primary pathogen responsible for wound infections, exhibiting multidrug resistance against all major antibiotics including β-lactamases, aminoglycosides, carbapenems, and more recently, colistin[4]. The rise in multidrug-resistant Gram-negative strains, especially those with significant healthcare implications like *A. baumannii*, underscores the urgent need for novel therapeutic strategies.

Antimicrobial peptides (AMPs) have emerged as promising candidates with broad-spectrum activity, superficial or internal targets, selectivity towards pathogens over mammalian cells, bactericidal and/or immunomodulatory capabilities[3]. Their broad range of actions, adaptability for modification, and low risk of resistance development compared with conventional antimicrobial drugs, identifies AMPs as valuable lead compounds[3]. Despite their many advantages, AMP development for the treatment of Gram-negative infections is challenging due to the complexity of the three-layered cell envelope, characteristic of Gram-negative bacteria. The outer membrane, a distinctive feature unique to Gram-negative bacteria and absent in Gram-positive bacteria, comprises a bilayer structure[5]. The outer leaflet consists mainly of lipopolysaccharides (LPS), while the inner leaflet consists of phospholipids. The LPS leaflet serves as a permeability barrier effectively blocking the entry of many antibacterial agents, thereby impeding their access to the peptidoglycan layer, cytoplasmic membrane or intracellular targets[6]. This renders Gram-negative bacteria intrinsically more resilient to drugs compared with Gram-positive bacteria[3]. The design of drugs, including AMPs, that can navigate the structural complexity of the cell envelope is challenging and have delayed the rational design of effective Gram-negative AMPs, resulting in a scenario where identifying novel potential molecules to inhibit Gram-positive bacteria is more attainable[7].

© University of Pretoria

In a previous study we identified Opis16a as a novel AMP with broad-spectrum antimicrobial activity[9]. Opis16a is derived from opistoporin 1, identified in the venom of the southern African *Opistophthalmus carinatus* scorpion (Table 3.1). Opistoporin 1 (44 amino acid residues) previously showed promising activity against both Gram-negative and -positive bacteria[8], however, its progress in development has been hindered by its toxicity, length and associated cost of synthesis. To overcome these challenges, the Collection of Anti-Microbial Peptides (CAMPR3) was used to identify the key active region of opistoporin 1 which is the N-terminal 16 amino acid residues[9]. Consequently, Opis16a was engineered as a truncated derivative comprising these 16 residues, including all original Trp residues to preserve hydrophobicity, along with four of the original Lys residues and an amidated C-terminus to maintain the cationic charge of +4 (Table 3.1). In contrast to the α-helix conformation adopted by the larger parent peptide, Opis16a displays reduced structural organisation in membrane-mimicking environments, likely due to its shorter length[8,9].

Importantly, while being derived from venom, Opis16a exhibits minimal toxicity toward mammalian cells, including HaCat and human red blood cells, compared with its parent peptide[8,9]. This is significant given that venom-derived peptides, such as melittin, are often highly antimicrobial but also associated with considerable mammalian toxicity[19].

The aim of this study was to further investigate the membrane interaction, activity, stability, and mechanism of action of Opis16a against the Gram-negative *E. coli* strain and a multidrug-resistant *A. baumannii* clinical isolate. Finally, the peptide was evaluated for its ability to protect *G. mellonella* larvae from *A. baumannii* infected burn wounds.

Table 3.1: *The sequence and physicochemical properties of opistoporin 1 from the venom of the Opistophthalmus carinatus scorpion and the shorter analogue Opis16a*

Peptide	**Sequence**	**#AA**	**Charge**	***M* (g/mol)**	**%[H]***
Opistoporin 1	GKVWDWIKSTAKKLWNSEPVKELKNTALNAAKNLVAEKIGATPS	44	+4	4837	45.45%
Opis16a	GKVWDWIKSTAKKLWN-NH_2	16	+4	1959	43.75%
Positive controls					
polymyxin B	Fatty acid–UUUTUUUFLU	10	+5	1200	-
melittin	GIGAVLKVLTTGLPALISWIKRKRQQ	26	+5	2847	50%

*Hydrophobicity percentage obtained from Peptide2.com; underlining represents common sequences; cationic Lys residues are indicated in blue, anionic Asp residues in red and hydrophobic Trp residues in purple.
U – unusual or non-standard amino acid: α,γ-diaminobutyric acid.

© University of Pretoria

3.3 Materials and methods

3.3.1 Opis16a purification

Opis16a was procured from Cambridge Research Biochemicals (Billingham, UK) at 80% purity. The peptide was further purified in reverse-phase high-performance liquid chromatography (RP-HPLC) on a Waters SymmetryPrep C8, 7 mm, 19 × 300 mm column as described in Van der Walt *et al* [9].

3.3.2 Antimicrobial activity assay

Antimicrobial activity was evaluated against four Gram-negative bacteria maintained by H3D, University of Cape Town, consisting of three standard laboratory strains (*E. coli* ATCC 25922 and 700928, and *A. baumannii* ATCC 19606) and one drug-resistant clinical isolate (*A. baumannii* NICD 15283[10]). Bacterial colonies from an LB agar plate were picked and cultured in cation-adjusted Mueller Hinton broth (MHB, Merck, Modderfontein, SA) at 37°C with 180 rpm shaking, overnight. Cultures were back diluted to an optical density at 600 nm (OD_{600}) of 0.1 and then diluted 100-fold to an inoculum of approximately 1 x 10^6 CFU/mL.

Opis16a was serially diluted (testing concentrations ranging from 0.125 to 64 µg/mL) in polypropylene 96-well plates using MHB. Inoculum at a starting cell density of ~5 x 10^5 CFU/mL was added at a 1:1 ratio. Gentamicin, polymyxin B and ciprofloxacin, at a concentration range of 0.063 to 32 µg/mL, were used as positive controls. Plates were incubated at 37°C for 20 h and the OD_{600} determined. Minimum inhibition concentrations (MICs) were determined from three biological repeats minimum. The MIC is the lowest concentration of peptide that reduces pathogen growth to 0.1 above the background absorbance.

3.3.3 In vitro cytotoxicity screening against HepG2 cells

HepG2 cell lines were purchased from ECACC (Salisbury, UK) and cultured in Dulbecco's Modified Eagle medium (DMEM, Sigma-Aldrich, St. Louis, USA) supplemented with 10% foetal bovine serum (FBS, Capricorn Scientific, Ebsdorfergrund, Germany) and 1% antibiotic-antimycotic (Abs, PAN Biotech, Aidenbach, Germany). The cells were seeded into 96-well plates to a density of 10^5 cells/well and allowed to attach for 24 h at 5–10% CO_2, 37°C, 95% humidity. After incubation, serial dilutions of Opis16a from 200 µg/mL (102 µM) down to 0.39 µg/mL (0.2 µM) were added and incubated for a further 48 h. Emetine (0.02 to 200 µg/mL), was used as control, since it shows non-specific cytotoxicity to mammalian cells. After 44 h of incubation the cells were stained with 10% 3-(4,5-dimethyl-2-thiazolyl)-2,5-diphenyl-2H-tetrazolium bromide (MTT) (1 mg/mL), for the remaining 4 h at 5–10% CO_2, 37°C, 95% humidity. Plates were centrifuged at 200 rpm for 5 min to pellet the reduced dye crystals, and the growth medium carefully aspirated. Crystals were solubilised using 50 µL of DMSO, and the plates were gently shaken to ensure complete dissolution. The viability of cells was determined by measuring the OD_{570} and converting it to a percentage relative to the untreated control. LC_{50}-values were obtained with non-linear dose response curve fitting analysis using the Dotmatics software.

© University of Pretoria

Selectivity towards the various bacterial species was determined using the selectivity index (SI). The SI of Opis16a was calculated as the ratio of the concentration required to cause 50% cytotoxicity in HaCat or HepG2 cell lines (LC_{50}) to the MIC per bacterial species. A higher SI value indicates greater selectivity of Opis16a towards specific bacteria over mammalian cells.

3.3.4 Outer membrane LPS competitive inhibition

For the LPS competitive assay, the ability of Opis16a to bind LPS was evaluated against *E. coli* ATCC 700928 and the multidrug-resistant *A. baumannii* NICD 15283 clinical strain in the presence of excess free LPS, as previously described[11]. Briefly, equal volumes of Opis16a and 10–640 µg/mL LPS (*E. coli* O111:B4), to a final volume of 100 µL, were incubated at 37°C in a 96-well plate for 2 h. Bacterial inoculum, as prepared above, were added to the LPS-peptide mixtures to achieve the final MIC of Opis16a and incubated overnight at 37°C. The untreated control contained bacteria and LPS alone. After incubation, the OD_{600} was measured and the percentage bacterial inhibition calculated using Equation 1:

$$\% \text{ Bacterial Inhibition} = ((A_P - A_B)/(A_{GC} - A_B) \times 100) - 100 \qquad \textbf{Equation 1}$$

where A_P is the optical density of bacterial cells exposed to peptide pretreated with LPS, A_B is the background absorbance of media and A_{GC} is the average optical density of untreated cells, plus LPS.

3.3.5 Outer membrane permeabilisation

An adapted 1-N-phenylnaphthylamine (NPN, Sigma-Aldrich, St. Louis, USA) uptake assay was used to determine whether Opis16a permeabilises the outer membrane of two representative Gram-negative bacteria: *E. coli* ATCC 700928 and a drug-resistant clinical *A. baumannii* NICD 15283 isolate[12]. Briefly, starting bacterial cultures with an OD_{600} of 0.1 were diluted 10-fold in phosphate buffered saline (PBS) containing NPN with a final concentration of 20 µM. This suspension was added to the wells of a black polypropylene 96-well plate containing Opis16a to achieve concentrations of 2, 4, 8 and 16 µg/mL (1, 2, 4 and 8 µM) peptide and 10 µM NPN. Polymyxin B, final concentration of 12.5 µg/mL (10 µM), was used as the positive control. Outer membrane permeabilisation was monitored at 37°C by measuring fluorescence intensity every two min at excitation/emission wavelengths of 350/420 nm, until the fluorescence plateaued. NPN uptake was calculated as follows:

$$\% \text{ NPN uptake} = (F_{obs} - F_0) / (F_{100} - F_0) \times 100 \qquad \textbf{Equation 2}$$

where the fluorescence intensity is $F_{obs,}$ for treated bacteria, F_0 for untreated bacteria and F_{100} for cells treated with the positive control.

3.3.6 Cytoplasmic membrane depolarisation

The effect of Opis16a on the cytoplasmic membrane potential was investigated using a potential sensitive probe bis-(1,3-dibutylbarbituric acid) trimethine oxonol ($DiBAC_4(3)$,ThermoFisher Scientific, Johannesburg, RSA.). Gram-negative *E. coli* ATCC 700928 and *A. baumannii* NICD 15283 were

© University of Pretoria

cultured as described above and were diluted 10-fold in PBS, before treatment with two-fold serial dilutions of the positive control melittin (1.6-11 µg/mL or 0.5-4 µM), and Opis16a (0.25, 0.5, 1 and 2x MIC), respectively. After 1 h incubation, the $DiBAC_4(3)$ probe at a final concentration of 2 µg/mL was added. After 30 min in the dark at 37°C, the cells were collected by centrifugation at 10000x g for 10 min. The pellets were resuspended in PBS and transferred to a black 96-well plate. Fluorescence intensity was measured with excitation/emission wavelengths of 490/516 nm. Membrane depolarisation was calculated as follows:

$$\% \text{ Cytoplasmic membrane depolarisation} = ((F_P - F_B) / (F_0 - F_B) \times 100) - 100 \qquad \textit{Equation 3}$$

where the fluorescence intensity is F_P following exposure to Opis16a or melittin, F_B, background fluorescence (PBS + $DiBAC_4(3)$ alone) and F_0, untreated bacteria.

3.3.7 Cytoplasmic membrane permeabilisation

The ability of Opis16a to permeabilise bacterial cytoplasmic membranes was assessed with the SYTOX Green assay (ThermoScientific, Massachusetts, USA). Briefly, bacterial cultures as prepared above were diluted 5-fold in PBS, before SYTOX Green (5 µM) was added at a 1:1 ratio. This suspension was then transferred to a black polypropylene 96-well plate containing Opis16a to reach final concentrations of 2, 4, 8 and 16 µg/mL (1, 2, 4 and 8 µM). Melittin, at a final concentration of 5.6 µg/mL (2 µM), was used as positive control (GenScript, Rijswijk, Netherlands). The increase in fluorescence at 37°C was measured every 2 min for 120 min at excitation/emission wavelengths of 485/535 nm.

3.3.8 Time-kill kinetics

The concentration- and time-dependent killing capability of Opis16a was determined against *E. coli* ATCC 700928 and the multidrug-resistant *A. baumannii* NICD 15283 bacterial isolate using a time-kill kinetics assay. A bacterial inoculum of 1 x 10^6 CFU/mL was established as described above. Killing kinetics were evaluated at 0.5x, 1x and 2x the MIC of Opis16a. Bacterial suspensions were added to each peptide concentration at a 1:1 ratio and incubated at 37°C. Samples were collected aseptically at the various timepoints of 0, 15, 30, 45, 60, 90, 120, and 180 min, which were then ten-fold serially diluted in sterile ddH_2O and plated on LB agar for colony counting.

3.3.9 Opis16a activity in the presence of trypsin and serum

The susceptibility of Opis16a to proteolytic degradation or the binding with serum proteins was evaluated *in vitro* using cation-adjusted MHB supplemented with trypsin (Merck, Modderfontein, SA) or foetal calf serum (FCS, Capricorn Scientific, Ebsdorfergrund, Germany). To evaluate trypsin stability, Opis16a was serially diluted in a 2 mM trypsin solution (pancreas protease) to reach a final concentration range of 0.125 to 64 µg/mL (0.064–32.67 µM) peptide to 1 mM trypsin (0.145 U/mL, pH 7.4). Samples were incubated for 1 h at 37°C. Peptide alone and protease alone were used as controls. After incubation the samples were heated at 60°C for 20 min for protease inactivation.

© University of Pretoria

A similar strategy was followed to determine whether FCS affects the antimicrobial activity of Opis16a due to possible serum protein binding. Serial dilutions of Opis16a in cation-adjusted MHB supplemented with 20% FCS were incubated for 1 h at 37°C. Peptide alone and FCS alone were used as controls. After Opis16a incubation with trypsin or FCS, the procedure described above for determining antimicrobial activity was followed whereby an equal volume of peptide and bacteria was added to the 96-well plates and incubated for 20 h at 37°C. The MIC of Opis16a pretreated with trypsin or preincubated with FCS was compared with peptide alone.

3.3.10 In vivo antibacterial activity of Opis16a in a G. mellonella burn wound model

The protection afforded by Opis16a against *A. baumannii* NICD 15283 infection in burn wounds was evaluated using *G. mellonella* larvae. The larvae were sourced from and maintained by the FABI Biocontrol Centre and Nursery at the University of Pretoria. A similar procedure as used by Clarke *et al.* and first introduced by Maslova *et al.,* was followed[15,38]. A group size of 10 larvae per condition were used for a total of three biological repeats. Prior to the experiment, *G. mellonella* larvae with similar size and weight (200-300 mg) were surface decontaminated using a cotton swab immersed in 70% ethanol. Burn wounds were induced by heating the flat head of a nail in a blue Bunsen burner flame until red hot, cooled for 11 s, and then topically applying it for 2 s to create a 2-mm^2 sized burn. The burn sites were then infected with 2-3 colonies of *A. baumannii* NICD 15283 from a fresh agar plate using an inoculating loop to topically spread the bacteria over the burn wound. Uninfected controls were treated with sterile PBS. Opis16a at 10 mg/kg in 5 µL was topically applied to the wound 1 h after infection. Each group of larvae was housed in separate containers within a static incubator at 37°C for the duration of the experiment. Survival was monitored every 24 h for 96 h. *G. mellonella* survival were analysed by the log rank (Mantel-Cox) method and plotted as Kaplan-Meier survival curves.

3.3.11 Activity data and statistical analysis

Triplicate dose response assays with three biological repeats each were performed against all pathogens. Data analyses for *in vitro* assays were performed using GraphPad Prism® V 7.0 software (San Diego, CA, USA), except for HepG2 toxicity screening data which were analysed using Dotmatics software. Statistical analyses were performed by determining Row totals/means with standard deviation (SD) or standard error of the mean (SEM) followed by One-way analysis of variance (ANOVA) with Dunnett's multiple/selected comparison post-test.

© University of Pretoria

3.4 Results

3.4.1 Opis16a displays promising Gram-negative antibacterial activity with high bacterial over mammalian cell selectivity

In a prior study, we highlighted the potent antimicrobial activity of Opis16a against seven Gram-negative strains[9]. The MICs in the present study were obtained in cation-adjusted MHB and are slightly higher compared with those in non-cation-adjusted MHB for three of the four strains, a phenomenon often observed due to the interactions between antimicrobial agents and the components of complex media[16]. Previously, the peptide demonstrated particularly strong efficacy against *E. coli* NCTC 12923 and LEC 001 strains, with MICs of 4 µg/mL, and even greater efficacy against *A. baumannii* ATCC 17978 and AYE strains, with MICs of 2 µg/mL[9]. The present study reaffirms the potential of Opis16a, with potent activity observed against additional strains of *E. coli* and *A. baumannii*, even when tested in cation-adjusted MHB.

In cation-adjusted MHB, Opis16a still achieves an MIC of 4 µg/mL against *E. coli* ATCC 700928, consistent with previous results in non-cation-adjusted MHB. In contrast, less activity is observed against *E. coli* ATCC 25922, with an MIC of 63.3 µg/mL. Notably, the potent activity of Opis16a is retained against the multidrug-resistant *A. baumannii* NICD 15283 clinical isolate as well as *A. baumannii* ATCC 19606 (Table 3.2). Both strains are more sensitive to Opis16a than to gentamicin, an antibiotic often indicated for wound infections, against which both strains are resistant (EUCAST breakpoint 4 µg/mL).

Table 3.2: *Antibacterial activity and selectivity of Opis16a against Gram-negative E. coli and A. baumannii strains*

Gram-negative bacteria	MIC µg/mL (µM)				Opis16a SI	
	Opis16a	Polymyxin B	Ciprofloxacin	Gentamicin	HaCat* (LC_{50} 311.2 µg/mL)	HepG2 (LC_{50} 118.2 µg/mL)
E. coli ATCC 700928	4 (2)	0.5 (0.4)	0.25 (0.75)	0.5 (1)	77.8	29.6
E. coli ATCC 25922	64 (32)	0.25 (0.2)	-	0.5 (1)	4.9	1.8
A. baumannii ATCC 19606	8 (4)	1 (0.8)	1 (3)	>32 (>16)	38.9	14.8
A. baumannii NICD 15283	8 (4)	1 (0.8)	1 (3)	>32 (>16)	38.9	14.8

Values in brackets are µM concentrations. * Data reproduced from van der Walt et al [9].

The toxicity of Opis16a was previously evaluated against human erythrocytes as well as epidermal HaCat keratinocytes from which HC_{50} or LC_{50} was determined[9]. The HC_{50} and LC_{50} values represent the concentrations of Opis16a required to cause 50% haemolysis, or 50% lethality of HaCat cells. Opis16a, is one of the few scorpion venom-derived peptides that showed little to no cytotoxicity against human cells.

© University of Pretoria

No haemolytic activity was observed towards human erythrocytes with an HC_{50} >256 µg/mL[9]. Low cytotoxicity against human HaCat cells was also reported with an LC_{50} of 311.2 ± 12.3 µg/mL[9]. This is similar to the previously reported LC_{50} of 0.35 mM (420 µg/mL) for polymyxin B against human kidney epithelial HK-2 cells[40].

In the present study the toxicity of Opis16a was further evaluated against the human hepatoblastoma HepG2 cell line to give an initial indication of potential liver toxicity. Opis16a shows increased toxicity against the HepG2 cells compared with erythrocytes and HaCat cells, with a lower LC_{50} of 118.2 µg/mL. Although toxicity increases in the more metabolically active cells, the LC_{50} of Opis16a is still higher than the MIC values required to inhibit the bacterial strains.

Opis16a shows promising bacterial selectivity with an SI >10 towards three of the four bacterial strains over HaCat or HepG2 cells (Table 3.2). The greatest selectivity is towards *E. coli* ATCC 700928, while high selectivity towards *A. baumannii* ATCC 19606 and the multidrug-resistant *A. baumannii* NICD 15283 clinical isolate is also observed.

3.4.2 LPS pretreatment inhibits Opis16a antibacterial activity suggesting LPS binding

To elucidate how Opis16a exerts its antimicrobial effects against Gram-negative bacteria, mechanism of action studies were conducted. Since AMPs generally target bacterial membranes, the interactions of Opis16a with various components of the Gram-negative membrane was investigated using two representative strains: *E. coli* ATCC 700928 and the multidrug-resistant clinical isolate *A. baumannii* NICD 15283.

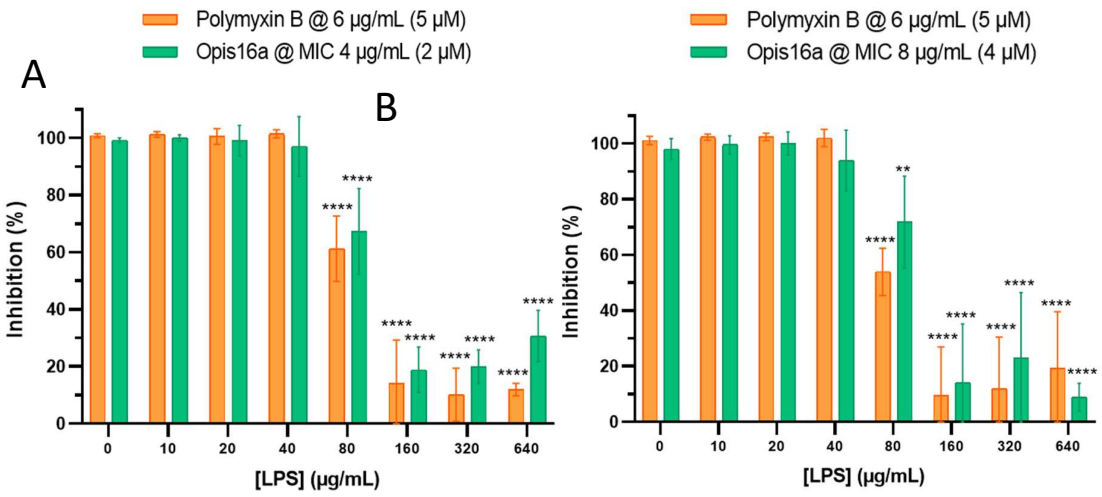


Figure 3.1: Effect of LPS on Opis16a efficacy against Gram-negative bacteria. (A) *E. coli ATCC 700928 and* ***(B)*** *A. baumannii NCID 15283 treated with the MIC of 4 or 8 µg/mL Opis16a [2 or 4 µM respectively for each species], compared with Polymyxin B at 6 µg/mL [5 µM]. Data represent the mean ± SEM, for three independent experiments performed in triplicate. (Statistical significance was assessed by one-way ANOVA followed by Dunnett's multiple comparisons test, comparing each LPS concentration to the 0 µg/mL control. A p-value < 0.01 was considered significant.**: p<0.05, ****: p<0.0001).*

© University of Pretoria

The outer membrane of Gram-negative bacteria is primarily composed of LPS, which are essential for membrane integrity and contribute to endotoxic shock in severe infections[6]. Polymyxin B is an example of a widely used Gram-negative drug, that electrostatically interacts with LPS on the outer membrane of Gram-negative bacteria[17]. Due to the anionic nature of LPS, cationic Opis16a potentially can target this outer membrane component. To test this hypothesis, Opis16a was pretreated with free LPS, and the consequence of potential binding, such as reduced activity, was determined against *E. coli* ATCC 700928 and *A. baumannii* NICD 15283.

In the presence of increasing concentrations of free LPS, the antimicrobial activity of both polymyxin B (6 µg/mL) and Opis16a (with MICs of 4 or 8 µg/mL) is reduced against *E. coli* ATCC 700928 and *A. baumannii* NICD 15283 (Fig. 3.1 A & B). This reduction in activity follows a similar trend for both polymyxin B and Opis16a, suggesting that free LPS competes with membrane-bound LPS for binding to both antimicrobials. As a result, the presence of free LPS decreases the availability of Opis16a and polymyxin B for binding to the bacterial membrane, leading to diminished bacterial inhibition. Thus, these findings indicate that Opis16a likely initially interacts with LPS when encountering Gram-negative bacteria.

3.4.3 Opis16a permeabilises the outer membrane

The consequence of the interaction of polymyxin B with LPS is the displacement of Mg^{2+} and Ca^{2+} ions allowing polymyxin B to insert into and destabilise the outer membrane[17]. This effect was further investigated using NPN, the hydrophobic fluorophore, that is membrane impermeable and can only enter and interact with the hydrophobic components of the cell membrane once the outer membrane is destabilised and disrupted[18]. This disruption leads to an associated increase in fluorescence intensity.

For comparison, outer membrane permeabilisation was also assessed using melittin, a membranolytic peptide derived from the honeybee *Apis mellifera*[19]. Like Opis16a, melittin is a venom-derived peptide, and is known for its ability to disrupt membranes, providing a relevant benchmark for evaluating the membrane-disrupting effects of Opis16a.

Opis16a treatment results in a dosage- and time-dependent increase in outer membrane permeabilisation of both *E. coli* ATCC 700928 and *A. baumannii* NICD 15283 (Fig. 3.2 A & B). Little to no membrane permeabilisation is observed at 0.5x MIC against either *E. coli* ATCC 700928 (2 µg/mL, 1 µM) or *A. baumannii* NICD 15283 (4 µg/mL, 2 µM). However, a rapid increase in fluorescence is detected within the first 15 min at the MIC (4 µg/mL, 2 µM) and 2x MIC (8 µg/mL, 4 µM), reaching 40% for *E. coli* ATCC 700928. The fluorescence then steadily increases to a maximum of 50% for the MIC and 85% for the 2x MIC (Fig. 3.2 A).

For *A. baumannii* NICD 15283, a more gradual increase in outer membrane permeabilisation is observed at the MIC (8 µg/mL, 4 µM), reaching a maximum of 55% after 2 h, similar to the maximum

© University of Pretoria

observed for *E. coli* ATCC 700928 (Fig. 3.2 B). At 2x MIC, rapid outer membrane permeabilisation occurrs, with fluorescence rising sharply in the first 15 min and reaching a maximum of 85%, comparable to that seen with *E. coli* ATCC 700928 (Fig. 3.2 B). This suggests that the binding of Opis16a to LPS causes dosage dependent disintegration of the outer membrane of Gram-negative *E. coli* and *A. baumannii* with maximum destabilisation at 2x MIC.

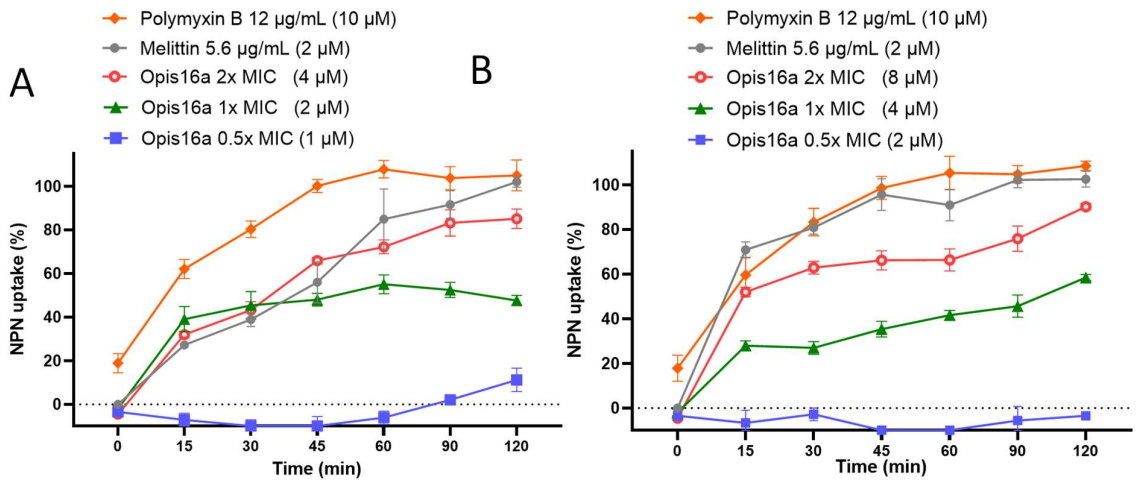


Figure 3.2: Opis16a mediated outer membrane permeabilisation using NPN uptake over a period of 2h. (A) *E. coli ATCC 700928 and* ***(B)*** *A. baumannii NCID 15283 membrane permeabilisation by Opis16a at 0.5, 1 and 2x MIC (2, 4 and 8 µg/mL for E. coli [1, 2 and 4 µM] or 4, 8 and 16 µg/mL for A. baumannii [2, 4 and 8 µM]) compared with polymyxin B (orange) at 12 µg/mL [10 µM], and melittin (grey) at 5.6 µg/mL [2 µM]. Data show one representative experiment with mean ± SD, of a total of three independent experiments performed in triplicate.*

3.4.4 Opis16a depolarises the cytoplasmic membrane at sub-MIC concentrations

Following the binding of Opis16a to LPS and the subsequent destabilisation of the outer membrane barrier, the ability of this peptide to target and depolarise the inner membrane of *E. coli* ATCC 700928 and *A. baumannii* NICD 15283 was evaluated.

$DiBAC_4(3)$ exhibits increased fluorescence intensity in response to changes in membrane potential, even when the membrane is not permeabilised. The dye's fluorescence is higher in depolarised cells compared to cells with normal membrane potential. This fluorescence increase is due to the dye's interaction with intracellular components and a change in the dye's environment[13].

Opis16a exhibits dose-dependent increases in $DiBAC_4(3)$ fluorescence intensity with cytoplasmic membrane depolarisation observed at concentrations as low as 0.5x MIC against *E. coli* ATCC 700928 and 0.25x MIC against *A. baumannii* NICD 15283 (Fig. 3.3 A & B).

The lowest concentration of 0.25x MIC Opis16a causes no depolarisation in *E. coli* ATCC700928, whereas in *A. baumannii* 20% depolarisation is induced. The 0.5x MIC Opis16a causes significant depolarisation of 20% against *E. coli* ATCC 700928 and 35% against *A. baumannii* NICD 15283. At the MIC, the cytoplasmic membrane depolarisation of Opis16a is 42% for both bacteria and reaches a maximum of 55-60% at 2x MIC. Therefore, membrane depolarisation is already induced

© University of Pretoria

by Opis16a at sub-MIC concentrations, not as a result of membrane permeabilisation—since permeabilisation only occurs at MIC and higher concentrations—but as a distinct mechanism.

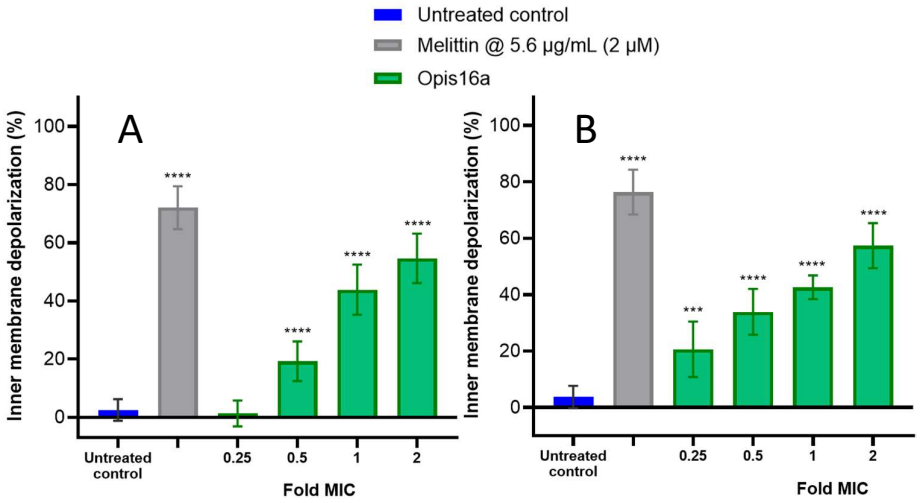


Figure 3.3: Percentage cytoplasmic membrane depolarisation after 1.5 h treatment with different concentrations of Opis16a. (A) *E. coli ATCC 700928 and* ***(B)*** *A. baumannii NICD 15283 treated with Opis16a at 0.25, 0.5, 1 and 2x MIC (1, 2, 4 and 8 µg/mL for E. coli [0.5, 1, 2 and 4 µM] or 2, 4, 8 and 16 µg/mL for A. baumannii [1, 2, 4 and 8 µM]). Melittin at 5.6 µg/mL [2 µM] is included as positive control. (Statistical significance was assessed by one-way ANOVA followed by Dunnett's multiple comparisons test, comparing each AMP concentration to the untreated control. ***: p<0.001, ****: p<0.0001).*

3.4.5 Opis16a shows rapid killing of E. coli ATCC 700928 and A. baumannii NICD 15283 via cytoplasmic membrane permeabilisation

LPS binding, destabilisation of the outer membrane and depolarisation of the inner plasma membrane can lead to increased cytoplasmic membrane permeability, and this was further investigated. SYTOX Green is impermeant to live cells with intact membranes but can enter cells with damaged membranes. Once inside it binds to nucleic acids and fluoresces. An increase in fluorescence is directly associated with an increase in membrane disruption[14].

SYTOX Green fluorescence, indicating membrane damage, is detected as early as 5 min and increases over time for both *E. coli* ATCC 700928 and *A. baumannii* NICD 15283 following Opis16a treatment.

In contrast to the membrane depolarisation observed at sub-MIC Opis16a concentrations, no cytoplasmic membrane permeabilisation occurs at 0.5x MIC for either *E. coli* ATCC 700928 (2 µg/mL, 1 µM) or *A. baumannii* NICD 15283 (4 µg/mL, 2 µM). An increase in fluorescence intensity indicating cytoplasmic membrane permeabilisation, is only observed at 1x MIC Opis16a and above (Fig. 3.4 A & B).

Against *E. coli* ATCC 700928 the MIC (4 µg/mL or 2 µM) starts to destabilise the cytoplasmic membrane, reaching a plateau around 45 min. At 2x MIC (8 µg/mL or 4 µM) a similar degree of permeabilisation to that induced by 2 µM melittin is observed, with the maximum reached about 45-60 min after treatment (Fig. 3.4 A).

© University of Pretoria

Membrane permeabilisation is more pronounced in *A. baumannii* NICD 15283, as demonstrated by the increased fluorescence intensity (Fig. 3.4 B). At the MIC of 8 µg/mL (4 µM), which is twice the concentration of melittin (2 µM), Opis16a initiates membrane permeabilisation in *A. baumannii* NICD 15283, reaching its peak approximately at 30-40 min. At 2x MIC (16 µg/mL or 8 µM), the level of permeabilisation is comparable to that induced by 2 µM melittin but occurs much more rapidly, peaking within 15 min. Following this peak, the fluorescence intensity gradually decreases due to cell death.

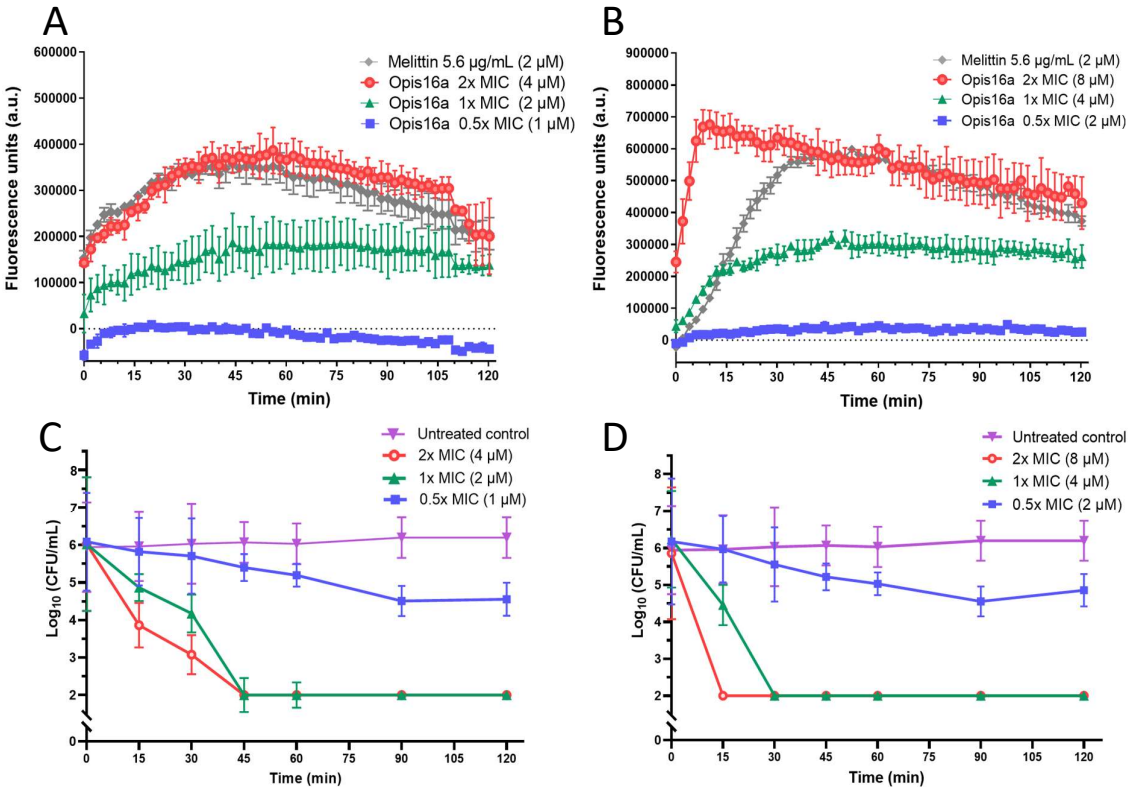


Figure 3.4: Inner membrane permeabilisation corresponds to the time-kill kinetics of Opis16a over a 2 h period. *Cytoplasmic membrane permeabilisation with melittin as control* ***(A&B)*** *and time-kill kinetics* ***(C&D)*** *of Opis16a against E. coli 700928* ***(A&C)*** *and A. baumannii NICD 15283* ***(B&D)*** *at 0.5 x, 1 x and 2 x MIC (2, 4 and 8 µg/mL or 4, 8 and 16 µg/mL respectively [1, 2 and 4 µM] or [2, 4 and 8 µM] respectively). Permeabilisation data show one representative experiment with mean ± SD, of a total of three independent experiments performed in duplicate. Time-kill data represent the mean ± SEM for three independent experiments performed in triplicate.*

Subsequent time-kill kinetics studies conducted on the *E. coli* ATCC 700928 strain and the multidrug-resistant clinical isolate *A. baumannii* NICD 15283 track closely with the observed cytoplasmic membrane permeabilisation results (Fig. 3.4 C & D). After 45 min of exposure to Opis16a at both 1x and 2x MIC, a reduction of approximately 99.9% (4 Log_{10} CFU/mL) is observed for *E. coli* ATCC 700928 (Fig. 3.4 C). This time point also coincides with the peak cytoplasmic membrane permeabilisation observed for these concentrations.

In addition, a threefold increase in the killing rate is observed for *A. baumannii* NICD 15283 compared with *E. coli* ATCC 700928 when exposed to 2x MIC of Opis16a, with killing occurring

© University of Pretoria

within 15 min (Fig. 3.4 D). This rapid killing correlates with the increased intensity of membrane permeabilisation seen for *A. baumannii* NICD 15283 at 2x MIC within 15 min (Fig. 3.4 B). At its MIC, Opis16a also demonstrates a fast-killing rate against *A. baumannii* NICD 15283, achieving substantial killing within 30 min (Fig. 3.4 D), again aligning with the peak cytoplasmic membrane permeabilisation observed for this concentration (Fig. 3.4 B). At 0.5x MIC, Opis16a shows minimal effect on either *E. coli* ATCC 700928 or *A. baumannii* NICD 15283, at least within the first hour post challenge.

The absence of bacterial regrowth following a 2-h treatment with 1x and 2x MIC of Opis16a, consistent with the observed cytoplasmic membrane permeabilisation, indicates that this AMP exerts a bactericidal effect.

3.4.6 Opis16a retains activity in FCS, but not in trypsin solution

The stability of Opis16a, in the presence of the proteolytic enzyme trypsin or in a more physiological environment such as FCS was evaluated. Opis16a pretreated with 1 mM trypsin (0.145 U/mL, pH 7.4), completely loses activity against the *A. baumannii* NICD 15283 clinical isolate even at the highest concentration tested (Fig. 3.5). This is attributed to the enzymatic degradation via hydrolytic cleavage of the peptide bonds at the carboxyl side of the four Lys residues in the peptide sequence. In 20% FCS, the activity of Opis16a is, however, retained indicating resistance to serum protein binding, a characteristic known to reduce the potential of AMPs for further topical and/or systemic applications[33].

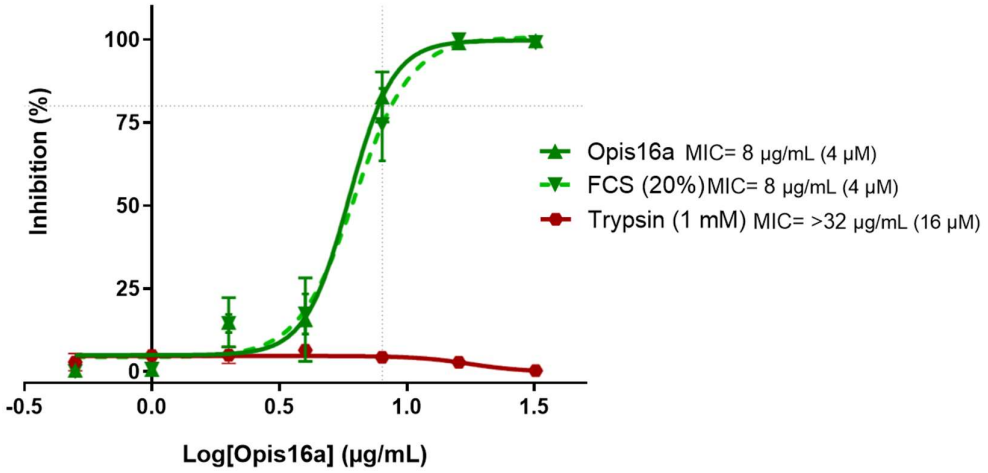


Figure 3.5: Antibacterial efficacy of Opis16a preincubated with trypsin 15283 (1 mM, 0.145 units/mL) or FCS (20%) against A. baumannii NICD 15283. *Data represents the mean ± SEM, for three independent experiments performed in triplicate.*

3.4.7 Opis16a shows activity against in vivo A. baumannii infected wounds

The *in vitro* planktonic potency, high selectivity of Opis16a for *A. baumannii* over mammalian epidermal cells, and stability in 20% FCS makes this AMP a suitable candidate for progression to a model of topical *A. baumannii* wound infection.

© University of Pretoria

While *G. mellonella* can tolerate superficial burns with a mortality of only 7%, subsequent infection with *A. baumannii* NICD 15283 leads to 70% mortality over 96 h ($p < 0.0001$, log rank [Mantel-Cox] test), allowing effective therapy to be quantified (Fig. 3.6). Treatment with 10 mg/kg polymyxin B rescued 83% of the *A. baumannii* NICD 15283 infected *G. mellonella* larvae ($p < 0.0001$, log rank [Mantel-Cox] test). At a concentration of 10 mg/kg, Opis16a showed comparable efficacy to polymyxin B, successfully rescuing 87% of the larvae ($p < 0.0001$, log rank [Mantel-Cox] test). This is a three-fold improvement compared with the survival of larvae with infected but untreated burn wounds.

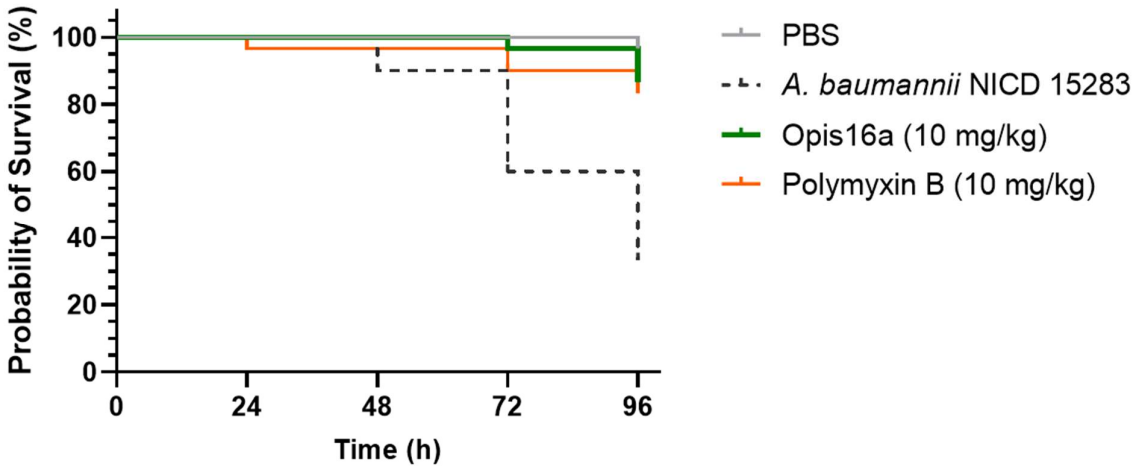


Figure 3.6: Opis16a provides protection in a G. mellonella burn wound infected with A. baumannii NICD 15283. *Survival curves are plotted for larvae with burn wounds only, with burn and A. baumannii NICD 15283 infected wounds or burn and infected wounds treated with 10 mg/kg Opis16a [5 µmol/kg] or polymyxin B [8 µmol/kg] over 96 h.* Data *are aggregated from three independent experiments consisting of 30 larvae in total.*

© University of Pretoria

3.5 Discussion

This study reveals the scorpion venom-derived peptide, Opis16a, as a promising anti-Gram-negative antimicrobial in *in vitro* as well as *in vivo* settings, with the ability to bind LPS and navigate the complex cell envelope of Gram-negative bacteria. Scorpion venom derived AMPs reported in literature are generally associated with cell toxicity and a lack of cell selectivity [20-23]. AMPs such as AamAP1, AamAP-S1a, A3a and K3-IsCTa derived from the venom of various African scorpion species show strong haemolysis and significant toxicity against mammalian cells[9].

Results herein show that Opis16a exhibits potent antimicrobial activity against WHO priority pathogens such as *E. coli* ATCC 700928, *A. baumannii* ATCC 19606 and *A. baumannii* NICD 15283 with MICs of 8 µg/mL or lower. This activity is comparable to other AMPs with reported Gram-negative activity such as the phage-derived AMP EC5 [24], the amphibian derived citropin1.1 or temporin A [25] or the fish-derived pleurocidin [26].

Additionally, Opis16a toxicity against HaCat or HepG2 cells only occurs at concentrations of 118 µg/mL and above, several fold greater than the MICs. This indicates high selectivity towards the three above mentioned bacterial strains over the representative topical and systemic mammalian cells. Generally, a SI greater than 10 is considered favourable, indicating a wide therapeutic window and lower risk of adverse effects on host cells[36]. Due to the potent activity of Opis16a, high SI values surpassing 38 for HaCat cells and 14 for HepG2 cells are yielded for *E. coli* ATCC 700928, *A. baumannii* ATCC 19606 and *A. baumannii* NICD 15283. These findings suggest a potential use for Opis16a in topical applications and possibly even systemically.

The selectivity of Opis16a can be attributed to several key factors. First, its overall positive charge of +4 facilitates specific electrostatic interactions with the negatively charged membranes of bacteria. This charge is notably high for a peptide comprising just 16 amino acids, especially when compared with other more toxic peptides like AamAP1 and AamAP-S1a, which have lower charges of +1 and +3, respectively, despite comprising 18 amino acids[9]. Moreover, Opis16a exhibits a relatively low hydrophobicity value of approximately -2.88 determined with the consensus scale of Eisenberg *et al.*[39]. This is significantly lower than the hydrophobicity of other toxic scorpion venom-derived peptides, such as AamAP1 (4.34), AamAP-S1a (3.64), A3a (1.91), and K3-IsCTa (0.21), as well as the well-known bee venom peptide melittin (-2.23). Previous studies have indicated a correlation between increased hydrophobicity and higher toxicity toward mammalian cells, suggesting that the lower hydrophobicity of Opis16a may contribute to its selective antimicrobial action[9].

Additionally, Opis16a has a lower lipophilicity of polar residues (LP) value of -6.9, in contrast to the higher LP values of -0.9, -2.06, -3.07, and -5.3 for AamAP1, AamAP-S1a, A3a, and K3-IsCTa, respectively. Previous work indicates that reduced LP is associated with more potent and selective antimicrobial activity[9]. Lastly, the interaction of Opis16a with LPS, a unique component of the Gram-

© University of Pretoria

negative outer membrane that is absent in mammalian membranes, may further enhance its selectivity.

Peptide susceptibility to degradation in systemic settings is another factor that limits Gram-negative AMP therapeutic development[27-32]. The presence of proteolytic enzymes such as trypsin in bodily fluids or wounds, can lead to the rapid degradation of AMPs, limiting their bioavailability and therapeutic efficacy[27]. For instance, magainin and temporin peptides, isolated from amphibian skin secretions, indolicidin from bovine neutrophils, human defensins, histatins, and numerous other AMPs have shown decreased activity in various bodily fluids, limiting their systemic stability and bioavailability [28-32]. Here we show that Opis16a undergoes degradation when exposed to trypsin which is attributed to the four Lys residues in the peptide sequence. However, in the presence of 20% FCS in cation-adjusted MHB, Opis16a maintains its antimicrobial effectiveness completely, suggesting that the peptide is not bound to or inhibited by serum proteins or complex media [33].

Since the rapid bactericidal action of Opis16a against *E. coli* ATCC 700928 and *A. baumannii* NICD 15283 matches closely to the permeabilisation kinetics we can infer that Opis16a acts on the outer surface of the bacterial membranes rather than internal components. This promoted the study of the mechanism of action of Opis16a, particularly its interaction with the membrane, starting with LPS, the major component of the outer membrane. Previous studies on cationic AMPs such as melittin or polymyxin B have shown that the initial interaction with anionic LPS on the cell surface plays a pivotal role in destabilising the cytoplasmic membrane, ultimately leading to the killing of Gram-negative bacteria [12]. LPS binding can also have anti-inflammatory effects, mitigating the risk of hypotension and septic shock by reducing the overwhelming immune response induced by this endotoxin[4, 34]. We find a decrease in the activity of Opis16a after pretreatment with excess free LPS. This suggests a reduction in the availability of Opis16a to bind to membrane LPS due to the binding with the excess free LPS. Notably, these results are comparable to those obtained for polymyxin B, a peptide well-known for its binding affinity to LPS and associated antibacterial activity[17]. Therefore, Opis16a binding to LPS likely marks the beginning of a series of events that contribute to Gram-negative bacterial death.

LPS binding often leads to the displacement of ions which triggers outer membrane destabilisation and could facilitate the entry of Opis16a into the periplasmic space[16]. The resulting exposure of the cytoplasmic membrane to Opis16a, combined with ion displacement renders the inner membrane susceptible to depolarisation even at sub-MIC concentrations. As noted by Wang *et al.*, the binding of AMPs to the cytoplasmic membrane can induce subtle changes in membrane potential, leading to bacterial cell death either directly or by triggering subsequent effects, such as a decrease in ATP production due to the disrupted ion gradient[34,37]. Membrane depolarisation can also affect other energy-intensive processes such as ion balance, transport of nutrients, protein, and lipids and bacterial motility[37]. These subtle disruptions could lead to a bacteriostatic effect which is supported by the slow killing-kinetics observed for this peptide at sub-MIC concentrations.

© University of Pretoria

Finally, given the potent and rapid activity of Opis16a against planktonic bacteria, LPS binding and potential anti-inflammatory activity, membrane depolarisation and disruption against *E. coli* and *A. baumannii*, selectivity for bacterial over mammalian epidermal cells, and stability in 20% FCS, the peptide was advanced to an evaluation in an *in vivo* wound infection model. Here, Opis16a offered significant protection against the multidrug-resistant *A. baumannii* NICD 15283 topical wound infection which led to an increase in larvae survival, comparable to the protection offered by polymyxin B. This is similar to the recently reported protection offered by 10 mg/kg pleurocidin or 5 mg/kg gentamicin or ciprofloxacin against *A. baumannii* ATCC 17978 infections of *G. mellonella* burn wounds[38]. These results bear considerable significance, particularly due to the frequent involvement of *A. baumannii* in hospital-acquired infections, severely affecting critically ill and immunocompromised individuals[35]. Moreover, the prevalence of multidrug resistance among various *A. baumannii* strains[35], emphasises the need for novel therapies. Therefore, the findings in the present study collectively highlight the potential of novel Opis16a for future therapeutic development, especially against challenging Gram-negative bacteria such as *A. baumannii*.

3.6 Conclusion

The scorpion venom-derived antimicrobial peptide Opis16a shows potent activity against a diverse range of Gram-negative bacteria, including a multidrug-resistant clinical isolate of *A. baumannii*. Remarkably, despite its venom origin, Opis16a exhibits low toxicity toward mammalian cells—a notable exception given that venom-derived peptides typically cause significant toxicity. Mechanism of action studies, with *E. coli* and *A. baumannii*, find that Opis16a binds to LPS comparable to polymyxin B and destabilises the outer membrane. The peptide also depolarises and permeabilises the cytoplasmic membrane similar to melittin. This indicates that Opis16a exhibits high efficacy akin to both polymyxin B and melittin, while offering the added benefit of minimal toxicity. Moreover, Opis16a shows high selectivity for bacterial over mammalian cells, rapid eradication of *E. coli* and *A. baumannii* within minutes and retained activity in 20% FCS. The *in vivo* application of Opis16a shows a three-fold improvement in larval survival compared to untreated *A. baumannii*-infected larvae, with an efficacy similar to that of polymyxin B. Consequently, this study identifies Opis16a as a novel AMP with potent Gram-negative activity, minimal toxicity to mammalian cells and promising potential for topical applications.

3.7 Acknowledgements

Research reported herein was funded by the South African Medical Research Council received from the South African National Department of Health and a SA-UK Newton Fund Antibiotic Accelerator (MC_PC_MR/T029552/1), awarded to AJM and ARMG, and managed by the Medical Research Council (UK). We also extend our gratitude to Sophie Nyoni and Pretti Khumalo from the FABI Biocontrol Centre and Nursery at the University of Pretoria, for their assistance in maintaining and providing *G. mellonella* larvae.

© University of Pretoria

3.8 References

[1] MAINA, J.W., ONYAMBU, F.G., KIBET, P.S. & MUSYOKI, A.M.(2023). Multidrug-resistant Gram-negative bacterial infections and associated factors in a Kenyan intensive care unit: a cross-sectional study. *Annals of Clinical Microbiology and Antimicrobials,* 22 (1), article 85. https://doi.org/10.1186/s12941-023-00636-5

[2] WORLD HEALTH ORGANIZATION. (2017). Antibacterial agents in clinical development: an analysis of the antibacterial clinical development pipeline, including tuberculosis. [Internet] Available from: WHO publishes list of bacteria for which new antibiotics are urgently needed, Accessed January 2024.

[3] BARRETO-SANTAMARÍA, A., ARÉVALO-PINZÓN, G., PATARROYO, M.A. & PATARROYO, M.E. (2021). How to combat Gram-negative bacteria using antimicrobial peptides: A challenge or an unattainable goal? *Antibiotics (Basel),* 10 (12), pg. 1499-1511. doi:10.3390/antibiotics10121499

[4] DEHARI, D., CHAUDHURI, A., KUMAR, D.N., PATIL, R., GANGWAR, M., RASTOGI, S., KUMAR, D., NATH, G. & AGRAWAL, A.K. (2023). A bacteriophage microgel effectively treats the multidrug-resistant Acinetobacter baumannii bacterial infections in burn wounds. Pharmaceuticals (Basel),16 (7), pg. 942-965. doi:10.3390/ph16070942

[5] JIMÉNEZ-JIMÉNEZ, C., MORENO, V.M. & VALLET-REGÍ, M. (2022). Bacteria-assisted transport of nanomaterials to improve drug delivery in cancer therapy. *Nanomaterials (Basel),* 12 (2), pg. 288-305. doi:10.3390/nano12020288

[6] ROMANO, K.P. & HUNG, D.T. (2023). Targeting LPS biosynthesis and transport in Gram-negative bacteria in the era of multidrug resistance. *Biochimica et Biophysica Acta Molecular Cell Research*, 1870 (3), article 119407. doi:10.1016/j.bbamcr.2022.119407

[7] WESSELING, C.M.J. & MARTIN, N.I. (2022). Synergy by perturbing the gram-negative outer membrane: Opening the door for gram-positive specific antibiotics. *ACS Infectious Diseases*, 8 (9), pg. 1731-1757.

[8] MOERMAN, L., BOSTEELS, S., NOPPE, W., WILLEMS, J., CLYNEN, E., SCHOOFS, L., THEVISSEN, K., TYTGAT, J., VAN ELDERE, J., VAN DER WALT, J. & VERDONCK, F. (2002). Antibacterial and antifungal properties of α-helical, cationic peptides in the venom of scorpions from southern Africa. *European Journal of Biochemistry*, 269, pg. 4799-4810. https://doi.org/10.1046/j.1432-1033.2002.03177.x

[9] VAN DER WALT, M., MÖLLER, D.S., VAN WYK, R.J., FERGUSON, P.M., HIND, C.K., CLIFFORD, M., DO CARMO SILVA, P., SUTTON, J.M, MASON, J.A., BESTER, M.J. & GASPAR, A.R.M. (2024). QSAR reveals cationic residues with decreased lipophilicity determine the selectivity of antimicrobial peptide activity. *ACS Omega,* doi: 10.1021/acsomega.4c01277

[10] VÁZQUEZ-LÓPEZ, R., SOLANO-GÁLVEZ, S.G., JUÁREZ VIGNON-WHALEY, J.J., ABELLO VAAMONDE, J.A., PADRÓ ALONZO, L.A., RIVERA RESÉNDIZ, A., MULEIRO ÁLVAREZ, M., VEGA LÓPEZ, E.N., FRANYUTI-KELLY, G. & ÁLVAREZ-HERNÁNDEZ, D.A. (2020). Acinetobacter baumannii resistance: A real challenge for clinicians. *Antibiotics, 9*, pg. 205-220. https://doi.org/10.3390/antibiotics9040205

[11] GIACOMETTI, A., CIRIONI, O., GHISELLI, R., MOCCHEGIANI, F., ORLANDO, F., SILVESTRI, C., BOZZI, A., DI GIULIO, A., LUZI, C., MANGONI, M.L., BARRA, D., SABA, V., SCALISE, G. & RINALDI, A.C. (2006). Interaction of antimicrobial peptide Temporin L with lipopolysaccharide in vitro and in experimental rat models of septic shock caused by Gram-negative bacteria. *Antimicrobial Agents in Chemotherapy,* 50, (7), pg. 2478-2486. https://doi.org/10.1128/aac.01553-05

© University of Pretoria

[12] HELANDER, I. M., & MATTILA-SANDHOLM, T. (2000). Fluorometric assessment of Gram-negative bacterial permeabilisation. *Journal of Applied Microbiology*, 88 (2), pg. 213–219. https://doi.org/10.1046/j.1365-2672.2000.00971.x

[13] EPPS, D.E., WOLFE, M.L. & GROPPI, V. (1994). Characterization of the steady-state and dynamic fluorescence properties of the potential-sensitive dye bis-(1,3-dibutylbarbituric acid)trimethine oxonol (DiBAC4(3)) in model systems and cells. *Chemistry and Physics of Lipids*, 69 (2), pg.137-150. doi: 10.1016/0009-3084(94)90035-3.

[14] HARHALA, M., GEMBARA, K., MIERNIKIEWICZ, P., OWCZAREK, B., KAŹMIERCZAK, Z., MAJEWSKA, J., NELSON, D.C. & DĄBROWSKA, K. (2021). DNA dye Sytox Green in detection of bacteriolytic activity: High speed, precision and sensitivity demonstrated with dndolysins. *Frontiers in Microbiology*, 12, article 752282. doi: 10.3389/fmicb.2021.752282.

[15] MASLOVA, E., SHI, Y., SJÖBERG, F., AZEVEDO, H.S., WAREHAM, D.W. & MCCARTHY, R.R. (2020). An invertebrate burn wound model that recapitulates the hallmarks of burn trauma and infection seen in mammalian models. *Frontiers in Microbiology*, 11, article 998. doi: 10.3389/fmicb.2020.00998.

[16] ERSOY, S.C., HEITHOFF, D.M., BARNES, L., TRIPP, G.K., HOUSE, J.K., MARTH, J.D., SMITH, J.W. & MAHAN, M.J. (2017). Correcting a fundamental flaw in the paradigm for antimicrobial susceptibility testing. EBioMedicine, 20, pg. 173– 181. doi:10.1016/j.ebiom. 2017.05.026.

[17] MOHAPATRA, S.S., DWIBEDY, S.K & PADHY, I. (2021). Polymyxins, the last-resort antibiotics: Mode of action, resistance emergence, and potential solutions. Journal of Biosciences, 46 (3), article 85. doi:10.1007/s12038-021-00209-8

[18] TIWARI, K., SINGH, M., KUMAR, P. & MUKHOPADHYAY, K. (2022). Binding of cationic analogues of α-MSH to lipopolysaccharide and disruption of the cytoplasmic membranes caused bactericidal action against Escherichia coli. Scientific Reports, 12, article 1987. https://doi.org/10.1038/s41598-022-05684-z

[19] ZHANG, H.Q., SUN, C., XU, N. & LIU, W. (2024). The current landscape of the antimicrobial peptide melittin and its therapeutic potential. *Frontiers in Immunology*, 15, pg. 1664-3224. doi: 10.3389/fimmu.2024.1326033.

[20] ALMAAYTAH, A., ABUALHAIJAA, A., & ALQUDAH, O. (2019). The evaluation of the synergistic antimicrobial and antibiofilm activity of AamAP1-Lysine with conventional antibiotics against representative resistant strains of both Gram-positive and Gram-negative bacteria. *Infection and Drug Resistance*, 12, pg. 1371-1380.

[21] ALMAAYTAH, A., FARAJALLAH, A., ABUALHAIJAA, A., & AL-BALAS, Q. (2018). A3, a scorpion venom derived peptide analogue with potent antimicrobial and potential antibiofilm activity against clinical isolates of multidrug resistant Gram-positive bacteria. *Molecules*, 23 (7), pg. 1603-1621.

[22] ALMAAYTAH, A., TARAZI, S., ABU-ALHAIJAA, A., ALTALL, Y., ALSHAR'I, N., BODOOR, K. & AL-BALAS, Q. (2014). Enhanced antimicrobial activity of AamAP1-Lysine, a novel synthetic peptide analog derived from the scorpion venom peptide AamAP1. *Pharmaceuticals (Basel)*, 7, pg. 502-516.

[23] ALMAAYTAH, A., ZHOU, M., WANG, L., CHEN, T., WALKER, B., & SHAW, C. (2012). Antimicrobial/cytolytic peptides from the venom of the North African scorpion, Androctonus amoreuxi: biochemical and functional characterization of natural peptides and a single site-substituted analog. *Peptides,* 35, pg. 291-299.

© University of Pretoria

[24] SAINATH RAO, S., MOHAN, K.V. & ATREYA, C.D. (2013). A peptide derived from phage display library exhibits antibacterial activity against *E. coli* and *Pseudomonas aeruginosa*. *PLoS One*, 8 (2), article e56081. doi:10.1371/journal.pone.0056081

[25] JAŚKIEWICZ, M., NEUBAUER, D., KAZOR, K., BARTOSZEWSKA, S. & KAMYSZ, W. (2019). Antimicrobial activity of selected antimicrobial peptides against planktonic culture and biofilm of *Acinetobacter baumannii. Probiotics and Antimicrobial Proteins*, 11 (1), pg. 317-324. doi:10.1007/s12602-018-9444-5

[26] MANZO, G., HIND, C. K., FERGUSON, P. M., AMISON, R. T., HODGSON-CASSON, A. C., CIAZYNSKA, K. A., WELLER, B. J., CLARKE, M., LAM, C., MAN, R. C. H., O' Shaughnessy, B. G., CLIFFORD, M., BUI, T. T., DRAKE, A. F., ATKINSON, R. A., LAM, J. K. W., PITCHFORD, S. C., PAGE, C. P., PHOENIX, D. A., LORENZ, C. D., SUTTON, J. M., & MASON, A. J. (2020). A pleurocidin analogue with greater flexibility, enhanced antimicrobial potency and in vivo therapeutic efficacy. *Communications Biology*, 3 (697), pg. 1-16.

[27] BÖTTGER, R., HOFFMANN, R. & KNAPPE, D. (2017). Differential stability of therapeutic peptides with different proteolytic cleavage sites in blood, plasma and serum. *PLOS ONE,* 12 (6), article e0178943. https://doi.org/10.1371/journal.pone.0178943

[28] HYUN, K., JU HYE, J., SUN, C.K. & JU, H.C. (2014). *De novo* generation of short antimicrobial peptides with enhanced stability and cell specificity. *Journal of Antimicrobial Chemotherapy*, 69 (1), pg. 121–132, https://doi.org/10.1093/jac/dkt322

[29] DOLLE, A., NAGATI, V.B., HUNASHAL, Y., KRISHNAMURTHY, K., PASUPULATI, A.K., RAGHOTHAMA, S., & GOWD, K.H. (2019). Disulfide engineering on temporin-SHf: Stabilizing the bioactive conformation of an ultra-short antimicrobial peptide. *Chemical Biology & Drug Design*, 94 (3), pg. 1634–1646. https://doi.org/10.1111/cbdd.13525

[30] STARR, C.G., & WIMLEY, W.C. (2017). Antimicrobial peptides are degraded by the cytosolic proteases of human erythrocytes. *Biochimica et Biophysica Acta. Biomembranes*, 1859 (12), pg. 2319–2326. https://doi.org/10.1016/j.bbamem.2017.09.008

[31] WENDLER, J., SCHROEDER, B.O., EHMANN, D., *et al.* (2019). Proteolytic degradation of reduced human beta defensin 1 generates a novel antibiotic octapeptide. *Scientific Reports*, 9 (1), article 3640. doi:10.1038/s41598-019-40216-2

[32] SUN, X., SALIH, E., OPPENHEIM, F.G. & HELMERHORST, E.J. (2009). Kinetics of histatin proteolysis in whole saliva and the effect on bioactive domains with metal-binding, antifungal, and wound-healing properties. *The Journal of the Federation of the American Societies for Experimental Biology*, 23 (8), pg. 2691-2701. doi:10.1096/fj.09-131045

[33] TANG, W.H., WANG, C.F. & LIAO, Y.D. (2021). Fetal bovine serum albumin inhibits antimicrobial peptide activity and binds drug only in complex with α1-antitrypsin. *Scientific Reports*, 11, article 1267. https://doi.org/10.1038/s41598-020-80540-6

[34] RAETZ, C.R. & WHITFIELD, C. (2002). Lipopolysaccharide endotoxins. *Annual Review of Biochemistry*, 71, pg. 635–700. doi: 10.1146/annurev.biochem.71.110601.135414

[35] NOCERA, F.P., ATTILI, A.R. & DE MARTINO L. (2021). Acinetobacter baumannii: Its clinical significance in human and veterinary medicine. *Pathogens*. 10 (2), pg. 127-139. doi:10.3390/pathogens10020127

[36] MULLER, P.Y. & MILTON, M. (2012). The determination and interpretation of the therapeutic index in drug development. *Nature Reviews Drug Discovery*, 11 (10), pg. 751-761. doi: http://dx.doi.org/10.1038/nrd3801

© University of Pretoria

[37] BUTTRESS, J.A., HALTE, M., TE WINKEL, J.D., ERHARDT, M., POPP, P.F., & STRAHL, H. (2022). A guide for membrane potential measurements in Gram-negative bacteria using voltage-sensitive dyes. *Microbiology (Reading, England*), 168 (9), pg. 1-11. doi.org/10.1099/mic.0.001227

[38] CLARKE, M., HIND, C.K., FERGUSON, P.M., MANZO, G., MISTRY, B., YUE, B., ROMANOPULOS, J., CLIFFORD, M., BUI, T.T., DRAKE, A.F., LORENZ, C.D., SUTTON, J.M. & MASON, A.J. (2023). Synergy between Winter Flounder antimicrobial peptides. *Nature Partner Journals: Antimicrobials and Resistance*, 1, article 8. https://doi.org/10.1038/s44259-023-00010-7

[39] EISENBERG, D., WEISS, R.M., TERWILLIGER, T.C. & WILCOX, W. (1982). Hydrophobic moments and protein structure. *Faraday Symposium of the Chemical Society*, 17, pg. 109-120.

[40] LI, M., AZAD, M. A. K., THOMPSON, P. E., ROBERTS, K. D., VELKOV, T., ZHU, Y., & LI, J. (2023). Transcriptomic responses to polymyxin B and analogues in human kidney tubular cells. *Antibiotics*, 12 (2), pg. 415-431. https://doi.org/10.3390/antibiotics12020415

© University of Pretoria

CHAPTER 4:

Enhanced Gram-negative membrane disruption and *in vivo* antibacterial efficacy through lysine and arginine enrichment in the Opis16a sequence

Van der Walt, M., Oosthuizen, C.B., Serian, M., Lorenz, C.D., Mason, A.J., Bester, M.J. and Gaspar, A.R.M. (2024).

This chapter is in preparation for publication. **Van der Walt, M. (writing of article as first author, responsible for most of the experimental work and all data analysis),** Oosthuizen, C.B. (screening of peptides for antimicrobial activity, co-writer and editor), Serian, M. (writing and editing of MD analysis scripts, trouble-shooting MD simulations), Lorenz, C.D. (MD data interpretation and editing), Mason, A.J. (co-writer and editor, critical evaluation of the study and data interpretation), Bester, M.J. (co-supervisor of study, co-writer and editor, critical evaluation of the study and data analysis) and Gaspar, A.R.M. (study supervisor and communicating author, co-writer and editor, critical evaluation of the study and data analysis).

© University of Pretoria

4.1 Abstract

Wound infections are a major challenge in burn wound care, further complicated by the rise of antimicrobial resistance. Antimicrobial peptides (AMPs) are promising alternatives amid the escalating antibiotic resistance crisis, offering significant potential for advancing wound care, especially in combating persistent Gram-negative bacterial infections. Opis16a, an AMP derived from scorpion venom, exhibits potent antibacterial activity by interacting with various components of Gram-negative bacterial membranes, leading to rapid membrane disruption and bacterial cell death. Here we explore modification strategies that yield four novel Opis16a analogues with significantly improved membrane targeting and antibacterial efficacy, with Opis16aCterKtoR demonstrating particular promise for topical application in Gram-negative burn wound infections. Enhanced peptide–lipid hydrogen bonding contributes to increased conformational stability, improved membrane insertion and rapid membrane permeabilisation. Among the new analogues, Opis16aCterKtoR demonstrated the most consistent improvement in activity, exhibiting high selectivity for pathogens over epidermal HaCat cells and stability in physiological serum conditions. In an *in vivo Galleria mellonella* burn wound model, infected with a clinical strain of *Enterobacter cloacae* NICD 16103 this analogue was well tolerated at a topical dose of 5 mg/kg and proved more effective than the original Opis16a peptide. These findings underscore the promising therapeutic potential of bactericidal AMPs for burn wound care.

Keywords: Wound infections, antimicrobial resistance, antimicrobial peptides, Gram-negative bacteria, Opis16a, Opis16aCterKtoR, Arginine substitution, membrane permeabilisation, molecular dynamics, *E. cloacae*

Abbreviations: AMP, antimicrobial peptide; MIC, minimum inhibition concentration; MD, molecular dynamics; LC, lethal concentration; SI, selectivity index

© University of Pretoria

4.2 Introduction

The management and prevention of wound infections is a growing challenge, as treatment options become limited due to the development of antimicrobial resistance (AMR) among pathogens. A comprehensive study by Murray *et al.* [1] revealed that an estimated 4.95 million deaths in 2019 alone were associated with antimicrobial resistant bacterial infections. This issue is particularly acute in wound care, where, over the past decade, the leading cause of patient mortality has shifted from anoxic injuries to infections and sepsis[2].

Patients with burn wounds are particularly vulnerable to infection due to compromised skin barrier function and impaired immune responses[2]. A significant challenge in treating these infections is the predominance of Gram-negative bacterial pathogens, such as highly virulent and resistant *Enterobacter cloacae*[2], compounded by the polymicrobial nature of these infections[3]. Research conducted in Naval hospitals in Vietnam and Afghanistan found that more than 50% of severe extremity wounds harboured Gram-negative organisms[4]. Alarmingly, 20% of these wounded patients developed bacteremia caused by *Enterobacter spp*. within just five days of hospitalisation[4]. This rapid onset makes *Enterobacter spp*. the second most commonly isolated Gram-negative organism from polymicrobial war wounds[4].

The rise of multidrug-resistant Gram-negative infections in military settings mirrors trends observed in civilian hospitals, especially with the rise of carbapenem-resistant *Enterobacterales*. *E. cloacae*, in particular, has shown increasing resistance rates, complicating treatment options as it can develop β-lactam resistance even when initially susceptible[4]. The current guidelines for treating *E. cloacae* predominantly address bacteraemia related to other infections, often overlooking wound infections[4,5]. This oversight highlights a critical gap and emphasises the need for targeted strategies to combat the growing threat of *Enterobacter* infections in wound care.

In response to these challenges, antimicrobial peptides (AMPs) have been identified as promising alternatives to conventional antibiotics due to their broad-spectrum efficacy and rapid action. Research into the pharmacological potential of AMPs has yielded encouraging results, with peptides such as colistin, polymyxin B, gramicidin, vancomycin, bacitracin, and daptomycin already in clinical use against antibiotic-resistant bacterial infections[6,7]. However, a significant disparity exists in the availability of antimicrobials that target Gram-negative bacteria, including *E. cloacae,* compared to those aimed at Gram-positive bacteria which could be attributed to the complex and resistant nature of the Gram-negative outer membrane[8]. This challenge is particularly pressing in burn wound care, where infections often involve multiple Gram-negative pathogens. Untreated or mistreated infected wounds can complicate recovery, leading delayed healing, extended hospitalisations, increased healthcare costs, and higher mortality rates[2]. Therefore, this study aimed to discover and develop

© University of Pretoria

novel AMPs with enhanced efficacy against Gram-negative *E. cloacae*, as well as a broad range of activity against other Gram-negative pathogens.

In a previous study, Opis16a, derived from the venom of the African scorpion *Opistophthalmus carinatus*, was identified as a promising AMP due to its potent antibacterial activity, particularly against Gram-negative bacteria and minimal mammalian cell toxicity[9]. In an *in vivo* burn wound infection model, Opis16a effectively treated burn wounds of *Galleria mellonella* larvae infected with gentamicin-resistant *Acinetobacter baumannii* infection, achieving results comparable to polymyxin B[9]. The peptide's efficacy against Gram-negative bacteria such as *Escherichia coli* and *A. baumannii* is attributed to its ability to interact with and disrupt various layers of the bacterial membrane[9]. Specifically, by binding lipopolysaccharides, damaging the outer membrane, and subsequently disrupting the plasma membrane through depolarisation and permeabilisation[9].

To investigate its potential for broader applications, particularly in addressing the polymicrobial infections commonly encountered in wounds, Opis16a was screened against a wider panel of bacteria, including *E. cloacae*. Further, we hypothesised that the antibacterial efficacy of this peptide could be enhanced by rational design strategies aimed at amplifying its membrane disruption effects.

Four such strategies were evaluated. First, the substitution of Asp5 with positively charged Lys is explored (Opis16aDtoK), anticipating improved electrostatic interactions with the membrane and enhanced insertion. Then, the replacement of Lys2 and Lys5 with Arg at the N-terminal (Opis16aNterKtoR), Lys12 and Lys13 with Arg at the C-terminal (Opis16aCterKtoR), or the replacement of all five Lys residues (Lys2, Lys5, Lys8, Lys12, Lys13) with Arg (Opis16aAllKtoR) is investigated (Table 4.1).

These analogues were designed based on previous findings showing a strong correlation between the lipophilicity of polar residues like Lys or Arg and selective antibacterial activity[10]. The positive charge located at the end of the long side chains of these residues can enhance electrostatic attraction to pathogen membranes, while the lipophilic central regions of the side chain are thought to facilitate membrane insertion.

To evaluate whether the modifications enhanced and/or altered the peptide activity and bactericidal mechanisms of action, a range of time-resolved and steady-state biophysical methods were employed. *In vitro* toxicity against mammalian cells and antibacterial performance against a panel of laboratory reference strains and resistant clinical isolates of Gram-negative bacteria for the four analogues compared with the parent Opis16a, was assessed in mammalian cell culture or bacteriological media. Bacterial membrane permeabilisation was investigated with *E. cloacae* and compared with the biophysical results. The time-kill kinetics, as well as the serum and protease stability, of the most promising analogue were further assessed. Finally, the *in vivo* therapeutic efficacy of Opis16a was reevaluated in the *Galleria mellonella* burn wound infection model, this time

© University of Pretoria

targeting a clinical isolate of *E. cloacae* and comparing its effectiveness with that of the most promising analogue.

Table 4.1: *Peptide sequences and physicochemical properties of parent Opis16a, and its four analogues. Substitutions relative to Opis16a shown in bold and underlined.*

	Peptide	Rationale	Sequence	M (g/mol)	Length	Charge (pH 7)
	Opis16a*	Original	GKVWDWIKSTAKKLWN-NH_2	1978	16	+4
1	Opis16aDtoK	Asp5 to Lys5: Increased charge, therefore increased membrane insertion	GKVW**K**WIKSTAKKLWN-NH_2	1972	16	+6
2	Opis16aNterKtoR	N terminal Lys2 and Asp5 to Arg: Increased membrane interaction	G**R**VW**R**WIKSTAKKLWN-NH_2	2028	16	+6
3	Opis16aCterKtoR	Asp5 to Lys5 as above and C terminal Lys12 and 13 to Arg: Increased membrane interaction	GKVW**K**WIKSTA**RR**LWN-NH_2	2028	16	+6
4	Opis16aAllKtoR	Asp5 to Lys5 and all Lys to Arg: Increased membrane interaction	G**R**VW**R**WI**R**STA**RR**LWN-NH_2	2112	16	+6

*Van der Walt *et al.* (2024) [9,10]

4.3 Materials and methods

4.3.1 Materials

All peptides were obtained from GenScript (Rijswijk, Netherlands) in 1 mg aliquots at ≥95% purity.

4.3.2 Molecular dynamic simulations

Molecular dynamics simulations were conducted using the GROMACS 2021 software package[11] and the CHARMM36 all-atom force field[12]. First the initial structures of peptides were built using Avogadro (version 1.2.0)[13] and then inserted into a water box with neutralising ions using CHARMM-GUI Solution Builder[14]. Energy minimisation was carried out using the steepest descent algorithm until the maximum force is less than 1000.0 kJ/mol/nm (~5000 steps). Equilibration was carried out using the canonical NVT ensemble (fixed number of simulated particles (N), simulation cell volume (V) and temperature (T)) at 303.15 K with the Nose-Hoover thermostat for 125 ps with position restraints on the peptides. Hydrogen-containing bond angles were constrained with the LINCS algorithm. The peptide in water box simulations were run in the NPT ensemble for 1 μs using 2-fs intervals, with trajectories recorded every 2 ps. The final configurations of the peptides from these simulations were then inserted above representative model Gram-negative bacterial membranes.

The representative Gram-negative bacterial membrane contained a total of 256 lipids, composed of POPE/POPG (3:1) lipids. Membranes were built using the CHARMM-GUI Membrane Builder[15]. For each run four peptides were inserted at least 8 Å above the lipid bilayer in a random position and orientation, at least 20 Å apart. The system was solvated with CHARMM-modified TIP3P[16] water

© University of Pretoria

and NaCl was added to neutralise. Energy minimisation was carried out using the steepest descent algorithm until the maximum force is less than 1000.0 kJ/ml/nm (~3000–4000 steps). Equilibration was carried out using the canonical (NVT) and isothermal-isobaric (NPT) ensembles at 300 K with the Berendsen thermostat for 500 ps with position restraints on the peptides. Hydrogen-containing bond angles were constrained with the LINCS algorithm. Final simulations were run in the NVT and NPT ensemble using Nose-Hoover and Parrinello-Rahman with 2-fs intervals and trajectories recorded every 2 ps. Simulations were run for a total of 200 ns each and repeated twice, with peptides inserted at different positions and orientations.

Membrane interaction via hydrogen bonding: To better elucidate the degree of initial interaction between the peptides and the Gram-negative model membrane, the number of hydrogen bonds between each residue and the membrane was calculated. The MDAnalysis software package [17,18] was used to identify the presence of hydrogen bonds by measuring the distance and bond-angle between possible hydrogen bond donors and acceptors. The number of hydrogen bonds and the variation thereof was determined for each residue that interacts with the Gram-negative bacterial model membrane.

Membrane binding and insertion: Membrane insertion was determined by calculating the distance between the *z*-position of the peptide α-carbons (CA) relative to the average *z*-position of the phosphate groups in the upper leaflet of the lipid bilayer. The relative *z*-position of each peptide was determined for the entire duration of the simulation and averaged across four copies.

Dihedral angle and circular variance calculations: Dihedral angles are circular quantities and the circular mean of the psi and phi angles for each residue was calculated as described in Manzo *et al.* 2019[19].

4.3.3 Circular dichroism spectroscopy

The secondary structures of the peptides (50 μM) were determined using far-UV CD spectra in Tris buffer (5 mM, pH 7.4, Melford Laboratories, Suffolk, UK), SDS micelles (50 mM in 5 mM Tris, pH 7.4, Melford Laboratories, Suffolk, UK) and in the presence of small unilamellar vesicles (SUVs) using a Jasco J-815 spectropolarimeter equipped with a PTC-423S Peltier temperature controller. The SUVs consisted of lipids, 1-palmitoyl-2-oleoyl-sn-glycero-3-phospho-(1′-rac-glycerol) (POPG) and 1-palmitoyl-2-oleoyl-sn-glycero-3-phosphoethanolamine (POPE) purchased from Avanti Polar Lipids, Inc. (Alabaster, AL) and were used without further purification. The lipid powders were solubilised using chloroform and dried under rotor-evaporation. The lipid films were left under vacuum overnight to completely remove the organic solvent, and then hydrated with 5 mM Tris buffer (pH 7.4). For further sample homogenisation, the lipid suspensions were subjected to five rapid freeze–thaw cycles. POPE/POPG (75:25, mol:mol) SUVs were formed by 2 × 5 min sonication with

© University of Pretoria

an amplitude of six microns, held cold with ice to avoid lipid degradation. The SUVs were stored at 4 °C for no longer than five days.

CD spectra between 260 to 180 nm were obtained, at a constant temperature of 296.15 K, a step size of 1 nm, a bandwidth of 2 nm, and a pathlength of 2 mm. The POPE/POPG SUV suspensions (5 mM) were used to dissolve the peptides to have a final concentration of 50 µM peptide. These experimental conditions were also used to determine peptide secondary structure in Tris (5 mM) and SDS micelles (50 mM). A spectrum of Tris solution, SDS solution or lipid suspension without peptide was subtracted during data processing. Peptide structures were identified by examining the CD spectra and mean residue molar ellipticities (MRME, [θ], deg.cm^2.dmol^{-1}).

4.3.4 Antibacterial activity against a panel of standard laboratory strains and clinical isolates

Antimicrobial activity was assessed against a panel of Gram-negative bacteria maintained by H3D, University of Cape Town, consisting of six laboratory reference strains and two clinical isolates. Briefly, bacterial colonies from an LB agar plate were picked and cultured in cation-adjusted Mueller Hinton broth (MHB) at 37°C with 180 rpm shaking, overnight. Cultures were back diluted to reach a starting optical density at 600 nm (OD_{600}) of 0.1 and then diluted 100-fold to an inoculum of approximately 1 x 10^6 CFU/mL.

The peptides were serially diluted in media across polypropylene 96-well plates, concentrations ranging from 0.125 to 64 µg/mL. Inoculum was added at a 1:1 ratio to give a cell density of ~5 x 10^5 CFU/mL. Gentamicin, polymyxin B, ciprofloxacin, meropenem and melittin at a concentration range of 0.063 to 32 µg/mL, were used in the antibiogram (Suppl. Table S2). Plates were incubated at 37°C for 20 h and the OD_{600} determined. Minimum inhibition concentrations (MICs) were determined from a minimum of three biological repeats. The MIC is defined as the lowest peptide concentration that resulted in pathogen growth of less than 0.1 above the background absorbance.

4.3.5 In vitro cytotoxicity screening against epidermal HaCat cells

The HaCat (Cellonex, South Africa) cell line was cultured in Dulbecco's Modified Eagle medium (DMEM, Sigma-Aldrich, St. Louis, USA) supplemented with 10% heat-inactivated FCS (Capricorn Scientific, Ebsdorfergrund, Germany) and 1% antibiotic-antimycotic (Abs, PAN Biotech, Aidenbach, Germany) and maintained at 5–10% CO_2, 37°C, 95% humidity.

For toxicity screening, 5.56 x 10^4 HaCat cells/mL were plated in a 96-well plate and incubated for 24 h. Thereafter the cells were exposed to serial dilutions of peptide from 512 to 1 µg/mL (256 to 0.5 µM) or 0.1% Triton-X-100 and incubated for 21 h. Cell viability was determined by adding 10% 3-(4,5-dimethyl-2-thiazolyl)-2,5-diphenyl-2H-tetrazolium bromide (MTT) (1 mg/mL), to each well for an additional 3 h. After incubation the media was discarded, and the formazan crystals dissolved by adding 25% DMSO in ethanol. The OD_{570} was measured, and the percentage cell viability calculated

© University of Pretoria

relative to the untreated control. The LC_{50} is the concentration of AMP treatment that results in 50% HaCat cell death.

Selectivity towards the various bacterial species was determined using the selectivity index (SI). The SI of each peptide was calculated as the ratio of the concentration required to cause 50% cytotoxicity in HaCat cells (LC_{50}) to the MIC per bacterial species. A higher SI value indicates greater selectivity of the peptides towards specific bacteria over mammalian cells.

4.3.6 Cytoplasmic membrane permeabilisation

The ability of the AMPs to permeabilise Gram-negative bacterial cytoplasmic membranes was assessed with the SYTOX Green assay (ThermoScientific, Massachusetts, USA). Briefly, bacterial cultures with an OD_{600} of 0.1 were diluted 5-fold in phosphate buffered saline (PBS), before SYTOX Green (10 µM) was added at a 1:1 ratio. The suspension was transferred to a black polypropylene 96-well plate containing the respective peptides to reach final concentrations of 0.5x, 1x and 2x the MIC. Melittin, at a final concentration of 11 µg/mL (4 µM), was used as positive control. The increase in fluorescence at 37°C was measured every 2 min for 120 min at excitation/emission wavelengths of 485/535 nm.

4.3.7 Time-kill kinetics

The concentration- and time-dependent killing capability of parent Opis16a and the most promising analogue Opis16aCterKtoR was determined against the resistant clinical isolate *E. cloacae* NICD 16103 using a time-kill kinetics assay. A bacterial inoculum with an OD_{600} of 0.1 was diluted 100-fold to reach 1 x 10^6 CFU/mL as described above. Killing kinetics were evaluated at 0.5x, 1x and 2x the MIC. Bacterial suspensions were added at a 1:1 ratio and incubated at 37°C. Samples were collected aseptically, at timepoints of 0, 5, 10, 15, 30, 45, 60, 90, 120, and 1200 min, each 10-fold serially diluted in sterile ddH_2O and plated on LB agar for colony counting.

4.3.8 Opis16aCterKtoR activity in the presence of trypsin and serum

The susceptibility of Opis16aCterKtoR to proteolytic degradation or the binding with serum proteins was evaluated *in vitro* using trypsin (Merck, Modderfontein, SA) or FCS. To evaluate trypsin stability, Opis16aCterKtoR was serially diluted in a trypsin solution (pancreas protease) to reach a final concentration range of 0.125 to 64 µg/mL (0.064–32.67 µM) peptide to 0.15 U/mL trypsin (pH 7.4). Samples were incubated for 1 h at 37°C. Peptide alone and protease alone were used as controls. After incubation the samples were heated at 60°C for 20 min for protease inactivation.

A similar strategy was followed to determine whether FCS affects the antimicrobial activity of Opis16aCterKtoR due to possible serum protein binding. Serial dilutions of Opis16aCterKtoR in a 20% FCS solution were incubated for 1 h at 37°C. Peptide alone and FCS alone were used as controls. After Opis16aCterKtoR incubation with trypsin or FCS, the procedure described above for determining antimicrobial activity was followed whereby an equal volume of peptide and bacteria

© University of Pretoria

was added to 96-well plates and incubated for 20 h at 37°C. The MIC of Opis16aCterKtoR pretreated with trypsin or preincubated with FCS was compared with peptide alone.

4.3.9 In vivo antibacterial activity of Opis16aCterKtoR in a G. mellonella burn wound model

The protection afforded by Opis16aCterKtoR against *E. cloacae* NICD 16103 infection in burn wounds was evaluated using G. *mellonella* larvae and compared with that of Opis16a. The larvae were sourced from and maintained by the FABI Biocontrol Centre and Nursery at the University of Pretoria. A similar procedure as used by Clarke *et al.* and first introduced by Maslova *et al.*, was followed [20,21]. All assays were performed on three separate occasions using a group size of 10 larvae. Prior to the experiment, *G. mellonella* larvae with similar size and weight (200-300 mg) were surface decontaminated using a cotton swab immersed in 70% ethanol. Burn wounds were induced by heating the flat head of a nail in a blue Bunsen burner flame until red hot, cooled for 12 s, and then superficially applying it for 2 s to create a 2-mm^2 burn. The burn sites were then infected with 2-3 colonies of *E. cloacae* NICD 16103 from a fresh agar plate using an inoculating loop to topically spread the bacteria over the burn wound. Uninfected controls were treated with sterile PBS. Opis16a or Opis16aCterKtoR at 5 or 10 mg/kg in 5 µL was topically applied to the wound 1 h after infection. Each group of larvae was housed in separate Petri dishes within a static incubator at 37°C during the duration of the experiment. Survival was monitored every 24 h over a period of 120 h. Changes in *G. mellonella* survival were analysed by the log rank (Mantel-Cox) method and plotted as Kaplan-Meier survival curves.

4.3.10 Activity data and statistical analysis

Triplicate dose response assays with three technical repeats each were performed against the target pathogens. Data analyses for all *in vitro* assays were performed using GraphPad Prism® V 7.0 software (San Diego, CA, USA). Statistical analyses were performed by determining Row totals/means with standard deviation (SD) or standard error of the mean (SEM) followed by One-way analysis of variance (ANOVA) with Dunnett's multiple/selected comparison post-test. Final MD simulation trajectories were analysed with various internal scripts written in Python and Bash using MDAnalysis[17,18] or GROMACS[11] analysis modules.

© University of Pretoria

4.4 Results

4.4.1 Opis16a analogues have increased hydrogen bonding with lipids

In peptide therapeutic development it is important to consider overall peptide charge as this will have a significant impact on the interaction with anionic pathogenic membranes. Here we investigated the impact an anionic to cationic substitution in the primary sequence of Opis16a has on model bacterial membrane binding and insertion, as well as compare the membrane interactions of peptides with Lys to Arg substitutions at an atomistic level using MD simulations. Mixed zwitterionic-anionic bilayers represent the plasma membrane of Gram-negative bacteria.

In contrast to aspartate, Lys and Arg are basic residues with high pKa values enabling them to carry a positive charge and form strong electrostatic interactions with anionic bacterial membranes[22]. This initial electrostatic pull between Lys or Arg residues and the anionic membrane lipid headgroups attracts the peptide toward the membrane promoting the formation of hydrogen bonds[22]. An increase in hydrogen bonding between the analogues and Gram-negative membranes is observed compared with Opis16a (Fig. 4.1, Suppl. Fig. 4.1). This is particularly evident when comparing the hydrogen bond formation of Opis16aDtoK (Fig. 4.1 B) with that of parent peptide Opis16a (Fig. 4.1 A). Lys5 makes a subtle contribution of over 100 hydrogen bonds on average where under 100 are observed for Asp5 in the parent peptide (Suppl. Fig. 4.1 A & B). The substitution also improves the hydrogen bonding of the other Lys residues within the sequence (Fig. 4.1 B). Consequently, Opis16aDtoK exhibits a slight increase in overall hydrogen bonding compared with Opis16a (Fig. 4.1 F).

An additional increase in total number of hydrogen bonds is observed when two Lys residues in the N-terminus or the C-terminus of Opis16aDtoK are replaced with Arg to form Opis16aNterKtoR or Opis16aCterKtoR, respectively (Fig. 4.1 C). Although similar in charge, Lys and Arg differ in chemical properties as Lys sidechains contain a primary amine group, whereas Arg sidechains contain a guanidinium group. As a result, Arg has more hydrogen donor atoms (five donor atoms per Arg, three donor atoms per Lys) and is believed to form more intermolecular hydrogen bonds than Lys[22]. Arg2 and Arg5 on the N-terminus of Opis16aNterKtoR more than double the amount of hydrogen bonding compared with Lys2 and Lys5 of Opis16aDtoK (Suppl. Fig. 4.1 C). This also leads to an increase in hydrogen bonding for Trp4 and Trp15 (Fig. 4.1 C). Similarly, an increase is also observed for Arg12 and Arg13 of Opis16aCterKtoR, that form an average of over 300 hydrogen bonds each, compared with around 100 hydrogen bonds for the C-terminal Lys residues of Opis16a and Opis16aDtoK (Fig. 4.1 D & Suppl. Fig. 4.1 D). Both these peptides, with Opis16aNterKtoR slightly surpassing Opis16aCterKtoR, exhibit a notable increase in the overall extent of hydrogen bonding compared to Opis16a and Opis16aDtoK (Fig. 4.1 F).

© University of Pretoria

Substituting all the Lys residues with Arg to form Opis16aAllKtoR results in the most substantial increase in number of hydrogen bonds which form across the length of the sequence rather than just at the termini (Fig. 4.1 E & F). The sequential enhancement in overall hydrogen bonding, highlights the importance of cationic residues, specifically Arg, in forming interactions with anionic bacterial membranes.

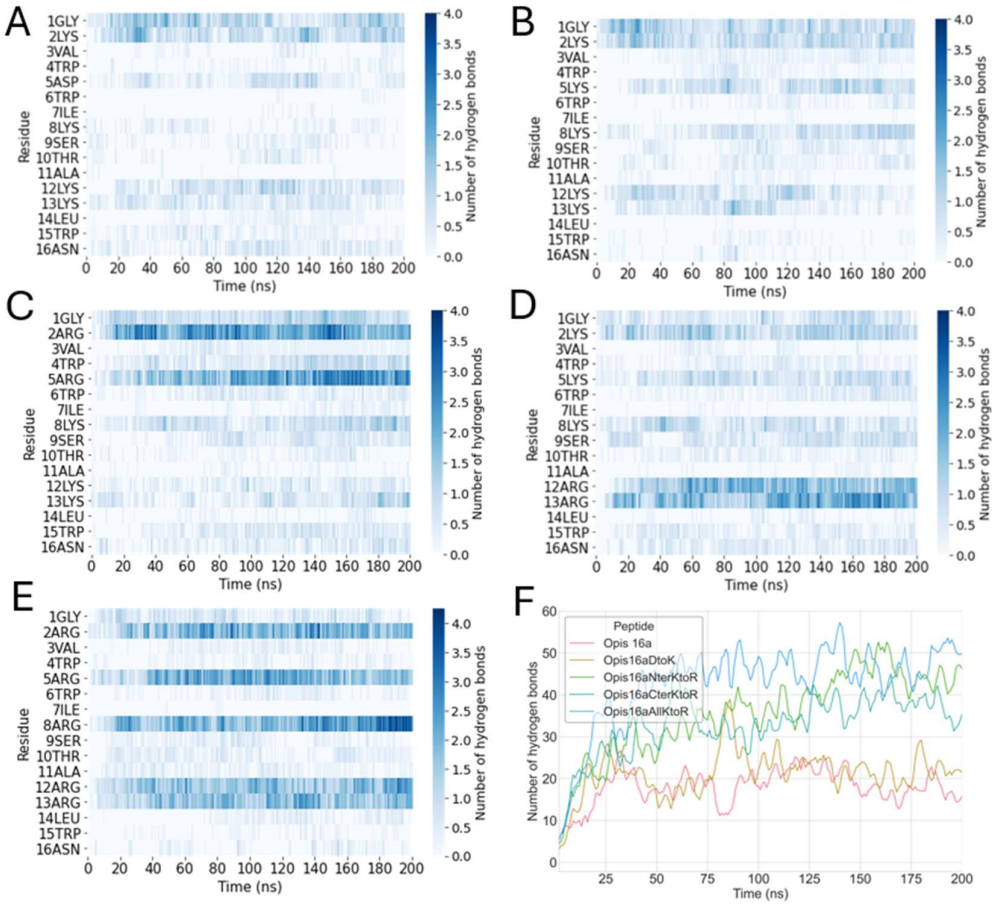


Figure 4.1: Hydrogen bonding between peptide and PEPG model lipids differ among Opis16a analogues and is driven by cationic residues. *Total* ***(F)*** *and residue specific peptide-membrane hydrogen bonds are shown as a function of time for Opis16a* ***(A, red)****, Opis16aDtoK* ***(B, orange)****, Opis16aNterKtoR* ***(C, lime green)****, Opis16aCterKtoR* ***(D, dark green)*** *and Opis16aAllKtoR* ***(F, blue)*** *in representative simulations of Gram-negative model membranes.*

4.4.2 Decreased conformational flexibility of the Opis16a analogues in model Gram-negative membranes

The impact of the four modification strategies on the conformational integrity of Opis16a was assessed through steady-state conformational analysis using CD spectroscopy and biophysical MD simulations. The CD spectrum obtained for Opis16a is consistent with previous work[9]. In both SDS micelles and PEPG liposomes, the spectra of the parent peptide and all four analogues are predominantly characteristic of α-helix conformation (Suppl. Fig. 4.2 & Table S4.3)[31]. However, the characteristic negative bands (208 and 222 nm) are less intense for Opis16a in PEPG, possibly indicating a slightly less ordered structure.

© University of Pretoria

To obtain molecular level insights into the initial secondary structure and conformational flexibility of the AMPs during the first few nanoseconds of membrane interaction, MD simulations were conducted. Here, the average psi and phi dihedral angles that each AMP adopts upon interaction with a Gram-negative bacterial PEPG model membrane were plotted on Ramachandran contour plots (Fig. 4.2). Alongside the secondary structures, the conformational flexibilities of the peptides were evaluated by determining the circular variance of the psi dihedral angles of each residue and examining changes in flexibility over time (Fig. 4.3 & Fig 4.4).

MD shows that there are notable differences in the conformational behaviour of the parent peptide compared with the four analogues (Fig. 4.2). Opis16a primarily adopts an extended conformation, dominated by polyproline II (φ -75°, ψ 140°), with some contribution from β-sheet (φ -135°, ψ 135°), while Trp6 participates in a type I β-turn in the middle of the sequence (φ -90°, ψ 10°) (Fig. 4.2. B & C). The peptide exhibits moderate circular variance around psi which is sensitive to conformational flexibility in Gram-negative membrane mimicking environments (Fig. 4.3 A & Fig 4.4 A).

Substitution of Asp5 with Lys5 in Opis16aDtoK results in a loss of the turn at Trp6 (Fig. 4.2 D) and a reduction in conformational flexibility at this position (Fig. 4.3 B). While most residues continue to adopt the extended conformation similar to Opis16a, the introduction of Lys5, along with the existing Lys13, induces turns in the structure (Fig. 4.2 D-F), resulting in an overall increase in conformational flexibility over time (Fig. 4.4 B). The deviation of these residues may indicate potential interaction sites with the membrane, as evidenced by the increase in hydrogen bonds shown for these residues in Fig. 4.1 and S4.1.

Opis16aNterKtoR exhibits a comparable conformation to Opis16aDtoK, characterised by the loss of the turn at Trp6 and the presence of an extended polyproline II structure adopted by most residues. The dihedral angles reveal two turns in this analogue, induced by Arg5 and Lys12. This suggests that replacing the anionic residue at position 5 with a cationic Lys or Arg significantly impacts the peptide structure, promoting turn formation in both analogues. In Opis16aNterKtoR, Arg5 induces a turn in the N-terminal region, which is absent in Opis16aDtoK, while Lys12 facilitates a turn in the C-terminal region, similar to that seen in Opis16aDtoK. Additionally, Opis16aNterKtoR displays reduced circular variance at the N-terminus compared to Opis16a, while showing increased flexibility around the C-terminus (Fig. 4.3 C). This may be due to stronger interactions between the Arg residues in the N-terminus and the bacterial membrane, which constrain movement in this region. In contrast, the Asp and Lys residues in the N-terminus of Opis16a and Opis16aDtoK exhibit weaker membrane interactions, resulting in greater flexibility (Fig. 4.2 G & H).

Opis16aCterKtoR exhibits the most notable change in conformation compared to Opis16a with Lys5 inducing a turn similar to Arg5 of Opis16aNterKtoR. Additionally, the sequential residues Ser9 to Ala11 demonstrate a preference for right-handed α-helix, with phi angles between -90° to -60° and psi angles from -30° to 0° (Fig. 4.2 J-L). This increase in structural order, along with the greater number of

© University of Pretoria

intermolecular hydrogen bonds with the membrane (Fig. 4.1), is consistent with the observation that this peptide exhibits the lowest overall conformational flexibility over time (Fig. 4.3 D & E).

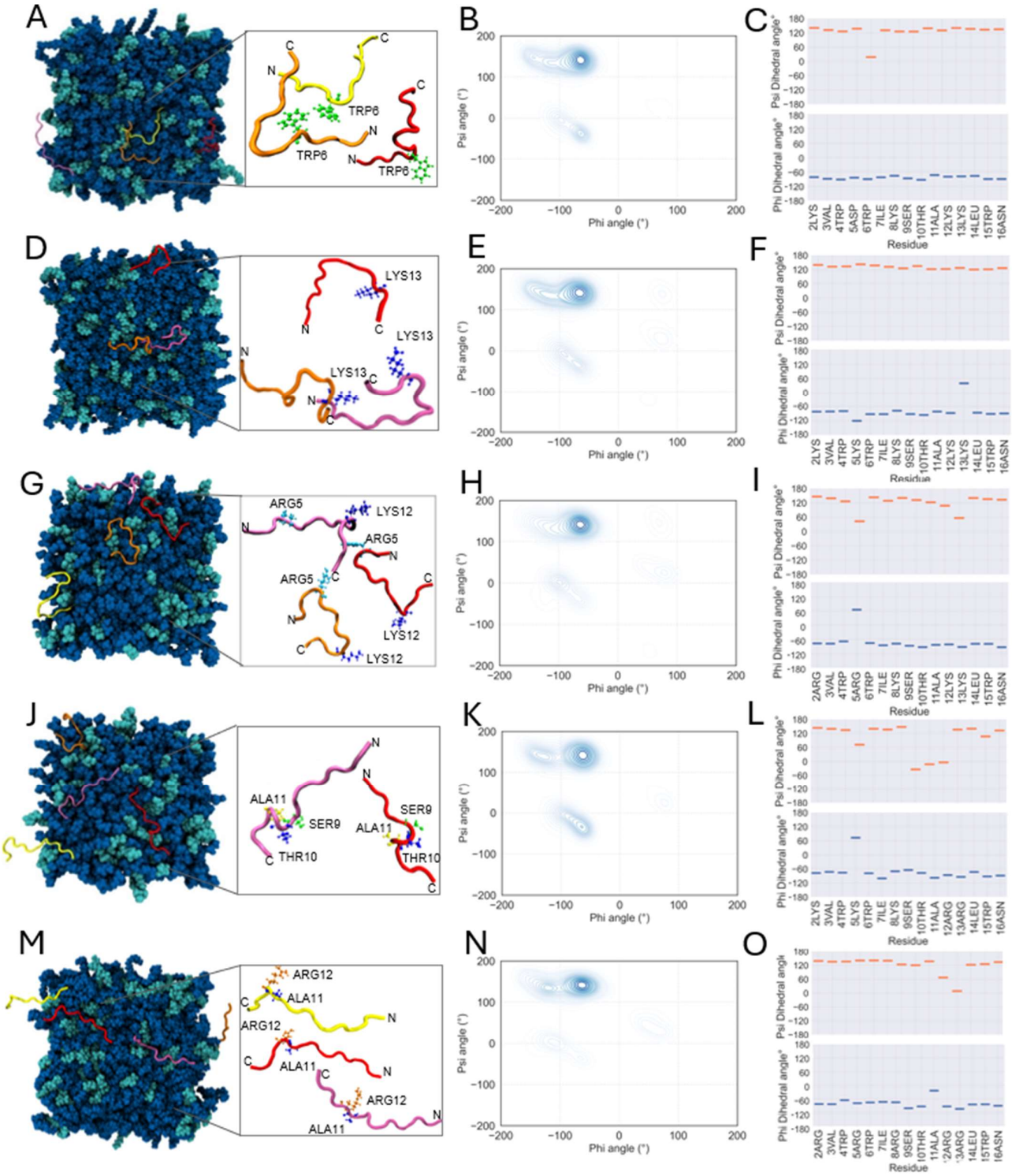


Figure 4.2: Secondary structure analysis of Opis16a and analogues in representative Gram-negative membranes. *Top view snapshots showing the conformation of each of four peptide monomers* ***(A, D, G, J, M)*** *binding to PEPG bilayers in silico. Ramachandran contour plots show the average dihedral angle concentration during the last 20 ns of the simulations* ***(B, E, H, K, N)****. Psi and phi dihedral angles are shown for each residue, averaged over 200 ns of simulation and four peptides* ***(C, F, I, L, O)****. Data are shown for Opis16a* ***(A–C)****, Opis16aDtoK* ***(D–F)****, Opis16aNterKtoR* ***(G-I)****, Opis16aCterKtoR* ***(J-L)*** *and Opis16aAllKtoR* ***(M-O)****.*

© University of Pretoria

Last, Opis16aAllKtoR predominantly adopts the extended conformation, similar to the other peptides however, sequential residues 11 and 12 introduce a kink in the structure. The absence of steric hindrance from Ala11 allows Arg12 to favour a type I β-turn conformation (φi 0°, ψi 60°; φi+1 -90°, ψi+1 0°) (Fig. 4.2 M-O). Overall, the peptide shows limited conformational flexibility over time (Fig. 4.4 D & E), likely due to increased intermolecular hydrogen bonding with the bacterial membrane, as observed for this analogue in Fig. 4.1.

Unlike CD, which reports on the average conformation adopted after 10s of seconds or several minutes, MD simulations are limited to initial binding events that happen within nanoseconds and provide residue specific information. Indeed, the MD simulations reveal that the initial interaction with a Gram-negative membrane induces subtle structural changes in certain residues within the analogue sequences, which was undetected by CD due to timescale differences. Specifically, the replacement of the anionic residue at position 5 with a cationic residue results in the loss of a type I β-turn at position 6, while facilitating the formation of additional type I β-turns in the N-terminal, C-terminal, or both around positions 5, 12, and 13. This effect may arise as the cationic residues in these positions serve as sites of membrane interaction, as shown in Fig. 4.1, disrupting the extended conformation to form turns. Notably, the peptide Opis16aCterKtoR, which features Lys residues in the N-terminus and Arg residues in the C-terminus, demonstrates the most ordered structural formation and the lowest conformational flexibility. This is attributed to the Lys residues interacting with the membrane, while the Arg residues promote α-helix formation.

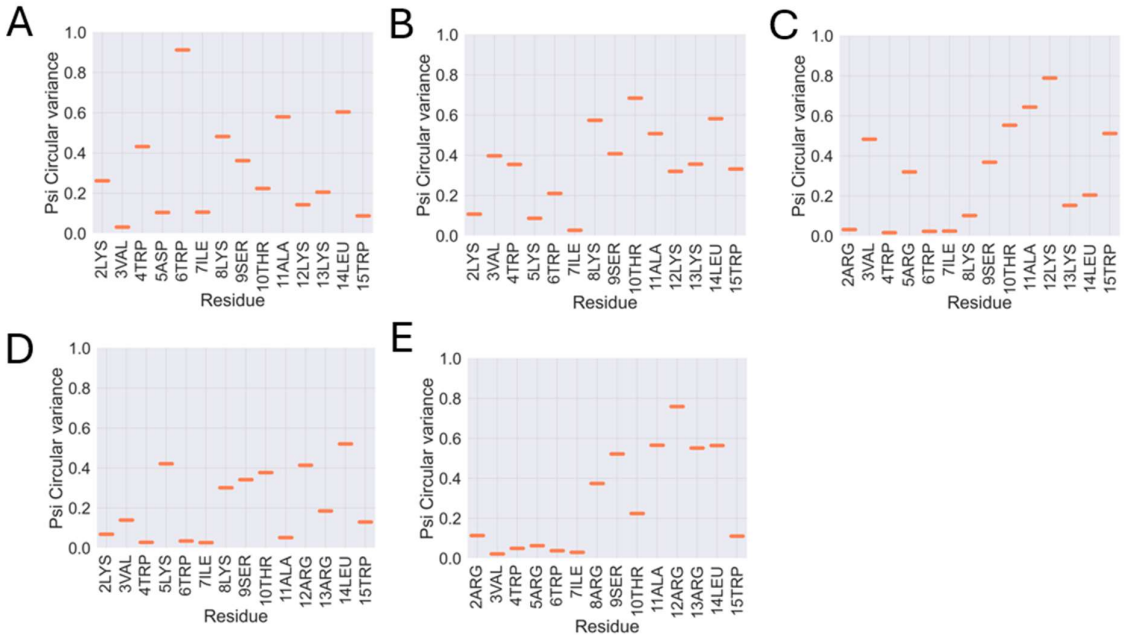


Figure 4.3: Average conformational flexibility of Opis16a and analogues in representative Gram-negative membranes. *Circular variance of the psi dihedral angles for each residue, averaged over 200 ns of simulation and four peptides. This is a measure of conformational flexibility and indicate the amount of variance (low = rigid, high = flexible) within the dihedral angles of each residue. Data are shown for Opis16a* ***(A)****, Opis16aDtoK* ***(B)****, Opis16aNterKtoR* ***(C)****, Opis16aCterKtoR* ***(D)*** *and Opis16aAllKtoR* ***(E)****.*

© University of Pretoria

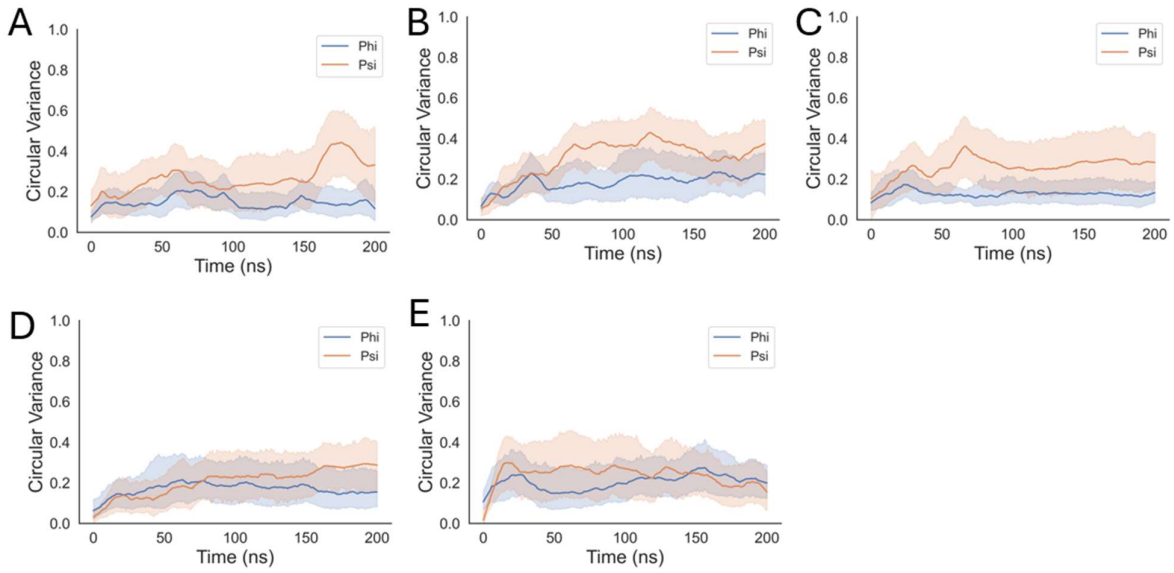


Figure 4.4: Change in conformational flexibility of Opis16a and analogues over time in representative Gram-negative membranes. *Change in circular variance of psi and phi dihedral angles over time averaged for four peptides. Data are shown for Opis16a* ***(A)****, Opis16aDtoK* ***(B)****, Opis16aNterKtoR* ***(C)****, Opis16aCterKtoR* ***(D)*** *and Opis16aAllKtoR* ***(E)****.*

4.4.3 Opis16a analogues offer improved antibacterial potency

The evident increase in hydrogen bonding and variation in secondary structure observed for the Opis16a analogues upon interaction with model bacterial bilayers, suggests altered antibacterial activity. The potency of the analogues was compared to that of the parent peptide in an *in vitro* assessment performed against a panel of Gram-negative bacteria (Table 4.2). Two of the eight bacterial strains in this panel are clinical isolates with *A. baumannii* NICD 15283 being multidrug-resistant to amikacin, gentamicin, meropenem, imipenem, tetracycline, tobramycin and borderline resistant to ciprofloxacin and *E. cloacae* NICD 16103 being multidrug resistant to sulbactam, ciprofloxacin, gentamicin, meropenem, imipenem, tetracycline and tobramycin (Suppl. Table S4.1). In addition, laboratory strains such as *A. baumannii* ATCC 19606 and *Klebsiella pneumoniae* ATCC BAA-1705 were included in this panel, both exhibiting resistance to gentamicin, while *A. baumannii* ATCC 19606 also demonstrate borderline resistance to ciprofloxacin (Suppl. Table S4.2). Susceptible strains, including *E. coli* ATCC 25922 and 700928, *Pseudomonas aeruginosa* PAO1, and *E. cloacae* ATCC 700323, were also included to ensure a comprehensive evaluation of the efficacy of the peptides across a broad spectrum of bacteria. (Suppl. Table S4.1).

Opis16a and all four analogues are effective against the entire panel, including the drug-resistant strains (Table 4.2). In addition to its previously reported activity against *E. coli* and *A. baumannii* [9], Opis16a also shows broad-spectrum activity against *P. aeruginosa, K. pneumoniae* and *E. cloacae.* Most notably,

© University of Pretoria

Opis16a is also effective against the multidrug-resistant *E. cloacae* NICD 16103 demonstrating a lower MIC than gentamicin and comparable efficacy to meropenem.

The four analogues show a substantial improvement in antibacterial potency compared to Opis16a across most strains (Table 4.2). The single substitution of Asp5 to Lys5 significantly enhances activity against *E. coli*, *K. pneumoniae*, and *E. cloacae,* achieving up to an 8-fold increase in effectiveness and an overall reduced MIC of 16 µg/mL or less. Replacing Lys with Arg residues yields similar or slightly greater enhancements in activity for the three Arg-containing analogues compared with Opis16aDtoK, resulting in up to a 16-fold improvement.

While the peptides exhibit similar antibacterial potency against most strains, Opis16aCterKtoR consistently slightly outperforms Opis16aDtoK and Opis16aNterKtoR. Although there is no significant difference in potency between Opis16aCterKtoR and Opis16aAllKtoR, among all the analogues Opis16aCterKtoR shows the most notable improvement in activity against *K. pneumoniae* ATCC BAA-1705, with an MIC of 8 µg/mL. This peptide, along with Opis16aAllKtoR, also exhibit enhanced effectiveness against both the laboratory *E. cloacae* ATCC 700323 and the resistant clinical *E. cloacae* NICD 161032 isolate (Table 4.2). With an MIC of 4 µg/mL against the multidrug-resistant clinical isolate *E. cloacae* NICD 161032, these two peptides demonstrate superior activity compared to all tested antibiotics, including ciprofloxacin, melittin, gentamicin, and meropenem (Suppl. Table S4.2).

Table 4.2: *Antibacterial activity of four Opis16a analogues against Gram-negative bacterial strains*

Isolate	Modal MICs in µg/mL (fold improvement)									
	Opis16a*	Opis16aDtoK		Opis16aNterKtoR		Opis16aCterKtoR		Opis16aAllKtoR	
Gram-negative									
E. coli ATCC 25922	64	**16**	**(4x)**	**8**	**(8x)**	**8**	**(8x)**	**8**	**(8x)**
E. coli ATCC 700928	4	8/4	(0.5/1x)	4	(1x)	4	(1x)	4	(1x)
P. aeruginosa PAO1	8	8	(1x)	4	(2x)	4	(2x)	4	(2x)
A. baumannii ATCC 19606	8	8	**(1x)**	4	(2x)	4	(2x)	4	(2x)
A. baumannii NICD 15283 (C)	8	8	(1x)	8	(1x)	8	(1x)	8	(1x)
K. pneumoniae ATCC BAA-1705	128	**16**	**(8x)**	**16**	**(8x)**	**8**	**(16x)**	**16**	**(8x)**
E. cloacae ATCC 700323	64	**16**	**(4x)**	**16**	**(4x)**	**8**	**(8x)**	**8**	**(8x)**
E. cloacae NICD 16103 (C)	16	8	(2x)	8	(2x)	**4**	**(4x)**	**4**	**(4x)**

* *Activity data obtained from* Van der Walt *et al.* (2024) [9] (C) Clinical isolate. Bold values indicate a significant improvement in potency over Opis16a with a factor of 4 or more.

© University of Pretoria

4.4.4 An increase in bacterial selectivity highlights the potential of the Opis16a analogues

A previous paper on Opis16a reported LC_{50} values of 311 µg/mL and 118.2 µg/mL towards mammalian keratinocyte HaCat and hepatoblastoma HepG2 cells, respectively [9,10]. Although these LC_{50} values are similar to some of the effective antibacterial concentrations, Opis16a still exhibits high selectivity towards *E. coli* ATCC 700928, *P. aeruginosa* PAO1, both *A. baumannii* strains as well as the resistant clinical *E. cloacae* NICD 16103 strain, for which it showed low MICs.

The increase in activity observed for the analogues is paralleled by an increase in mammalian cytotoxicity. HaCat toxicity has nearly doubled, with LC_{50} values ranging from 131.4 to 180.8 µg/mL (Table 4.3). Although toxicity is observed, two-way ANOVA analysis shows that Opis16aCterKtoR is significantly less toxic than Opis16aDtoK ($p<0.05$), Opis16aNterKtoR ($p<0.05$) and Opis16aAllKtoR ($p<0.01$). Moreover, the enhanced antibacterial activity of the analogues compared with Opis16a has led to an overall improvement in selectivity for bacteria over HaCat cells.

Similar to Opis16a, Opis16aDtoK retains selectivity for five out of eight bacterial strains (Table 4.3). However, the more active Arg-containing peptides—Opis16aNterKtoR, Opis16aCterKtoR, and Opis16aAllKtoR—exhibit an extended range of bacterial selectivity. Opis16aNterKtoR demonstrates selectivity for six of the eight strains, including an SI > 10 for *E. coli* ATCC 25922, which was not observed with Opis16aDtoK. Opis16aAllKtoR improves the selectivity even further with SI > 10 against seven of the bacteria, including *E. cloacae* ATCC 700323.

Finally, Opis16aCterKtoR emerges as the most promising analogue, displaying selectivity against all tested bacterial strains with SI values of 22.6 and higher. Opis16aCterKtoR is the only peptide to show a significant SI > 10 for *K. pneumoniae* ATCC BAA-1705 over HaCat cells (Table 4.3). Additionally, this peptide exhibits slightly higher SI values against *P. aeruginosa* PAO1, *A. baumannii* ATCC 19606 and *E. cloacae* NICD 16103 compared with Opis16a.

© University of Pretoria

Table 4.3: *The toxicity and resulting selectivity indexes of Opis16a and analogues towards Gram-negative bacteria*

Isolate	HaCat toxicity and SI				
	Opis16a	**Opis16aDtoK**	**Opis16aNterKtoR**	**Opis16aCterKtoR**	**Opis16aAllKtoR**
HaCat toxicity					
LC_{50} **(µg/mL)**	311.2 ± 12.3	148.3 ± 5.8	138.3 ± 14.26	180.8 ± 7.8	131.4 ± 4.5
Gram-negative bacteria					
E. coli ATCC 25922	4.86	9.27	**17.29**	**22.60**	**16.43**
E. coli ATCC 700928	**77.80**	**37.08/18.54**	**34.58**	**45.20**	**32.85**
P. aeruginosa PAO1	**38.90**	**18.54**	**34.58**	**45.20**	**32.85**
A. baumannii ATCC 19606	**38.90**	**18.54**	**34.58**	**45.20**	**32.85**
A. baumannii NICD 15283 (C)	**38.90**	**18.54**	**17.29**	**22.60**	**16.43**
K. pneumoniae ATCC BAA-1705	2.47	9.27	8.64	**22.60**	8.21
E. cloacae ATCC 700323	4.86	9.27	8.64	**22.60**	**16.43**
E. cloacae NICD 16103 (C)	**19.45**	**18.54**	**17.29**	**45.20**	**32.85**

Bold values indicate SI values > 10.

4.4.5 Opis16a analogues show enhanced membrane insertion and permeabilisation

The significant increase in antibacterial activity and broader selectivity of the analogues compared to Opis16a, suggests that compared with Opis16a the mechanisms of action differ. Membrane penetration and permeabilisation studies show that overall, PEPG membrane insertion significantly increases for the analogues compared to the parent Opis16a peptide (Fig. 4.5). Consistent with previous research, the time-resolved membrane insertion of all five peptides over 200 ns MD simulations proceeds predominantly via the N-terminus[23,24]. Being strongly hydrogen bonded and deeper inserted into the membrane as seen for the N-termini of the peptide, there is less freedom to move around for these residues compared to those floating above the membrane. The strong hydrogen bonds (Fig. 4.1) and deeper insertion of the N-termini into the model bacterial membrane likely limit the mobility of these residues compared to the C-terminal residues that remain above the membrane. This reduced mobility correlates with the decreased conformational flexibility observed around the N-terminus for all analogues, as illustrated in Fig. 4.2.

Opis16a inserts via the first three N-terminal and last three C-terminal residues with a loss of insertion observed for the middle of the sequence (Fig. 4.5 A). This is likely due to the electrostatic clash between anionic Asp5 and the anionic membrane phospholipid headgroups. The substitution of Asp5 with cationic Lys5 in Opis16aDtoK leads to an increase in membrane interaction and insertion of the N-terminal residues up until 8Lys (Fig. 4.5 B). Less insertion is now observed for the residues located in the C-terminus. Membrane insertion follows a trend similar to that of hydrogen bonding where the Arg-containing analogues interact and insert more readily than the parent or the Opis16aDtoK analogue.

© University of Pretoria

In the PEPG environment Opis16aNterKtoR insertion also proceeds via the N-terminus with continuous interaction and insertion from 10 to 200 ns for the first six N-terminal residues (Fig. 4.5 C). Beyond 80 ns, four C-terminal residues also undergo insertion for the remainder of the simulation. Opis16aCterKtoR and Opis16aAllKtoR show membrane interaction and insertion across the length of their sequences. Opis16aCterKtoR exhibits more superficial insertion with all residues inserting toward the end of the simulation (Fig. 4.5 D), while Opis16aAllKtoR show quicker and deeper membrane penetration for all except the last two C-terminal residues (Fig. 4.5 E). Thus, an increase in the number of Arg residues causes an increase in hydrogen bonding as well as peptide insertion into model PEPG membranes.

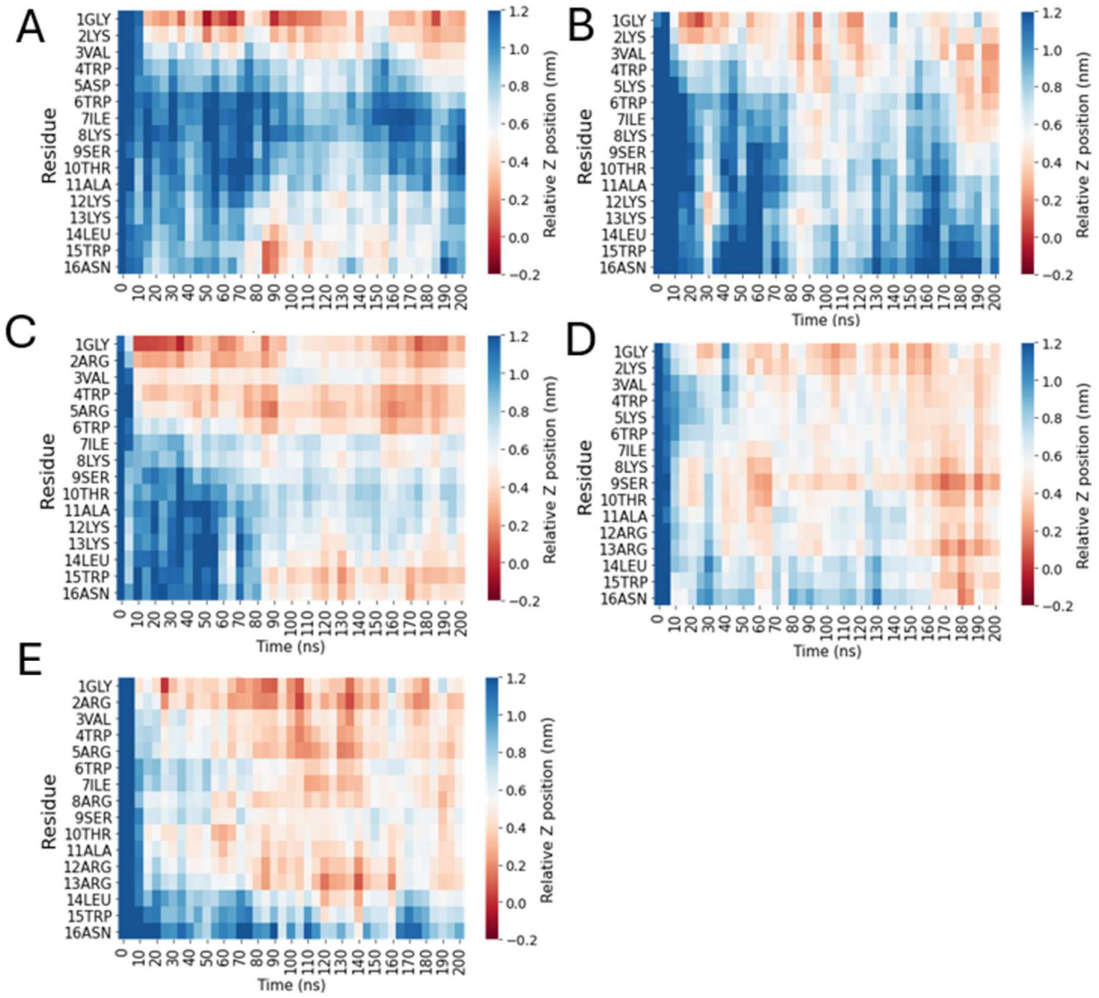


Figure 4.5: Membrane activity of Opis16a and analogues against Gram-negative bacterial membranes in silico. *The depth of Opis16a* ***(A)****, Opis16aDtoK* ***(B)****, Opis16aNterKtoR* ***(C)****, Opis16aCterKtoR* ***(D)*** *or Opis16aAllKtoR* ***(E)*** *insertion into model Gram-negative membranes is shown as the average z-position of each residue relative to the phosphate plane in the upper bilayer leaflet during a 200 ns simulation. Positive or negative values indicate the residues are above or below the phosphate group.*

© University of Pretoria

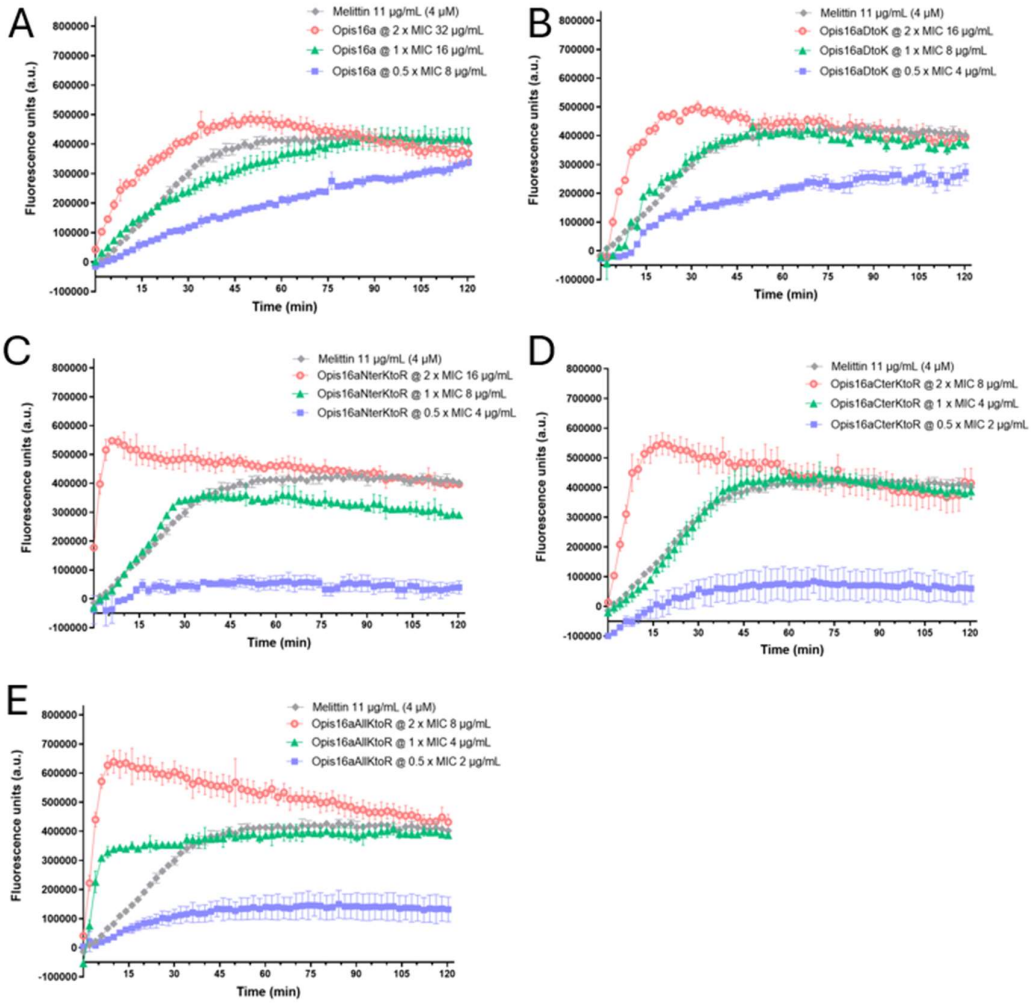


Figure 4.6: Membrane activity of Opis16a and analogues against Gram-negative bacterial membranes in vitro. *E. cloacae NICD 16103 cytoplasmic membrane permeabilisation by Opis16a* ***(A)****, Opis16aDtoK* ***(B)****, Opis16aNterKtoR* ***(C)****, Opis16aCterKtoR* ***(D)*** *and Opis16aAllKtoR* ***(E)*** *at 0.5x, 1x and 2x MIC over 2 h. Melittin at 11 µg/mL is used as positive control. Data show one representative experiment with mean ± SEM, of a total of 3 biological repeats performed in triplicate.*

In vitro membrane permeabilisation assays provide insight into the subsequent damage caused by the initial membrane interaction and insertion of residues predicted by *in silico* MD simulations. All four analogues exhibit faster rates of membrane permeabilisation compared with Opis16a (Fig. 4.6). The increased rate in membrane permeabilisation of the resistant clinical isolate *E. cloacae* NICD 16103 is of particular interest, although similar trends are observed against the *E. coli* ATCC 700928 laboratory strain as well as the resistant *A. baumannii* NICD 15283 clinical isolate confirming broad-spectrum bacterial membrane targeting (Suppl. Fig. S4.3).

At supra-MIC, all four analogues demonstrate markedly faster membrane permeabilisation compared with Opis16a (Fig. 4.6). Notably, the analogues rich in Arg—Opis16aNterKtoR, Opis16aCterKtoR, and Opis16aAllKtoR—exhibit the highest rates of permeabilisation (within 5-10 min). This observation aligns with the *in silico* hydrogen bonding data (Fig. 4.1) and the membrane insertion results (Fig. 4.5).

© University of Pretoria

At MIC, Opis16a induces a steady, nearly linear increase in membrane permeabilisation of *E. cloacae* NICD 161032, reaching its peak after approximately 60-80 min (Fig. 4.6 A & Suppl. Fig. S4.4). In contrast, Opis16aDtoK achieves membrane permeabilisation at a significantly faster rate, with notable differences observed within 15 min and maximum permeabilisation reached in about 45 min (Fig. 4.6 B & Suppl Fig. S4.4). Opis16aNterKtoR also shows a rapid increase in rate of permeabilisation, with its peak effect occurring around 30 min, twice as fast as Opis16a (Fig. 4.6 C & Suppl. Fig. S4.4). Although the MIC of Opis16aCterKtoR shows the lowest level of permeabilisation at 15 or 30 min, it achieves its maximum effect in approximately 35-40 min and displays the greatest overall increase in permeabilisation among the analogues (Fig. 4.6 D & Suppl. Fig. S4.4). Finally, Opis16aAllKtoR demonstrates the fastest rate of membrane permeabilisation, similar to the fastest membrane insertion observed *in silico* (Fig. 4.6 E) with the MIC reaching its maximum effect within the first 15 min, 4 times faster than Opis16a (Suppl. Fig. S4.4).

4.4.6 Opis16aCterKtoR shows rapid killing of resistant E. cloacae NICD 16103

Having identified enhanced membrane disruption capabilities for Opis16aCterKtoR compared to parent Opis16a and considering its superior antibacterial potency and selectivity for bacteria relative to HaCat cells among all analogues tested, we proceeded to advance this peptide for further in-depth studies.

Time-kill studies of Opis16a and Opis16aCterKtoR against the resistant clinical *E. cloacae* NICD 16103 isolate over a 20-h period identify that membrane permeabilisation resulted in bacterial eradication (Fig. 4.7). Both peptides demonstrate rapid antimicrobial activity, with Opis16a achieving complete eradication at 1x MIC within 60 min and Opis16aCterKtoR within 45 min. This quick action aligns with the membrane permeabilisation rates observed in Fig. 4.6, suggesting that both peptides employ membrane-targeting mechanisms of action.

Overall, Opis16aCterKtoR achieves a similarly rapid rate of bacterial killing compared to Opis16a, while requiring significantly less peptide. The 2x and 1x MIC (32 or 16 µg/mL) of Opis16a achieves a 4 Log_{10} reduction in CFU/mL within 30 and 60 min, respectively. In contrast, Opis16aCterKtoR attains the same level of bacterial eradication at four-fold lower concentrations (2x and 1x MIC of 8 or 4 µg/mL) within the same time frame. The 0.5x MIC of both peptides cause a 2 to 3 Log_{10} decrease in CFU/mL within 60 min; however, complete eradication is not achieved, and bacterial regrowth is evident after 20 h, a phenomenon not observed at the 1x and 2x MIC levels.

© University of Pretoria

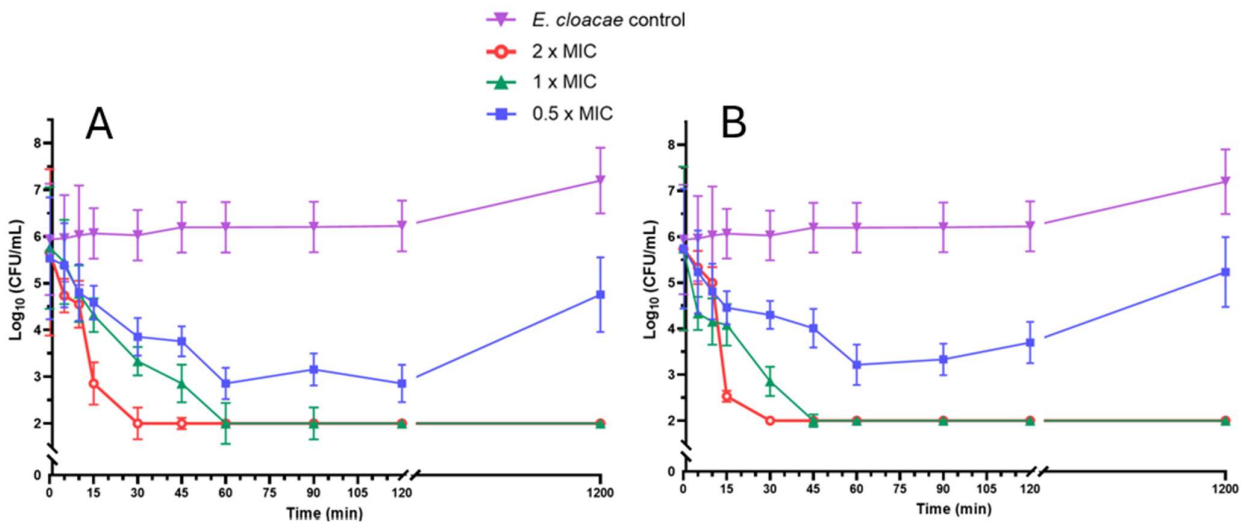


Figure 4.7: Bacterial time-kill kinetics of Opis16a compared with Opis16aCterKtoR over a 20-h period. *E. cloacae NICD 15283 treated with Opis16a* ***(A)*** *or Opis16aCterKtoR* ***(B)*** *at 0.25 x, 0.5 x, 1 x and 2 x MIC. Data represent the mean ± SEM, for three independent experiments performed in triplicate.*

4.4.7 Opis16aCterKtoR retains activity in FCS, but not in trypsin solution

The stability of Opis16a and Opis16aCterKtoR was evaluated in the presence of the proteolytic enzyme trypsin or in a more physiological environment such as FCS. Both peptides completely lost activity against the *E. cloacae* NICD 16103 isolate when pretreated with trypsin (0.15 U/mL, pH 7.4), even at the highest concentrations tested (Fig. 4.8 A). This result aligns with previous findings for the parent peptide Opis16a[9]. The decrease in activity is attributed to trypsin-induced hydrolytic cleavage at the carboxyl side of Lys and Arg residues present in the sequence of both peptides.

In 20% FCS, Opis16a exhibited significantly reduced activity with the MIC increasing from 16 to 64 µg/mL (Fig. 4.8 A). In contrast, Opis16aCterKtoR retained full activity in FCS, indicating resistance to serum protein binding, a characteristic known to reduce the potential of AMPs for further topical and/or systemic applications[25].

4.4.8 Opis16aCterKtoR efficacy against in vivo E. cloacae NICD 16103 infected burn wounds

The improved *in vitro* planktonic activity of Opis16aCterKtoR compared to Opis16a, combined with the high selectivity for *E. cloacae* over mammalian epidermal cells, particularly towards the resistant clinical isolate of *E. cloacae*, as well as its stability in 20% FCS, makes this AMP an excellent candidate for advancement to a model of topical *E. cloacae* wound infection.

Despite the *G. mellonella* larvae tolerance for superficial wounds with only 7% mortality, subsequent infection with *E. cloacae* NICD 16103 leads to 70% mortality over 120 h ($p < 0.0001$, log rank [Mantel-Cox] test), enabling effective therapy to be quantified (Fig. 4.8 B & C). Treatment with 10 mg/kg doses of either Opis16a or Opis16aCterKtoR rescues 93% of the *E. cloacae* NICD 16103 infected *G. mellonella* larvae ($p < 0.0001$, log rank [Mantel-Cox] test).

© University of Pretoria

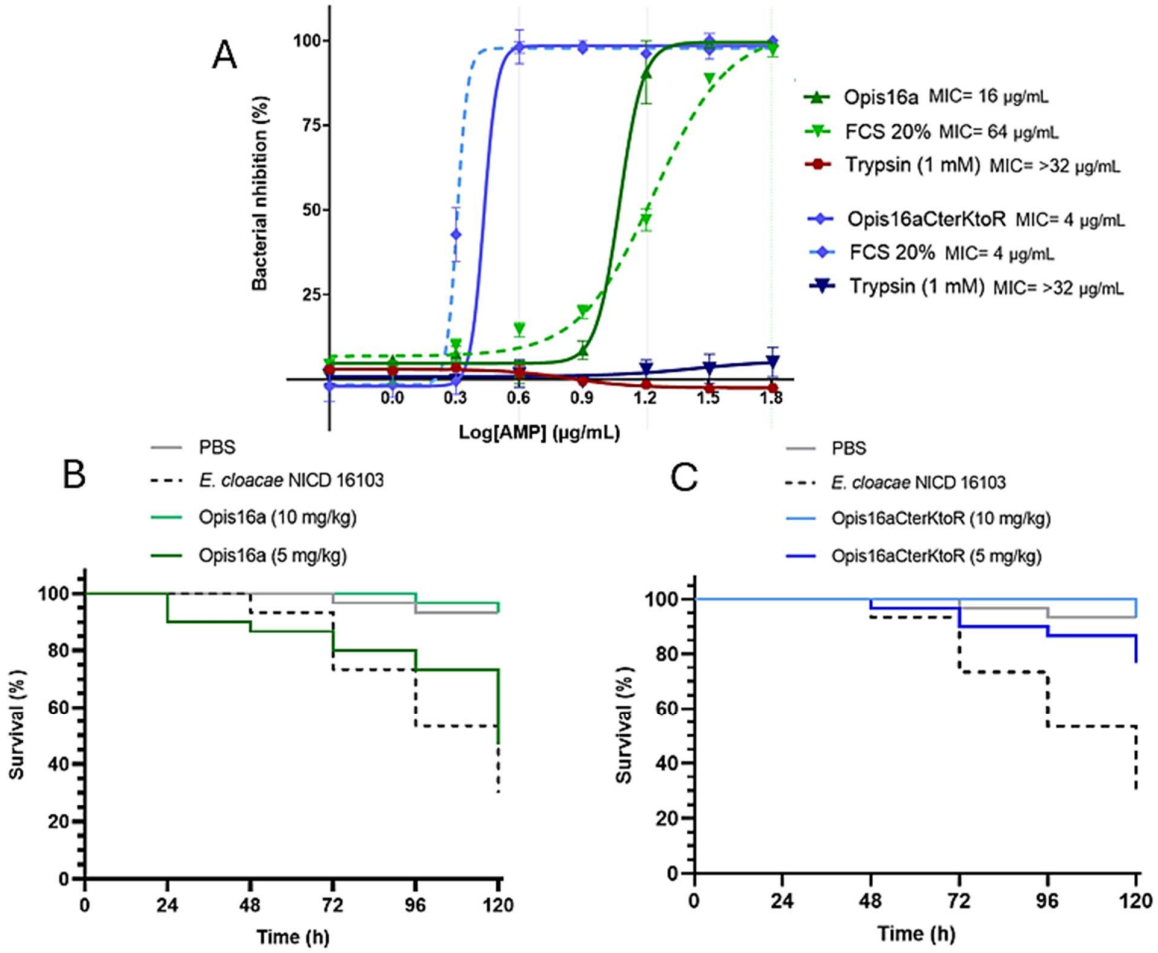


Figure 4.8: Comparison of Opis16a and Opis16aCterKtoR activity against E. cloacae NICD 16103 in serum, and in a G. mellonella – E. cloacae NICD 16103 burn wound infection model. *MIC testing was repeated for Opis16a and Opis16aCterKtoR in the presence of trypsin (0.15 U/mL) or FCS (20%)* ***(A)****. Data represents the mean ± SEM, for three independent experiments performed in triplicate. Survival curves over 120 h are plotted for larvae with burn wounds only (PBS), with burn and E. cloacae NICD 16103 infected wounds or burn and infected wounds treated with the indicated doses of Opis16a* ***(B)*** *or Opis16aCterKtoR* ***(C)****. Data represent the aggregate of three independent experiments consisting of 30 larvae in total per condition.*

However, at a lower dose of 5 mg/kg, Opis16a shows diminished efficacy, rescuing only 46% of the infected larvae over 120 h ($p > 0.5$ nonsignificant, log-rank [Mantel-Cox] test) (Fig. 4.8 B). In contrast, Opis16aCterKtoR retains a significant protective effect at this lower concentration, rescuing 77% of the larvae ($p < 0.001$, log-rank [Mantel-Cox] test) (Fig. 4.8 C). Opis16aCterKtoR is therefore capable of producing a substantial and significant therapeutic effect at a lower dose than the parent Opis16a peptide.

© University of Pretoria

4.5 Discussion

Over the years, the demand for peptide therapeutics has grown significantly, with peptide drugs now representing approximately 5-6% of the global pharmaceutical market[27]. A list of 114 peptides approved by regulatory authorities for clinical use and the $50 billion in peptide drug sales for 2024 highlight the substantial interest and potential in the development of AMP therapeutics[27,28]. However, of the 114 approved AMPs, only seven are specifically aimed at wound recovery or the treatment of skin infections. Of these seven, four are primarily used for Gram-positive bacterial wound infections, and one functions via immune modulation [28]. Colistin and polymyxin B are currently the only peptide drugs listed for the direct treatment of wound infections caused by Gram-negative bacteria. These AMPs are often reserved for cases where other treatments are ineffective or contraindicated.

Consequently, Gram-negative wound infections present a significant clinical challenge due to the limited effectiveness of current treatment options. This issue is particularly acute in burn wound infections, where research indicates that bacterial infections account for 42 to 65 percent of deaths among burn patients[2]. Additionally, the mortality rate for burn patients with infections is nearly twice as high as that for those with non-infectious burns[2]. The situation is further complicated by the escalating resistance of Gram-negative bacteria to existing antibiotics and the inherent complexity of their protective membranes.

Extensive research has shown that AMPs can effectively facilitate wound healing and offer substantial therapeutic potential for treating skin and other epithelial injuries. For example, AMPs such as pexiganan, AP114, and iseganan have advanced to clinical trials for burn wound treatment. Despite their promise, these peptides have encountered setbacks including variable efficacy, toxicity, and formulation stability issues[30]. Nonetheless, ongoing research into AMPs for wound care underscores their potential in this area and highlights the urgent need for novel peptides that can effectively target resistant infections with high selectivity, minimal toxicity, and enhanced stability.

This study introduces four novel analogues of the Gram-negative-targeting peptide Opis16a, that exhibits enhanced membrane targeting and improved antibacterial activity, with Opis16aCterKtoR showing promise for topical use in Gram-negative burn wound infections. Sequence substitutions of an anionic residue with a cationic one or Lys residues with Arg, delivered potent AMPs with up to a 16-fold improvement in activity and 4-fold improvement in selectivity compared with Opis16a.

© University of Pretoria

MD simulations using bacterial plasma membrane models reveals an increase in the number of hydrogen bonds between the analogues and the Gram-negative model membranes compared with Opis16a. As reported by Li *et al.*[22], the incorporation of Lys or Arg residues into an AMP sequence enhances electrostatic interactions, which draws the peptide closer to the anionic membrane and facilitates more hydrogen bonding. Although both Lys and Arg substitutions improved membrane interaction, Arg, with its guanidinium group, provides a more dispersed positive charge[22]. Consequently, the three analogues with increasing Arg substitutions exhibited greater hydrogen bonding compared with the analogue with the single Asp to Lys substitution or the parent Opis16a peptide.

The increased hydrogen bonding observed for the Arg-containing analogues enhances the stability of their interaction with the membrane, resulting in reduced conformational flexibility compared with the Lys-containing analogue and the parent peptide, which are more loosely associated with the membrane. *In silico* conformational analyses and CD spectroscopy provide complementary insights into the structural changes induced by these modifications. Specifically, substituting Asp with Lys in Opis16aDtoK results in the loss of the β-turn type I in the mid-sequence, leading to a coiled structure with reduced flexibility around the N-terminal. This change likely arises from the closer interaction of the N-terminal and mid-sequence with the membrane, contrasting with the mid-sequence of Opis16a, where the Asp residue protrudes away from the membrane.

While stronger interactions with the membrane and reduced conformational flexibility are also noted for the Arg-containing analogues, each of these peptides adopts a β-turn at various locations along their sequences that are stabilised by either Lys or Arg residues. Opis16aNterKtoR and Opis16aCterKtoR each form a β-turn type II around the fifth residue, while Opis16aNterKtoR and Opis16aAllKtoR exhibit a β-turn type I around the twelfth residue. The long, cationic side chains of Lys and Arg residues facilitate multiple interactions with the membrane but also with other residues within the peptide sequence[22]. These residues can form non-covalent cation-π interactions with nearby Trp residues[22], as in the case of residues 4 to 6, where the positive charge on the sidechain of either Lys or Arg in position 5 can interact with the electron-rich indole ring of the flanking Trp residues. This interaction contributes to the stabilisation of peptide structures such as the β-turns that are formed.

Not only did the analogues show increased membrane hydrogen bonding, less conformational flexibility and a slight increase in ordered structure formation, but also a broader spectrum of antibacterial activity and improved efficacy compared with the parent Opis16a peptide. Although all four analogues showed improved efficacy, the Arg containing peptides, especially Opis16aCterKtoR, showed the best improvement. This aligns with the increased number of hydrogen bonds observed for these analogues, which highlights the importance of peptide–lipid hydrogen bonding in modulating the interaction of Opis16a analogues with membranes of varying compositions. The increased charge of these analogues further contributes to this enhanced activity, highlighting how both structural stabilisation and electrostatic effects positively influence antimicrobial performance.

© University of Pretoria

Increased membrane insertion, demonstrated by MD simulations, and greater membrane damage, indicated by permeabilisation assays, were observed for the analogues, with particularly pronounced effects in the Arg-containing variants compared with Opis16a. This agrees with findings reported by Li *et al.*, which highlight that the guanidinium group of Arg interacts more favourably with the membrane interface, leading to more extensive hydrogen bonding with lipids, and consequently induces more significant membrane deformations compared with Lys[22].

Membrane insertion for all four analogues occur via an interaction between the cationic N-terminus and anionic lipid phosphate headgroups, effectively anchoring the peptide to the membrane. This correlates well with other membrane insertion studies on AMPs such as temporin L, temporin B, cecropin B and pleurocidin, where initial membrane contact also proceeds via the N-terminus of the peptides[19,23,24,26].

The outward protrusion of the central region in Opis16a, attributed to the anionic Asp residue, was eliminated by substituting Asp with Lys in Opis16aDtoK. This modification facilitates more extensive insertion of the analogue into the model Gram-negative membrane, engaging both its N-terminal and central regions. Additionally, this change resulted in a twofold increase in the time required to permeabilise *E. cloacae* NICD 16103 membranes, a representative of Gram-negative membranes.

The systematic introduction of Arg further enhanced membrane interaction and insertion, following a similar trend to that observed with hydrogen bonding. While the Opis16aNterKtoR analogue also showed increased insertion along the N-terminal and central regions, Opis16aCterKtoR and Opis16aAllKtoR exhibited membrane interaction and insertion across the entire length of their sequences, without any regions protruding outward. This increased membrane insertion was accompanied by enhanced and more rapid membrane permeabilisation *in vitro*.

Among the four analogues, Opis16aCterKtoR exhibited the most significant improvement in MIC compared with Opis16a and demonstrated the highest selectivity for pathogens over mammalian HaCat cells. This analogue also displayed the most pronounced conformational changes, with increased helicity observed in the central region of the sequence. The enhanced helicity, combined with increased hydrogen bonding, results in the lowest conformational flexibility among the analogues. Therefore, despite the significant potential of all four analogues, the changes in conformation and increased membrane interaction, along with its promising antimicrobial activity, led to the selection of Opis16aCterKtoR for further evaluation.

Notably, Opis16aCterKtoR is the only peptide active against all Gram-negative bacteria in a concentration range as low as 4 to 8 µg/ml, except for *P. aeruginosa* PAO1. This peptide also showed promising activity against resistant clinical Gram-negative isolates, with a fourfold improvement in in efficacy compared with Opis16a against *E. cloacae* NICD 16103. Additionally, Opis16aCterKtoR outperformed all the antibiotics screened against this strain.

© University of Pretoria

The significant efficacy of Opis16aCterKtoR against *E. cloacae* NICD 16103 at a concentration as low as 4 µg/mL, where conventional antibiotics fail, warranted further investigation into its potential applications. This included examining its time-kill kinetics, stability in physiological environments, and efficacy in providing protection in an *in vivo* burn wound infection model.

Time-kill kinetics against the resistant clinical isolate *E. cloacae* NICD 16103 demonstrated that both Opis16a and Opis16aCterKtoR exhibit bactericidal effects at both the MIC and 2x MIC, with comparable rates of bacterial killing. Notably, Opis16aCterKtoR demonstrated a slight enhancement, reducing the time to kill at MIC from 60 min to 45 min. This improvement aligns with the increased rate and extent of membrane permeabilisation observed within 45 min for this analogue, suggesting that membrane targeting is the primary mechanism of action for Opis16aCterKtoR.

Although both Opis16a and Opis16aCterKtoR lose activity in the presence of trypsin, Opis16aCterKtoR retains full activity in 20% FCS, while Opis16a shows a fourfold reduction in activity. This reduction in Opis16a activity could be due to its binding with serum proteins such as anionic albumin, which decreases the free peptide concentration available for interaction with its target, thereby reducing its antimicrobial effectiveness[25]. Interestingly, in contrast, against a clinical *A. baumannii* isolate, activity was maintained in 20% FCS[9]. The observed difference may be attributed to variations in peptide interactions with different bacterial species, such as differences in membrane interactions. This is supported by the faster eradication times observed in time-kill assays for *A. baumannii*[9]. In contrast, eradication of *E. cloacae* occurs at a slower rate, suggesting that the mechanisms of action and the impact of serum on peptide efficacy may differ between these bacteria.

Both peptides were subsequently tested in an *in vivo* wound infection model. At a dose of 10 mg/kg, both Opis16a and Opis16aCterKtoR provided substantial protection against topical wound infections caused by the clinical isolate *E. cloacae* NICD 16103, resulting in improved survival rates of larvae. This protective effect is consistent with recent findings where 10 mg/kg of Opis16a protected against the clinical isolate *A. baumannii* NICD 16103, and 10 mg/kg of pleurocidin was effective against *A. baumannii* ATCC 17978 in *G. mellonella* burn wound models [9, 20].

However, at a lower concentration of 5 mg/kg, Opis16a lost its protective efficacy, while Opis16aCterKtoR still provided significant protection. This finding reinforces the superior potency of Opis16aCterKtoR over Opis16a, as observed in both *in silico* and *in vitro* assays. This is especially significant given the common prevalence of *E. cloacae* in hospital-acquired wound infections, particularly in burn wounds. The extensive multidrug resistance observed in *E. cloacae* strains further highlights the critical need for new and effective treatment alternatives. Consequently, the study highlights the benefits of incorporating Arg into peptide sequences, positioning Opis16aCterKtoR as a promising candidate for future therapeutic development, especially against challenging Gram-negative bacteria such as *E. cloacae*.

© University of Pretoria

4.6 Conclusion

The study contributes to antimicrobial peptide research in two significant ways: first, it confirms that incorporating Arg into peptide sequences enhances antibacterial activity and increases selectivity against Gram-negative bacteria; and second, it identifies Opis16aCterKtoR as a novel peptide with considerable potential for future therapeutic development, particularly for combating challenging Gram-negative pathogens such as *E. cloacae* especially in the context of burn wound care.

4.7 Acknowledgements

The research in this publication was facilitated by the South African Medical Research Council with funding received from the South African National Department of Health and a SA-UK Newton Fund Antibiotic Accelerator (MC_PC_MR/T029552/1), awarded to AJM and ARMG, and managed by the Medical Research Council (UK). A special thanks to the UK Materials and Molecular Modelling Hub, which is partially funded by EPSRC (EP/P020194/1 and EP/T022213/1), and the UK HPC Materials Chemistry Consortium, which is also funded by EPSRC (EP/R029431), for providing us access to computational resources. This work also benefited from access to the King's Computational Research, Engineering and Technology Environment (CREATE) at King's College London[29]. We also extend our gratitude to Sophie Nyoni and Pretti Khumalo from the FABI Biocontrol Centre and Nursery at the University of Pretoria, for their assistance in maintaining and providing *G. mellonella* larvae.

© University of Pretoria

4.8 References

[1] MURRAY, C.J.L., IKUTA, K.S., RAO, P., WOOL, E., AGARWAL, R., BEKKER, A., DAY, N.P.J., DUNACHIE, S.J., HAY, S.I., NANAVATI, R., NOVOTNEY, A., STEENKESTE, N., SARTORIUS, B., LOPEZ, A.D., MOORE, C.E. & NAGHAVI, M. (2019). Global burden of bacterial antimicrobial resistance in 2019: a systematic analysis. *The Lancet*, 399 (10325), pg. 629 – 655.

[2] VINAIK, R., BARAYAN, D., SHAHROKHI, S. & JESCHKE, M. G. (2019). Management and prevention of drug-resistant infections in burn patients. *Expert Review of Anti-infective Therapy,* 17 (8), pg. 607–619. doi: 10.1080/14787210.2019.1648208

[3] MAITZ, J., MERLINO, J., RIZZO, S., MCKEW, G. & MAITZ, P. (2023). Burn wound infections microbiome and novel approaches using therapeutic microorganisms in burn wound infection control. *Advanced Drug Delivery Reviews*, 196, article 114769. doi: 10.1016/j.addr.2023.114769.

[4] BENNETT, W., MENDE, K., CAMPBELL, W.R., BECKIUS, M., STEWART, L., SHAIKH, F., RAHMAN, A., TRIBBLE, D.R. & YABES, J.M. (2023) Enterobacter cloacae infection characteristics and outcomes in battlefield trauma patients. *PLoS One*, 18 (8), article e0290735. doi: 10.1371/journal.pone.0290735.

[5] HARRIS, P. N., WEI, J. Y., SHEN, A. W., ABDILE, A. A., PAYNTER, S., HUXLEY, R. R., PANDEYA, N., DOI, Y., HUH, K., O'NEAL, C. S., TALBOT, T. R. & PATERSON, D. L. (2016). Carbapenems versus alternative antibiotics for the treatment of bloodstream infections caused by Enterobacter, Citrobacter or Serratia species: a systematic review with meta-analysis. *Journal of Antimicrobial Chemotherapy*, 71 (2), pg. 296–306. doi: 10.1093/jac/dkv346.

[6] WANG, C., HONG, T., CUI, P., WANG, J. & XIA, J. (2021). Antimicrobial peptides towards clinical application: Delivery and formulation. *Advanced Drug Delivery Reviews*, 175, article 113818.

[7] MAHLAPUU, M., BJÖRN, C. & EKBLOM, J. (2020) Antimicrobial peptides as therapeutic agents: opportunities and challenges. *Critical Reviews in Biotechnology*, 40 (7), pg. 978-992.

[8] BARRETO-SANTAMARÍA, A., ARÉVALO-PINZÓN, G., PATARROYO, M. A. & PATARROYO, M. E. (2021). How to combat Gram-negative bacteria using antimicrobial peptides: A challenge or an unattainable goal? *Antibiotics (Basel),* 10 (12), article 1499. doi: 10.3390/antibiotics10121499.

[9] VAN DER WALT, M., OOSTHUIZEN, C. B, LORENZ, C. D., SERIAN, M., MASON, J. A., BESTER, M. J. & GASPAR, A. R. M. (2024). Scorpion venom-derived Opis16a shows potent membrane-destabilising Gram-negative activity and promising *in vivo* topical efficacy. Submitted.

[10] VAN DER WALT, M., MÖLLER, D. S., VAN WYK, R. J., FERGUSON, P. M., HIND, C. K., CLIFFORD, M., DO CARMO SILVA, P., SUTTON, J. M, MASON, J. A., BESTER, M. J. & GASPAR, A. R. M. (2024). QSAR reveals cationic residues with decreased lipophilicity determine the selectivity of antimicrobial peptide activity. *ACS Omega,* doi: 10.1021/acsomega.4c01277.

[11] LINDAHL, E., ABRAHAM, M., HESS, B. & VAN DER SPOEL, D. (2021). GROMACS 2021 Manual (Version 2021). Zenodo. https://doi.org/10.5281/zenodo.4457591.

[12] HUANG, J. & MACKERELL. J. A. D. (2013). CHARMM36 all-atom additive protein force field: Validation based on comparison to NMR data. *Computational Chemistry*, 34 (25), pg. 2135–2145. doi: 10.1002/jcc.23354.

[13] AVOGADRO: An open-source molecular builder and visualization tool. Version 1.2.0. Retrieved June 2, 2024, from http://avogadro.cc/

© University of Pretoria

[14] JO, S., KIM, T., IYER, V. G. & IM, W. (2008) CHARMM-GUI: A Web-based graphical user interface for CHARMM. *Journal of Computational Chemistry*, 29, pg. 1859-1865. https://doi.org/10.1002/jcc.20945

[15] WU, E. L., CHENG, X., JO, S., RUI, H., SONG, K. C., DÁVILA-CONTRERAS, E. M., QI, Y., LEE, J., MONJE-GALVAN, V., VENABLE, R. M., KLAUDA, J. B. & IM, W. (2014) CHARMM-GUI Membrane Builder toward realistic biological membrane simulations. *Journal of Computational Chemistry*, 35 (27), pg. 1997-2004. https://doi.org/10.1002/jcc.23702

[16] BOONSTRA, S., ONCK, P.R., & GIESSEN, E.V. (2016). CHARMM TIP3P water model suppresses peptide folding by solvating the unfolded state. *The Journal of Physical Chemistry B,* 120 (15), pg. 3692-3698. doi: 10.1021/acs.jpcb.6b01316.

[17] GOWERS, R. J., LINKE, M., BARNOUD, J., REDDY, T. J. E., MELO, M. N., SEYLER, S. L., DOTSON, D. L., DOMANSKI, J., BUCHOUX, S., KENNEY, I. M. & BECKSTEIN, O. (2016). MDAnalysis: A Python package for the rapid analysis of molecular dynamics simulations. In S. Benthall and S. Rostrup, editors, *Proceedings of the 15th Python in Science Conference*, pg. 98-105. Austin, TX. SciPy. doi:10.25080/majora-629e541a-00e.

[18] MICHAUD-AGRAWAL, N., DENNING, E. J., WOOLF, T. B. & BECKSTEIN, O. (2011). MDAnalysis: A toolkit for the analysis of molecular dynamics simulations. *Journal of Computational Chemistry*, 32, pg. 2319-232. doi:10.1002/jcc.21787.

[19] MANZO, G., FERGUSON, P. M., HIND, C. K., CLIFFORD, M., GUSTILO, V. B., ALI, H., BANSAL, S. S., BUI, T. T., DRAKE, A. F., ATKINSON, R. A., SUTTON, J. M., LORENZ, C. D., PHOENIX, D. A. & MASON, A. J. (2019). Temporin L and aurein 2.5 have identical conformations but subtly distinct membrane and antibacterial activities. *Scientific Reports,* 9, article 10934. https://doi.org/10.1038/s41598-019-47327-w

[20] CLARKE, M., HIND, C.K., FERGUSON, P.M., MANZO, G., MISTRY, B., YUE, B., ROMANOPULOS, J., CLIFFORD, M., BUI, T.T., DRAKE, A.F., LORENZ, C.D., SUTTON, J.M. & MASON, A.J. (2023). Synergy between Winter Flounder antimicrobial peptides. *Nature Partner Journals: Antimicrobials and Resistance*, 1, article 8. https://doi.org/10.1038/s44259-023-00010-7.

[21] MASLOVA, E., SHI, Y., SJÖBERG, F., AZEVEDO, H.S., WAREHAM, D.W. & MCCARTHY, R.R. (2020). An invertebrate burn wound model that recapitulates the hallmarks of burn trauma and infection seen in mammalian models. *Frontiers in Microbiology*, 11, article 998. doi: 10.3389/fmicb.2020.00998.

[22] LI, L., VOROBYOV, I. & ALLEN, T.W. (2013). The different interactions of lysine and arginine side chains with lipid membranes. *Journal of Physical Chemistry B*, 117 (40), pg.11906–11920.

[23] MANZO, G., FERGUSON, P. M., GUSTILO, V. B., HIND, C. K., CLIFFORD, M., BUI, T. T., DRAKE, A. F., ATKINSON, R. A., SUTTON, J. M., BATONI, G., LORENZ, C. D., PHOENIX, D. A. & MASON, A. J. (2019). Minor sequence modifications in Temporin B cause drastic changes in antibacterial potency and selectivity by fundamentally altering membrane activity. *Scientific Reports,* 9, pg. 1385-1400.

[24] MANZO, G., HIND, C. K., FERGUSON, P. M., AMISON, R. T., HODGSON-CASSON, A. C., CIAZYNSKA, K. A., WELLER, B. J., CLARKE, M., LAM, C., MAN, R. C. H., O' Shaughnessy, B. G., CLIFFORD, M., BUI, T. T., DRAKE, A. F., ATKINSON, R. A., LAM, J. K. W., PITCHFORD, S. C., PAGE, C. P., PHOENIX, D. A., LORENZ, C. D., SUTTON, J. M., & MASON, A. J. (2020). A pleurocidin analogue with greater flexibility, enhanced antimicrobial potency and in vivo therapeutic efficacy. *Communications Biology*, 3 (697), pg. 1-16.

© University of Pretoria

[25] TANG, W.H., WANG, C.F. & LIAO, Y.D. (2021). Fetal bovine serum albumin inhibits antimicrobial peptide activity and binds drug only in complex with α1-antitrypsin. *Scientific Reports*, 11, article 1267. https://doi.org/10.1038/s41598-020-80540-6

[26] WANG, X., VAN BEEKVELD, R.A.M, XU, Y., PARMAR, A., DAS, S., SINGH, I. & BREUKINK, E. (2023). Analyzing mechanisms of action of antimicrobial peptides on bacterial membranes requires multiple complimentary assays and different bacterial strains. *Biochimica et Biophysica Acta - Biomembranes*, 1865 (6), article 184160. doi.org/10.1016/j.bbamem.2023.184160.

[27] CRESTI, L., CAPPELLO, G. & PINI, A. (2024). Antimicrobial peptides towards clinical application—A long history to be concluded. *International Journal of Molecular Sciences,* 25 (9), article 4870. https://doi.org/10.3390/ijms25094870

[28] PEPTHERDIA. Available online: http://peptherdia.herokuapp.com/ (accessed on 29 August 2024).

[29] KING'S COLLEGE LONDON. (2022). King's Computational Research, Engineering and Technology Environment (CREATE). Retrieved June 2, 2024, from https://doi.org/10.18742/rnvf-m076

[30] DIJKSTEEL, G.S., ULRICH, M.M.W., MIDDELKOOP, E. & BOEKEMA, B.K.H.L. (2021). Review: Lessons learned from clinical trials using antimicrobial peptides (AMPs). *Frontiers in Microbiology*, 12. Available at: https://www.frontiersin.org/journals/microbiology/articles/10.3389/fmicb.2021.616979 [Accessed 17 September 2024]. doi: 10.3389/fmicb.2021.616979.

[31] MICSONAI, A., WIEN, F., KERNYA, L., LEE, Y., GOTO, Y., RÉFRÉGIERS, M., & KARDOS, J. (2015). Accurate secondary structure prediction and fold recognition for circular dichroism spectroscopy. *Proceedings of the National Academy of Sciences, U.S.A.*, 112 (24), pg. E3095-E3103. https://doi.org/10.1073/pnas.1500851112

© University of Pretoria

Supplementary Material

Table S4.1: *Antimicrobial susceptibility profile provided by the NICD*

Clinical Isolate	Antimicrobials							
	Amikacin	Sulbactam	Ciprofloxacin	Gentamicin	Meropenem	Imipenem	Tetracycline	Tobramycin
A. baumannii NICD 15283 (C)	R	I	R	R	R	R	R	R
E. cloacae NICD 16103 (C)	S	R	R	R	R	R	R	R

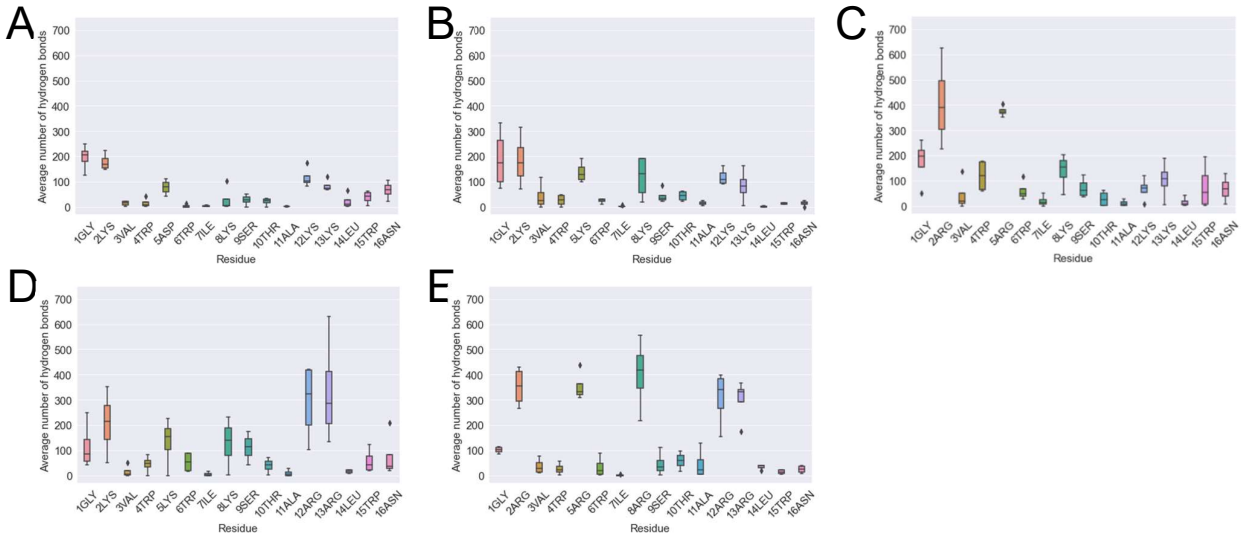
S - Susceptible, R - Resistant, I – Intermediate

Table S4.2: *Antibacterial activity of four clinically used antibacterial agents, and melittin, against Gram-negative bacterial strains*

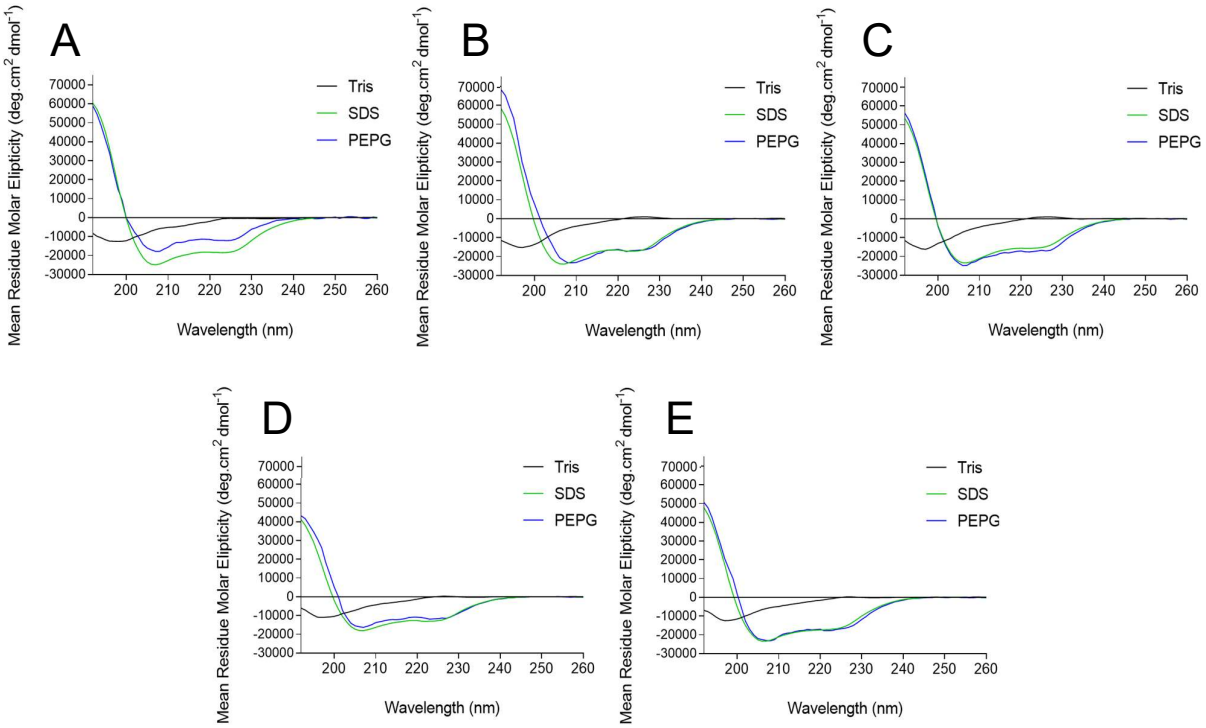
Isolate	Modal MICs in µg/mL				
	Polymyxin B	Ciprofloxacin	Gentamicin	Meropenem	Melittin
Gram-negative bacteria					
E. coli ATCC 25922 (S)	**0.25**	**-**	0.5	-	-
E. coli ATCC 700928 (S)	0.5	0.25	0.5	-	4
P. aeruginosa PAO1 (S)	-	0.5	4	-	2
A. baumannii ATCC 19606 (S)	**1**	**1**	**32**	-	-
A. baumannii NICD 15283 (C)	1	1	**16/32**	**32**	4
K. pneumoniae ATCC BAA-1705 (S)	**0.5**	**>32**	1/2	-	-
E. cloacae ATCC 700323 (S)	**0.25**	**0.13**	2	-	-
E. cloacae NICD 16103 (C)	-	**8**	**>32**	**16**	8

Bold values indicate MICs above the 2024 EUCAST breakpoint for susceptibility.

© University of Pretoria



Supplementary Figure 4.1: Hydrogen bonding between peptide and PEPG model lipids differ among Opis16a analogues and is driven by cationic residues. *Residue specific peptide-membrane hydrogen bonds are shown cummulatively for Opis16a* ***(A)****, Opis16aDtoK* ***(B)****, Opis16aNterKtoR* ***(C)****, Opis16aCterKtoR* ***(D)*** *and Opis16aAllKtoR* ***(E)*** *in representative simulations of Gram-negative model membranes.*



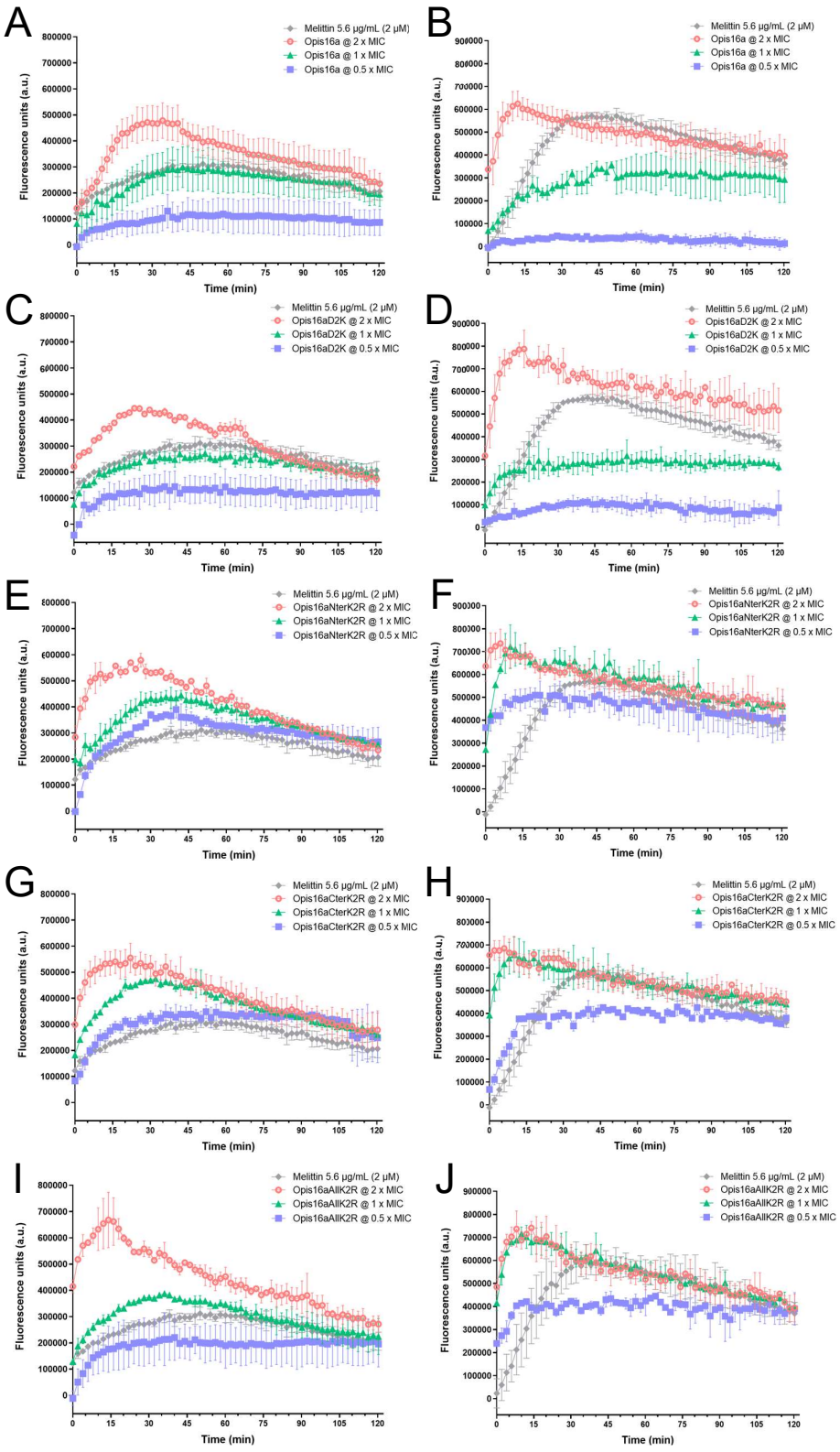
Supplementary Figure 4.2: Steady-state secondary structure analysis of Opis16a and analogues. *Far-UV CD spectra obtained in Tris buffer, anionic SDS detergent micelles or model Gram-negative plasma membranes comprising POPE/POPG lipids. Data are shown for Opis16a* ***(A)****, Opis16aDtoK* ***(B)****, Opis16aNterKtoR* ***(C)****, Opis16aCterKtoR* ***(D)*** *and Opis16aAllKtoR* ***(E)****.*

© University of Pretoria

Table S4.3: *Peptide secondary structure content determined with BestSel using CD spectra*

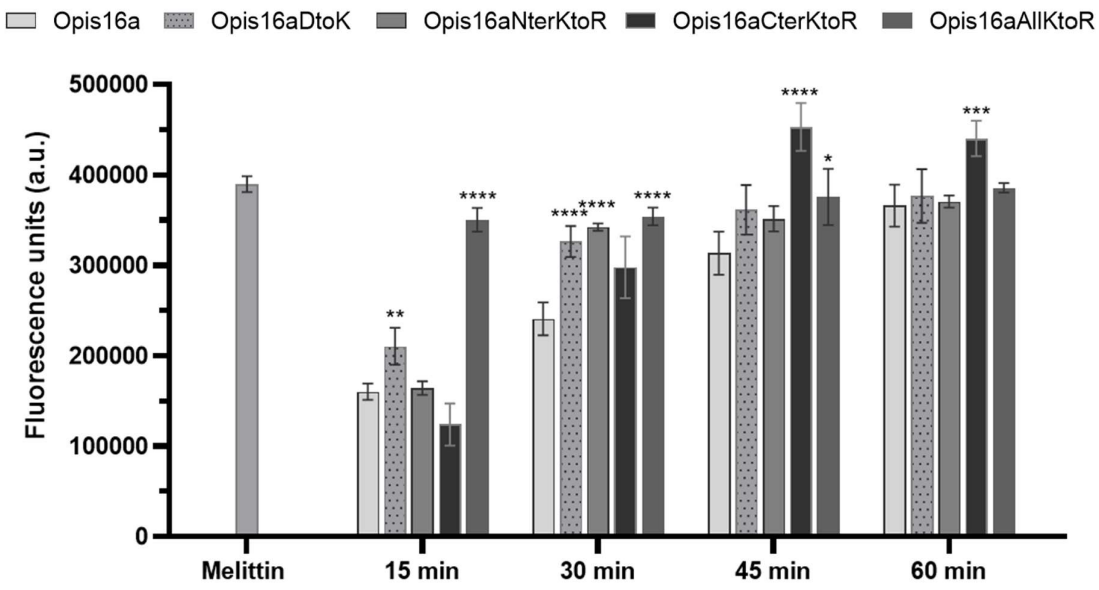
Peptide	Percentage structural content in **SDS (%)**				Percentage structural content in **PEPG (%)**			
	α-helix	*β-sheet*	*turns*	*other*	*α-helix*	*β-sheet*	*turns*	*other*
Opis16a	42.9	-	-	57.1	35.2	16.8	7.6	40.4
Opis16aDtoK	48.3	-	2.7	49	44.2	18.3	-	37.4
Opis16aNterKtoR	45	-	1.2	53.8	50.4	-	-	49.6
Opis16aCterKtoR	32.1	14.6	17.9	35.4	36.3	11.7	12.6	39.4
Opis16aAllKtoR	48.8	3.3	-	47.9	42.8	14.5	3.7	39

© University of Pretoria



Supplementary Figure 4.3: Membrane permeabilisation of Opis16a and analogues against in vitro Gram-negative bacterial membranes. (Left) *E. coli ATCC 700928 and* ***(Right)*** *A. baumannii NICD 15283 cytoplasmic membrane permeabilisation by Opis16a* ***(A or B)****, Opis16aDtoK* ***(C or D)****, Opis16aNterKtoR* ***(E or F)****, Opis16aCterKtoR* ***(G or H)*** *and Opis16aAllKtoR* ***(I or J)*** *at 0.5x, 1x and 2x MIC over a 2 h period. Data shows one representative experiment with mean ± SEM, of a total of 3 biological repeats performed in duplicate.*

© University of Pretoria



Supplementary Figure 4.4: Comparison of membrane permeabilisation in E. cloacae NICD 16103 induced by 1x MIC of Opis16a and analogues at different time points. *E. cloacae NICD 16103 cytoplasmic membrane permeabilisation by Opis16a (16 µg/mL), Opis16aDtoK (8 µg/mL), Opis16aNterKtoR (8 µg/mL), Opis16aCterKtoR (4 µg/mL) and Opis16aAllKtoR (4 µg/mL) at 1x MIC. Melittin at 11 µg/mL is used as positive control. Data show one representative experiment with mean ± SEM, of a total of 3 biological repeats performed in triplicate. (*: p<0.01, **: p<0.05, ***: p<0.001, ****: p<0.0001 relative to permeabilisation by Opis16a per timepoint).*

© University of Pretoria

CHAPTER 5: Conclusions and future perspectives

5.1 Summary of findings and future perspectives

Current antibacterial therapies effective against multidrug-resistant bacteria are scant. Carbapenems have previously been valued as the best broad-spectrum β-lactam antibiotics for treatment of multidrug-resistant Gram-negative bacteria. Recently, carbapenem-resistant bacteria have emerged leaving only colistin (polymyxin E) and tigecycline as the last-resort therapeutics for carbapenem-resistant bacterial infections. However, the increased consumption of these antibiotics resulted in an increase in colistin- or tigecycline-resistant bacteria over the last 6 years (Zhang *et al.,* 2018; Karakonstantis *et al.,* 2024). Therefore, there is an urgent need to develop novel therapies and classes of antimicrobials to fight bacterial infections.

This study highlights the promise of AMPs as potential therapeutic drugs to combat antimicrobial resistance. In Chapter 2, 46 peptide candidates were subjected to comprehensive *in vitro* screenings to evaluate their antimicrobial efficacy against a range of pathogens, as well as their potential toxicity. The tick-derived peptides primarily exhibited inactivity against most pathogens and showed no haemolytic activity. This is attributed to their salt sensitivity, especially in complex media. Notably, only the hydrophobic Trp-tagged tick peptides demonstrated some activity against a select few bacterial species. The frog peptides emerged as the second-best performing group, displaying strong antibacterial properties, moderate antifungal activity, and minimal mammalian toxicity. In contrast, the scorpion peptides exhibited the most effective antibacterial and antifungal activities, with four specific peptides—Opis-16a, AamP1-Lys, AamP1-Lys-NH_2, and A3-NH_2—showing effectiveness against all tested bacteria, including the resistant strain *P. aeruginosa* NCTC 13437. However, despite their promising antimicrobial capabilities, the scorpion peptides also displayed varying degrees of toxicity against human erythrocytes and keratinocytes, highlighting the need for improved selectivity for future developments. Among the primate peptides, BTD2-15a demonstrated strong antibacterial and antifungal activity but also targeted mammalian cells. Interestingly, a shorter derivative, BTD2-9a, exhibited no bacterial or haemolytic activity while showing promising antifungal effects.

Overall, this research reveals the potential but also the challenges in developing AMPs into effective drugs, particularly regarding selectivity. Chapter 2 specifically addresses issues related to host cell toxicity and low target selectivity. Despite over 70 peptides advancing to drug development over recent years, only a few have reached the market, partly due to safety concerns (Boto *et al.,* 2018; Wang *et al.,* 2021). This emphasises the importance of understanding the structure-activity relationships of AMPs, focusing on how physicochemical properties influence activity and selectivity.

© University of Pretoria

A QSAR model revealed that an essential molecular parameter, the negative lipophilicity of polar residues (LP), correlates with antimicrobial activity while minimising cytotoxicity (Van der Walt *et al.,* 2024). To our knowledge, this study is the first to identify LP as a key property for enhancing peptide selectivity, thus paving the way for more effective and targeted AMP design.

Decreasing LP can enhance AMP selectivity, suggesting that increasing the number of polar residues with very low LP values can boost antimicrobial action without raising toxicity. Cationic residues, such as Arg and Lys, are particularly effective in achieving pathogen selectivity. The study further reveals that while overall hydrophobicity and total lipophilicity are essential for AMP activity, they also contribute to cytotoxicity, complicating the design process. Consequently, identifying specific properties like LP facilitates the rational design of potent and selective AMPs, allowing for a more strategic approach to developing therapies that minimise harmful side effects. Additional factors, including charge and peptide size, also play significant roles in determining selectivity. Overall, this study provides new insights into optimising AMPs by identifying specific molecular properties that enhance selectivity, aiming to mitigate the toxic side effects that hinder AMP therapeutic potential.

Among the 46 AMPs screened in Chapter 2, the scorpion venom-derived peptide Opis16a emerged as one of the most promising candidates with broad-spectrum antimicrobial activity and minimal mammalian toxicity. Chapter 3 presents a comprehensive analysis of the novel Opis16a peptide, highlighting its promise as an effective anti-Gram-negative agent both *in vitro* and *in vivo*. The study demonstrates that Opis16a exhibits potent antimicrobial activity against critical WHO priority pathogens, including *E. coli* and *A. baumannii*, with minimal cytotoxicity to mammalian cells, yielding significant selectivity ratios (Table 5.1).

While several factors may contribute to the selectivity of Opis16a, the relatively high positive charge and lower hydrophobicity in comparison with other, more toxic venom-derived peptides such as AamAP1, AamAP-S1a, A3a, and K3-IsCTa are noted in this chapter. Opis16a also has a lower LP value of -6.9 compared with the higher LP values of -0.9, -2.06, -3.07, -5.3 for AamAP1, AamAP-S1a, A3a and K3-IsCTa. Therefore, a reduced LP leads to potent and selective activity as concluded in Chapter 2 and the first publication from this study.

Additionally, the ability of Opis16a to bind LPS, a unique component of Gram-negative bacteria, enhances its efficacy and selectivity while potentially providing anti-inflammatory effects. The mechanism of action of Opis16a involves LPS binding, destabilising the outer membrane, and leading to membrane permeabilisation, which is crucial for its bactericidal effect (Table 5.1). Opis16a demonstrates stability in serum and maintains its antimicrobial properties in 20% FCS and cation-adjusted MHB. In an *in vivo* burn wound infection model, Opis16a showed significant protective effects against multidrug-resistant *A. baumannii*, comparable with established treatments like polymyxin B.

© University of Pretoria

These findings show the potential of Opis16a as a novel therapeutic candidate for addressing multidrug-resistant Gram-negative infections, particularly in hospitals where such pathogens present a significant threat to vulnerable populations. Future research could focus on investigating the initial binding of Opis16a to LPS using techniques such as isothermal titration calorimetry and a quantitative chromogenic *Limulus amebocyte* lysate assay (LAL) kit (Malan *et al.,* 2015). This would clarify how Opis16a interacts with Gram-negative cells and assess its anti-inflammatory potential, an important target in reducing infection associated inflammation.

Given the promising activity in the *G. mellonella* burn wound model, the wound healing properties of Opis16a warrant further investigation using various methods. These could include the cell migration "scratch" assay, assessing migration inhibition with mitomycin C, and measuring transforming growth factor β1 (TGF-β1) production in macrophages (Di Grazia *et al.,* 2014, Wang *et al.,* 2023). Furthermore, a HaCat cell proliferation assay could be employed to evaluate its effects on keratinocyte growth during wound healing (Wang *et al.,* 2023). Chronic wounds present an even greater challenge due to antimicrobial resistance. These wounds are characterised by persistent bacterial infections, reduced angiogenesis, compromised epithelialisation, and an excess of ROS. Therefore, the immune-modulating effects of Opis16a should be further explored. This could involve evaluating the antioxidant activity of the peptide using the oxygen radical absorbance capacity (ORAC) assay, assessing its impact on tumour necrosis factor-α (TNF-α) and nitric oxide production, and examining its ability to regulate ROS levels (Malan *et al.,* 2015; Taute *et al.,* 2019).

Chapter 4 of this study introduces four new analogues of the Gram-negative-targeting peptide Opis16a, that exhibits enhanced membrane targeting and improved antibacterial activity. The chapter outlines four rational design strategies that proved successful. First, substituting Asp with a positively charged Lys resulted in Opis16aDtoK, which demonstrated increased potency and improved selectivity. However, the most significant improvements were observed with the replacement of Lys residues with Arg at various positions to yield Opis16aNterKtoR, Opis16aCterKtoR and Opis16aAllKtoR. These novel Arg-containing peptides exhibited superior antibacterial activity and selectivity compared with the original Opis16a. MD simulations demonstrated that the analogues formed more hydrogen bonds with Gram-negative model membranes, leading to stronger membrane interactions. The incorporation of Lys or Arg residues facilitated closer binding to the anionic membrane, improving overall peptide stability. While both Lys and Arg substitutions enhanced membrane interaction, the unique guanidinium group of Arg provided a more favourable charge distribution, contributing to greater hydrogen bonding, deeper membrane insertion and subsequent reduced conformational flexibility of the peptides.

Of the four analogues, Opis16aCterKtoR holds the most promise, achieving an MIC as low as 4 μg/mL against Gram-negative bacteria. This peptide outperformed conventional antibiotics against resistant strains, particularly *E. cloacae* NICD 16103, highlighting its potential for treating difficult

© University of Pretoria

infections (Table 5.1). In an *in vivo* wound infection model, both Opis16a and Opis16aCterKtoR conferred protection against *E. cloacae* NICD 16103; however, only Opis16aCterKtoR maintained efficacy at lower doses. This suggests superior potency, especially given the prevalence of multidrug-resistant *E. cloacae* in wound infections. These findings highlight the benefits of incorporating Arg into peptide sequences, positioning the novel Opis16aCterKtoR analogue as a strong candidate for future therapeutic development against challenging Gram-negative bacteria.

Future research on all four analogues of Opis16a, particularly Opis16aCterKtoR, is essential due to their significant broad-spectrum activities at low concentrations. Given that AMPs exhibit multifaceted properties, it would be beneficial to investigate their immune modulation potential and wound healing capabilities alongside their antimicrobial effects (Branco *et al.,* 2023). The strong performance of Opis16aCterKtoR in the *G. mellonella* burn wound model further supports the need for in-depth wound healing studies, similar to those planned for Opis16a.

This research has led to the discovery of two novel AMPs, Opis16a and Opis16aCterKtoR, that exhibit promising antimicrobial potential and distinct mechanisms of action as summarised in Table 5.1. However, both peptides demonstrate sensitivity to the protease trypsin. Generally, the strategy to increase resistance to proteases is further structural modifications. This requires extensive retesting with unpredictable outcomes. A more effective approach is the development of drug-delivery vehicles for these peptides. Current investigations by our research group show the potential of conjugating gold nanoparticles to promising AMPs (Van Wyk *et al.,* manuscript in preparation). Loading AMPs onto gold nanoparticles is a novel strategy used to protect, control the release, and extend resident times, of AMPs while minimising their associated cytotoxic effects. Van Wyk *et al.* showed that the loading of AamAP1-Lys-NH2, onto gold nanoparticles (AuNPs) using tyrosine capped gold surfaces (Tyr-AuNPs), affords a delivery system that improves the *in vivo* protection of *G. mellonella* larvae against *P. aeruginosa* infection. This approach can therefore improve target selectivity, reduce toxicity, and increase peptide stability. Encapsulating AMPs in liposomes to extend the half-life and enhance target specificity is a further focus of research (Nguyen *et al.,* 2022).

Future studies on treating infected wounds and the topical application of the AMPs in *in vivo* wound models could explore the incorporation of these peptides into wound dressings. A promising approach is the use of electrospun fibre matrices, which can effectively embed the peptides for slow release. This method not only optimises therapeutic outcomes but also promotes wound healing (Ramos *et al.*, 2024). Similar strategies have already been implemented for Os, a multifunctional AMP developed in our laboratory (Jiao *et al.,* 2021).

5.2 Last word

Scorpion venom-derived peptides, especially analogues derived from the N-terminal of opistoporin 1, hold significant promise as antimicrobial agents to combat antibiotic-resistant infections. These

© University of Pretoria

peptides demonstrate faster action, broad-spectrum activity, and a reduced likelihood of inducing resistance among pathogens as summarised in Table 5.1. Although the peptides may initially lack specificity, research herein shows that rational design strategies such as increasing Lys or Arg content in their sequences, can enhance target specificity, improve bacterial membrane interaction and damage, and expedite their action. Optimising the formulation of these peptides is crucial for enhancing their delivery and therapeutic efficacy. Future research should prioritise the development of effective delivery vehicles, conduct additional *in vivo* testing, and evaluation of their ADMET profiles. These steps are crucial for advancing the translation of these promising laboratory agents into viable drug candidates.

Table 5.1: *Summary of the activities, mechanisms of action and clinical potential of Opis16a and Opis16aCterKtoR, delivered by this research*

	Property	Opis16a	Opis16aCterKtoR
Activity	Antibacterial including against drug-resistant strains	✓	✓
	Haemolytic	X	nd
	HaCat toxicity	X	✓
	Bacterial over mammalian selectivity	✓	✓
	In vivo G. mellonella infection protection	✓ (10 mg/kg)	✓ (5 mg/kg)
Structure	Obtained CD secondary structure	✓ (predominantly α-helical)	✓ (predominantly α-helical)
	In silico secondary structure via dihedral angles and Ramachandran plots	✓ (coil/helix)	✓ (coil/helix)
Mechanism of bacterial action	Hydrogen bonding with lipids (*in silico*)	✓	✓
	Membrane insertion (*in silico*)	✓	✓
	LPS binding	✓	nd
	Outer membrane permeabilisation	✓	nd
	Cytoplasmic membrane depolarisation	✓	nd
	Cytoplasmic membrane permeabilisation	✓	✓
	Rapid killing kinetics	✓ (30-60 min)	✓ (30-45 min)
Stability	Activity in cation-adjusted MHB	✓	✓
	Activity in 20% FCS	✓	✓
	Activity in trypsin	X	X
Potential for further development		✓	✓

Green= Desirable outcome, Orange= Observed to some extent, Red= Undesirable outcome.
Check mark (✓)= yes, X mark (X)= no, nd = not determined.

© University of Pretoria

5.3 References

BRANCO, P., MAURÍCIO, E.M., COSTA, A., VENTURA, D., ROMA-RODRIGUES, C., DUARTE, M.P., FERNANDES, A.R. & PRISTA, C. (2023). Exploring the multifaceted potential of a peptide fraction derived from *Saccharomyces cerevisiae* metabolism: antimicrobial, antioxidant, antidiabetic, and anti-inflammatory properties. *Antibiotics*, 12 (8), pg.1332-1347. doi:10.3390/antibiotics12081332.

BOTO A, PÉREZ DE LA LASTRA J. M. & GONZÁLEZ C. C. (2018). The road from host-defense peptides to a generation of antimicrobial drugs. *Molecules*, 23 (2), pg. 311-320. doi:10.3390/molecules23020311

DI GRAZIA, A., LUCA, V., SEGEV-ZARKO, L.T., SHAI, Y. & MANGONI, M.L. (2014). Temporins A and B stimulate migration of HaCaT keratinocytes and kill intracellular *Staphylococcus aureus*. *Antimicrobial Agents and Chemotherapy*, 58 (5), pg. 2520–2527.

JIAO, J., PENG, C., LI, C., QI, Z., ZHAN, J. & PAN, S. (2021). Dual bio-active factors with adhesion function modified electrospun fibrous scaffold for skin wound and infections therapeutics. *Scientific Reports*, 11 (1), article 457. doi: 10.1038/s41598-020-80269-2.

KARAKONSTANTIS, S., ROUSAKI, M., VASSILOPOULOU, L. & KRITSOTAKIS, E.I. (2024). Global prevalence of cefiderocol non-susceptibility in *Enterobacterales*, *Pseudomonas aeruginosa*, *Acinetobacter baumannii*, and *Stenotrophomonas maltophilia*: a systematic review and meta-analysis. *Clinical Microbiology and Infection*, 30 (2), pg.178-188. doi:10.1016/j.cmi.2023.08.029.

MALAN, M., SEREM, J., BESTER, M., NEITZ, A. & GASPAR, A. (2015). Anti-inflammatory and anti-endotoxin properties of peptides derived from the carboxy-terminal region of a defensin from the tick *Ornithodoros savignyi*. *Journal of Peptide Science*, 22 (1), pg. 1-10. doi:10.1002/psc.2838.

NGUYEN, V.H., NGUYEN THUY, V., VO VAN, T. & HOANG DAO, A. (2022). Nanostructured lipid carriers and their potential applications for versatile drug delivery via oral administration. *OpenNano*, *8*, article 100064. doi:10.1016/j.onano.2022.100064.

RAMOS, C., LORENZ, K., PUTRINŠ, M., HIND, C.K., MEOS, A., LAIDMÄE, I., TENSON, T., SUTTON, J.M., MASON, A.J. & KOGERMANN, K. (2024). Fibrous matrices facilitate pleurocidin killing of wound-associated bacterial pathogens. *European Journal of Pharmaceutical Sciences*, 192 (1), pg.106648-106662. doi:10.1016/j.ejps.2023.106648.

TAUTE, H., BESTER, M.J. & GASPAR, A.R.M. (2019). The dual functionality of antimicrobial peptides Os and Os-C in human leukocytes. *Journal of Peptide Science*, 25 (1), article e3156. doi:10.1002/psc.3156.

VAN WYK, R.J., LORENZ, C.D., MASON, A.J., BESTER, M.J. & GASPAR, A.R.M. (2024). A nana-gold delivery system improves the therapeutic potential of scorpion-derived peptide, AamAP1-Lys-NH_2. *Manuscript in preparation.*

WANG, C., HONG, T., CUI, P., WANG, J. & XIA, J. (2021). Antimicrobial peptides towards clinical application: Delivery and formulation. *Advanced Drug Delivery Reviews*, 175 (1), article 113818. https://doi.org/10.1016/j.addr.2021.05.028

WANG, X., DUAN, H., LI, M., XU, W. & WEI, L. (2023). Characterization and mechanism of action of amphibian-derived wound-healing-promoting peptides. *Frontiers in Cell and Developmental Biology*, 11 (1), article 1219427. doi:10.3389/fcell.2023.1219427.

ZHANG, Y., WANG, Q., YIN, Y., CHEN, H., JIN, L., GU, B., XIE, L., YANG, C., MA, X., LI, H., LI, W., ZHANG, X., LIAO, K., MAN, S., WANG, S., WEN, H., LI, B., GUO, Z., TIAN, J., PEI, F., LIU, L., ZHANG, L., ZOU, C., HU, T., CAI, J., YANG, H., HUANG, J., JIA, X., HUANG, W., CAO, B. & WANG H. (2018). Epidemiology of carbapenem-resistant Enterobacteriaceae infections: Report from the China CRE Network. *Antimicrobial Agents and Chemotherapy*, 62 (2), pg. e01882-17. doi: 10.1128/AAC.01882-17

© University of Pretoria

Supplementary information

GenScript — Make Research Easy

CERTIFICATE OF ANALYSIS

Product Name	Opis16a
Order ID	U113KSCKG0_9
Lot No.	U113KSCKG0-9/PE3296
Sequence	GKVWDWIKSTAKKLWN
Modification	C - Terminal: Amidation
Length	16AA
Storage*	-20°C
Recommended Solvent*	Ultrapure water
Comments	TFA salt

Test Items	Specifications	Results
Molecular Weight	Theoretical MW: 1959.31	Consistent
HPLC purity	≥98.0%	99.7%
Appearance	White lyophilized powder	Conforms
Gross Weight	9 mg	9*1.0mg

*Note: Above recommended solvents for reference only. If there is any request for detailed dissolution conditions,we suggest you choose our 'Peptide Solubility Test Service'.

For long-term storage, it is suggested to store at -20°C and avoid freeze-thaw cycles. Since the expiration date of different peptides is different, if you are interested in more information about the expiration date, please feel free to consult the stability test service.

Caution:
For laboratory or further manufacturing use only. Not intended for household use. If you have any questions about the Certificate of Analysis, please contact our customer service representative at 1-877-436-7274 (Toll-Free), or 1-732-885-9188.

Certified by: Yi Gao Date:04/02/2024

Thank you for your patronage to our Peptide services! To maintain this working relationship, we shall be grateful if you can add our webpage URL into your lab website. As a token of appreciation, you will be rewarded by 1,000 EZcoupon™ points. For more information, please contact us by e-mail at web@genscript.com

860 Centennial Ave., Piscataway, NJ 08854, USA
Toll-Free: 1-877-436-7274 Tel: 1-732-885-9188 Fax: 1-732-210-0262 Email: order@genscript.com Web: www.genscript.com

© University of Pretoria

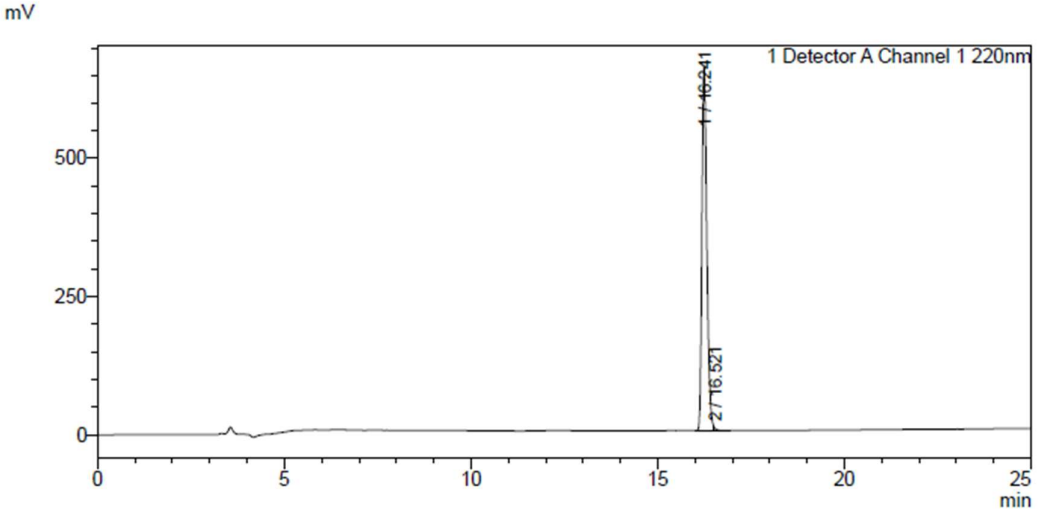
Sample Name :Opis16a
Sample ID :U113KSCKG0-9
Time Processed :21:34:26
Month-Day-Year Processed :03/30/2024

Pump A : 0.065% trifluoroacetic in 100% water (v/v)
Pump B : 0.05% trifluoroacetic in 100% acetonitrile (v/v)
Total Flow:1 ml/min
Wavelength:220 nm
<<LC Time Program>>

Time	Module	Command	Value
0.01	Pumps	B.Conc	5
25.00	Pumps	B.Conc	65
25.01	Pumps	B.Conc	95
27.00	Pumps	B.Conc	95
27.01	Pumps	B.Conc	5
35.00	Pumps	B.Conc	5
35.01	Controller	Stop	

<<Column Performance>>
<Detector A>
Column :Inertsil ODS-SP 4.6 x 250 mm
Equipment: GR11010440

<Chromatogram>

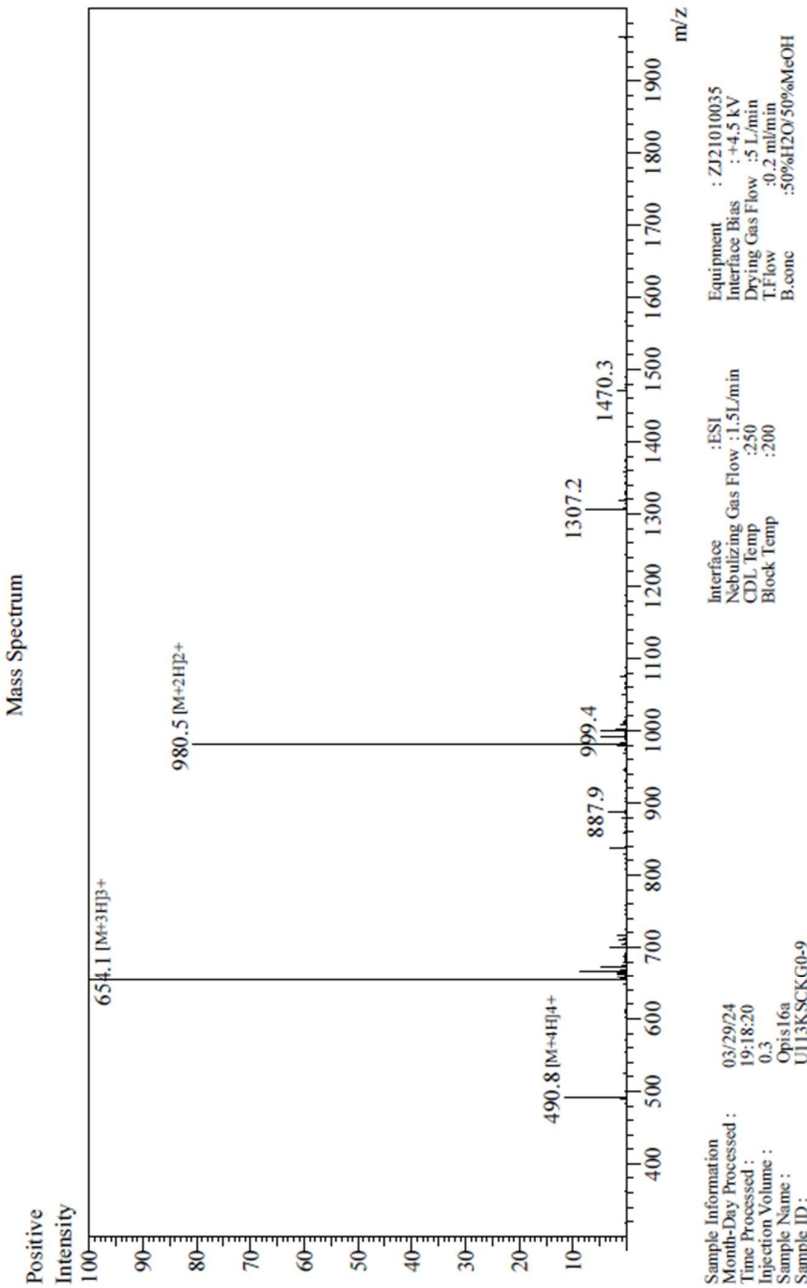


<Peak Table>

Detector A Channel 1 220nm

Peak#	Ret. Time	Area	Height	Area%
1	16.241	6013590	660646	99.688
2	16.521	18812	5320	0.312
Total		6032403	665966	100.000

© University of Pretoria



© University of Pretoria

GenScript Make Research Easy

CERTIFICATE OF ANALYSIS

Product Name	Opis16aD2K
Order ID	U8559HJ270_1
Lot No.	U8559HJ270-1/PE8261
Sequence	GKVWKWIKSTAKKLWN
Modification	C - Terminal: Amidation
Length	16AA
Storage	-20°C
Recommended Solvent*	Ultrapure water
Comments	TFA salt
Gross Weight	4*3.0mg+1.5mg

Test Items	Specifications	Results
Molecular Weight	Theoretical MW: 1972.39	Consistent
HPLC purity	≥95.0%	97.9%
Appearance	White lyophilized powder	Conforms
Net Weight	9 mg	4*2.0mg+1.0mg

*Note: Above recommended solvents for reference only. If there is any request for detailed dissolution conditions,we suggest you choose our 'Peptide Solubility Test Service'.

Caution:
For laboratory or further manufacturing use only. Not intended for household use. If you have any questions about the Certificate of Analysis, please contact our customer service representative at 1-877-436-7274 (Toll-Free), or 1-732-885-9188.

Certified by: Yi Gao Date:11/20/2022

Thank you for your patronage to our Peptide services! To maintain this working relationship, we shall be grateful if you can add our webpage URL into your lab website. As a token of appreciation, you will be rewarded by 1,000 EZcoupon™ points. For more information, please contact us by e-mail at web@genscript.com

860 Centennial Ave., Piscataway, NJ 08854, USA
Toll-Free: 1-877-436-7274 Tel: 1-732-885-9188 Fax: 1-732-210-0262 Email: order@genscript.com Web: www.genscript.com

© University of Pretoria

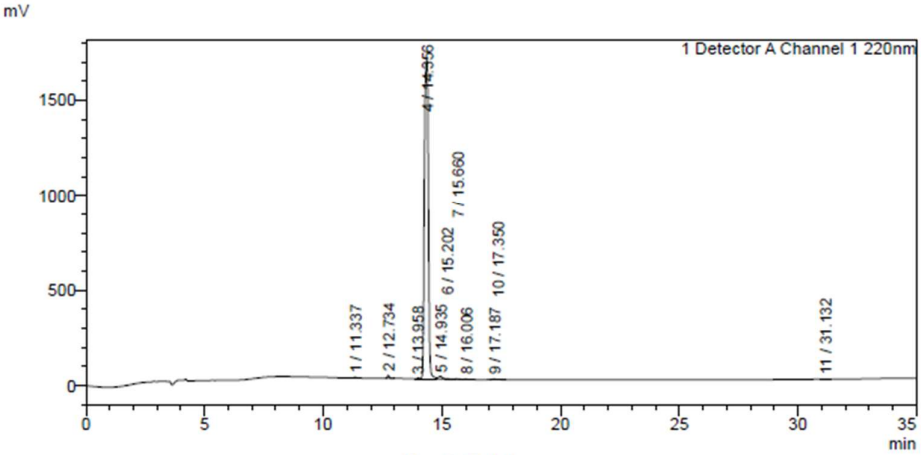
Sample Name :Opis16aD2K
Sample ID :U8559HJ270-1
Time Processed :4:45:38 PM
Month-Day-Year Processed :11/15/2022

Pump A : 0.065% trifluoroacetic in 100% water (v/v)
Pump B : 0.05% trifluoroacetic in 100% acetonitrile (v/v)
Total Flow:1 ml/min
Wavelength:220 nm
<<LC Time Program>>

Time	Module	Command	Value
0.01	Pumps	B.Conc	5
10.00	Pumps	B.Conc	35
35.00	Pumps	B.Conc	95
37.00	Pumps	B.Conc	95
37.01	Pumps	B.Conc	5
43.00	Pumps	B.Conc	5
43.01	Controller	Stop	

<<Column Performance>>
<Detector A>
Column :Inertsil ODS-3 4.6 x 250 mm
Equipment: ZJ17010508

<Chromatogram>

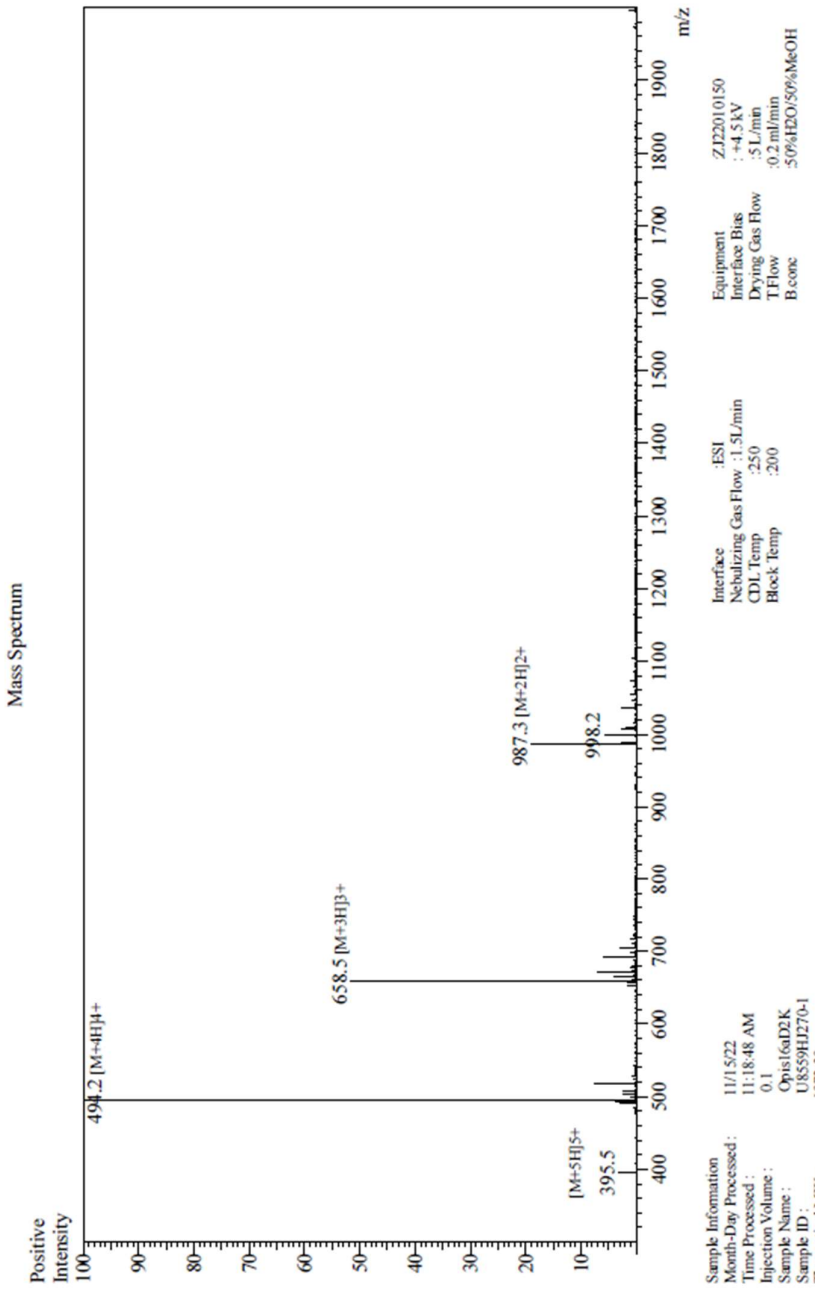


<Peak Table>

Detector A Channel 1 220nm

Peak#	Ret. Time	Area	Height	Area%
1	11.337	28427	5124	0.142
2	12.734	97373	15930	0.487
3	13.958	11315	1532	0.057
4	14.356	19595425	1686982	97.916
5	14.935	170835	14094	0.854
6	15.202	30698	2734	0.153
7	15.660	8034	984	0.040
8	16.006	15193	2802	0.076
9	17.187	26252	3164	0.131
10	17.350	11687	1166	0.058
11	31.132	17221	1584	0.086
Total		20012460	1736096	100.000

© University of Pretoria



© University of Pretoria

GenScript Make Research Easy

CERTIFICATE OF ANALYSIS

Product Name	Opis16aNterK2R
Order ID	U8559HJ270_7
Lot No.	U8559HJ270-7/PE8267
Sequence	GRVWRWIKSTAKKLWN
Modification	C - Terminal: Amidation
Length	16AA
Storage	-20°C
Recommended Solvent*	Ultrapure water
Comments	TFA salt
Gross Weight	4*2.8mg+1.4mg

Test Items	Specifications	Results
Molecular Weight	Theoretical MW: 2028.42	Consistent
HPLC purity	≥95.0%	96.1%
Appearance	White lyophilized powder	Conforms
Net Weight	9 mg	4*2.0mg+1.0mg

*Note: Above recommended solvents for reference only. If there is any request for detailed dissolution conditions,we suggest you choose our 'Peptide Solubility Test Service'.

Caution:
For laboratory or further manufacturing use only. Not intended for household use. If you have any questions about the Certificate of Analysis, please contact our customer service representative at 1-877-436-7274 (Toll-Free), or 1-732-885-9188.

Certified by: Li Hai Wei Date:11/21/2022

Thank you for your patronage to our Peptide services! To maintain this working relationship, we shall be grateful if you can add our webpage URL into your lab website. As a token of appreciation, you will be rewarded by 1,000 EZcoupon™ points. For more information, please contact us by e-mail at web@genscript.com

860 Centennial Ave., Piscataway, NJ 08854, USA
Toll-Free: 1-877-436-7274 Tel: 1-732-885-9188 Fax: 1-732-210-0262 Email: order@genscript.com Web: www.genscript.com

© University of Pretoria

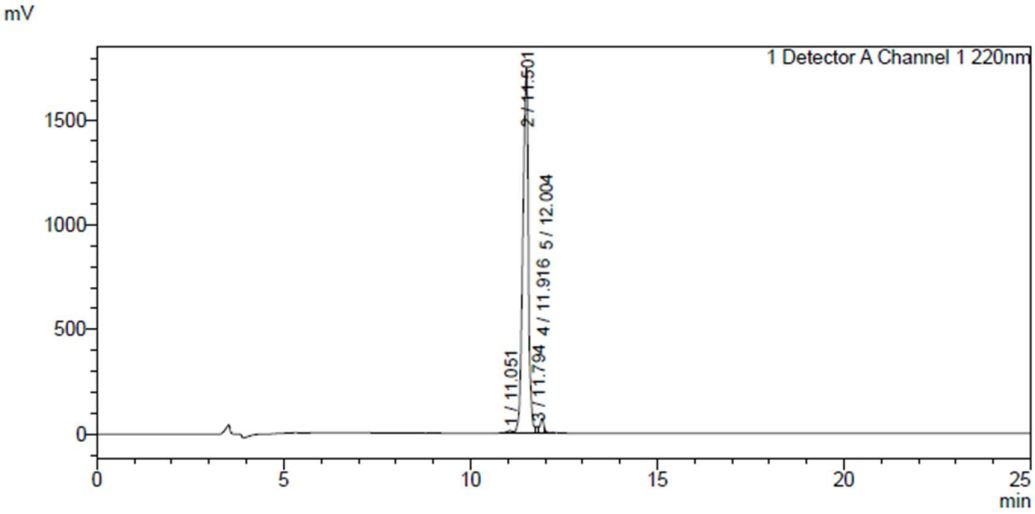
Sample Name :Opis16aNterK2R
Sample ID :U8559HJ270-7
Time Processed :10:51:10
Month-Day-Year Processed :11/16/2022

Pump A : 0.065% trifluoroacetic in 100% water (v/v)
Pump B : 0.05% trifluoroacetic in 100% acetonitrile (v/v)
Total Flow:1 ml/min
Wavelength:220 nm
<<LC Time Program>>

Time	Module	Command	Value
0.01	Pumps	B.Conc	5
25.00	Pumps	B.Conc	65
25.01	Pumps	B.Conc	95
27.00	Pumps	B.Conc	95
27.01	Pumps	B.Conc	5
35.00	Pumps	B.Conc	5
35.01	Controller	Stop	

<<Column Performance>>
<Detector A>
Column :Inertsil ODS-SP 4.6 x 250 mm
Equipment: GR11010440

<Chromatogram>

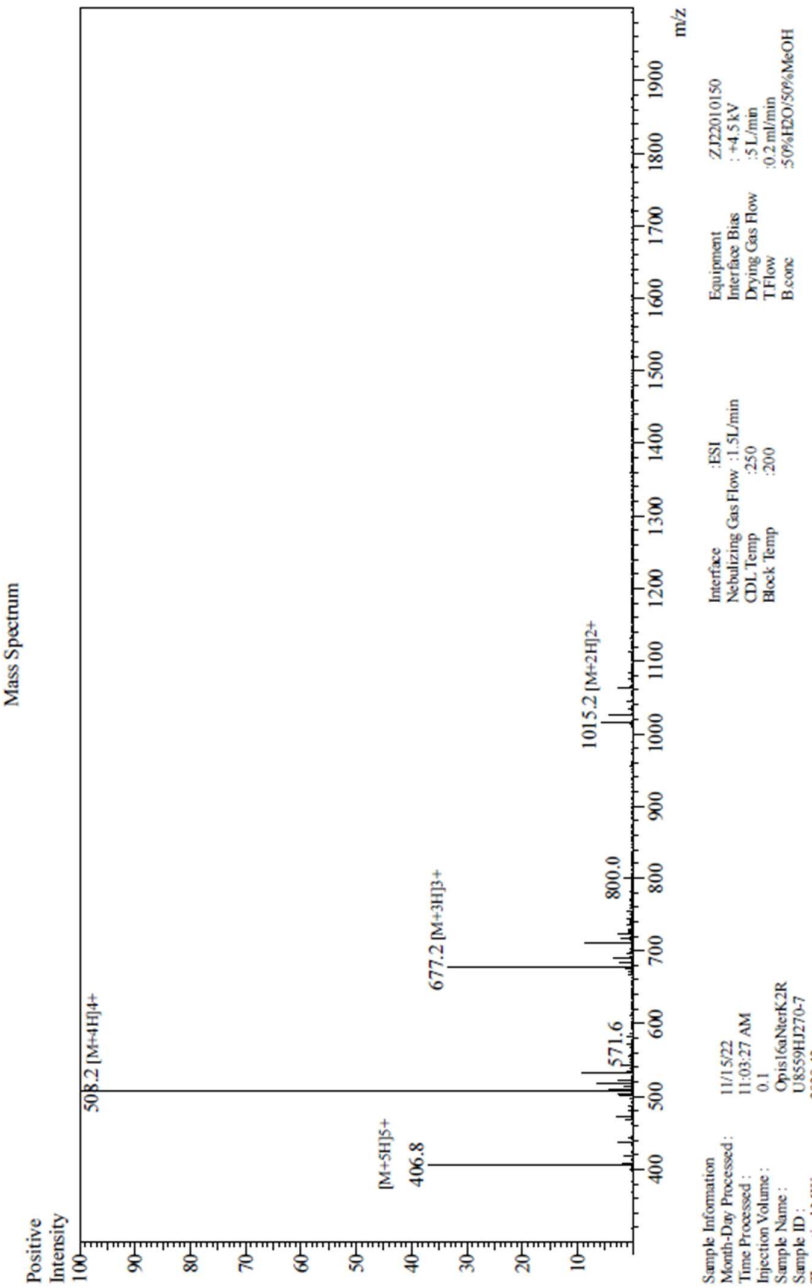


<Peak Table>

Detector A Channel 1 220nm

Peak#	Ret. Time	Area	Height	Area%
1	11.051	95777	10815	0.508
2	11.501	18114568	1750574	96.057
3	11.794	102596	31174	0.544
4	11.916	499579	70096	2.649
5	12.004	45655	13470	0.242
Total		18858175	1876129	100.000

© University of Pretoria



© University of Pretoria

UNIVERSITEIT VAN PRETORIA
UNIVERSITY OF PRETORIA
YUNIBESITHI YA PRETORIA

CERTIFICATE OF ANALYSIS

Product Name	Opis16aCterK2R
Order ID	U113KSCKG0_1
Lot No.	U113KSCKG0-1/PE4167
Sequence	GKVWKWIKSTARRLWN
Modification	C - Terminal: Amidation
Length	16AA
Storage*	-20°C
Recommended Solvent*	Ultrapure water
Comments	TFA salt

Test Items	Specifications	Results
Molecular Weight	Theoretical MW: 2028.42	Consistent
HPLC purity	≥98.0%	98.1%
Appearance	White lyophilized powder	Conforms
Gross Weight	9 mg	9*1.0mg

*Note: Above recommended solvents for reference only. If there is any request for detailed dissolution conditions,we suggest you choose our 'Peptide Solubility Test Service'.

For long-term storage, it is suggested to store at -20°C and avoid freeze-thaw cycles. Since the expiration date of different peptides is different, if you are interested in more information about the expiration date, please feel free to consult the stability test service.

Caution:
For laboratory or further manufacturing use only. Not intended for household use. If you have any questions about the Certificate of Analysis, please contact our customer service representative at 1-877-436-7274 (Toll-Free), or 1-732-885-9188.

Certified by: Dengyin Ge Date:03/28/2024

Thank you for your patronage to our Peptide services! To maintain this working relationship, we shall be grateful if you can add our webpage URL into your lab website. As a token of appreciation, you will be rewarded by 1,000 EZcoupon™ points. For more information, please contact us by e-mail at web@genscript.com

860 Centennial Ave., Piscataway, NJ 08854, USA
Toll-Free: 1-877-436-7274 Tel: 1-732-885-9188 Fax: 1-732-210-0262 Email: order @genscript.com Web: www.genscript.com

© University of Pretoria

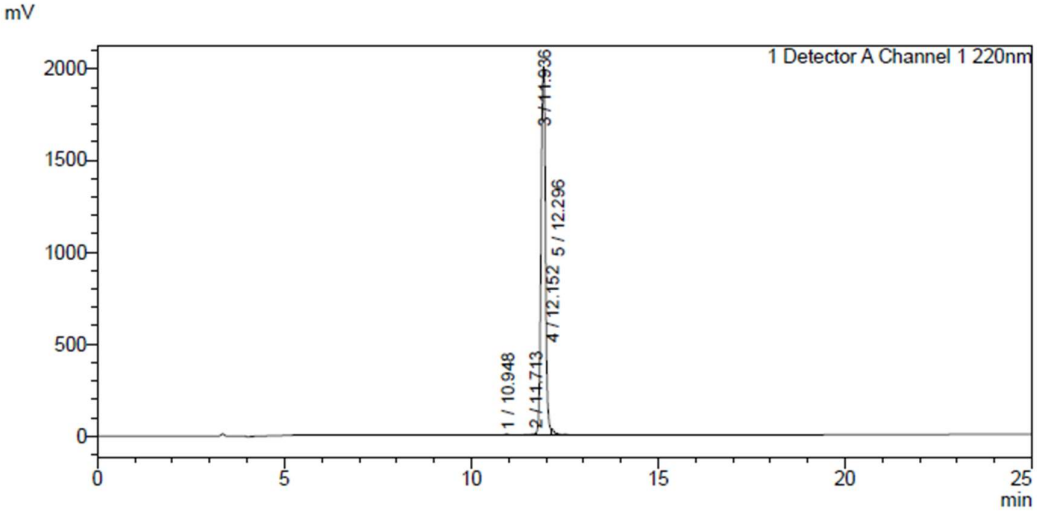
Sample Name :Opis16aCterK2R
Sample ID :U113KSCKG0-1
Time Processed :0:11:19
Month-Day-Year Processed :03/26/2024

Pump A : 0.065% trifluoroacetic in 100% water (v/v)
Pump B : 0.05% trifluoroacetic in 100% acetonitrile (v/v)
Total Flow:1 ml/min
Wavelength:220 nm
<<LC Time Program>>

Time	Module	Command	Value
0.01	Pumps	B.Conc	5
25.00	Pumps	B.Conc	65
25.01	Pumps	B.Conc	95
27.00	Pumps	B.Conc	95
27.01	Pumps	B.Conc	5
35.00	Pumps	B.Conc	5
35.01	Controller	Stop	

<<Column Performance>>
<Detector A>
Column :Inertsil ODS-SP 4.6 x 250 mm
Equipment: GR11010440

<Chromatogram>

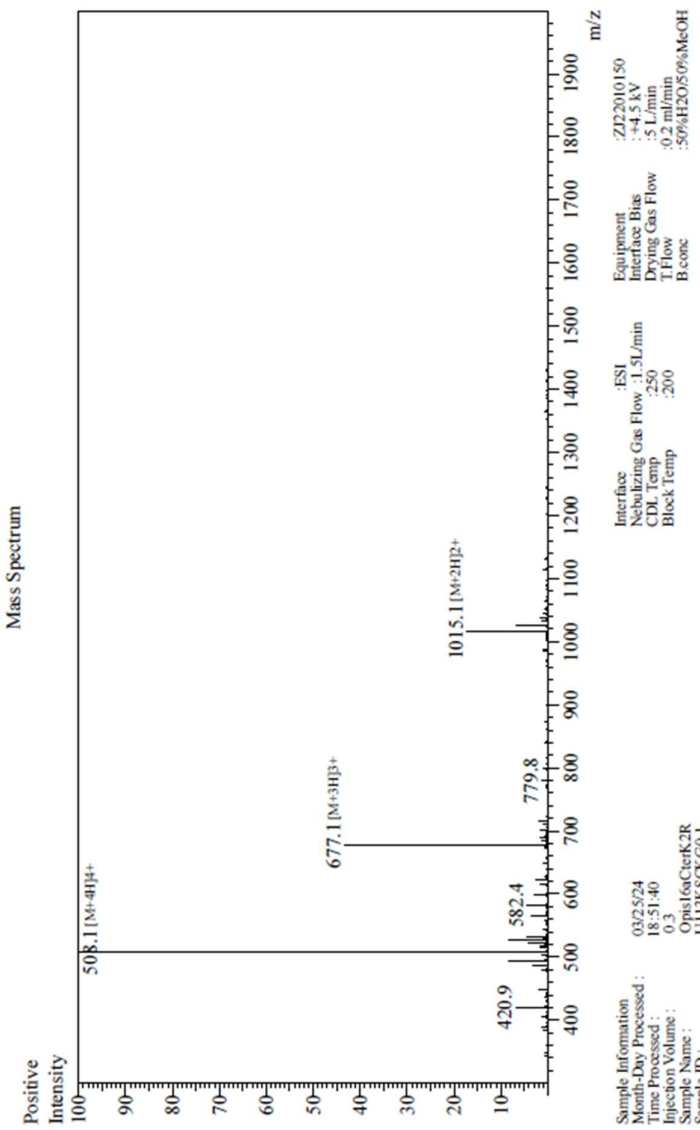


<Peak Table>

Detector A Channel 1 220nm

Peak#	Ret. Time	Area	Height	Area%
1	10.948	36513	4925	0.213
2	11.713	61371	6219	0.358
3	11.936	16826734	2008210	98.133
4	12.152	158399	33166	0.924
5	12.296	63811	5064	0.372
Total		17146828	2057584	100.000

© University of Pretoria



© University of Pretoria

GenScript Make Research Easy

CERTIFICATE OF ANALYSIS

Product Name	Opis16aAllK2R
Order ID	U8559HJ270_4
Lot No.	U8559HJ270-4/PE8264
Sequence	GRVWRWIRSTARRLWN
Modification	C - Terminal: Amidation
Length	16AA
Storage	-20°C
Recommended Solvent*	Ultrapure water
Comments	TFA salt
Gross Weight	4*3.0mg+1.5mg

Test Items	Specifications	Results
Molecular Weight	Theoretical MW: 2112.46	Consistent
HPLC purity	≥95.0%	97.6%
Appearance	White lyophilized powder	Conforms
Net Weight	9 mg	4*2.0mg+1.0mg

*Note: Above recommended solvents for reference only. If there is any request for detailed dissolution conditions,we suggest you choose our 'Peptide Solubility Test Service'.

Caution:
For laboratory or further manufacturing use only. Not intended for household use. If you have any questions about the Certificate of Analysis, please contact our customer service representative at 1-877-436-7274 (Toll-Free), or 1-732-885-9188.

Certified by: Li Hai Wei Date:11/22/2022

Thank you for your patronage to our Peptide services! To maintain this working relationship, we shall be grateful if you can add our webpage URL into your lab website. As a token of appreciation, you will be rewarded by 1,000 EZcoupon™ points. For more information, please contact us by e-mail at web@genscript.com

860 Centennial Ave., Piscataway, NJ 08854, USA
Toll-Free: 1-877-436-7274 Tel: 1-732-885-9188 Fax: 1-732-210-0262 Email: order@genscript.com Web: www.genscript.com

© University of Pretoria

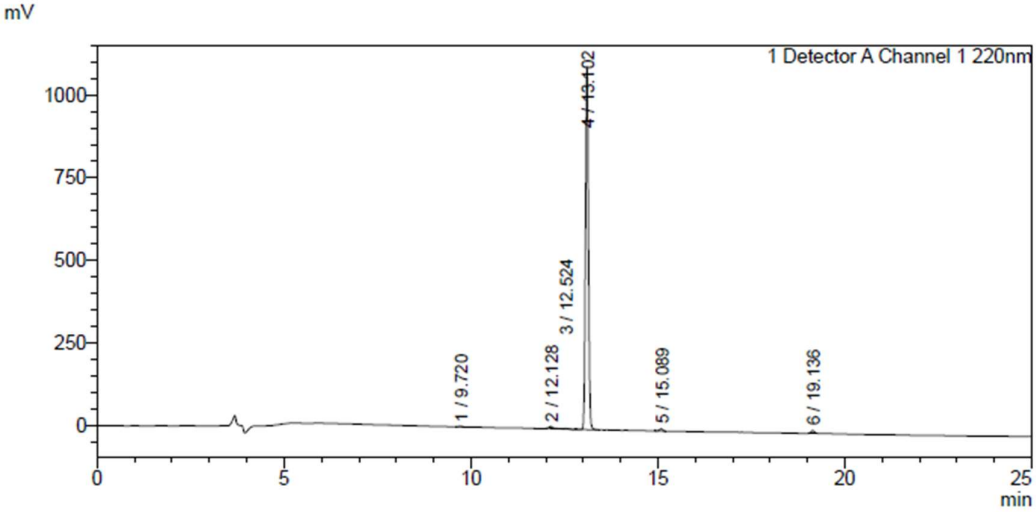
Sample Name :Opis16aAllK2R
Sample ID :U8559HJ270-4
Time Processed :1:53:58
Month-Day-Year Processed :11/18/2022

Pump A : 0.065% trifluoroacetic in 100% water (v/v)
Pump B : 0.05% trifluoroacetic in 100% acetonitrile (v/v)
Total Flow:1 ml/min
Wavelength:220 nm
<<LC Time Program>>

Time	Module	Command	Value
0.01	Pumps	B.Conc	5
25.00	Pumps	B.Conc	65
25.01	Pumps	B.Conc	95
27.00	Pumps	B.Conc	95
27.01	Pumps	B.Conc	5
35.00	Pumps	B.Conc	5
35.01	Controller	Stop	

<<Column Performance>>
<Detector A>
Column :Inertsil ODS-SP 4.6 x 250 mm
Equipment: GR11010440

<Chromatogram>

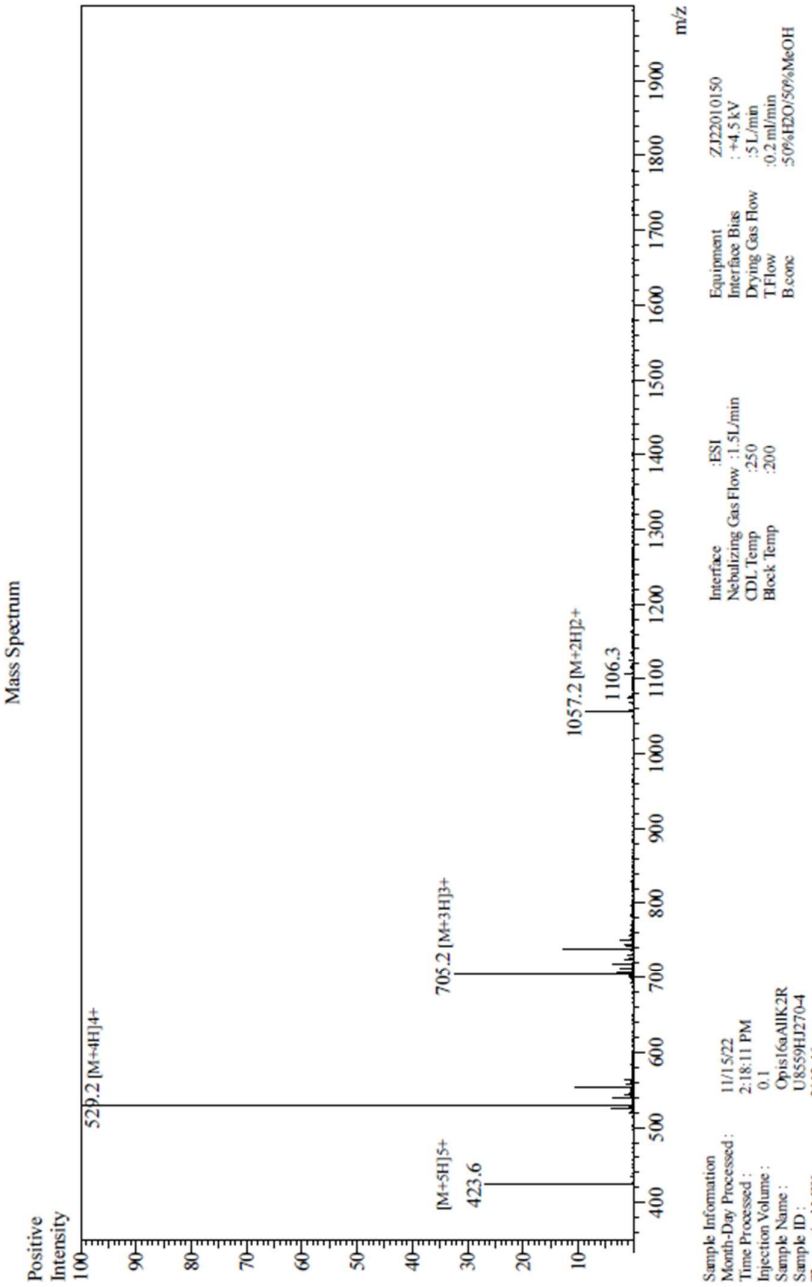


<Peak Table>

Detector A Channel 1 220nm

Peak#	Ret. Time	Area	Height	Area%
1	9.720	10163	1784	0.165
2	12.128	44305	5907	0.720
3	12.524	12352	1907	0.201
4	13.102	6000501	1101770	97.559
5	15.089	37476	6248	0.609
6	19.136	45823	8054	0.745
Total		6150621	1125671	100.000

© University of Pretoria



© University of Pretoria

Table S1: Total MD simulations carried out within this research project

Source	Peptide	Sequence	Environ-ment	Simulation duration (ns)	Repli-cates
O. carinatus (BioT-SA; Southern Africa)	**Opis8a**	WIKSTAKK-NH_2	Water	1000	1
	Opis16a	GKVWDWIKSTAKKLWN-NH_2	Water	1000	1
	Opis14a	GKVWWIKSTAKKLW-NH_2	Water	1000	1
	Opis18a	KGKKVWKWIKSTAKKLWN-NH_2	Water	1000	1
	Opis16	GKVWDWIKSTAKKLWN	Water	1000	1
	Opis16aKtoRwithD	GRVWDWIRSTARRLWN-NH_2	Water	1000	1
	Opis16aDtoG	GKVWGWIKSTAKKLWN-NH_2	Water	1000	1
	Opis16aDtoN	GKVWNWIKSTAKKLWN-NH_2	Water	1000	1
	Opis16aDtoK	GKVWKWIKSTAKKLWN-NH_2	Water	1000	1
	Opis16aAllKtoR	GRVWRWIRSTARRLWN-NH_2	Water	1000	1
	Opis16aNterKtoR	GRVWRWIKSTAKKLWN-NH_2	Water	1000	1
	Opis16aCterKtoR	GKVWKWIKSTARRLWN-NH_2	Water	1000	1
	Opis8a	WIKSTAKK-NH_2	PEPG POPG	200 200	1 1
	Opis16a	GKVWDWIKSTAKKLWN-NH_2	PEPG POPG	200 200	2 2
	Opis14a	GKVWWIKSTAKKLW-NH_2	PEPG POPG	200 200	1 1
	Opis18a	KGKKVWKWIKSTAKKLWN-NH_2	PEPG POPG	200 200	1 1
	Opis16	GKVWDWIKSTAKKLWN	PEPG POPG	200 200	1 1
	Opis16aKtoRwithD	GRVWDWIRSTARRLWN-NH_2	PEPG POPG	200 200	1 1
	Opis16aDtoG	GKVWGWIKSTAKKLWN-NH_2	PEPG POPG	200 200	1 1
	Opis16aDtoN	GKVWNWIKSTAKKLWN-NH_2	PEPG POPG	200 200	1 1
	Opis16aDtoK	GKVWKWIKSTAKKLWN-NH_2	PEPG POPG	200 200	2 2
	Opis16aAllKtoR	GRVWRWIRSTARRLWN-NH_2	PEPG POPG	200 200	2 2
	Opis16aNterKtoR	GRVWRWIKSTAKKLWN-NH_2	PEPG POPG	200 200	2 2
	Opis16aCterKtoR	GKVWKWIKSTARRLWN-NH_2	PEPG POPG	200 200	2 2
	Opis16a	GKVWDWIKSTAKKLWN-NH_2	Erythrocyte	200	2
	Opis16aDtoK	GKVWKWIKSTAKKLWN-NH_2	Erythrocyte	200	2
	Opis16aAllKtoR	GRVWRWIRSTARRLWN-NH_2	Erythrocyte	200	2
	Opis16aNterKtoR	GRVWRWIKSTAKKLWN-NH_2	Erythrocyte	200	2
	Opis16aCterKtoR	GKVWKWIKSTARRLWN-NH_2	Erythrocyte	200	2
Total no. of simulations		56			
Total simulation time (ns)		20 800			

© University of Pretoria